The reaction pathways of hydrogen peroxide in the presence of scavengers and its transition metal catalyzed oxidation of disulfide bridge containing peptides

By

Christopher Erik Helmut Asmus

Submitted to the graduate degree program in Pharmaceutical Chemistry and the Graduate Faculty of the University of Kansas in partial fulfillment of the requirements for the degree of Doctor of Philosophy.

_____

Chairperson: Dr. Christian Schöneich

_____

Dr. Susan Lunte

_____

Dr. John Stobaugh

_____

Dr. Valentino Stella

_____

Dr. Mario Rivera

Date Defended: 02-23-2015

The Dissertation Committee for Christopher Erik Helmut Asmus
certifies that this is the approved version of the following dissertation:

The reaction pathways of hydrogen peroxide in the presence of scavengers and its transition metal catalyzed oxidation of disulfide bridge containing peptides

_____

Chairperson Dr. Christian Schöneich

Date approved: 05-12-2015

Abstract

This thesis addresses two different reaction pathways of hydrogen peroxide.

The degradation pathway of hydrogen peroxide (H_2O_2) with sodium pyruvate elucidates the formation and breakdown of an intermediate formed during the reaction. Sodium pyruvate is a potential base for the creation of a peroxide scavenger. It readily reacts with H_2O_2 to yield sodium acetate, carbon dioxide and water as final products. A low temperature nuclear magnetic resonance protocol has been developed in order to observe the formation and breakdown of a proposed intermediate, 2-hydroxy-hydroperoxy-propanoate. Samples of ^{13}C-enriched sodium pyruvate were used to verify the formation of the intermediate and identify its structure by the heteronuclear multiband correlation spectroscopy NMR method. The observed chemical shifts have been compared with the predicted chemical shifts obtained from density functional theory calculations.

In order to calculate the activation parameters of the formation and breakdown of the intermediate a low temperature ^{13}C-NMR protocol has been developed that allowed to record intergable spectra of sodium pyruvate, the intermediate and the products formed by the reaction with H_2O_2 at various temperatures. The integrated data have been plotted vs. time which allowed to calculate the individual rate constants of the reaction steps at various temperatures. Based on the rate constants the activation parameters, the

enthalpy, entropy and free energy of the transition states of the formation and breakdown of the intermediate have been calculated.

The metal-catalyzed pathway of hydrogen peroxide is dealing with the effect of hydroxyl radicals created by the Fenton reaction and their potential to oxidize the disulfide bridge of small peptides. Based on the reduction potential, which is an indicator for the oxidizability by radicals, disulfide bridges in a peptide or protein are more facile targets for radical attack than methionine (Met) which is known to be easily oxidized by reactive oxygen species. The effects of the Fenton reaction on the peptides pressinoic acid (PA), oxytocin (Oxt) and a custom made peptide containing a disulfide bridge have been studied.

The experiments showed that the aromatic residues tyrosine (Tyr), which present on both PA and Oxt and Phenylalanine (Phe), which occurs on PA as well as arginine (Arg) located on the custom made peptide have been subject to hydroxylation by the ROS created through the Fenton reaction. No modification of the disulfide bridge such as oxidation, disulfide scrambling or formation of new carbon-sulfur bonds was detected on these peptides after the Fenton reaction has been applied.

Dedication

In memory of my father Prof. Dr. Klaus-Dieter Asmus

*12/13/1937 †07/10/2012

Do not stand at my grave and weep.
I am not there. I do not sleep.
I am a thousand winds that blow.
I am the diamond glints on snow.
I am the sunlight on ripened grain.
I am the gentle autumn rain.
When you awaken in the morning's hush
I am the swift uplifting rush
Of quiet birds in circled flight.
I am the soft stars that shine at night.
Do not stand at my grave and cry;
I am not there. I did not die.

Mary Elizabeth Frye

Acknowledgements

First I want to thank the love of my life, my wife Rahel for her support throughout the time, she stood beside me through good and bad and I value every day since we first met.

My mother Sibylle Asmus and my sister Ariane Asmus and my late father Klaus-Dieter Asmus for their neverending support and love during all stages of my life.

My advisor Christian Schöneich for his help and advice during these years.

My thanks also go to Sue Lunte, John Stobaugh, Val Stella and Mario Rivera for their support as my committee members and the support during my time at KU.

I'd like to thank my research group members for the help and especially Jessica, Olivier, Daniel and Riccardo.

The introduction to the NMR and all the help by Justin Douglas, Sarah Neuenswander and Asokan Anbanandam was invaluable for my thesis.

Gabi and Ahmed Aced as well as Dirk Guldi I'd like to thank for their more than helpful discussions.

I will never forget my "private" chemistry lesson from Richard Givens and I am glad he came by to support me during my oral defense.

Tracy Wechselblatt has given me so much comfort over the past years and always had an open ear for all my problems.

My thanks go to Nancy Helm and Karen Hall for solving so many non-research related problems.

Finally thanks to all my friends who believed in me.

Table of Contents

1 Introduction

1.1 Oxidative stress

Oxidative stress occurs from reactive oxygen species (ROS), which include hydroxyl radicals, ozone, singlet oxygen or peroxides.[1] In vivo, ROS such as peroxides and hydroxyl radicals are produced during normal cell metabolism as well as during the humoral defense mechanism.[2,3] Singlet oxygen, on the other hand, is formed in the retina due to high oxygen uptake combined with an increased UV radiation absorption from sunlight.[4] Therefore, cells possess enzymes, such as catalase or superoxide dismutase, as well as scavengers, such as tocopherol or pyruvate, to protect themselves from oxidative stress.[1,5]

ROS are also known to occur in protein drug formulations, e.g. calmodulin,[6] human parathyroid hormone,[7] or glutamine synthetase[8] and significantly reduce their shelf-life and stability.[9] Oxidation products, which stem from a reaction of ROS with proteins and/or peptides, may exert detrimental effects. For example, hydrogen peroxide, even in trace amounts, lowers the viscosity of hydroxyethylcellulose gels.[10] Protein based enzymes are known to lose their binding capacity towards specific receptors and to be inactivated in the process. Residues, which are originally buried within the three-dimensional structure of proteins, might become exposed to ROS, which is likely to

result in decreased cellular uptake of substances or even in aggregation of drug substances when newly exposed residues bind metal ions.[1,11]

Metal catalyzed oxidation is linked to chemical instabilities of proteins and peptides.[11] Unlike proteins, most peptides, however, lack a distinct higher order structure and as such fail to bury facile oxidation targets including aromatic side chains and to protect them from solvents.[12]

H_2O_2 and reduced transition metals are the substrates of Fenton reaction (**Reaction 1**), which is believed to yield hydroxyl radicals. Both substrates occur in trace amounts in pharmaceutical formulations.[13]

Reaction 1

Hydroxyl radicals have a very high reduction potential, which is a reflection of their oxidizing strength and is a demonstration that they are capable to oxidize most organic matter.[14] Hydroxyl radicals originate from both organic and inorganic peroxides.[9] They usually react with organic substrates via H-abstraction, for example, from saturated carbon sites of the protein backbone or residues of amino acids as well as hydroxylation of unsaturated carbon sites and oxidation of sulfur.[15]

Carbon centered radicals created by oxygen radicals are shown to react with molecular oxygen and form peroxyl radicals during the course of the reaction.[16] In this context, the sulfur containing amino acids cystein (Cys) and Met are oxidized by hydroxyl radical attack to form sulfoxides.[15,17]

While the Fenton reaction is beneficial for the treatment of waste water, as it is known to eliminate active pharmaceutical ingredients[18] or to degrade dyes,[19] it is, however, crucial to prevent it from happening when drugs are still stored in their original containers. A powerful way to circumvent Fenton reaction induced degradation involves the addition of oxygen scavengers such as ascorbate to drug formulations.

1.2 Origins of peroxides and metal traces

In pharmaceutical formulations, reactive impurities such as H_2O_2 and transition metal ions are present in trace levels and lead to the formation of highly ROS.[9,10] Water typically accelerates the degradation effects, which stem from these oxidizing species.[20]

These impurities might origin from additives in the form of buffers, which contain trace amounts of transition metals capable of catalyzing oxidation processes.[21] Other sources are antioxidants, surfactants, or solubilizing agents required to provide desired dosage forms.[22] Surfactants include polysorbate 20/80. These are used in freeze drying processes[11] and they facilitate the solubility of hydrophobic substances in aqueous solution.[13] Polyethylene glycol stabilizes the conformational character of proteins[11] and polyvinylpyrrolidone is used as a binder for wet granulation in solid dosage forms.[9]

Any of the aforementioned surfactants contain appreciable amounts of peroxides. The amounts of peroxides vary depending on manufacturers, batches, and storage times with concentrations ranging from 50 to 10,000 nmol/g.[9]

Even glass syringes used in laboratory settings introduce significant iron levels to solutions.[21] Metal ions, such as iron, used as coloring agent for glass leach from amber glass containers used for drug storage.[23]

1.3 Preventing oxidative damage

Prevention of oxidative damage to pharmaceutical formulations is crucial for the extension of their shelf life. Some damaging effects are easily prevented. For example, effects due to UV and light damage are minimized by secondary packaging. For the prevention of potential degradation by heat, cooling devices are usually available for optimal storage conditions.[24]

Prevention of oxidative damage, however, is a more challenging task. For a liquid drug formulation, the amount of oxygen in a container may be reduced but not totally eliminated by limiting the headspace in a vial.[11] Container closure issues that lead to oxygen uptake within the container result in the accumulation of ROS.[22]

Chelating agents such as ethylenediaminetetraacetic acid (EDTA) are often used to avoid the metal-catalyzed formation of hydroxyl radicals from H_2O_2. EDTA, on one

hand, successfully blocks the reaction with copper ions, but, on the other hand, it increases the reaction rate with Fe^{2+}.[25]

Radical chain reactions are stoppable by scavengers – tocopherol (E^0 = +0.5 V) or ascorbate (E^0 = +0.28 V) – with oxidation potentials lower than those substrates involved in the chain reaction.[25,26] However, antioxidants such as ascorbate reduce Fe^{3+} to Fe^{2+}, which then catalyzes the formation of peroxides and yields hydroxyl radicals.[27]

1.4 Specific aims of this dissertation

As described before, it is virtually impossible to prevent oxygen uptake leading to the further formation of peroxides and metal traces in pharmaceutical formulations. Two different reaction pathways involving hydrogen peroxide will be elucidated in this thesis. The first pathway focuses on the reaction mechanism of hydrogen peroxide with sodium pyruvate – a potential peroxide scavenger. The second pathway is looking at the damaging effect of the Fenton reaction, which is based on the reaction of H_2O_2 with reduced transition metals, on small, disulfide-bridge containing peptides.

1.4.1 Aim #1: Elucidation of the reaction mechanism of H_2O_2 and sodium pyruvate

The exact reaction mechanism of sodium pyruvate with hydrogen peroxide, resulting in the formation and breakdown of an intermediate, and the reaction products have been

analyzed using low temperature ^{13}C-NMR spectroscopy. This enabled the direct observation of all the molecules formed and the determination of all the kinetic data relevant to the corresponding reaction.

1.4.2 Aim #2: Effect of the Fenton reaction on small ring shaped, disulfide containing peptides

The effects of hydroxyl radicals created by the Fenton reaction on a small ring shaped, disulfide bridge containing model peptide, namely pressinoic acid, have been studied. It was of particular interest to test if the disulfide bridges of the peptides are a target of the hydroxyl radicals. As model peptides pressinoic acid and oxytocin have been studied as well as a custom made peptide lacking aromatic residues.

1.5 References

(1) Dalle-Donne, I.; Scaloni, A.; Giustarini, D.; Cavarra, E.; Tell, G.; Lungarella, G.; Colombo, R.; Rossi, R.; Milzani, A. *Mass Spectrom Rev* **2005**, *24*, 55.

(2) Fridovich, I. *Annu. Rev. Biochem.* **1975**, *44*, 147.

(3) Chance, B.; Sies, H.; Boveris, A. *Physiol Rev* **1979**, *59*, 527.

(4) Beatty, S.; Koh, H.; Phil, M.; Henson, D.; Boulton, M. *Survey of ophthalm* **2000**, *45*, 115.

(5) Hassan, H. M.; Fridovich, I.; Academic: 1980; Vol. 1, p 311.

(6) Gao, J.; Yin, D. H.; Yao, Y.; Sun, H.; Qin, Z.; Schöneich, C.; Williams, T. D.; Squier, T. C. *Biophys J* **1998**, *74*, 1115.

(7) Chu, J.-W.; Yin, J.; Wang, D. I. C.; Trout, B. L. *Biochem* **2004**, *43*, 14139.

(8) Levine, R. L. *J of Bio Chem* **1983**, *258*, 11823.

(9) Wasylaschuk, W. R.; Harmon, P. A.; Wagner, G.; Harman, A. B.; Templeton, A. C.; Xu, H.; Reed, R. A. *J Pharm Sci* **2007**, *96*, 106.

(10) Dahl, T.; He, G.-X.; Samuels, G. *Pharm. Res.* **1998**, *15*, 1137.

(11) Cornell Manning, M.; Chou, D. K.; Murphy, B. M.; Payne, R. W.; Katayama, D. S. *Pharm. Res.* **2010**, *27*, 544.

(12) Payne, R. W.; Manning, M. C. *Innovations Pharm. Technol.* **2009**, *28*, 64.

(13) Harmon, P. A.; Kosuda, K.; Nelson, E.; Mowery, M.; Reed, R. A. *J. Pharm. Sci.* **2006**, *95*, 2014.

(14) Meyer, T. E.; Przysiecki, C. T.; Watkins, J. A.; Bhattacharyya, A.; Simondsen, R. P.; Cusanovich, M. A.; Tollin, G. *Proc of the Nat Academy of Sciences* **1983**, *80*, 6740.

(15) Xu, G.; Chance, M. R. *Chem. Rev. (Washington, DC, U. S.)* **2007**, *107*, 3514.

(16) Davies, M. J.; Gilbert, B. C. *Adv. Detailed React. Mech.* **1991**, *1*, 35.

(17) Schöneich, C. *Chem Res in Tox* **2008**, *21*, 1175.

(18) Giri, A. S.; Golder, A. K. *Industrial & Engineering Chem Res* **2014**, *53*, 1351.

(19) Xu, X. R.; Li, H. B.; Wang, W. H.; Gu, J. D. *Chemosphere* **2004**, *57*, 595.

(20) Hemenway, J. N.; Carvalho, T. C.; Rao, V. M.; Wu, Y.; Levons, J. K.; Narang, A. S.; Paruchuri, S. R.; Stamato, H. J.; Varia, S. A. *J of Pharm Sc* **2012**, *101*, 3305.

(21) Buettner, G. R.; Jurkiewicz, B. A. *Radiat. Res.* **1996**, *145*, 532.

(22) Kasraian, K.; Kuzniar, A. A.; Wilson, G. G.; Wood, J. A. *Pharm. Dev. Technol.* **1999**, *4*, 475.

(23) Sanga, S. V. *J. Parenter. Drug Assoc.* **1979**, *33*, 61.

(24) Kerwin, B. A.; Remmele, R. L., Jr. *J. Pharm. Sci.* **2007**, *96*, 1468.

(25) Hovorka, S. W.; Schoneich, C. *J. Pharm. Sci.* **2001**, *90*, 253.

(26) Niki, E. *The Am J of Clin Nut* **1991**, *54*, 1119S.

(27) Buettner, G. R. *Arch. Biochem. Biophys.* **1993**, *300*, 535.

2 Identification of the intermediate formed during the reaction of sodium pyruvate and hydrogen peroxide

2.1 Introduction

Pyruvic acid (Chart 1, Structure 1), an alpha keto acid, is known to be an efficient peroxide scavenger.[1] The low temperature NMR experiments have been performed with deuterated solvents. Therefore in this chapter all exchangeable protons have been substituted with deuterons. The mechanism of the reaction of pyruvate with H_2O_2 was proposed to proceed through the formation of an intermediate, 2-hydroperoxy-hydroxypropanoate or 2-deuteroperoxy-deuteroxypropanoate in deuterated solvents. This intermediate further breaks down to acetate, carbon dioxide and water.[2] Experimental observations of the products with $H_2{}^{18}O$ and $H_2{}^{18}O_2$ as substrates have supported the proposed mechanism, here shown with deuterons instead of protons, as shown in **Scheme 1**.[2,3] However, no direct observation of this intermediate has been reported before. Those experiments were performed at room temperature where the lifetime of 2-hydroperoxy-hydroxypropanoate is too short for spectroscopic observation.

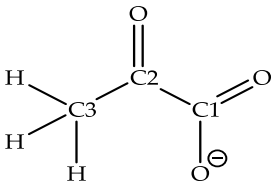

1: Pyruvate

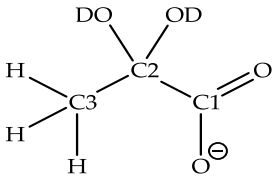

2: Hydrate

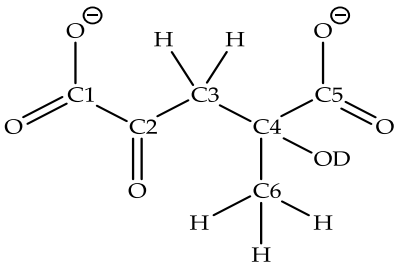

3: Dimer

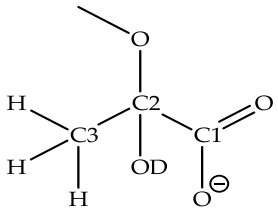

4: Hemiacetal

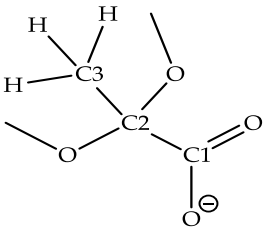

5: Full acetal

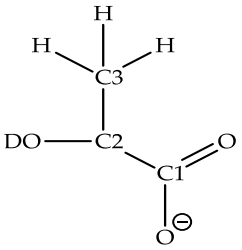

6: Lactate

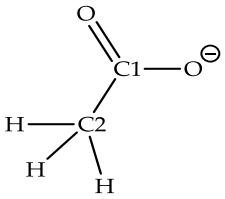

7: Acetate

8: CO_2

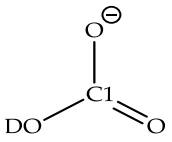

9: Bicarbonate

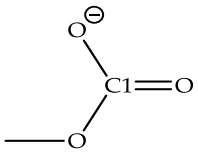

10: Methylcarbonate

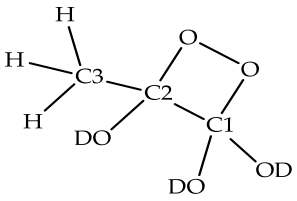

11: Dioxetane

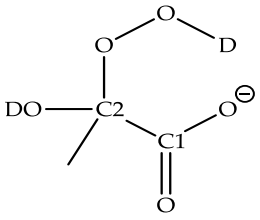

12: 2-hydroperoxy-2-hydroxypropanoate (Intermediate)

Chart 1: Chemical structures with the carbon position number

Chemical structures of the molecules that may be observed with ^{13}C NMR spectroscopy have been drawn with ChemDraw v 13.0. Carbon identifiers are based

on IUPAC rules. All exchangeable protons have been replaced by deuterons because the experiments were performed in protic, deuterated solvents.

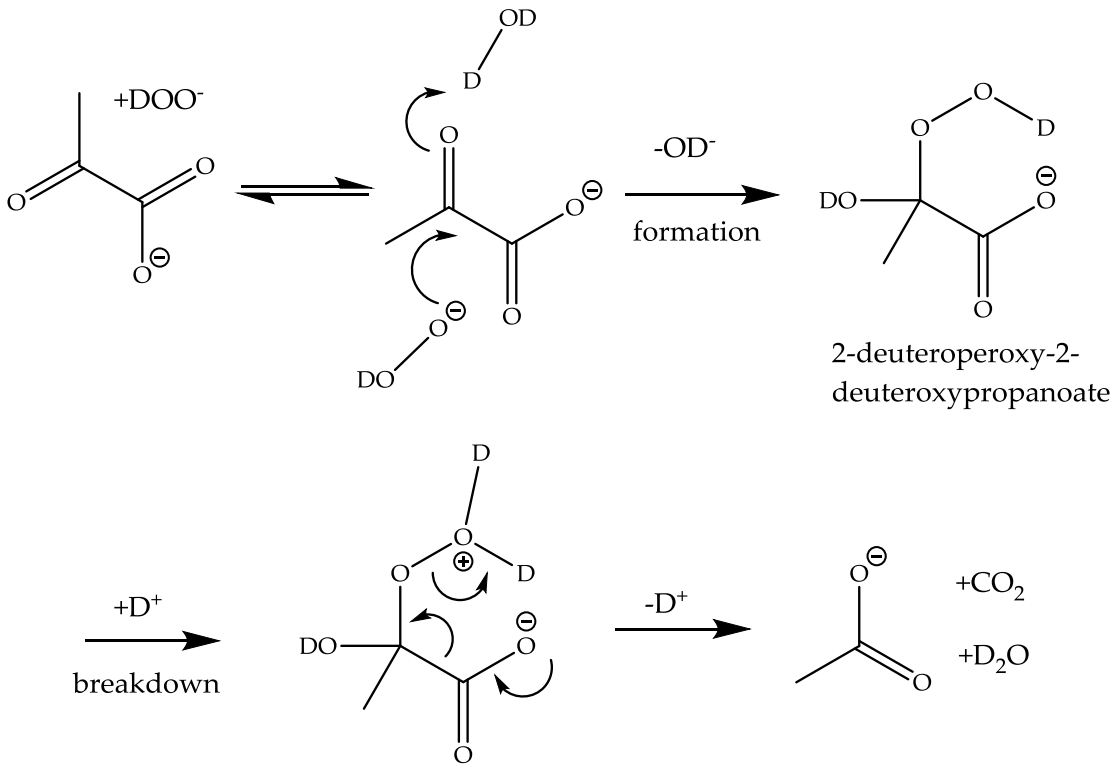

Scheme 1: The reaction mechanism of pyruvate and D_2O_2 forming an intermediate followed by the breakdown to the products at neutral pD.

Depending on the pH the rate limiting step of the reaction is either the formation of the intermediate (pH > 3.8) or the breakdown of the intermediate (pH < 3.8). This pH dependency of the rate limiting step has been shown by kinetic isotope effect experiments. The decarboxylation at the C1 position of pyruvate samples showed no significant carbon kinetic isotope effect in the pH range of 2 – 3.8, as the total reaction rate is not dependent of the C1 isotope, the attack of H_2O_2 at the C2 position and not the

decarboxylation is rate limiting. With increasing pH the kinetic isotope effect for the decarboxylation is increasing from nearly 1.001 at pH 3 to 1.0283 at pH 10 and the attack of H_2O_2 is less significant for the reaction rate.[4]

In aqueous solution pyruvic acid exists in equilibrium with its hydrate form, 2,2 dihyroxypropanoate (Chart 1, Structure 2) or simply hydrate. Under acidic conditions the equilibrium is shifted to the hydrate form. The hydrate structure is stabilized through protonation of the carboxyl group.[5] The stability of the hydrate is directly correlated with the pKa values of pyruvic acid (2.2) and the hydrate (3.6).[6] This means below pH 2.2 almost all pyruvic acid is converted into the hydrate form. The hydrate form is stabilized through two water molecules. The hydrate has an entropy value, calculated from the equilibrium constant, of (-112.13 J / mol x K) suggesting this highly structured form.[6]

Pyruvic acid is unstable if stored at neutral or basic conditions. It undergoes aldol condensation to form 2-hydroxy-2-methyl-3-oxosuccinate (Chart 1, Figure 3).[7] This dimer is also referred to as parapyruvate. The acidic proton on the methyl group allows for the keto-enol conversion which forms the dimer. The enol form occurs in very low yields (K = [enol form / keto form] = 8.2×10^{-6}) under neutral conditions and readily converts to the dimer in the presence of another pyruvic acid molecule. The enol form is therefore unlikely to be observable. At pH > 6 pyruvic acid is converted into parapyruvate due to that acidic proton and can even further polymerize. A hydrate

form of this parapyruvate has not been observed possibly due the intermolecular stabilization of parapyruvate through the adjacent hydroxyl and keto groups.[7]

The base catalyzed formation of parapyruvate is becoming self-catalyzed as the pKa of parapyruvate is higher than the pKa of pyruvic acid.[8] Therefore storage of pyruvic acid is recommended at temperatures below -20 °C and slightly acidic conditions. This makes pyruvic acid unsuitable as a peroxide scavenger in pharmaceutical formulations that are stored at room temperature or require a neutral or basic storage condition.

Hydrogen peroxide has a lower basicity than water leading to a higher nucleophilicity of hydrogen peroxide compared to water.[9] Therefore the hydrogen peroxide adduct on pyruvic acid is more stable than a water adduct. This results in an equilibrium shift to the intermediate form and the acid or water catalyzed dissociation to pyruvic acid is significantly slower compared to the water adduct.[9]

In addition to the formation of the intermediate 2-hydroperoxy-hydroxypropanoate it was taken into account that a dioxetane (Chart 1, Structure 11) can be formed. The newly formed 3-methyl-1,2-dioxetane-1,1-diol would yield acetate, bicarbonate and H_2O as products. Bicarbonate exists in equilibrium with CO_2 and H_2O but is rather stable in aqueous solution at low temperatures.[10]

Lactic acid differs from pyruvic acid only by the presence of a hydroxyl group at the C2 position instead of a carbonyl group. Lactic acid does not readily react with hydrogen peroxide, in fact the conversion to pyruvic acid is required first.[11] In the experiments it

served as a model for the C1 carboxyl group to check whether hydrogen peroxide will attach to the C1 position.

Because of the fast reaction rate at temperatures above 0 °C a low temperature NMR protocol was developed to observe the formation of the proposed intermediate. Experiments were performed with ^{13}C-enriched sodium pyruvate in a D_2O/d4-methanol solution which allowed to perform experiments in solution at temperatures as low as -40 °C.

2.2 Materials and methods

2.2.1 Chemicals

Deuterium oxide (99.8%), d4-methanol (99.6%) , ^{13}C-enriched (99%) sodium pyruvate at either positions C1 or C2, ^{13}C-enriched (99%) sodium acetate and ^{13}C-enriched (99%) sodium bicarbonate (Chart 1, Structure 9) were obtained from Cambridge Isotopes Laboratories (Tewksbury, MA, USA); non enriched sodium pyruvate was supplied by Aldrich (Milwaukee, WI, USA); lactic acid (85%) and H_2O_2 (30% in H_2O) were supplied by Fisher Scientific (Waltham, MA, USA). All chemicals were used without further purification. A solution (S_0) of 49.9%:0.1%:49.8%:0.2% D_2O:H_2O:CD_3OD:CH_3OH (v:v:v:v) was used as solvent for the NMR experiments.

2.2.2 Instruments

NMR spectra were acquired on a 500 MHz (11.74 T) Bruker DRX spectrometer equipped with an X-channel observe broadband probe. Samples were cooled using a gas flow from liquid nitrogen through the probe. Standard 5mm-7″ NMR tubes were purchased from Wilmad LabGlass (Vineland, NJ 08360, USA).

2.2.3 Software

Chemical structures were drawn with ChemBioDraw Ultra 13.0 (Perkin Elmer, Waltham, MA 02451, USA). Chemical shifts were initially predicted with the integrated predictor function in ChemBioDraw Ultra 13.0, which is based on empirical data. Subsequently, NMR data were predicted by density functional theory (DFT) calculations. The DFT calculations were performed with the Gaussian-03 (G03) molecular orbital packages.[12] NMR data were analyzed using MNova version 9.0 (Mestrelab Research, Santiago de Compostela, Spain). Kinetic data were fitted with a customized algorithm written in the Python® programming language.

2.2.4 Experimental protocol

Standard solutions of 15 mM of ^{13}C-sodium pyruvate, ^{13}C-acetate, ^{13}C-bicarbonate were prepared in both D_2O and S_0. Because of the use of deuterated, protic solvents all subsequent formulas with exchangeable sites are written with deuterons. The spectra of the substances were recorded in both solutions in order to identify any substrate-solvent

interactions which yield new products. In addition this allowed the comparison of the individual chemical shifts with the predicted values.

A non-enriched CO_2 solution was prepared by purging gas created from a dry ice in water bath through D_2O for 2 min. Non-enriched lactic acid standard was dissolved in D_2O to yield 15 mM concentration.

The solutions were not buffered because non-carbon buffers, which would not interfere with the carbon signal of the substrates, such as sodium phosphate salts were not well soluble at low temperatures in S_0. The pD in D_2O solutions and the apparent pD* in S_0 were measured before and after each experiment.

For the observation of the intermediate structure NMR tubes were filled with 600 µl of 15 mM ^{13}C enriched sodium pyruvate in S_0 (pD* = 6.8). The samples were cooled in an acetone bath that was cooled to approximately -40 °C with dry ice. Then 21 µl of 7 M H_2O_2 were added to yield 150 mM D_2O_2 concentration in the solution, which resulted in a 10:1 ratio of D_2O_2 : pyruvate. The cooled NMR tubes were shaken several times to allow even distribution of D_2O_2 and were then inserted into the precooled (-38 °C) NMR probe.

As an initial experiment, the spectra of non-enriched sodium pyruvate samples were recorded.

By comparison of the data before and after addition of hydrogen peroxide and with the the spectra of the known product standards the chemical shifts of the intermediate had been identified. The ^{13}C1 and ^{13}C2 chemical shifts of sodium pyruvate (205.3 ppm), sodium acetate (181.3 ppm), sodium bicarbonate (161.7 ppm), CO_2 (126.2 ppm) and methanol as reference standard (49 ppm) had been assigned individually based on the predictions. The not assigned new peaks after addition of hydrogen peroxide belong to the intermediate. Based on the predictions the chemical shifts of the intermediate had been assigned (102.9 ppm).

A standard carbon NMR experiment with a non-enriched sample usually requires about 30 min recording time. The good spectrum quality indicated that at -38 °C the reaction rate is very slow and the intermediate can be trapped for the preparation of the NMR and further observation. For kinetic observation of the samples the temperature was raised to the desired temperature point of each experiment after sample injection and preparation of the instrument.

In order to calculate kinetic reaction data, the exact temperature of the sample needs to be known. Although the temperature of the NMR probe can be set to a fixed value, the measured temperature on the probe can differ significantly from the temperature inside the NMR tube due to air fluctuations.[13] Depending on the temperature range either ethylene glycol for higher temperatures or methanol for lower temperatures is used to measure the exact temperature. The protons of the hydroxyl group of the protonated

methanol have a lower intermolecular distance to the adjacent methyl groups at lower temperatures, see **Figure 1**.

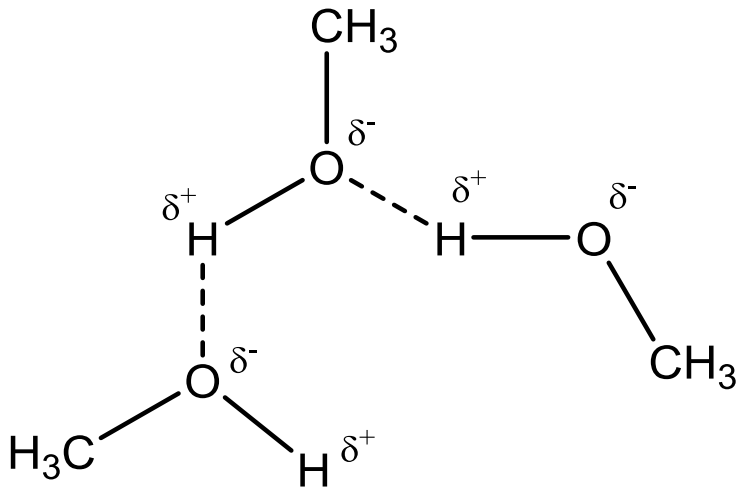

Figure 1: Interaction of hydroxyl groups of methanol

The closer proximity to the oxygen is deshielding the proton which leads to a downfield move of the peaks and increased difference between the methyl group proton signal and the hydroxyl group proton signal. The chemical shift of the methyl group remains constant as it is not affected by adjacent hydrogens. It is common practice to use a (4%:96% CH_3OH:CD_3OD) standard which allows to lock the NMR signal on the d4-methanol signal and provide a clear spectrum.[14,15] For the calculation of the temperature **Equation 1** was used:

Equation 1

$$T = (3.92 - \Delta_{Proton\ signals})/0.008$$

The above mentioned uncertainties with the temperature measurements at the NMR probe did not allow repeating two experiments at the exact same temperature. Although the temperature of the sample was stable over several hours once it was injected, every insertion of a new sample lead to a change of the internal temperature, e.g. in two different experiments the preset temperature of -17 °C resulted in measured temperatures of -32.5 °C and -30.1 °C.

Initial experiments showed that sodium pyruvate is not soluble in pure methanol. Therefore a water/methanol mixture has been used for the experiments. Mixtures of water and methanol can form clusters of unmixed solvents. This may lead to a significantly increased pyruvate concentration in water clusters and falsification of the concentration data. However since water clusters are occurring in less than 1% of the solution volume[16] under the experimental conditions they have not been taken into account, as those pyruvate concentrations would not be high enough to yield significant NMR signals.

The temperature window for kinetic observation was set from -10 °C to -35 °C. The upper temperature limit was based on the fact that the reaction occurred too fast to properly observe the intermediate structure with NMR. The lower temperature limit was close to the freezing point of the mixture (ca. -40 °C)[17] at which the viscosity of the solution was increased, leading to peak broadening and loss of the NMR lock signal.

For a better assignment of the NMR data to the proposed structures Heteronuclear Multiple-Bond Correlation (HMBC) NMR experiments where applied. This method allows observation of the interaction of hydrogen not directly attached to the observed carbons. In the case of pyruvate the methyl hydrogens interact with the C1 and C2 carbon.

1-D ^{13}C-NMR spectroscopy was determined for CO_2 and sodium bicarbonate as no distant hydrogens are coupled to the carbons observed.

2.2.5 Distinguishing between hydrate, pyruvate and dimer

In aqueous solution sodium pyruvate is partially converted to its hydrate form.[6] The amount of hydrate relative to pyruvate can be increased by lowering the pH of the solution.[6] Therefore the pD of the sodium pyruvate solution was lowered below pD 2 by addition of 1 M DCl. By addition of 1 M NaOD the pD* of the sodium pyruvate solution was set to > 12 for observation of the dimer form.

2.2.6 Distinguishing between hemiacetal and acetal

Additional peaks occurred in the NMR spectra after addition of d4-methanol. Similar to the hydrate form a half acetal was formed from sodium pyruvate and methanol. To create the full acetal form, acid catalysis is required.[18] By creating and observing the full acetal form with addition of 1 M DCl hemi- and full acetal can be distinguished and the creation of a full acetal under acidic conditions proofs the formation of a hemiacetal in

the beginning. The fraction of d4-methanol in the S_0 solution was varied from 0% to 75% in order to observe increasing hemi- or full acetal concentration.

2.2.7 Kinetic NMR measurement

For the acquisition of kinetic data 1-D ^{13}C-NMR spectra were recorded with inverse gated ^{1}H decoupling at a rate of 4 scans/2 min for one data point every two minutes for the whole experiment. For ^{13}C1-pyruvate the spectral width and offset were set to 160 ppm and 115 ppm and for ^{13}C2-pyruvate to 190 ppm and 125 ppm respectively. To ensure reproducible quantitative integration, the interscan delay was set to 25 s which is 5 times longer than the average ^{13}C longitudinal relaxation time constant for carboxylate carbons.

The highest signal quality can be obtained by applying a 90° pulse to the observed nucleus. The pulse length was acquired by finding the Null value of the 360° pulse and dividing the value by four. The Null value was found at 70 μs and the pulse was set to 17.5 μs.

Sodium pyruvate was dissolved in S_0 which is not a standard NMR solvent and therefore no lock program was available for this mixture. The lock signal was set to the D_2O which gave a clearer signal than d4-methanol.

It is not recommended for long time experiments to spin the samples. Although spinning is supposed to cancel out field inhomogeneity in the Z direction of the sample,

over an extended period of time the spin rate may differ and create spinning side bands in the spectrum.

The probe was cooled to the desired temperature at least 10 min before the initial experiment. Temperature measurement with the method described above showed that by the time the instrument was prepared for the first measurement the content of the NMR tube had already been adjusted to the desired temperature. For the quantification of the amount of hydrate, hemiacetal and acetal formed, a total of 64 scans with a rate of 2 scans/min has been acquired. Based on **Equation 2** the concentration of each species from the kinetic data has been calculated, with A being the integrated NMR signal of the species X, S being the sum of all integrated areas of the NMR signals of the species and C_0 the initial concentration of pyruvate in the sample.

Equation 2

$$[X] = \frac{A}{S} \times C_0$$

The hydrate and dimeric form of sodium pyruvate had a rather low abundance at neutral pD* and did not yield a significant signal under the conditions used for the kinetic observation. Therefore these species were not considered for kinetic calculations. Based on the reactions in **Scheme 2** equations 3-6 were used to calculate the rate constants of the reaction scheme with the following variables: [A] = sodium pyruvate concentration; [B_0] = initial hydrogen peroxide concentration; [I] = intermediate concentration; [C_0] = initial methanol concentration and [D] = hemiacetal concentration.

Equation 3

$$\frac{dA}{dt} = -k_1 \times [A] \times [B]_0 + k_2 \times [I] - k_4[C]_0 \times [A] + k_5 \times [D]$$

Equation 4

$$\frac{dI}{dt} = k_1 \times [A] \times [B]_0 - k_2 \times [I] - k_3 \times [I]$$

Equation 5

$$\frac{dP}{dt} = k_3 \times [I]$$

Equation 6

$$\frac{dD}{dt} = k_4 \times [C]_0 \times [A] - k_5[D]$$

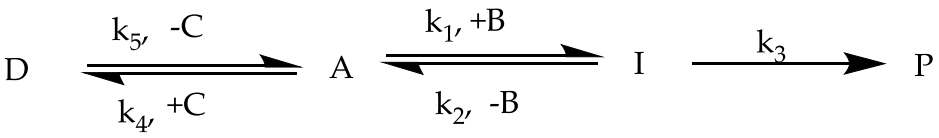

Scheme 2: Reaction pathway on which the calculation of the kinetic data is based

With A: Pyruvate; B: H_2O_2; C: d4-methanol; D: Hemiacetal; I: Intermediate; P: products; k_x: rate constant of the reaction

2.2.8 Density function theory (DFT) calculations

Most prediction software such as the one utilized in ChemDraw is based on empirical data associated to certain functional groups. The chemical shift of a carbon is predicted by the average influence of the adjacent functional groups and their nuclei and the distance from the carbon. This method does not take into account any solvent or steric effects or through space effects. Based on DFT the prediction can take into account the

whole molecule, its 3-D structure and the solvent environment. While an empirical prediction requires only minimal resources and time, the DFT calculation is a rather time and resource intense method to predict chemical shifts.

2.3 Results

2.3.1 Characterization of the standards

The chemical shifts recorded of the known standards sodium pyruvate, sodium acetate, sodium bicarbonate and CO_2 in D_2O observed with HMBC or ^{13}C NMR are listed in **Table 1**.

Table 1: HMBC chemical shifts

Compound	Experimental ^{13}C-1 chemical shifts	Experimental ^{13}C-2 chemical shifts	Experimental ^{1}H chemical shifts
Pyruvate	170.2 ppm	204.9 ppm	2.3 ppm
Hydrate	178.4 ppm	93.7 ppm	1.4 ppm
Dimer	182.1 ppm	73.4 ppm	1.3 ppm
Hemiacetal	177.9 ppm	99.2 ppm	2.9 ppm
Acetal	174.0 ppm	101.4 ppm	2.9 ppm
Intermediate	177.3 ppm	102.9 ppm	2.8 ppm
Acetate	181.8 ppm	n/a	3.3 ppm

^{13}C chemical shifts recorded from HMBC spectra assigned to the carbon atoms in the structures presented in Chart 1

2.3.2 Characterization of the reactants

2.3.2.1 Hydrate, dimer and enol

The HMBC spectra recorded of sodium pyruvate in D_2O (pD = 6.8), **Figure 2**, showed three different species in the solution, which is consistent with the fact that sodium pyruvate is in equilibrium with its hydrate and dimer form in solution. Based on the DFT calculations and predictions the C2 chemical shift of 205.3 ppm was assigned to the pyruvate form, the 94.5 ppm chemical shift was assigned to the hydrate form and the 73.4 ppm chemical shift was assigned to the dimer form.

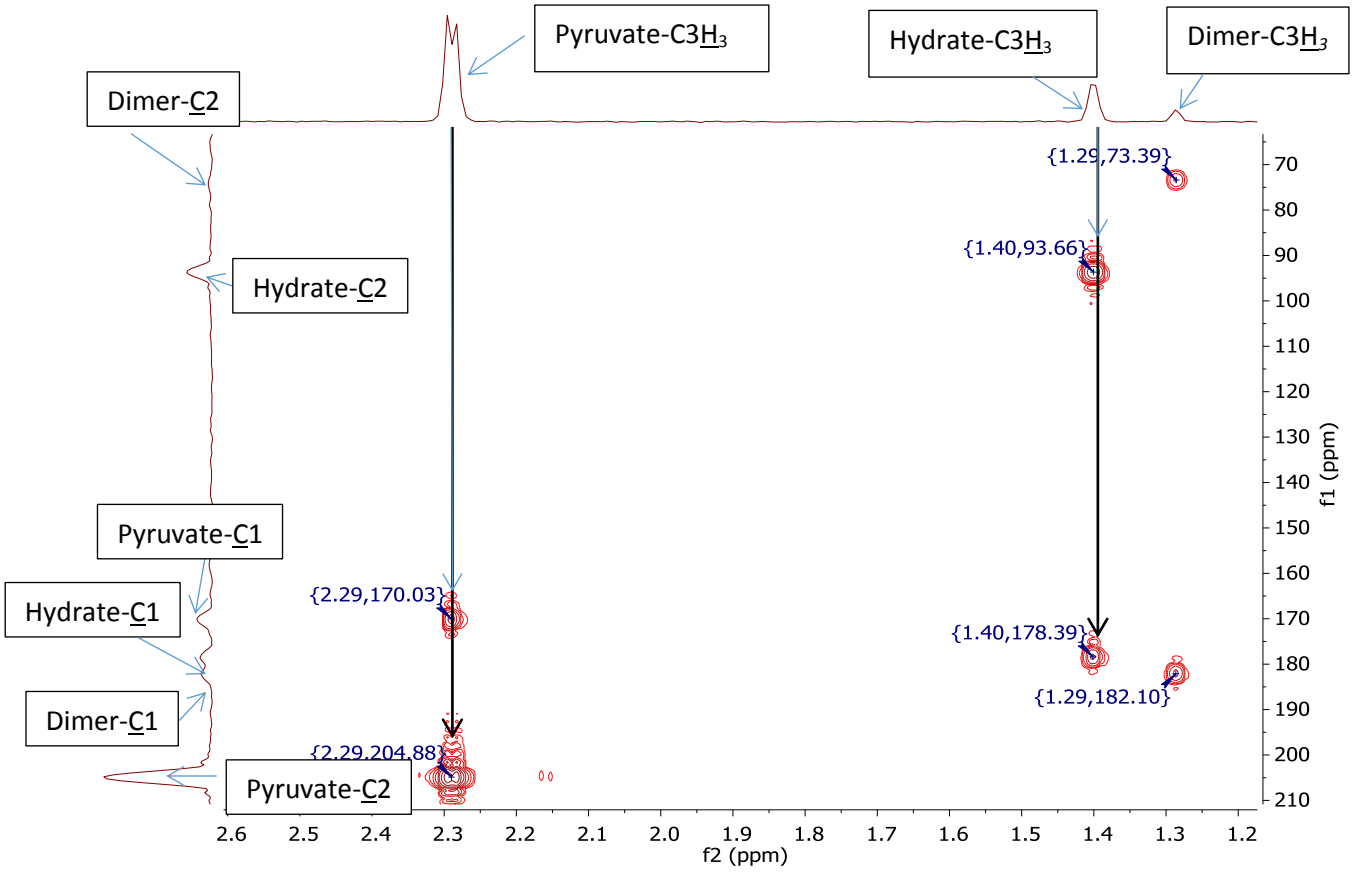

Figure 2: HMBC data of a 1:1 mixture of ^{13}C1 and ^{13}C2 enriched sodium pyruvate in D_2O, spectrum recorded at room temperature and near neutral pD*. Frequency 1 (f1) carbon chemical shift in ppm; frequency 2 (f2) hydrogen chemical shift in ppm.

Under neutral conditions the hydrate form accounted for 6±4% of the total pyruvate content and in an acidic environment (pD < 2) the hydrate content increased to 69±3% of the total pyruvate content.

Under basic conditions (pD > 12) only the dimer was observed with an apparent content of 100% dimer.

The isolated enol form of sodium pyruvate had a predicted ^{13}C2 chemical shift at 110 ppm which was not observed in the spectrum. The yield of the enol form is expected to be very low (K = [enol form / keto form] = 8.2 x 10^{-6}) under neutral conditions and any enol quickly forms a dimer.[19]

2.3.2.2 Hemiacetal and full acetal

Figure 3 shows the HMBC spectrum of sodium pyruvate in S_0. When sodium pyruvate was dissolved in S_0 additional peaks occurred in the NMR spectrum. Those were believed to occur from a hemiacetal formed from methanol and pyruvate in a similar way as the hydrate form. The hemiacetal had ^{13}C2 and ^{13}C1 chemical shifts at 99.2 ppm and 177.9 ppm, respectively.

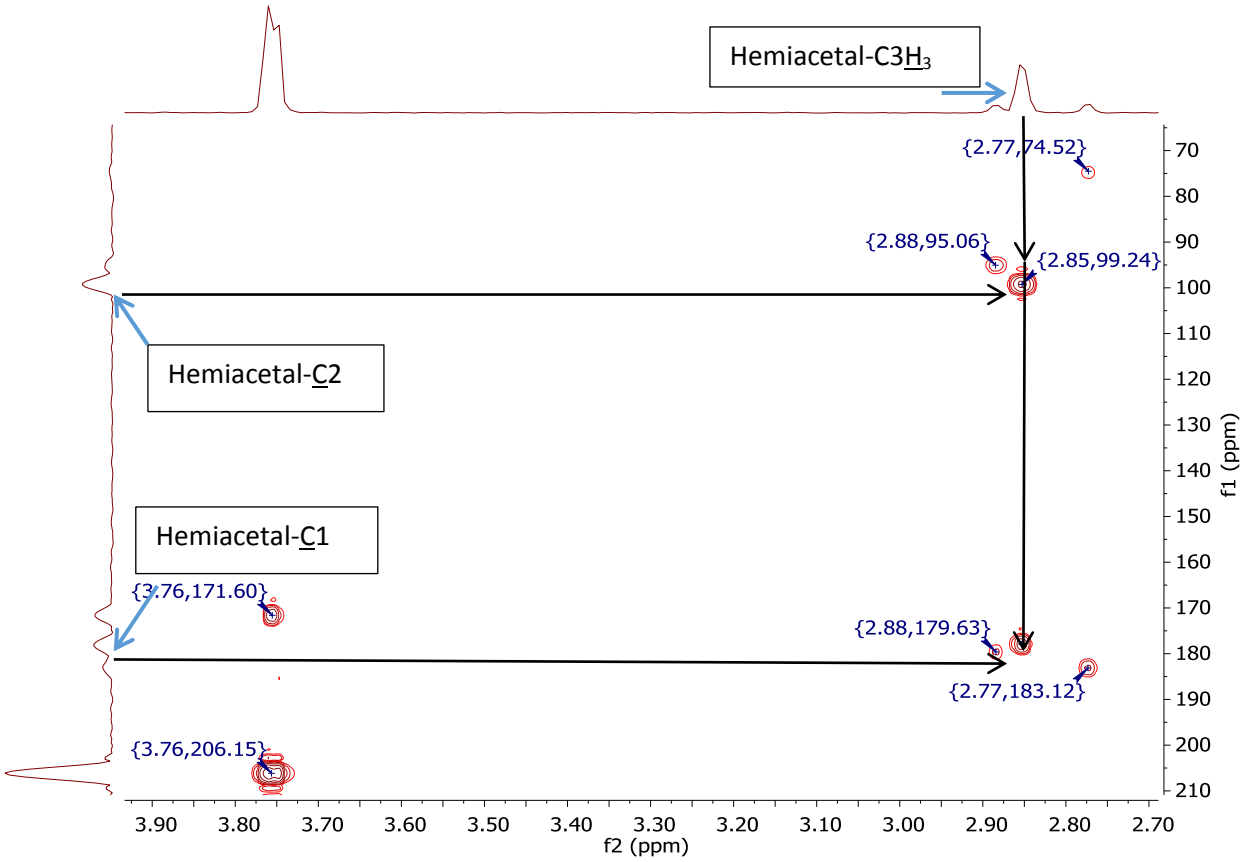

Figure 3: HMBC spectrum of sodium pyruvate in 50% D_2O / 50% d4-MeOD, spectrum recorded at room temperature and near neutral pD*. Frequency 1 (f1) carbon chemical shift in ppm; frequency 2 (f2) hydrogen chemical shift in ppm.

The variation of the methanol content in S_0 showed an increased hemiacetal content with a higher methanol fraction as shown in **Table 2**.

Table 2: Influence of the methanol concentration on the hemiacetal formation at neutral pD*

Sample	Pyruvate	Hemiacetal	Hydrate
MeOD 0%	94 % ±4%	0 %	6 % ±4%

MeOD 25%	90 % ±3%	7 % ±2%	3 % ±1%
MeOD 50%	85 % ±5%	10 % ±3%	5 %±3%
MeOD 75%	85 % ±5%	13 % ±3%	3 % ±1%

The recorded signals from the ^{13}C-NMR spectra were integrated and the relative values were calculated in %.

As the formation of a full acetal requires acid catalysis this experiment has been repeated under acidic (pD < 2) conditions which also allowed to distinguish the chemical shifts of the hemiacetal and the full acetal form. The values for the full acetal are shown in **Table 3**.

Table 3: hemiacetal and full acetal formation under acidic conditions (pD* < 2)

Sample	Pyruvate	Hemiacetal	Acetal	Hydrate
MeOD 0%	31 % ±3%	0 %	0 %	69 % ±3%
MeOD 25%	19 % ±4%	38 % ±11%	4 % ±3%	39 % ±9%
MeOD 50%	18 % ±1%	52 % ±2%	14 % ±10%	16 % ±10%
MeOD 75%	16 % ±1%	60 % ±4%	6 % ±1%	19 % ±3%

The recorded signals from the ^{13}C-NMR spectra were integrated and the relative values were calculated in %.

The full acetal form had new ^{13}C2 and ^{13}C1 signals at 101.4 ppm and 174.0 ppm, see **Figure 4**.

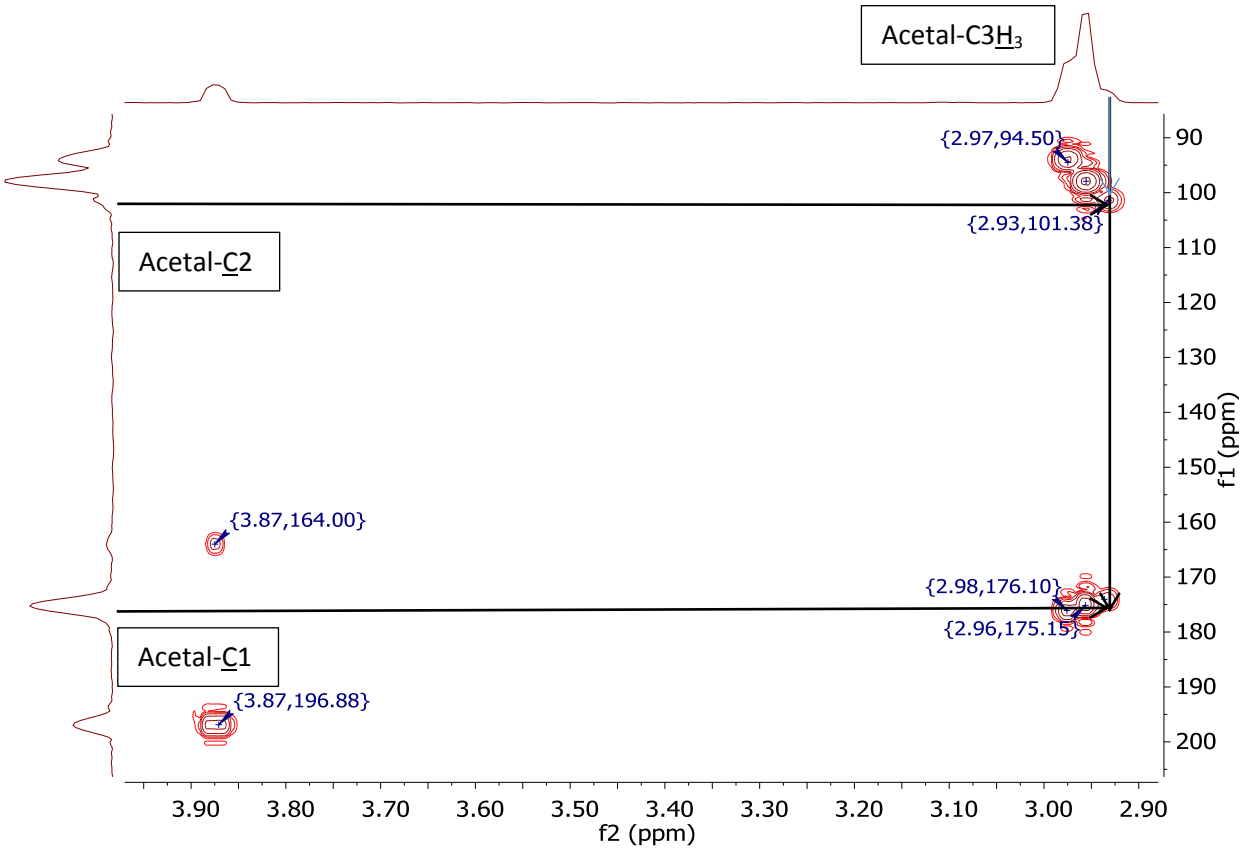

Figure 4: HMBC spectrum of sodium pyruvate in 50% D_2O / 50% d4-MeOD, spectrum recorded at room temperature at low pD* (<2). Frequency 1 (f1) carbon chemical shift in ppm; frequency 2 (f2) hydrogen chemical shift in ppm.

2.3.3 Characterization of the intermediate

In **Figure 5** spectroscopic data of the newly formed intermediate after addition of D_2O_2 to S_0 at -35 ˚C is shown as an HMBC spectrum. The cross peaks at 2.8 ppm frequency (f)2 (^{1}H), 102.9 f1 (^{13}C) ppm for C2 and 2.8 ppm f2, 178.3 f1 ppm for C1 in the HMBC spectrum were assigned to the intermediate I (Chart 1, Structure 12), consistent with the

structure of 2-deuteroperoxy-2-deuteroxypropanoate. This assignment was supported by the DFT calculation as shown in **Table 1**.

Only minor changes to the chemical shifts occurred at the C1 and C3 sites, the latter observed in a non-enriched sodium pyruvate sample. This shows that the intermediate is formed solely by the nucleophilic attack of the peroxide on the C2 position of sodium pyruvate.

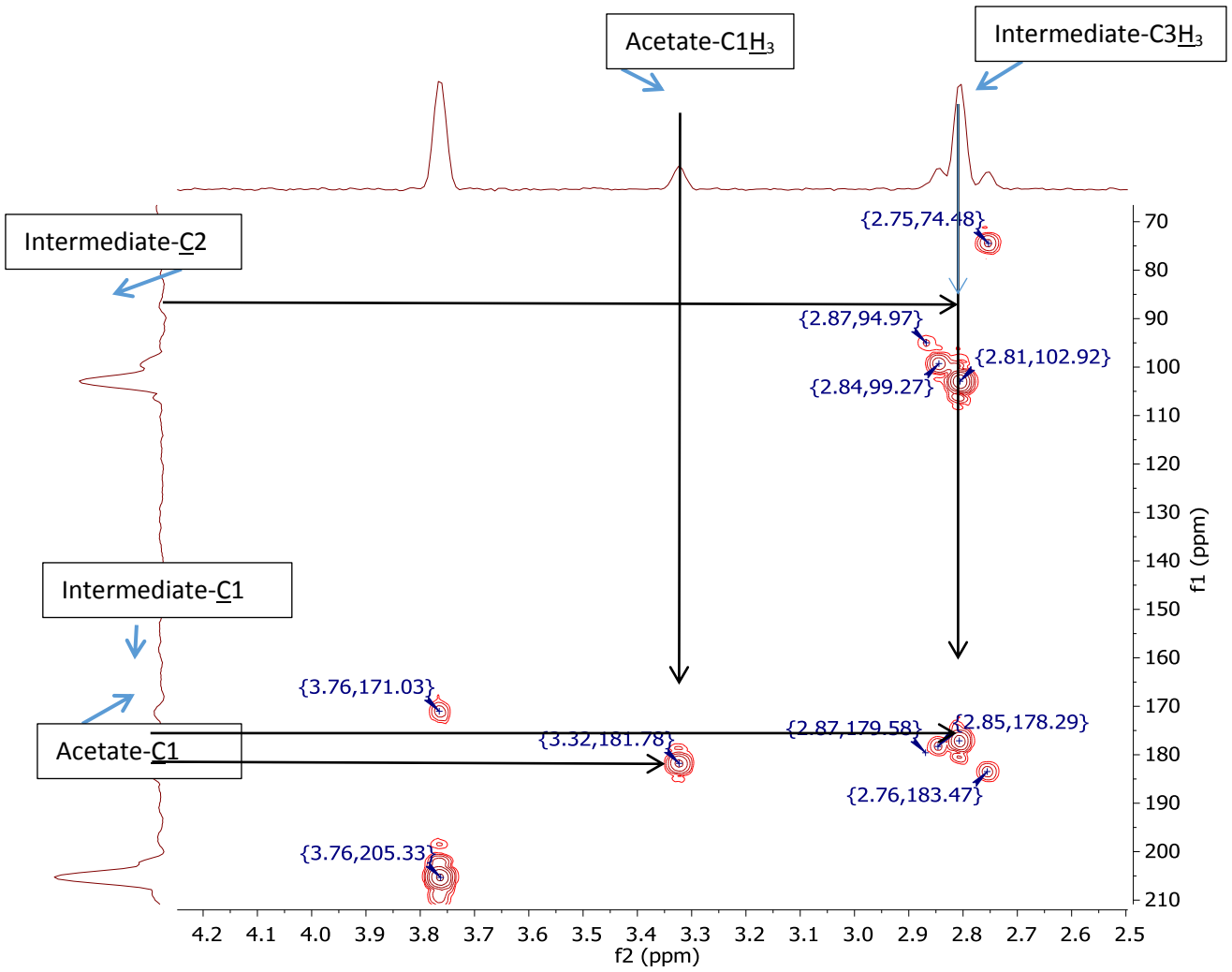

Figure 5: HMBC spectrum of sodium pyruvate in 50% D_2O / 50% d4-MeOD, spectrum recorded after D_2O_2 addition at near neutral pH and -35 ˚C. Frequency 1 (f1) carbon chemical shift in ppm; frequency 2 (f2) hydrogen chemical shift in ppm.

2.3.4 Characterization of the reaction products

The final products of the mechanism shown in **Error! Reference source not found.** observable with ^{13}C-NMR are sodium acetate and CO_2 with the latter being in equilibrium with sodium bicarbonate and sodium methyl carbonate (Chart 1, Figure 10).

Non ^{13}C-enriched CO_2 purged in D_2O yielded one peak in the ^{13}C NMR spectrum at 125 ppm, consistent with the prediction. ^{13}C-enriched sodium bicarbonate in D_2O yielded one peak at 161.7 ppm and in S_0 an additional peak occurred at 162 ppm which was assigned to methyl carbonate.

The assigned chemical shifts of the standards allowed to identify the reaction products. In addition to those standard products the dimer form of sodium pyruvate has been identified with HMBC NMR after the reaction mixture was heated to room temperature again. This indicated that the dimer form is inert against H_2O_2.

2.3.5 DFT calculations and experimental results

DFT calculations take into account the shielding effect on a specific nucleus by the molecule it is attached to. In addition the solvent effect can be calculated. However, the accuracy of the prediction is limited by the NMR instrument and the reaction conditions. Modern NMR instruments do not require Tetramethylsilan (TMS) as an internal standard but rather calibrate the signal to the lock solvent used. For the experiment the lock signal was calibrated to D_2O which can slightly differ from the S_0 signal shift. It was not possible to calibrate the HMBC spectrum to methanol because the one-bond proton-carbon signal of methanol is obscured in an HMBC experiment. The DFT calculations were performed for a neutral environment, under acidic conditions the chemical shifts differ as well.

Table 4 shows the DFT calculated values for the C2 chemical shifts compared with the experimental data and **Table 5** shows the Chemdraw predictions.

Table 4: DFT predicted and experimental ^{13}C2 NMR shifts

Structure	Computed ^{13}C chemical shifts	Experimental ^{13}C chemical shifts
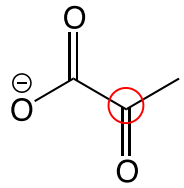	196 ppm	205.3 ppm
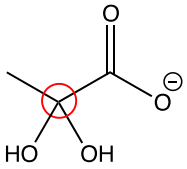	93 ppm	94.5 ppm
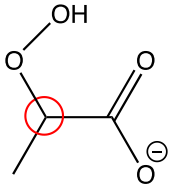	102 ppm	102.9 ppm
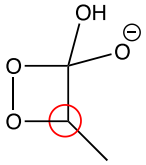	92 ppm	n.o.*
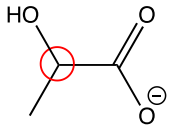	68 ppm	67.3 ppm
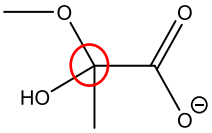	95 ppm	99.3 ppm
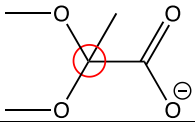	98 ppm	102.2 ppm

n.o. not observed, ^{13}C chemical shifts calculated with DFT and measured in the HMBC spectra

Table 5: Chemdraw predicted and measured ^{13}C chemical shifts of product standards

Position	Acetate	Carbon dioxide	Bicarbonate	Methyl carbonate	Dimer C1	Dimer C2
Measured	181.3 ppm	126.2 ppm	161.7 ppm	162.0 ppm	182.1 ppm	73.4 ppm
Predicted	173.2 ppm	124.2 ppm	166.0 ppm	161.0 ppm	183.0 ppm	78.0 ppm

^{13}C chemical shifts predicted on the basis of Chemdraw and measured in the HMBC or ^{13}C spectra

2.3.6 Exclusion of alternative reaction pathways

The solvents used for the experiments and the product standards were tested for any reactions that may occur in the presence of D_2O_2 which can for example react with acetic acid at acidic conditions (pD < 2) to form peracetic acid.[20] Solvents and standards were incubated over 24 h with D_2O_2 and analyzed both at -30 °C and room temperature but no modification was observed.

2.3.7 Lactic acid

Lactic acid differs from pyruvic acid only at the C2 position where the carbonyl group is replaced by a hydroxyl group. While it is known that lactic acid is inert against H_2O_2

attack at its C2 position[11] this experiment also allowed excluding an attack on the carboxyl group. No changes of the chemical shifts of lactic acid were observed after addition of water, methanol or D_2O_2 to lactic acid. This demonstrated the inertness against the D_2O_2 attack which was also observed for the dimer, hydrate and hemiacetal form of pyruvate.

2.3.8 Changes of the pD* value

The pD* value was tested before and after the reaction occurred, a slight decrease of 0.5 units was observed in all experiments. While pyruvic acid (pKa = 2.2) is a stronger acid than acetic acid (pKa = 4.75) and carbonic acid (pKa = 6.37) this decrease can be explained by the fact that one pyruvic acid molecule yields two new acid molecules (acetic and carbonic acid).

2.4 Kinetics

The 1-D ^{13}C-NMR spectra, an example is shown in **Figure 6**, allowed to integrate the individual peaks for calculation of the kinetics. In this example the signal of sodium pyruvate was recorded in S_0 34 min after addition of D_2O_2 at -35 °C. At this time point all chemical shifts of the species occurring during the reaction are visible in the spectrum.

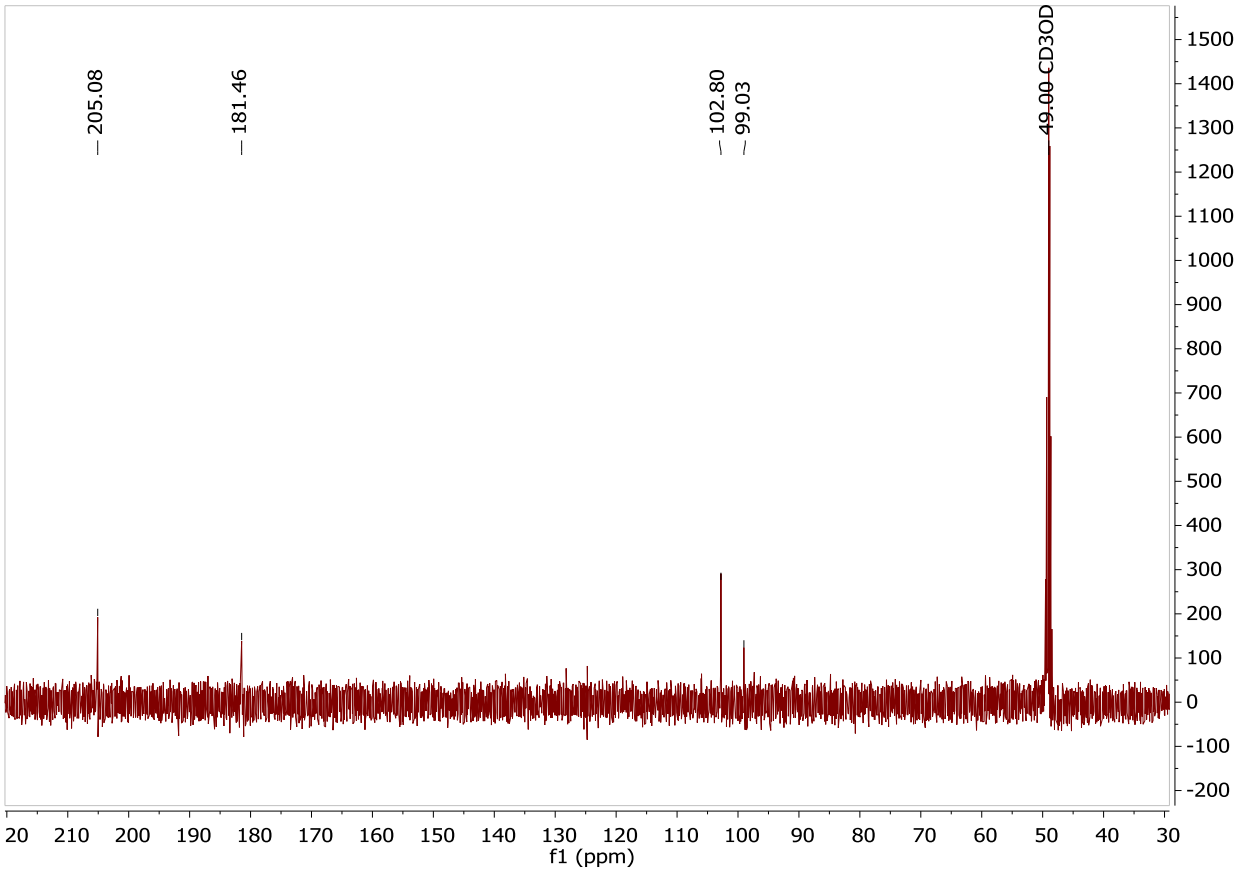

Figure 6: Representative 1-D ^{13}C NMR spectrum of sodium pyruvate in 50% D_2O / 50% d4-MeOD, sample recorded after addition of H_2O_2 at -33.6 °C (pD* = 6,8) after 34 min

The integrated values of the ^{13}C signals were plotted vs. time as shown in **Figure 7** and **Figure 8**.

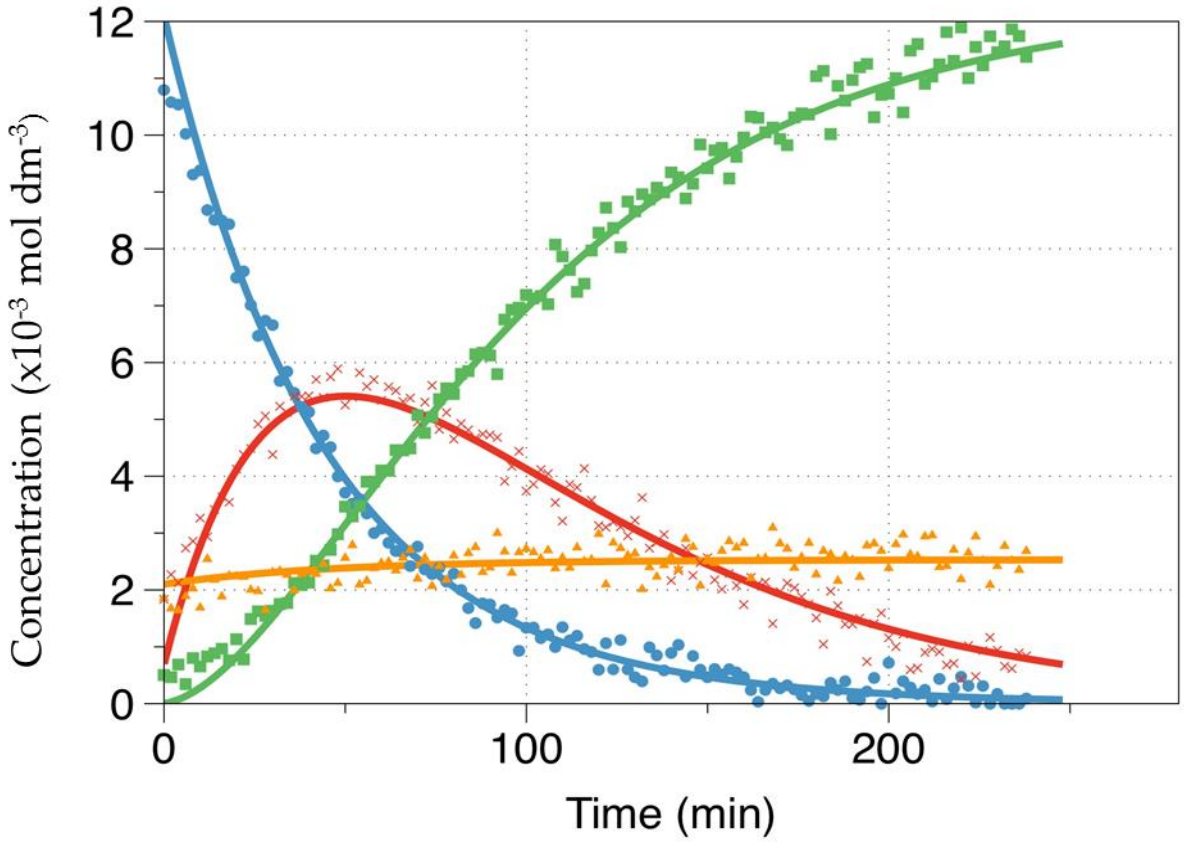

Figure 7: Concentration versus time (i.e., 0 to 280 min) during the reaction of ^{13}C2 enriched pyruvate in S_0 with D_2O_2 at -34.85 °C - Pyruvate (●, blue); acetate (■, green); hemiacetal (▲, orange); intermediate (×, red)

Depending on the starting temperature t=0 the signal of sodium pyruvate and the hemiacetal are present in the spectrum and the intermediate and the product signals occurred when the experiments were performed at higher temperatures than -30 °C. Due to the increased reaction rate which increases with the temperature the reaction had already started before the first spectrum could be recorded. **Figure 8** reveals a maximum of intermediate formation after 2400 s with a concentration of 3.5 mM. While ^{13}C2-enriched sodium pyruvate allowed monitoring of the formation of acetate, ^{13}C1-enriched

sodium pyruvate enabled insights into the CO_2 formation as a product. The calculated curves match quite well with the recorded data points.

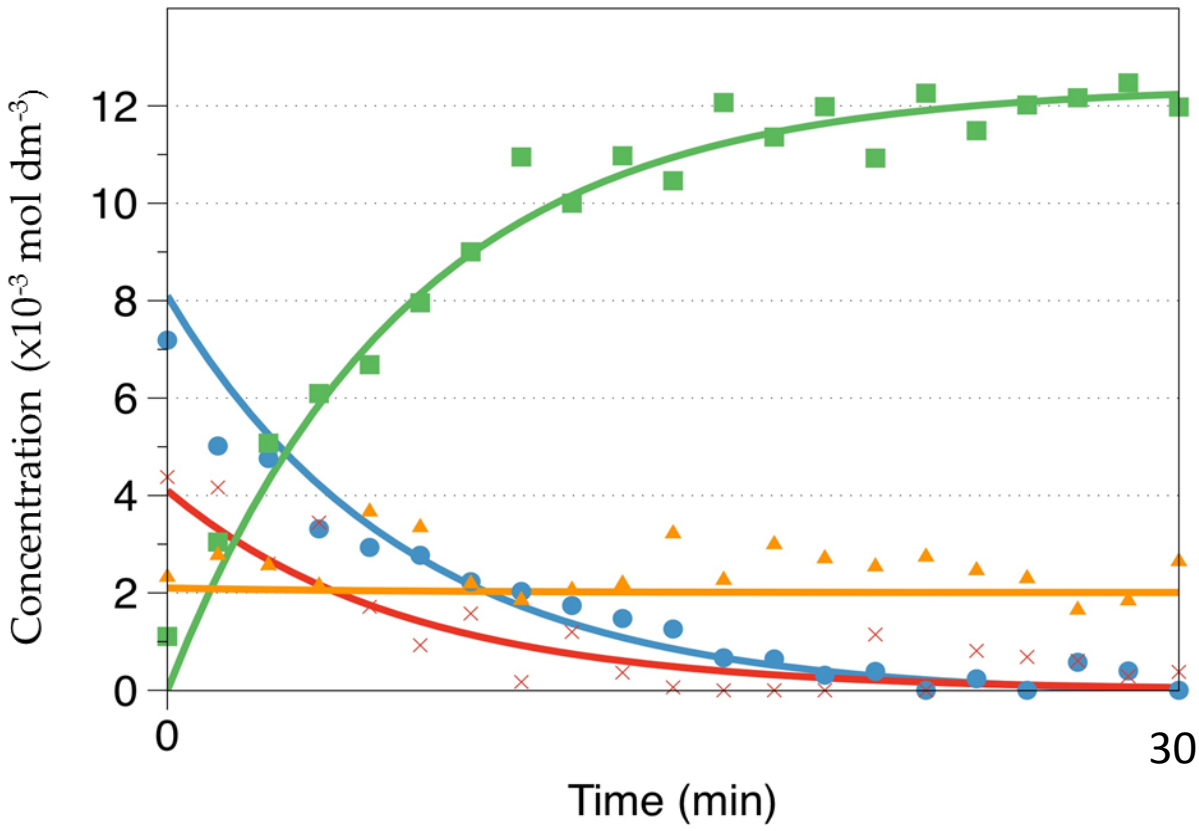

Figure 8: Concentration versus time (i.e., 0 to 30 min) during the reaction of $^{13}C2$ enriched pyruvate in S_0 with D_2O_2 at -13.94 °C - Pyruvate (●, blue); acetate (■, green); hemiacetal (▲, orange); intermediate (×, red)

In **Figure 8** the integrated values for the reaction of $^{13}C1$ enriched pyruvate at a higher temperature – -13.94 °C – are presented. Under these conditions, the intermediate formation is not observed, owing to the fact that the reaction is too fast to be detected.

Within 30 min practically all pyruvate was converted to carbon dioxide except for remaining hemiacetal.

The data shown in **Figure 9** are recorded at -19.18 °C. It infers that the degradation of sodium pyruvate is significantly slower than at -13.94 °C. The intermediate was already formed when the data recording started but only small amounts of the product, less than 0.5 mM, was formed. No significant changes of the hemiacetal concentration are observed during the recorded time.

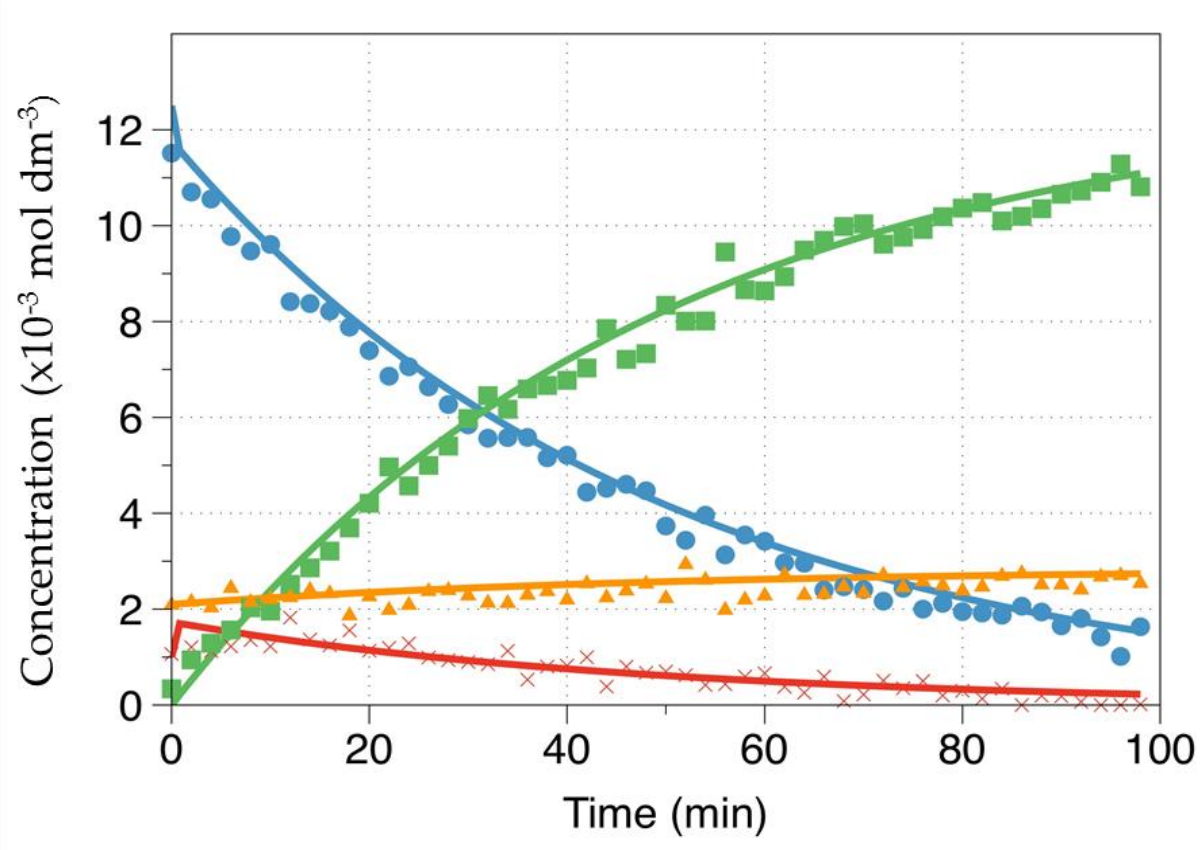

Figure 9: Concentration versus time (i.e., 0 to 30 min) during the reaction of ^{13}C1 enriched pyruvate in S_0 with D_2O_2 at -19.18 °C - Pyruvate (●, blue); CO_2 (■, green); hemiacetal (▲, orange); intermediate (×, red)

The kinetic data shown in **Figure 10** is very scattered. The original sodium pyruvate concentration of 15 mM had already been reduced to 7 mM at the time when the first spectrum was recorded. The intermediate had been formed in amounts of 6 mM and was already breaking with the formation of some product. After 133 min most of the product was formed and the pyruvate and the intermediate were degraded. The hemiacetal concentration remained stable over the recorded time. The calculated curves do not match the measured data points.

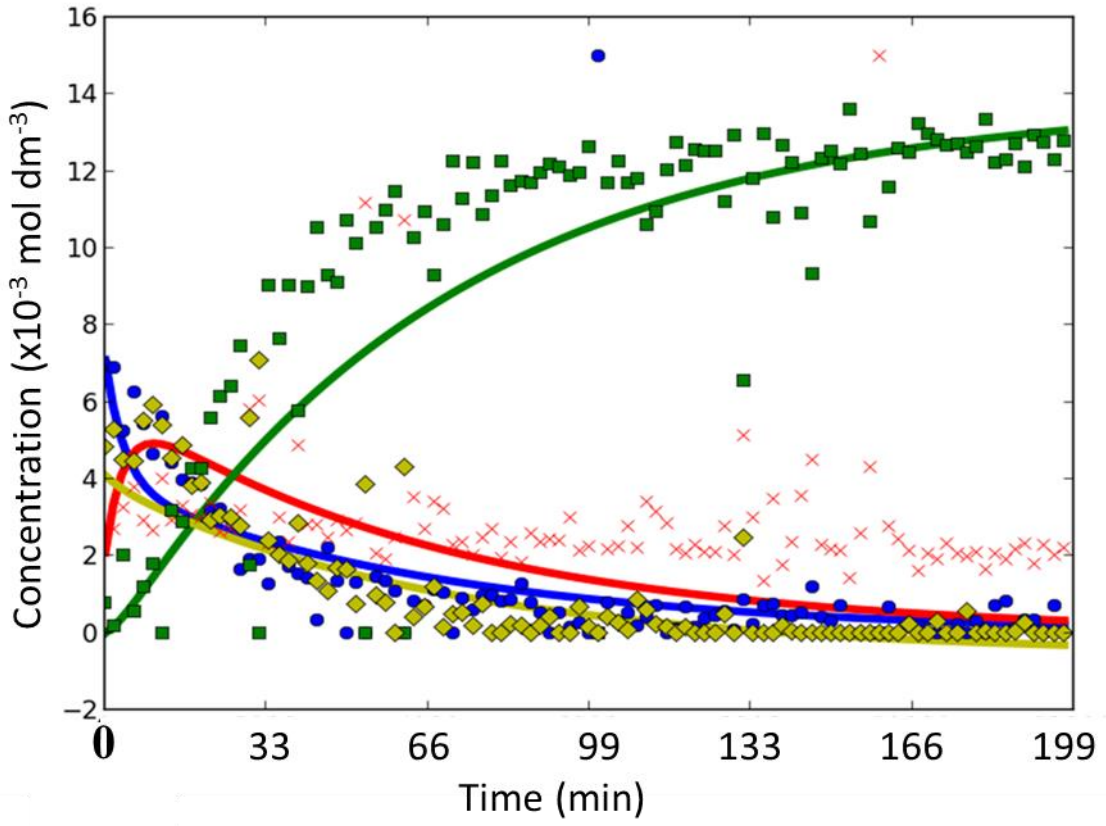

Figure 10: Concentration versus time (i.e., 0 to 200 min) during the reaction of ^{13}C2 enriched pyruvate in S_0 with D_2O_2 at -25.52 °C - Pyruvate (●, blue); acetate (■, green); intermediate (◆, orange); hemiacetal (×, red)

Figure 11 shows the integrated data points recorded at reaction temperature of -28.2 °C. The sodium pyruvate content decreased over 100 min without reaching zero. This sample had the highest temperature among the shown experiments, where the formation of the intermediate had been recorded before the breakdown phase started. Most of the intermediate had been degraded after 100 min but the product had still been

formed. The hemiacetal concentration remained stable during the experiment. The calculated lines match quite well the experimental data.

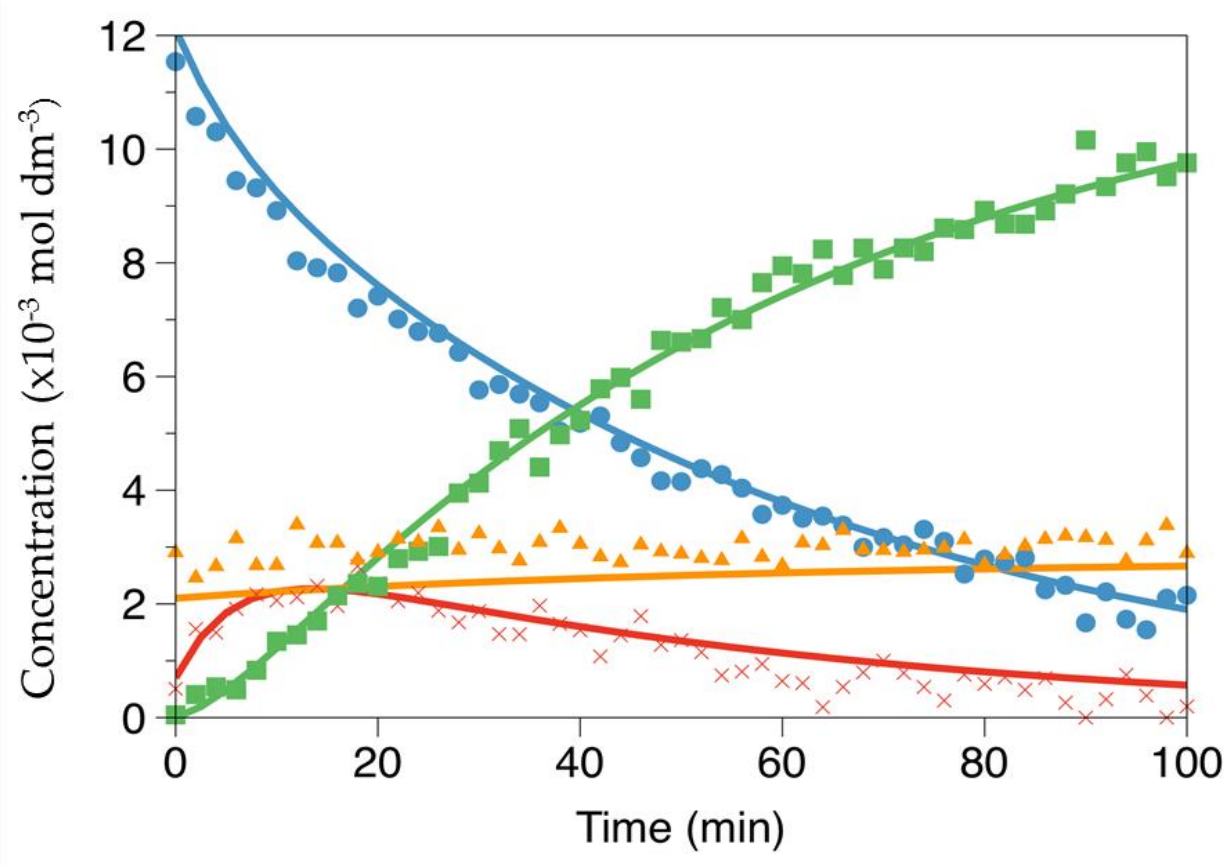

Figure 11: Concentration versus time (i.e., 0 to 100 min) during the reaction of ^{13}C1 enriched pyruvate in S_0 with D_2O_2 at -28.20 °C - Pyruvate (●, blue); CO_2 (■, green); hemiacetal (▲, orange); intermediate (×, red)

Shown in **Figure 12** is the kinetic data recorded at -31.21 °C, over a time period of 240 min. In the beginning, only the signal due to sodium pyruvate and the hemiacetal were discernable in the spectrum. Most of the pyruvate and the intermediate were degraded after 240 min. The hemiacetal concentration did not change over the time. The simulated curves match well with the experimental data points.

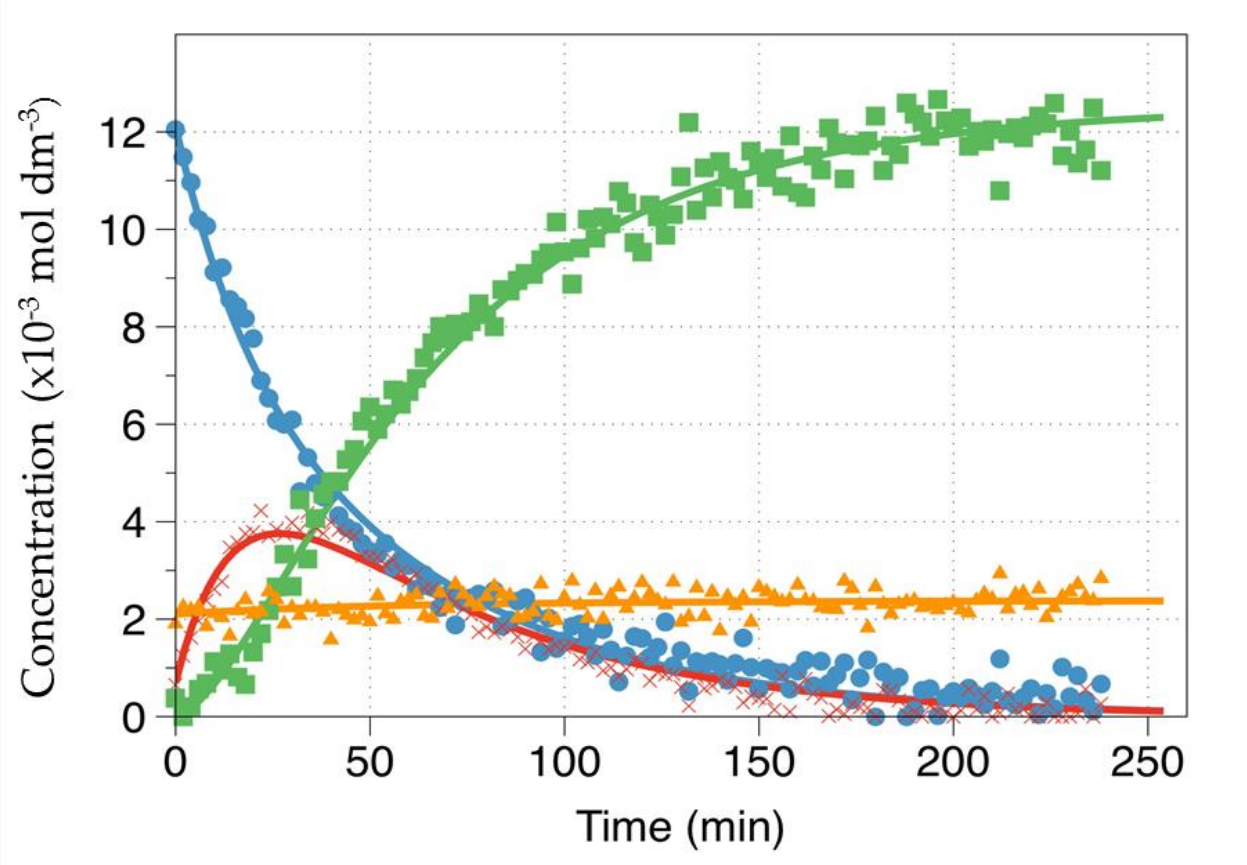

Figure 12: Concentration versus time (i.e., 0 to 240 min) during the reaction of ^{13}C2 enriched pyruvate in S_0 with D_2O_2 at -31.21 °C Signal intensities vs. time during the reaction of ^{13}C2-enriched pyruvate with D_2O_2 in S_0 at -31.21˚C - Pyruvate (●, blue); acetate (■, green); hemiacetal (▲, orange); intermediate (×, red)

The kinetic data recorded at -33.19 °C in **Figure 13** shows the slow formation and breakdown of the intermediate. After 240 min there was still some pyruvate left and the intermediate concentration was around 1 mM. The calculated lines match well with the experimental data.

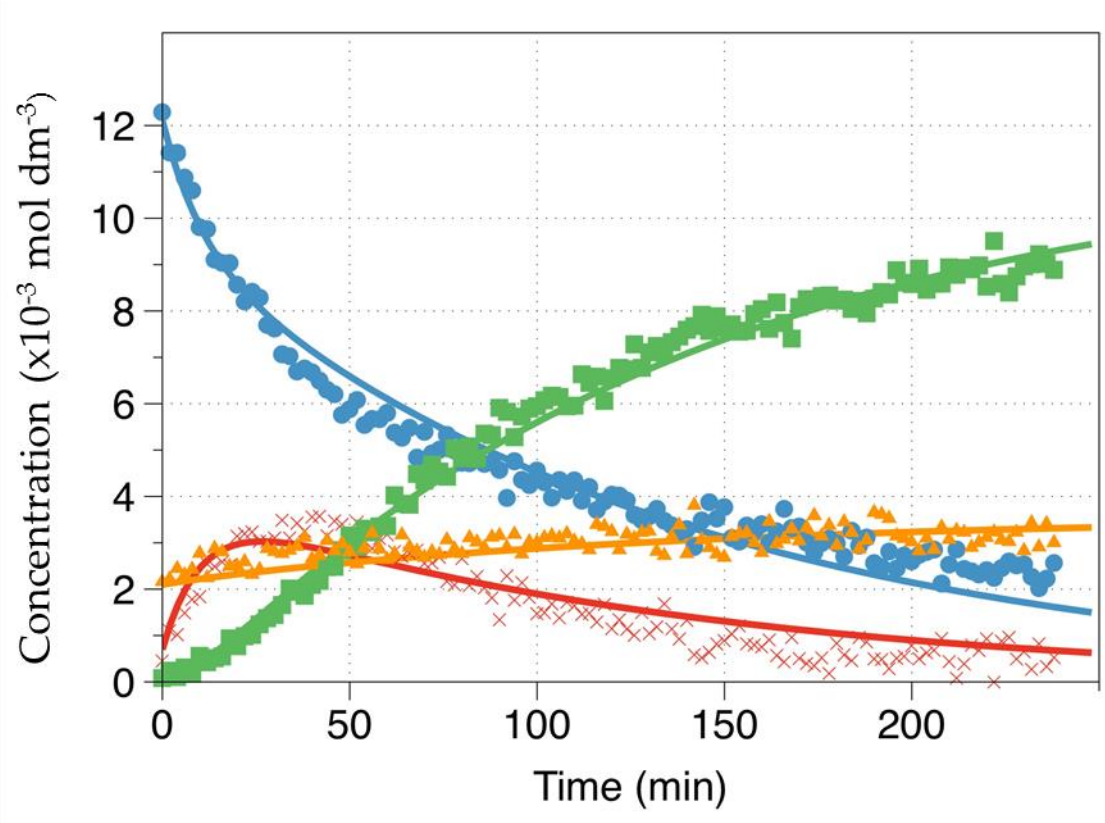

Figure 13: Concentration versus time (i.e., 0 to 240 min) during the reaction of ^{13}C1 enriched pyruvate in S_0 with D_2O_2 at -33.19 °C - Pyruvate (●, blue); CO_2 (■, green); hemiacetal (▲, orange); intermediate (×, red)

The kinetic data in **Figure 14** recorded at -33.64 °C prompt to the fact that already significant amounts of the intermediate were formed before the first spectrum was recorded. When comparing this data set with the other data sets at similar temperatures the sample may have not been cooled properly before injection into the NMR. After addition of H_2O_2 to the sample the solution was not readily homogenized. Right before the mixing process higher concentrations of H_2O_2 can be mixed with sodium pyruvate and the sample can be partially heated if some liquid had moved to the upper part of

the NMR tube, which could not be well cooled before the sample was inserted in the precooled NMR instrument.

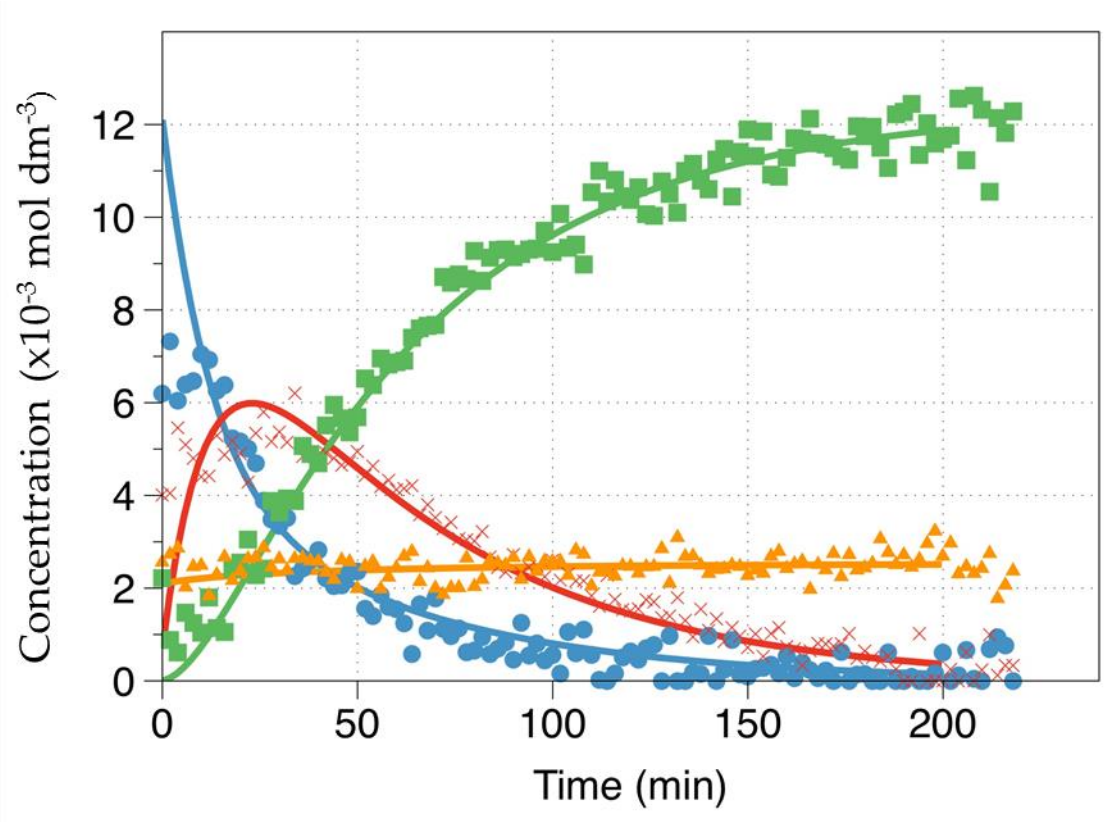

Figure 14: Concentration versus time (i.e., 0 to 240 min) during the reaction of ^{13}C2 enriched pyruvate in S_0 with D_2O_2 at -33.64 °C - Pyruvate (●, blue); acetate (■, green); hemiacetal (▲, orange); intermediate (×, red)

2.4.1 Stability of the hemiacetal

The kinetic data in **Figure 7** shows no visible degradation of the hemiacetal over time at -35 °C. The hemiacetal form of pyruvate is therefore considered as inert against D_2O_2 and neutral conditions. This is likely due to a very slow elimination of CD_3OD from the hemiacetal. After the reaction mixture had been heated to room temperature the hemiacetal form could no longer be detected, see **Figure 15**. This is consistent with the fact that pyruvate and methanol exist in equilibrium with the hemiacetal form. Pyruvate can completely react with D_2O_2 if it is not in a hemiacetal or hydrate form.

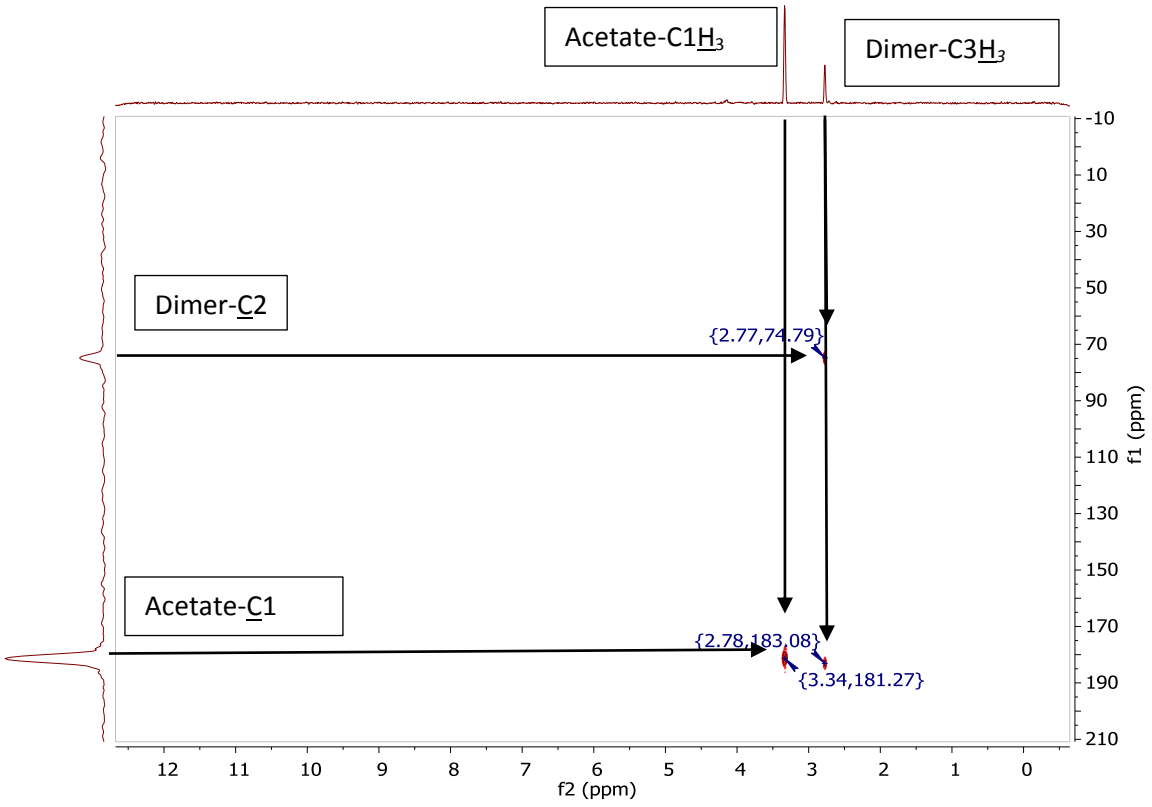

Figure 15: HMBC spectrum after complete reaction of 0.015 dm^3mol^{-1} ^{13}C2-enriched sodium pyruvate with 0.15 dm^3mol^{-1} D_2O_2 at near neutral pH and room temperature in

S_0. Frequency 1 (f1) carbon chemical shift in ppm; frequency 2 (f2) hydrogen chemical shift in ppm

2.4.2 Fitting of the kinetic data

Shown in **Scheme 2** is the proposed reaction pathway from which the rate constants k1 to k5 have been derived. The reaction scheme includes the equilibria of sodium pyruvate with d4-methanol and the hemiacetal as well as D_2O_2, the intermediate and the final products. The reaction scheme does not include the hydrate and dimer form of pyruvate because these species have not been detected at integrable levels during the kinetic experiments. The full acetal form was not observed under neutral conditions and was not included in the calculations. Although CO_2, bicarbonate and methyl carbonate are in equilibrium as well, their reaction mechanism was not relevant for the investigation of the intermediate and therefore the sum of the three integrals obtained from ^{13}C1-enriched sodium pyruvate was treated as one product integral in the same way as acetate observed from ^{13}C2-enriched sodium pyruvate.

The kinetic data were fit with first order kinetics. Both the hemiacetal and the intermediate were formed in a solution were d4-methanol and D_2O_2 were present in excess to allow observation of pseudo first-order kinetics. In order to convert the pseudo first-order into second order rate constants, the respective calculated values have been divided by [D_2O_2] = 0.15 M. The rate constants calculated for the reactions at different

temperatures are shown in **Table 6**. Significant variability of k1 and k2 was observed for lower (≤ -33 °C) and higher (≥ -19.18 °C) temperatures. With higher temperatures the intermediate was increasingly faster formed and a fraction of the intermediate was already formed before the observation started. This lead to variations of the k1 and k2 values. The values for k3, however, show a clearer increasing trend with increasing temperature.

Table 6: Compilation of rate constants for the reaction of pyruvate with D_2O_2 in S_0 with ^{13}C1 and ^{13}C2 enriched pyruvate. The values for k were obtained by kinetic fitting as described in the experimental section. Calculated values below 10^{-9} were not considered by the program because they were too low to be significant.

Temp °C	k_1 [$dm^3 \times mol^{-1} s^{-1}$]	k_2 [s^{-1}]	k_3 [s^{-1}]	k_4 [$dm^3 \times mol^{-1} s^{-1}$]	k_5 [s^{-1}]
-13.94[a]	1.34×10^{-2}	$<2.92 \times 10^{-9}$	4.99×10^{-3}	3.50×10^{-7}	7.23×10^{-5}
-19.18[a]	2.45×10^{-3}	$<1.00 \times 10^{-9}$	2.87×10^{-3}	9.06×10^{-8}	$< 1.00 \times 10^{-9}$
-25.52[b]	1.87×10^{-2}	1.46×10^{-3}	5.82×10^{-4}	$< 1.00 \times 10^{-9}$	$< 1.00 \times 10^{-9}$
-28.20[a]	4.33×10^{-3}	3.44×10^{-4}	7.66×10^{-4}	2.29×10^{-7}	$< 1.00 \times 10^{-9}$
-31.21[b]	3.30×10^{-3}	2.39×10^{-4}	5.81×10^{-4}	5.40×10^{-8}	$< 1.00 \times 10^{-9}$
-33.19[a]	3.13×10^{-3}	8.67×10^{-4}	3.77×10^{-4}	1.22×10^{-7}	$< 1.00 \times 10^{-9}$

-33.64[b]	6.48×10^{-3}	2.81×10^{-4}	3.92×10^{-4}	1.33×10^{-7}	$< 1.00 \times 10^{-9}$
-34.85[a]	2.43×10^{-3}	6.87×10^{-6}	2.58×10^{-4}	8.77×10^{-8}	$< 1.00 \times 10^{-9}$

[a]C1 pyruvate data [b]C2 pyruvate data

At temperatures above -20 °C the values of k2 became insignificantly small and the back reaction to form pyruvate was negligible. The breakdown of the intermediate is defined by the rate constant k3, which is of first order.

For the formation of the hemiacetal the observed rate constant $k4_{obs}$ was calculated by dividing the d4-methanol concentration in S_0 (12.3 M) in order to calculate the second order rate constant. The hemiacetal breakdown followed first order rate constant k5. Those values were below the reasonable minimum value for the calculations for temperatures below -14 °C. This lead to the conclusion that the hemiacetal structure is apparently inert towards the nucleophilic attack of D_2O_2 under the experimental conditions.

Equation 7 was used to calculate the entropy and enthalpy of the transition state (TS) for the reaction **Scheme 2**.

Equation 7

$$ln\frac{kh}{\kappa k_B T} = \frac{-\Delta H^{\ddagger}}{R} \times \frac{1}{T} + \frac{\Delta S^{\ddagger}}{R}$$

In order to draw a line, $ln\frac{kh}{\kappa k_B T}$ was plotted vs. 1/T (**Figure 16**) with the rate constants given in **Table 6**, $h = 6.62697 \times 10^{-34} J \times s$, $\kappa = 1$, $k_B = 1.3807 \times 10^{-23} \frac{J}{K}$, $R =$

1.987 $cal/(K \times mol)$, T = measured temperature in K. The entropy of the TS $\Delta S^{\ddagger}$ was calculated by multiplying the negative slope of the line shown in **Figure 16** with R and the enthalpy $\Delta H^{\ddagger}$ of the TS was calculated by multiplying the intercept value with R. The data is summarized in **Table 7**.

Table 7: Entropy, enthalpy and Gibbs free energy of activation for k_1 and k_3

Parameter	k_1	k_3
Slope	-4686.0	-8000.3
Intercept	-15.56	-3.83
$\Delta H^{\ddagger}$ [kJ/mol]	38.96	66.51
$\Delta S^{\ddagger}$ [J/mol*K]	-129.34	-31.84
$\Delta G^{\ddagger}$ at 298 K (kJ/mol)	77.51	76.00

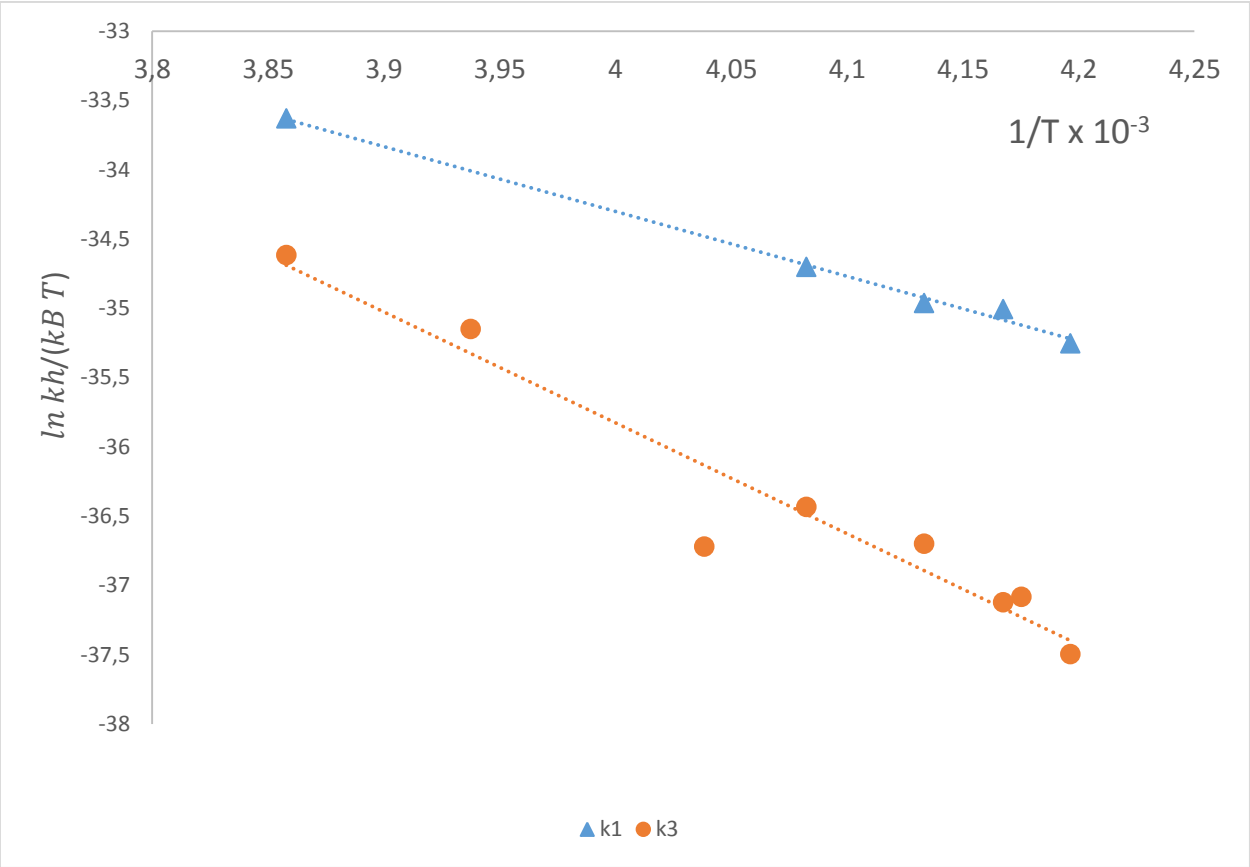

Figure 16: Eyring plot of the dependence of k_1 (▲, blue) and k_3 (●, red) on temperature

Eyring plot of the dependence of k_1 (▲, blue) and k_3 (●, red) on temperature. Linear regression was performed in Microsoft Excel® and k values that had a p-value above 0.05 were not considered. This lead to the rejection of the k_1 values at temperatures -19.18, -25.52 and -33.64 ˚C, because the p-value exceeded 0.05. For k_3 no values were rejected.

2.4.3 Exclusion of dioxetane formation

As an additional pathway the formation of a second intermediate, a dioxetane structure as shown in Chart 1, Structure 11, generated through the reaction of sodium pyruvate with D_2O_2, had been proposed. For this dioxetane structure a significant change of the $^{13}C1$ chemical shift was expected to occur due to covalent bonding of an additional oxygen. The recorded HMBC spectra however showed no additional signals for the $^{13}C1$ chemical shifts. The proposed additional pathway would yield sodium bicarbonate instead of CO_2 as a product. Even though both exist in equilibrium experiments with sodium bicarbonate standard indicated that under the experimental conditions applied the bicarbonate form is stable and does not yield relevant amounts of CO_2.

2.5 Discussion

2.5.1 Characterization of the intermediate

The reaction pathway shown in **Scheme 1** has been proposed earlier.[2] So far no spectroscopic data was available about the direct observation of the intermediate. The observation with low temperature NMR spectroscopy allowed to assign a structure to the proposed intermediate (Chart 1, Structure 12) based on the chemical shifts observed in the HMBC **Figure 5** spectrum. Of particular interest for the structural elucidation of the intermediate were the $^{13}C2$ chemical shifts observed in the HMBC spectra. Here the most significant changes of the chemical shifts were expected due to the formation of

new bonds. Major changes to the $^{13}C1$ chemical shifts were observed after the breakdown of the intermediate when the carboxyl group had been converted to CO_2.

The comparison of the experimental data and the DFT calculations presented in **Table 4** show that the DFT calculations are appropriate to predict and assign the chemical shifts to the respective structures. The predicted values differed less than 4 ppm from the experimental values.

Chemical shifts in an NMR spectrum correlate with the shielding effect from the electron density provided by the substituents attached to the carbon. The shielding effect was expected to increase and move the chemical shift upfield in the order hydrate (-OD group), hemiacetal (-OMe group) and intermediate (-OOD group) which is consistent with the experimental data.

The experimental data allow to assign the newly observed chemical shifts to the proposed structure of 2-deuteroperoxy-2-deuteroxypropanoate.

2.5.2 Formation of the intermediate by deuterium peroxide and pyruvate

The formation of the intermediate 2-deuteroperoxy-2-deuteroxypropanoate is the first step of the reaction between D_2O_2 and sodium pyruvate as proposed before.[2,4,21] The first step of this reaction is reversible similar to the formation of the hydrate or the hemiacetal form.[9]

With a very low value (-129.34 J / (mol x K) for the entropy of activation to form the intermediate it is clear that this is a highly ordered system. As shown in **Error! Reference source not found.** the attack of D_2O_2 occurs at the back site of carbonyl simultaneously with the addition of a deuterium to form a deuteroxyl group.

2.5.3 Breakdown mechanism

In reaction **Scheme 1** the breakdown mechanism of the intermediate is shown. This can be considered as one concerted step. The decarboxylation of the carboxyl group shows similarities to the enzymatic decarboxylation of pyruvate by pyruvate dehydrogenase yielding AcetylCoA or by pyruvate decarboxylase yielding acetaldehyde.[22] During the enzymatic degradation of pyruvate a nucleophilic attack occurs at the C2 position through 4-amino-C2-carbanion thiamin pyrophosphate (TTP) and forms an intermediate 4-imino-2-(2-hydroxypropionyl)-TTP.[22] During the decarboxylation step the negative charge from the carboxylate group is transferred to the C2 position of pyruvate by breaking the C2-C1 electron bond which results in the release of CO_2 and formation of acetate. In the enzymatic pathway a new carbon-carbon double bond is formed while the peroxide pathway will yield a carbon-oxygen double bond which further results in the formation of acetic acid after dehydration.

The high enthalpy of activation ($\Delta H^{\ddagger}$) for the breakdown of 66.57 kJ / mol can be attributed to the breaking of several covalent bonds during the second step of the reaction scheme. The entropy of activation for this step is -31.84 J / (mol x K) and

indicates that several product molecules are formed out of one substrate molecule, being acetate, CO_2 and D_2O.

2.6 Additional Experiments

2.6.1 Other solvents tested

The solvent used for the NMR experiments needed to fulfill several requirements: It was required dissolve sodium pyruvate, it had to be inert against all substrates and products, it had to be available as deuterated substance, its freezing point had to be below -40 °C, and it needed to remain of low viscosity.

As no pure solvent was available which fulfilled all the aforementioned requirements, a methanol/water mixture was used. Other solvents tested were tetrahydrofuran, dimethylsulfoxide, ethanol, ethylene glycol and isopropanol. The experiments showed that these solvents, mixed with water, had very high melting temperatures. When the samples were cooled to desired low temperatures for the observation of the reaction kinetics, the NMR could not lock to deuterium signal of the solvent.

2.6.2 Experiment below and above pH 7

An additional sample of sodium pyruvate was run at pD* = 4.5 at ca. -35 °C. The protocol as described in the methods section 2.2.4 was applied for the experiment. The integrated data are shown in **Figure 17**.

The breakdown of pyruvate was slower than at neutral pD*. For the first 500 min no acetate was formed. In fact, the concentration of hemiacetal was increasing significantly with only a minor formation of the intermediate. As soon as the formation of hemiacetal was reaching a plateau, the acetate was formed and the concentration of the intermediate appeared to remain stable.

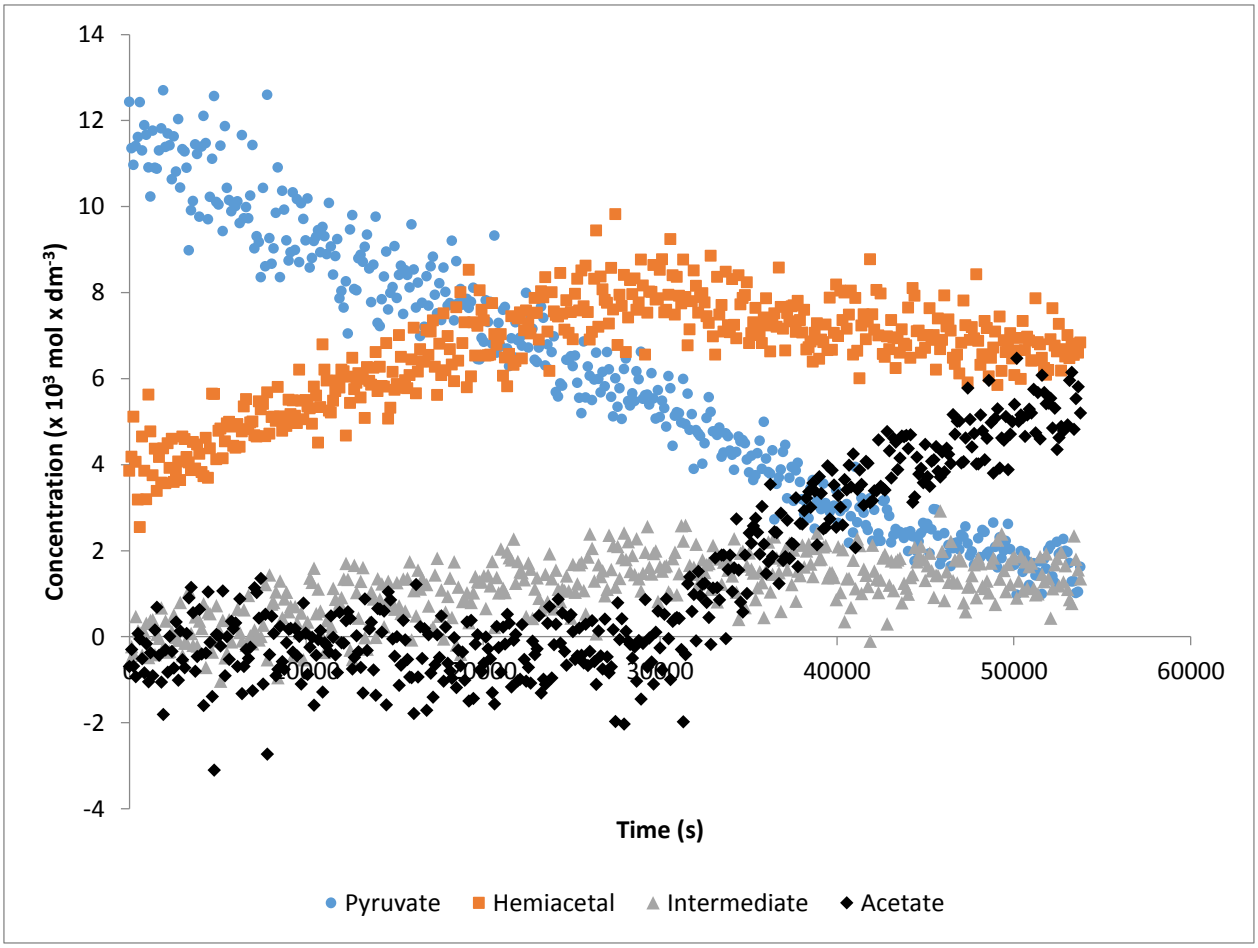

Figure 17: Concentration versus time (i.e., 0 to 900 min) during the reaction of $^{13}C2$ enriched pyruvate in S_0 with D_2O_2 at -35 °C, pD* = 4.5

In **Figure 18** the ^{13}C-NMR data of ^{13}C2 enriched sodium pyruvate recorded at pD* = 10.7 at ca. -35 °C is shown. Initially, no pyruvate was detected. In fact, only the signals of acetate, the hemiacetal, and the intermediate were visible in the spectrum. A maximal intermediate concentration was already formed when the NMR measurement started and the product, sodium acetate, was already formed and increased over the time of the observation. The hemiacetal concentration remained steady over the first 5.5 h and then slowly increased. At the same time it appeared that the sodium acetate concentration was slower increasing, indicating that the remaining sodium pyruvate was reacting with methanol in the solvent rather than with H_2O_2.

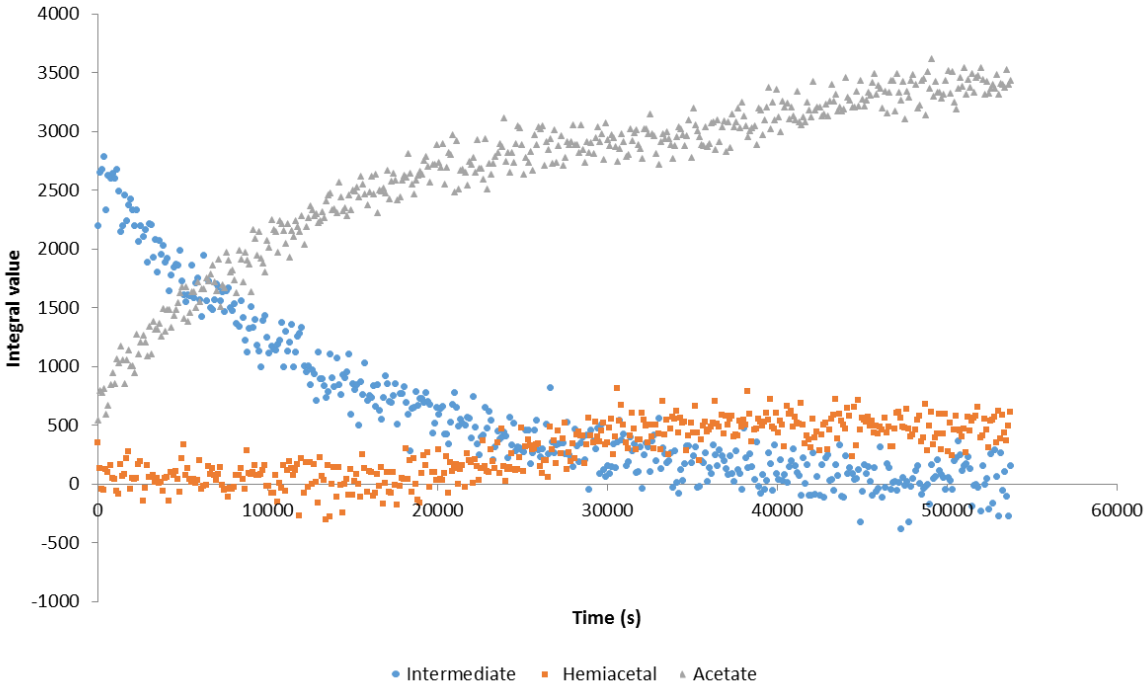

Figure 18: Concentration versus time (i.e., 0 to 900 min) during the reaction of ^{13}C2 enriched pyruvate in S_0 with D_2O_2 at -35 °C, pD* = 10.7

2.6.3 Testing the preset temperature over an extended time frame

As mentioned before, the measurement of the exact temperature was important for the kinetic experiments. Therefore a test was performed if the system could keep a constant temperature over time. The signal of a mixture of 4% methanol-d4 with 96% methanol (protonated) was recorded over 14 h at a preset temperature. **Figure 19** shows the results.

The temperature of the NMR was set to -15 °C. Every 30 min the NMR spectrum was recorded and the exact temperature was calculated with **Equation 1**. The graph shows that the temperature was stable over the time frame with only minor variations of 1 K or

less. The scattering of the integrated points from the kinetic measurement were actually more significant than the temperature fluctuations.

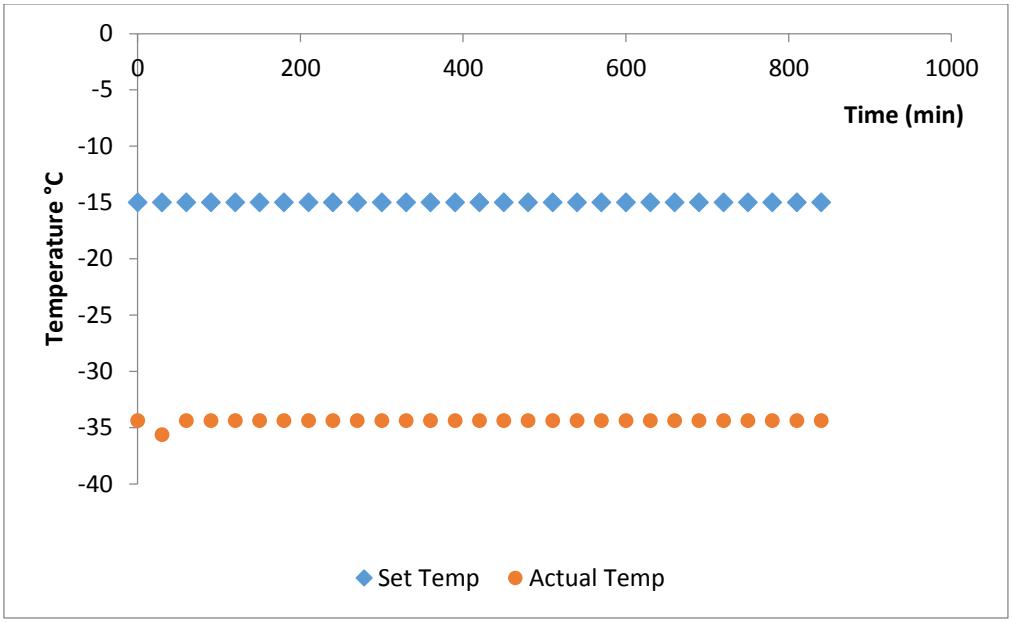

Figure 19: Temperature measurement over an extended time frame calculated from the ^{1}H-NMR data of 4:96 d4-Methanol:h4-methanol solution

2.6.4 Variation of the temperature

For establishing the observation protocols, the spectrum of a sample containing ^{13}C2 enriched sodium pyruvate in S_0 was monitored over time after addition of H_2O_2. Shown in **Figure 20** are the integral values as a function of time with temperatures, which were increased in 5 K intervals every 15 min. This experiment allowed to initially test the optimal temperature for observing the formation and breakdown of the intermediate. Based on the predicted pathway and the experimental conditions it was expected to see the breakdown of pyruvate following (pseudo) first order kinetics. In this graph one can

also follow the degradation of the hemiacetal with increasing temperature. It appears that the conversion from hemiacetal to pyruvate occurs rather slowly compared to the formation of the intermediate from sodium pyruvate as no increase of the pyruvate concentration was detected during the decrease of the hemiacetal concentration.

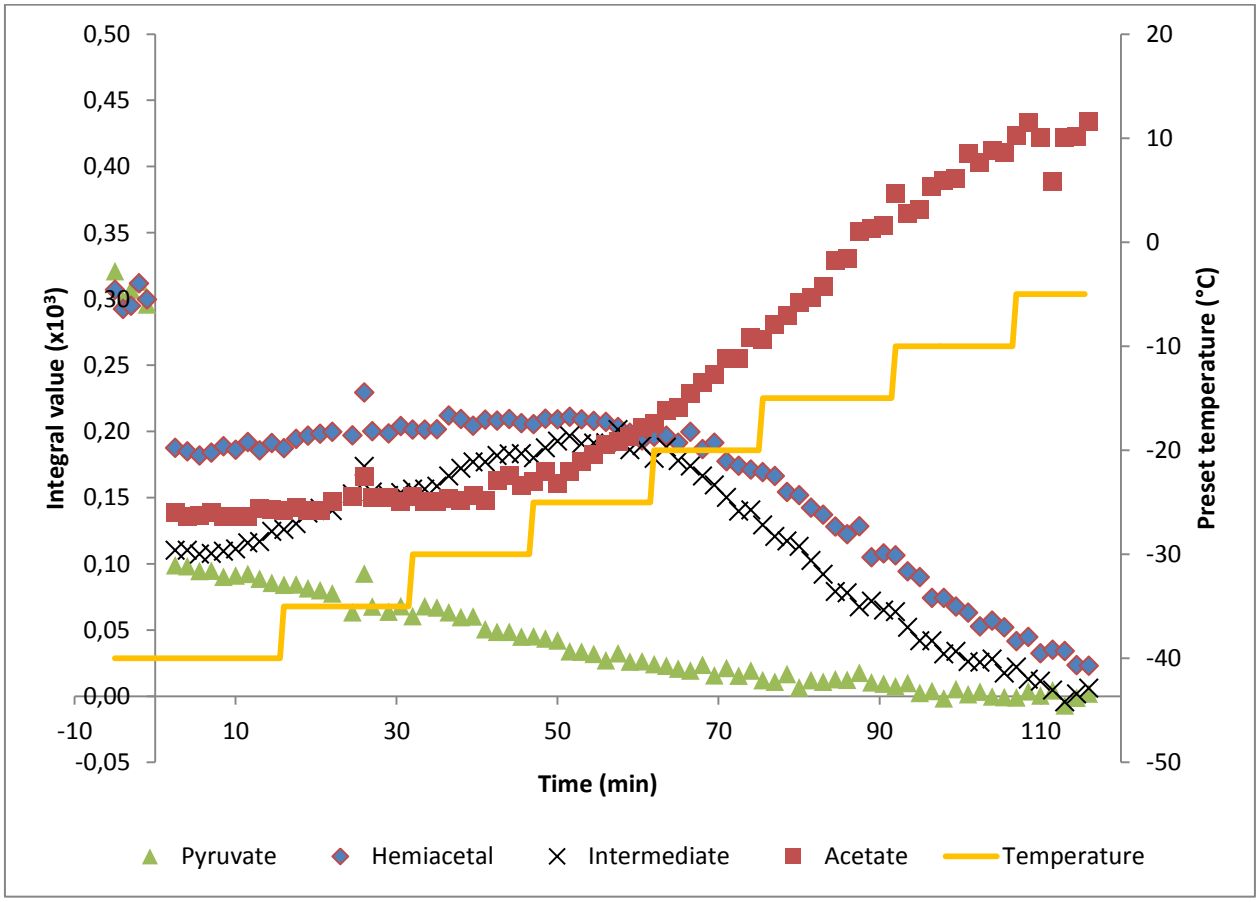

Figure 20: Concentration versus time (i.e., 0 to 120 min) during the reaction of $^{13}C2$ enriched pyruvate in S_0 with D_2O_2 at neutral pD*. The temperature was increased in 5 K intervals every 15 min.

2.6.5 Increased hydrogen peroxide concentration

Figure 21 shows an experiment that included a 30-fold excess of D_2O_2 in comparison to the 10-fold excess used in the other experiments. No degradation of the hemiacetal was observed under these conditions as well.

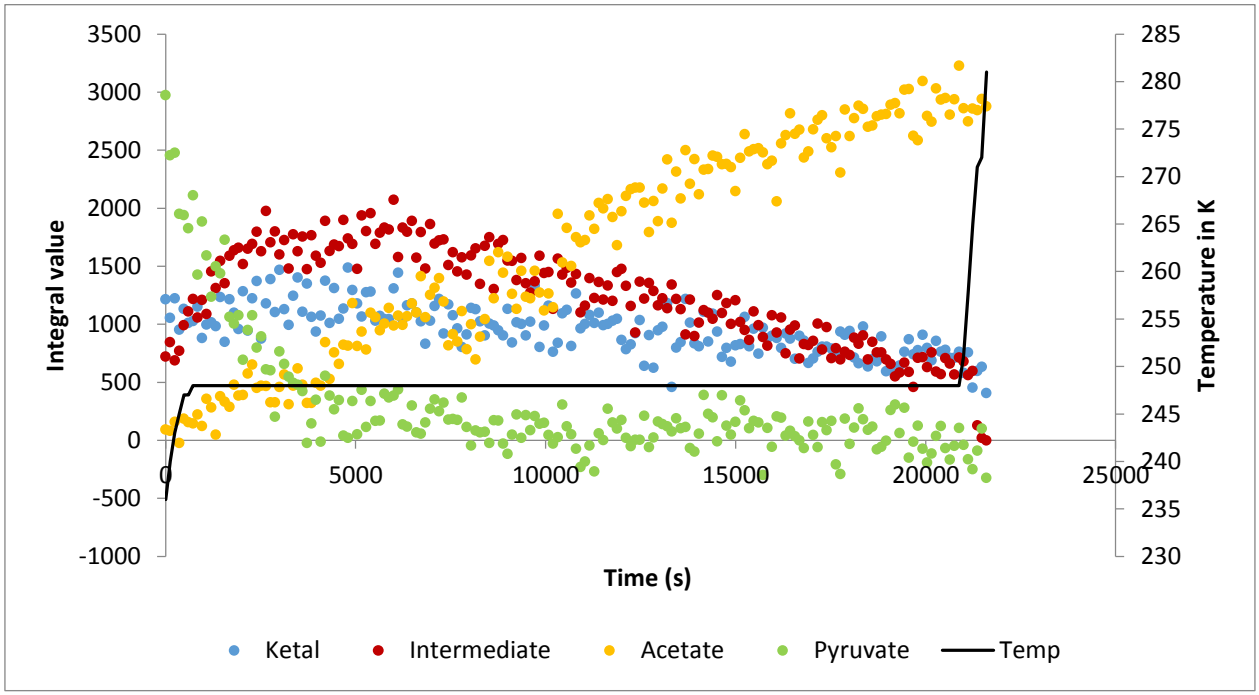

Figure 21: Concentration versus time (i.e., 0 to 360 min) during the reaction of $^{13}C2$ enriched pyruvate in S_0 with 30 fold excess of D_2O_2 at -25 °C.

2.7 Experiments performed that did not give further insight into the elucidation of the reaction mechanism

2.7.1 Temperature measurement with the internal probe

The temperature set on the NMR probe can differ from the actual sample temperature. The first experiments were run based on the temperature shown by the internal probe. Although the temperature was stable over the time course of the experiment the exact temperature was unknown, making the experiments not reproducible. Several kinetic curves were drawn that looked similar to the curves presented in the kinetics section 2.4. However, those were not suitable for exact calculations.

Even if the probe is calibrated it is advised to make an additional temperature measurement if the exact temperature is crucial. The method of choice for temperature calculation was using a solution of 4% deuterated methanol and 96% protonated methanol, which can be used for various temperature ranges. The recommended equations for the calculation of the exact temperatures are shown in **Figure 22**:

Source: Bruker Instruments, Inc. VT-Calibration Manual
4% Methanol in Methanol-d4:
180-300K, T = (3.86 - Δ)/0.00782 (approximate)

for more accurate values, use the following, depending on T:
180-230K, T = (3.72 - Δ)/0.007143
230-270K, T = (3.92 -Δ)/0.008
270-300K, T = (4.109 - Δ)/0.008708

(Δ is the shift difference (ppm) between the CH_3 and OH peaks)

Figure 22: Calculation formulas to measure the temperatures with 4% deuterated methanol (source: Bruker Inc. manual)

The temperature can also be measured with a 100% protonated solvent. Due to its high concentration only one free induction decay (FID), i.e. one scan, is required and the sample cannot be locked because no deuterium is available. **Figure 23** shows a sample spectrum of unlocked MeOH for temperature measurement.

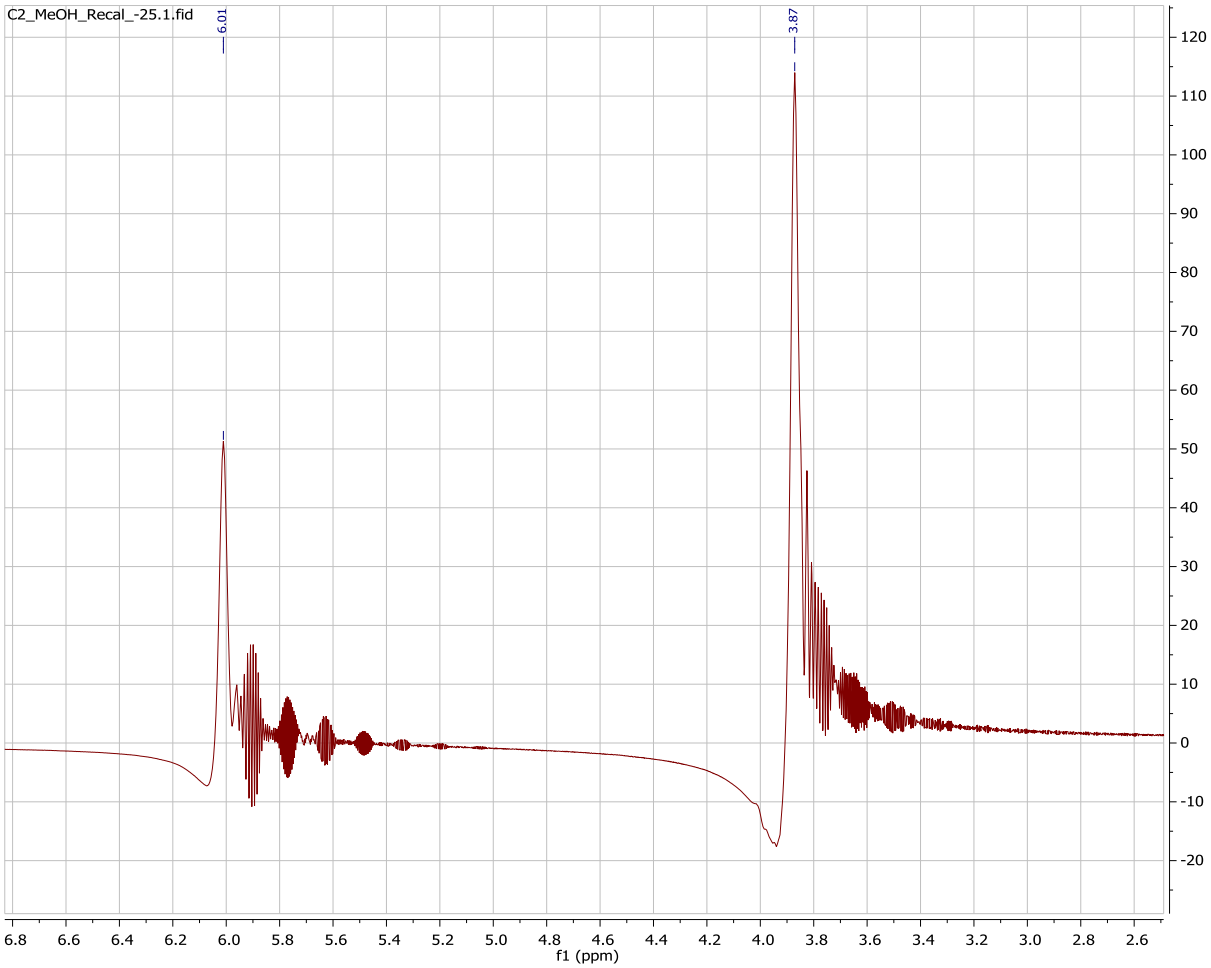

Figure 23 – Spectrum of unlocked protonated methanol. ^{1}H-NMR spectrum recorded of protonated methanol with one FID (scan) at room temperature.

For pure MeOH **Equation 8** has been used:

Equation 8

$T = -23.832\Delta^2 - 29{,}46\Delta + 403.0$

With Δ = the difference between the $C\underline{H}_3$ and the $O\underline{H}$ chemical shifts in ppm

It is also possible to use 99.8:0.2 deuterated:protonated methanol which is the commercially available solvent. Here the signal of the deuterium is recorded. The temperature can be calculated according to **Equation 9**.[13] However, deuterium has a spin of 1 and will yield broader peaks than hydrogen.[23]

Equation 9

$$T = -16.7467 \times (\Delta\delta)^2 - 52.5130 \times \Delta\delta + 419.1381$$

2.7.2 NMR protocol for ^{13}C-enriched samples

The standard experimental protocols that are preset for ^{13}C NMR experiments are optimized for 10-50 mM organic compounds in $CDCl_3$ with the natural 1.1% ^{13}C content. For the initial experiments with ^{13}C enriched sodium pyruvate the number of FID (scans) was reduced from 1024 to 32 scans. Although it allowed for structural observation, this method was not suitable for the integration of the data, because it does not provide a sufficient relaxation time for the nuclei after the FID. This time is required to avoid oversaturation of the sample signal over time, which will lead to decreasing signal intensity of the same observed sample.

2.7.3 Internal standards

An internal standard, which does not interact with the observed reactants, can be used to create a calibration line and to convert the signal intensity to the sample

concentration. For every NMR experiment, the receiver gain is adjusted to the deuterium signal of the solvent. The value is set automatically and differs with each experiments leading to different signal intensities for each recorded spectrum. In other words, the integrated values from the same sample can be different for two separate experiments. However, the relative integral values within the spectrum remain the same. It was intended to use ^{13}C enriched sodium acetate standard for the $^{13}C1$ sodium pyruvate experiment. The $^{13}C1$ sodium pyruvate sample would yield observable amounts of ^{13}C CO_2 and sodium bicarbonate but no significant amounts of ^{13}C sodium acetate. The $^{13}C2$ sodium pyruvate experiments yield sodium acetate as observable product. Under the experimental conditions the non-enriched products, e.g. acetate from $^{13}C1$ enriched sodium pyruvate, have a natural ^{13}C abundance of only 1.1%. That means the amount of observable internal standard increases about 1% over the time of the experiments if equimolar amounts of pyruvate and internal standard are used.

The breakdown mechanism from intermediate to product is not reversible and it is therefore unlikely that the presence of the product standard has a significant influence on the reaction rate or equilibrium.

The data scattering observed during the experiments was not significantly reduced by the use of an internal standard for the calculation of the relative concentrations.

2.7.4 Solubility of sodium pyruvate in pure solvents

The ^{13}C-NMR observation regarding the kinetics of the reaction mechanism of sodium pyruvate with H_2O_2 rendered impossible at temperatures above -5 °C due to the very fast reaction rate. As far as the observation of the ^{13}C NMR signal due the formation of the intermediate in pure D_2O is concerned, this proofed to be impossible at temperatures above the freezing point of D_2O. Pure solutions of alcohols and tetrahydrofuran (THF) as replacements for D_2O were tested. Solubility tests were performed with non-enriched sodium pyruvate in protonated solvents. Sodium pyruvate was, however, insoluble at the desired concentration of 15 mM in pure methanol, ethanol, tetrahydrofuran (THF) or isopropanol. Therefore, sodium pyruvate was first dissolved in water and then methanol was added to create S_0. Besides the high freezing point of a THF/water mixture the deuterated solution turned cloudy when THF was added. This was not observed with the protonated solvent mixture.

2.7.5 Solvents used for low temperature experiments

Tetrahydrofurane does not form a hemiacetal since it is not a protic solvent. Therefore it was considered as a substitute for methanol. The melting temperature of a water/tetrahydrofurane mixture is -10 °C with only 10% water content.[24] This mixture was therefore not suitable for low temperature NMR observation. Other solvents tested like ethylene glycol, DMSO, ethanol or isopropanol all showed significant viscosity increase when cooled. The lock signal of those viscous substances was very bad or the

NMR could not lock at all to the sample. The broadened peaks were hardly possible to integrate correctly.

Acetone can form an explosive product with hydrogen peroxide and should therefore be avoided.[25]

2.7.6 Phosphate Buffer

When sodium pyruvate reacts with H_2O_2 the pH is dropping due to the fact that acetic acid and carbonic acid are formed. A suitable buffer must not contain any carbon as the signal may interfere with the products of interest. A mixture of sodium phosphate salts had been deuterated by alternating addition of D_2O and freeze drying. However, this buffer was not well soluble in S_0 at low temperatures probably due to the high sodium concentration in the sample.

2.7.7 Trifluorethanol for the identification of the hemiacetal

^{19}F NMR spectroscopy is a method that is very sensitive to structural changes due to the high amount of valence electrons in ^{19}F and its 100% natural abundance.[26]

Trifluorethanol was used for the identification of the hemiacetal formed with sodium pyruvate. The proton of the hydroxyl group of trifluorethanol is more acidic (pKa = 12.4) than methanol (pKa = 15.5)[27] which allows a nucleophilic attack on sodium pyruvate. For this experiment 15 mM non-enriched sodium pyruvate was dissolved in D_2O and mixed with an aliquot of trifluorethanol.

The ^{19}F NMR experiments showed no spectral changes of the trifluorethanol sample after addition to sodium pyruvate solution.

2.7.8 Distillation of methanol

Although methanol-d4 was newly purchased it may have contained impurities that interfere in the NMR experiments. Methanol-d4 was distilled and tested for changes in the NMR signal, which may indicate non-volatile impurities such as metals in the solvent.[28]

Although all glassware had been cleaned with acetone and water, the distilled fraction contained solid particles that had to be filtered off before further use. Volatile impurities may be found by GC-MS, both deuterated and protonated methanol samples were tested and no impurities were found.

2.7.9 Kinetic isotope effect

The kinetic isotope effect (KIE) can give further insight in the reaction mechanism. [29]KIE may tell what bonds have been broken or formed. The KIE testing is limited to H/D for the experiments as ^{12}C is not observable with NMR (Spin = 0). NMR requires a minimum of 10% deuterated solvent, usually D_2O. Since both methanol and water are protic they exchange protons. Therefore about 15% D_2O are needed to get a 10% D_2O solution. No clear effect has been observed and the system was difficult to lock to the deuterium signal resulting in broad peaks that were not well integrable.

2.8 Conclusion

A low temperature NMR protocol has been developed to observe the formation and breakdown of 2-deuteroperoxy-2-deuteroxypropanoate. The structure has been observed by HMBC NMR spectra and the chemical shifts have been assigned according to DFT calculations. The kinetic data allowed to calculate the rate constants for the reaction **Scheme 2** and to calculate the activation parameters of the transition states during the formation and breakdown of the intermediate 2-deuteroperoxy-2-deuteroxypropanoate.

2.9 References

(1) Andrae, U.; Singh, J.; Ziegler-Skylakakis, K. *Toxicol Lett* **1985**, *28*, 93.
(2) Aleksankin, M. M.; Vysotskaya, N. A.; Brodskii, A. E. *Kernenergie* **1962**, *5*, 362.
(3) Hamilton, G. A. *Progr. Bioorganic Chem.* **1971**, *1*, 83.
(4) Melzer, E.; Schmidt, H. L. *Biochem J* **1988**, *252*, 913.
(5) Cooper, A. J. L.; Redfield, A. G. *J. Biol. Chem.* **1975**, *250*, 527.
(6) Pocker, Y.; Meany, J. E.; Nist, B. J.; Zadorojny, C. *J. Phys. Chem.* **1969**, *73*, 2879.
(7) Margolis, S. A.; Coxon, B. *Anal Chem* **1986**, *58*, 2504.
(8) Von Korff, R. W. In *Met in Enzym*; John, M. L., Ed.; Academic Press: 1969; Vol. 13, p 519.
(9) Sander, E. G.; Jencks, W. P. *J. Amer. Chem. Soc.* **1968**, *90*, 4377.
(10) Lechtken, P.; Yekta, A.; Turro, N. J. *J of the Am Chem Soc* **1973**, *95*, 3027.
(11) Olek, R. A.; Antosiewicz, J.; Popinigis, J.; Gabbianelli, R.; Fedeli, D.; Falcioni, G. *Free Radic Biol Med* **2005**, *38*, 1484.
(12) Frisch, M. J. T., et al; Gaussian, Inc., Wallingford CT: 2004.
(13) Findeisen, M.; Brand, T.; Berger, S. *Magn Reson Chem* **2007**, *45*, 175.
(14) Ammann, C.; Meier, P.; Merbach, A. E. *J. Magn. Reson.* **1982**, *46*, 319.
(15) Van, G. A. L. *Anal. Chem.* **1970**, *42*, 679.
(16) Dougan, L.; Hargreaves, R.; Bates, S. P.; Finney, J. L.; Reat, V.; Soper, A. K.; Crain, J. *J. Chem. Phys.* **2005**, *122*, 174514/1.
(17) In *Chem Rubber Company handbook of chem and phys*; Chemical Rubber; Chemical Rubber Publishing, C., Eds.; Boca Raton : CRC Press: Boca Raton], 1977.
(18) Vollhardt, K. P. C.; Vollhardt, K. P. C. *Organic chemistry : structure and function*; 4th ed.. ed.; New York : W.H. Freeman and Co.: New York, 2003.
(19) Damitio, J.; Smith, G.; Meany, J. E.; Pocker, Y. *J. Am. Chem. Soc.* **1992**, *114*, 3081.
(20) Zhao, X.; Zhang, T.; Zhou, Y.; Liu, D. *J of Mol Cat A: Chem* **2007**, *271*, 246.
(21) Siegel, B.; Lanphear, J. *J. Am. Chem. Soc.* **1979**, *101*, 2221.
(22) Ciszak, E. M.; Korotchkina, L. G.; Dominiak, P. M.; Sidhu, S.; Patel, M. S. *J of Biol Chem* **2003**, *278*, 21240.
(23) Brevard, C. *Handbook of high resolution multinuclear NMR*; New York : Wiley: New York, 1981.
(24) Hayduk, W.; Laudie, H.; Smith, O. H. *J of Chem & Eng Data* **1973**, *18*, 373.
(25) Wolffenstein, R. *Berichte der deut chem Gesell* **1895**, *28*, 2265.
(26) Danielson, M. A.; Falke, J. J. *An rev of biophys and biomol struc* **1996**, *25*, 163.
(27) Brown, W. F., C.; Iverson, B.; Anslyn, E. **2010**.
(28) *Pure Appl. Chem.* **1985**, *57*, 855.
(29) Roth, J. P.; Klinman, J. P.; Elsevier Ltd.: 2004; Vol. 2, p 522.

3 Metal-catalyzed degradation pathway of hydrogen peroxide and its effect on Pressinoic Acid via Fenton Reaction

3.1 Introduction

The Fenton reaction is known as the reaction of ferrous iron with hydrogen peroxide and is believed to yield highly reactive hydroxyl radicals.[33,34] The oxidizing effect of the Fenton reaction on a disulfide bridge containing peptide has been studied and the results are presented in this chapter. According to its reduction potential, which ranks the easiness of an oxidizing radical attack, the disulfide bridge (for dimethyldisulfide E^0 = +1.39 V)[1] is believed to be a facile target for hydroxyl radicals (E^0 = +2.72 V)[2]. Other studies have shown that in Met containing peptides the sulfur of Met is easily oxidized by the Fenton reaction. Met (E^0 = +1.46 V)[3] has a higher reduction potential than a disulfide bridge, in turn, the latter are potentially a more susceptible target for hydroxyl radical oxidation.

3.1.1 The biological role of PA and vasopressin

Pressinoic acid (PA) is a synthetic peptide also known as the pressin ring of vasopressin, a hormone type nonapeptide.[4] In most mammalians vasopressin is referred to as Arg-vasopressin (AVP).[5] Vasopressin is non-protein bound in plasma and circulating in the extracellular fluid space with a rather short half-life (16-24 min). About one fourth of AVP is excreted with the urine and the rest is metabolically degraded by

vasopressinase, which is located in the liver and kidney.[6] The half-life of AVP was estimated based on the duration of the antidiuretic action of AVP.[7,8]

Other forms of vasopressin that are found in vivo are Lys-vasopressin (LVP) where the Arg residue is substituted by a Lys residue or vasotocin (or Arg-oxytocin), with an Ile instead of a Phe residue.[5]

AVP is one of the most important nonapeptide hormones. AVP is best known for its antidiuretic activity. Its main function is to regulate the water excretion from the kidney. AVP regulates urea and water permeability by activating the urea transporter protein leading to a change of osmotic pressure in the kidney and increasing the water permeability of renal collecting duct cells.[9,10]

AVP is synthesized in the hypothalamus, when dehydration occurs.[11-13] It also has several other physiological roles as it originates from different organs in the body. AVP can be found in the pancreas[14] where it exhibits hepatic effects like stimulating the release of glucagon, which is responsible for triggering the gluconeogenesis.[15-18] AVP and its derivatives such as LVP or Oxt have regulating effects on the glucose metabolism in the liver.[19]

In the adrenal gland AVP is stimulating the release of catecholamines, e.g. adrenaline or dopamine.[11,20] For the treatment of septic shock, which can lead to multiple organ dysfunction, AVP has beneficial effects by improving the vascular reactivity. In the emergency room it is commonly used to raise reduced blood pressure.[21] During a septic

shock, vasopressin levels are reduced and low doses of AVP are therefore recommended as first response.[22-24]

PA has been considered as the inactive form of AVP as its three dimensional structure differs from AVP. The biological active site of PA, which contains the Asn residue, is not stabilized by the C-terminal tripeptide (Pro-Arg-Gly), which is missing in PA. The Asn residue in PA does not point away from the macrocyclic ring in AVP but rather lays over the ring.[4] It was however shown that PA has the same effects but less biological activity than AVP.[25] For example, PA and Vasopressin are both known to stimulate the release of corticotrophin as a response to stress.[26-28]

3.1.2 Structure of PA

Pressinoic acid (PA) is a small ring-shaped peptide made of six amino acids: Cys-Tyr-Phe-Asn-Gln-Cys. The ring is closed by a disulfide bridge between two Cys.[4] AVP has an additional Pro-Arg-Gly attached to the C-terminus of PA. It has been shown by means of x-ray crystallography that the two aromatic residues span a 72 degree angle with respect to each other rather than being parallel.[4,29] This conformation of the two aromatic residues is very common in proteins and peptides.[30] The structure has a hydrophilic site based of the Asn and Gln residues which lay over the ring moiety. The hydrophobic site consists of the aromatic residues which both point away from the inner ring creating one edge of the peptide. On the opposite edge of the peptide the disulfide bridge is also exposed.[4] Both, the aromatic residues and the disulfide bridge of PA are

therefore easily accessible for solvents and ROS. A radical attack from a hydroxyl radical on the disulfide bridge is not limited due to steric hindrance.

Figure 24 shows the 3-D model of PA drawn with the ChemDraw 3-D program Version 14.0. The structure was optimized by minimizing the internal energy of the molecule based on the integrated MM2 function. This method performs iteration to minimize the energy until the root-mean-square gradient is less than the preset 0.01 value. The simulation was performed to demonstrate the free accessibility of the disulfide bridge and the aromatic residues of PA. However, the simulated structure is similar to the structure that was obtained with x-ray crystallography.[4]

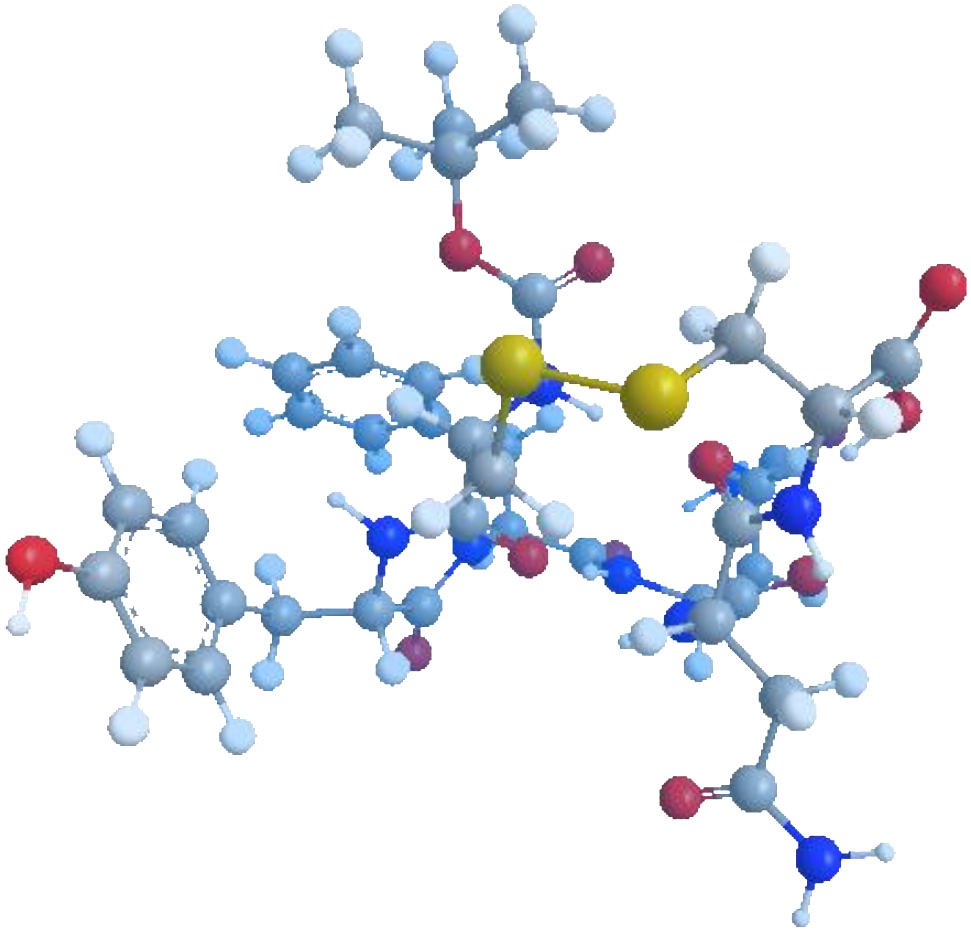

Figure 24: ChemDraw 3-D structure of pressinoic acid

The three-dimensional simulation of the structure of PA has been obtained by first drawing the 2-D model of PA and then performing the MM2 based energy minimization function included in ChemDraw 3-D with the RMS-gradient minimum of 0.01 and a maximum number of 10,000 iterations.

For this study PA with the N-terminus blocked by a tert-butyloxycarbonyl group (tboc) has been used. This modification made the peptide more hydrophobic which supported the separation process with a C18 analytical column. PA is therefore an ideal model

peptide to study the potential radical attack of hydroxyl radicals on the disulfide bridge of a peptide.

3.1.3 The Fenton reaction

The Fenton reaction was originally described by Henry Fenton as the reaction of H_2O_2 and ferrous iron salt that oxidize tartaric acid to yield dihydroxymaleic acid.[31] Although Fenton did not explain the actual mechanism of this reaction himself, the reaction of ferrous iron with H_2O_2 is named the Fenton reaction.[32-35] The mechanism of forming dihydroxymaleic acid is proposed[36] as presented in **Scheme 3**. The hydroxyl radical formed during the Fenton reaction abstracts a hydrogen from tartaric acid and forms H_2O. The new carbon centered radical can then donate an electron to Fe^{3+} which is formed during the Fenton reaction[32-34] to yield Fe^{2+} which can further react with H_2O_2, see **Reaction 2**. The electron pair of the neighboring hydrogen can then form a C-C double bond and release the proton. This results in the formation of dihydroxymaleic acid.

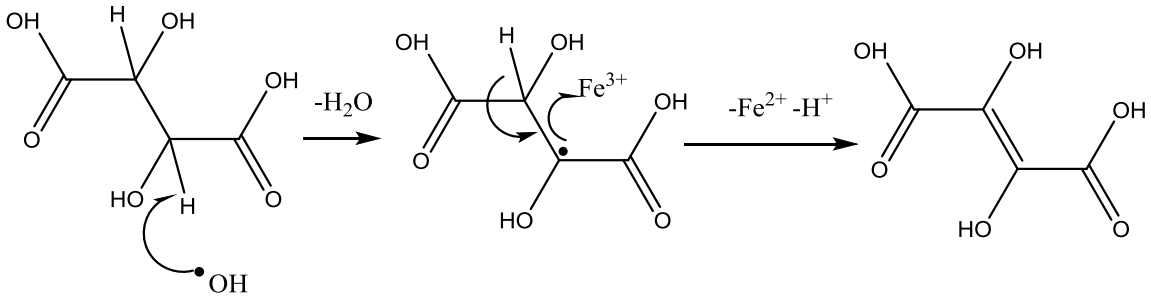

Scheme 3: proposed mechanism for the oxidation of tartaric acid to yield dihydroxymaleic acid

Haber and Weiss suggested that the Fenton reaction yielded hydroxyl radicals as the primary active species as shown in **Reaction 2**.[32,34,37]

Reaction 2

This reaction is not limited to iron. The Fenton reaction can also be performed with other reduced transition metals (M) such as copper(I)[38,39], titanium(III)[40,41], chromium(II)[42] or cobalt(II) [43] and will follow the generic reaction path shown in **Reaction 3**. This reaction and the reagents are also referred to as "Fenton-like". The Fenton-like reaction yields the same products as the actual Fenton reaction.[33,44]

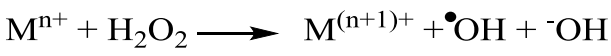

Reaction 3

It is still widely discussed whether the Fenton reaction yields free or bound hydroxyl radicals or higher oxidation state ferryl ions (FeO^{2+}), or perhaps even all of them.[33,37,40,45]

No clear evidence for the formation of only free hydroxyl radicals exists. The most promising methods for proving the formation of free hydroxyl radicals by the Fenton reaction are electron spin resonance (ESR) and the hydroxylation of aromatic compounds,[37,40] but the reaction rate is either too fast to be observable or the products

formed are not clearly assignable to one specific form of reactive species from the Fenton reaction.[46] Hydroxyl radicals react too fast with each other or organic compounds to be directly observed by ESR.[34] Hydroxylation of aromatic compounds can occur from both free hydroxyl radicals and ferryl ions.[33,45]

Free hydroxyl radicals can be created by ionizing radiation with H_2O which creates solvated electrons (e^-_{aq}). In the presence of nitrous oxide e^-_{aq} will form free hydroxyl radicals (**Reaction 4**).[47-50]

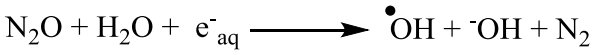

Reaction 4

Therefore the irradiation method allows to compare products which are formed by a reaction that is not known to yield free hydroxyl radicals with a reaction that is known to form free hydroxyl radicals.

Bound hydroxyl radicals may be formed during the Fenton reaction and may yield more selective, i.e. less reactive, radicals than free hydroxyl radicals and with a slower reaction rate (**Reaction 5**).[45,51] The hydrogen peroxide molecule attaches to the $Fe(EDTA)^{2-}$ complex, forming $Fe(EDTA)^-$ with the H_2O_2 still attached to the complex and the hydroxyl radical is trapped in that complex as it is not fully separated from the hydroxyl group.

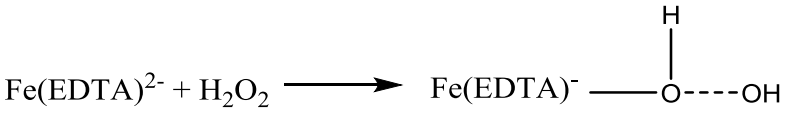

Reaction 5

Ferryl ions (FeO^{2+}) can be formed during the Fenton reaction and contain iron with the oxidation state IV[52] with an oxygen attached that can react similar to hydroxyl radicals.[53] Theoretical studies calculated that the formation of Ferryl ions in aqueous solutions is energetically favorable to the formation of hydroxyl radicals.[54] The ferryl ion is more selective towards amino acids than free hydroxyl radicals[55] and is formed as shown in **Reaction 6**. Hydrogen peroxide first attaches to $Fe(EDTA)^{2-}$ and then a ferryl ion is created with the release of a water molecule.

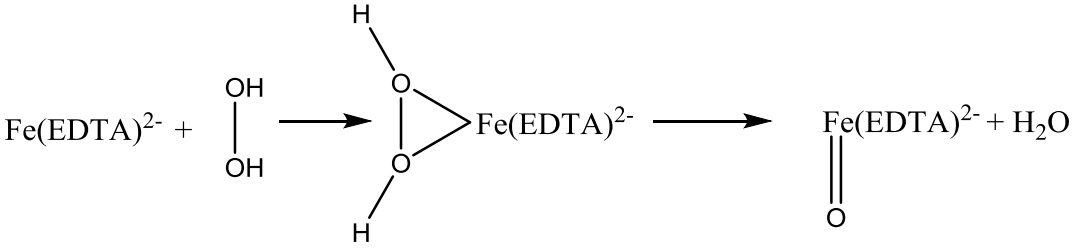

Reaction 6

It is suggested that the type of oxidizing species formed during the Fenton reaction depends on the iron concentration in the reaction mixture and the chelating agent used.[45] Iron chelated with diethylenetriaminepentaacetic acid creates mostly hydroxyl radicals[56] while EDTA generates both hydroxyl radicals and ferryl ions.[56]

Ferric iron (Fe^{3+}) can react with H_2O_2 to yield a peroxyl radical anion $^{\bullet-}OO$, which is less reactive than a hydroxyl radical, and a reduced ferrous iron (Fe^{2+}) as shown in **Reaction 7**.[34,57] Reduced Fe^{2+} can again react with H_2O_2 (**Reaction 2**). Therefore only catalytic traces of iron may initiate a Fenton reaction cascade. In order to gain a high yield of oxidation products it is suggested to use an excess of H_2O_2 for the experimental Fenton reaction.

$$Fe^{3+} + H_2O_2 \longrightarrow Fe^{2+} + {}^{\bullet}OO + 2H^+$$

Reaction 7

The reaction rate of the Fenton reaction (**Reaction 2**) varies depending on the type of the reduced metal involved. In addition, a chelating agent such as EDTA can significantly influence the reaction rate. In aqueous solution Fe^{2+} forms $Fe(H_2O)_6^{2+}$ complexes.[34] Fenton reaction occurring with this non-chelated Fe^{2+} has a reaction rate constant of about $k = 65\ M^{-1}s^{-1}$. EDTA can increase the solubility of iron and the efficiency to create hydroxyl radicals.[44] With a $Fe(EDTA)^{2-}$ complex the Fenton reaction has a reaction rate constant of $k = 7 \times 10^3\ M^{-1}s^{-1}$.[33,34,45]

Hydroxyl radicals are electrophilic species, regardless of whether they are formed by radiolysis or Fenton reaction.[58] When hydroxyl radicals react with amino acids they can either abstract hydrogen atoms from aliphatic residues, add to unsaturated and aromatic molecules or oxidize sulfur atoms.[32,44,97] Oxidative damage through hydroxyl radicals in proteins occurs preferably on His (Asn, Asp formation),[59,60] Tyr

(hydroxylation, dimerization), Phe (hydroxylation),[40,61] Trp (e.g. kynurenine formation),[62] Met (sulfoxide) and Cys (sulfenic, sulfinic and sulfonic acid)[63] side chains during all stages of protein development and storage.[64]

3.1.4 The reduction potential

The likelihood for the oxidation of a specific side of an amino acid residue can be predicted by its reduction potential E° vs. the standard hydrogen electrode (SHE).[65] The standard hydrogen electrode is a hypothetical construction as shown in **Figure 25**.[66]

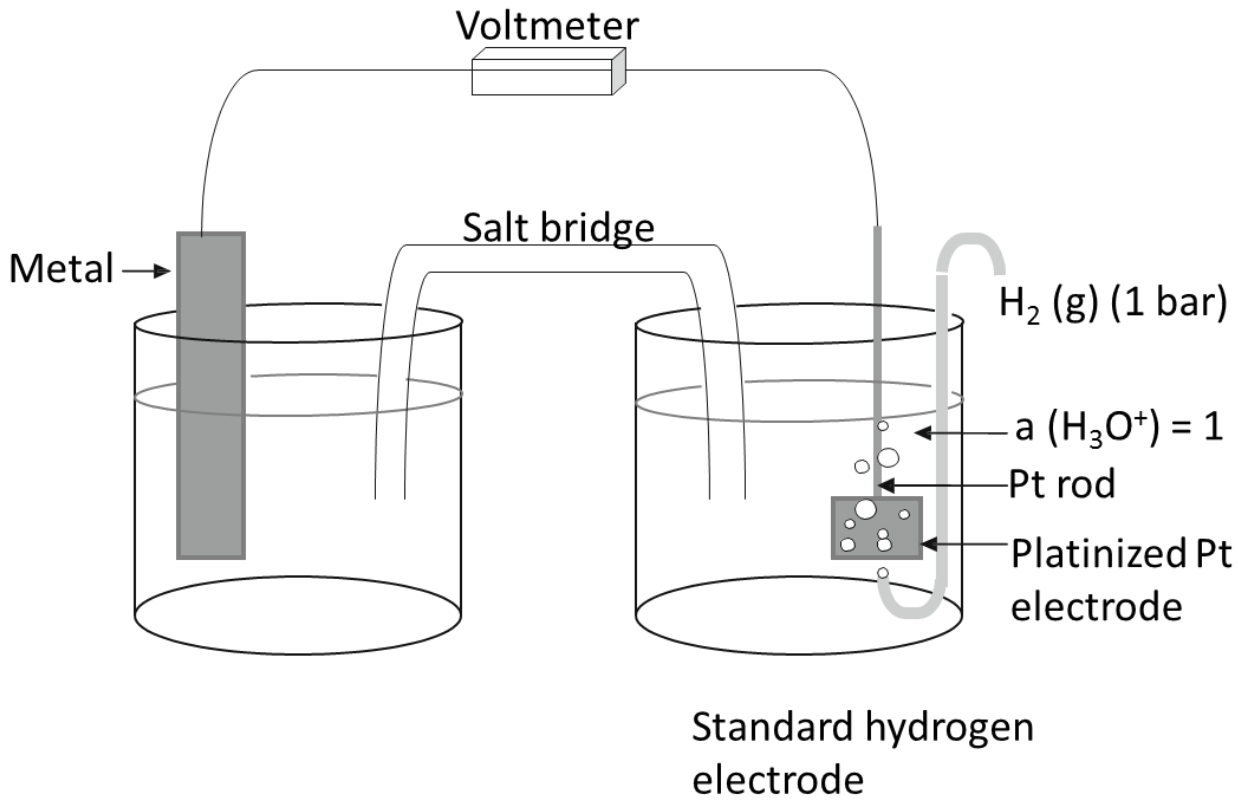

Figure 25: Standard hydrogen electrode setup; source see reference [66]

The half-cell is immersed in 1 M H^+ solution and the platinum electrode is constantly purged with hydrogen gas at atmospheric pressure. The reduction potential for this half-cell is defined as $E^0 = 0$ V (E^0 is the reduction potential vs. SHE). The original normal hydrogen electrode[67] as a reference was replaced by the theoretical SHE which assumes that no ion activity exists at pH = 0, which is impossible to observe in practical experiments due to high proton concentration.[68] The potential (E) measured by a practical working hydrogen electrode can be converted to the standardized SHE value with the Nernst **Equation 10**:

Equation 10

$E = E^0 - 29.6\ mV \times \log (\text{air pressure})/(\text{ion activity})^2$

The number 29.6 is derived from Equation 11.

Equation 11

$29.6\ mV = (R \times T) / (F \times z)$

With R (gas constant) T (absolute temperature) / F (Faraday constant) z (electrons transferred), with z = 2, because $2\ H^+ + 2e^- = H_2$. Here the unit for E is mV.[69]

The reduction potential is a measure of how likely a substance will oxidize, i.e. withdraw electrons, from another substance. A substance with a higher reduction potential can withdraw an electron from a substance with a lower reduction potential. Therefore a radical with a low reduction potential is considered more stable or more selective.[70,71] A hydroxyl radical has a reduction potential of $E^0 = +2.72$ V[2] and is known

to be a very strong oxidant.[72] A hydroxyl radical will oxidize, i.e. withdraw an electron, from a substance with a lower reduction potential, e.g. Met E^0 = +1.46 V[3] as shown in **Scheme 4**.

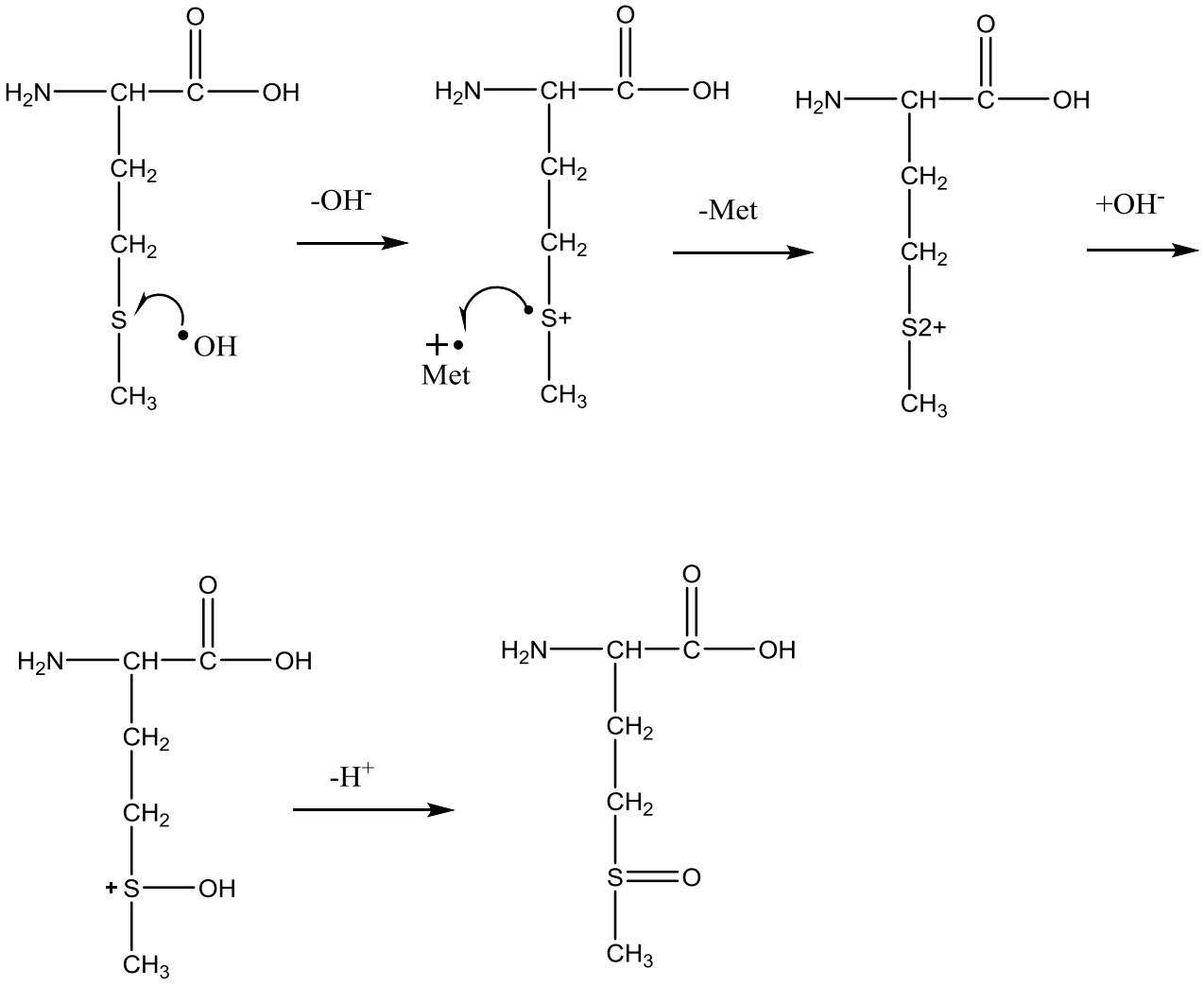

Scheme 4: Radical attack of a hydroxyl radical on Met and subsequent oxidation

The hydroxyl radical which has a higher reduction potential than Met abstracts an electron from the sulfur group and forms a hydroxide anion and the sulfur radical

cation. This reaction is irreversible. However, the Met radical cation can abstract an electron from another Met radical cation or from a substance with a lower redox potential. Then a hydroxide anion can attach to the sulfur and create a sulfoxide group after releasing the proton.

On the contrary to a high reduction potential, a lower reduction potential means that the substance will more likely reduce, i.e. donate an electron to another substance. An aqueous electron, known to be a very potent reducing agent, has a reduction potential of E^0 = -2.87 V.[70]

Radicals with a higher reduction potential are therefore more reactive and less selective towards other substances. The hydroxyl radical with E^0 = +2.72 V[2] can oxidize all amino acids, it is not selective. On the other hand a superoxide radical anion ($^{-\bullet}OO$) with E^0 = +0.89 V[2] is very selective as it can only oxidize Cys or Phe residues but not an aliphatic amino acid such as Leu. The superoxide radical anion is less reactive and can be considered to be more stable and is less likely to oxidize other substances. [1,70]

Met is known to be a facile target for oxidation by ROS. Even H_2O_2 in aqueous solution can oxidize the sulfur of Met.[73] The oxidation of Met by Fenton reagents has been studied before.[74] The reduction potential of a disulfide bridge, e.g. dimethyldisulfide E^0 = +1.39 V[1], is lower than Met E^0 = +1.46 V[3]. A disulfide bridge, as in cystine, can be

therefore considered as an even more likely target for oxidation by a hydroxyl radical than the sulfur of Met.

The reduction potential of an amino acid side chain is influenced by the pH of the solution and the neighboring amino acids in the protein structure.[44] Therefore the reduction potential for isolated amino acids can significantly differ from the values within a protein or peptide.[44,75] For example, depending on the adjacent amino acids the reduction potential for Met can be E^0 = +1.19-1.86 V.[76]

The reduction potential of a disulfide bridge is significantly lower within a rigid five membered ring (e.g. E^0 = +1.13 V for lipoic acid) compared to an open chain form (E^0 = +1.39 V dimethyldisulfide). This is believed to be based on the higher electron density in this ring structure because the torsion angle in the five-membered ring is lower than in an open chain disulfide bridge.[1]

Aromatic amino acids are also known to be facile targets for hydroxyl radicals. The reduction potential of Tyr residues at neutral pH is E^0 = +0.93 V.[75] The Tyr residue has a lower reduction potential at basic conditions, E^0 = +0.72 V at pH 13.[75] Since the hydroxyl group on the phenol group of Tyr is deprotonated the electron density in the aromatic ring is increased, making it a more facile target for nucleophilic hydroxyl radicals.[44]

3.1.5 Reaction kinetics of radical reactions

Hydroxyl radicals are highly reactive and can react with most organic matter at diffusion limited rates.[40,77] The reaction rate constant of hydroxyl radicals with the disulfide bridge of cystine is $k = 2.1 \times 10^9 M^{-1}s^{-1}$.[44] For the reaction of the Met sulfur with hydroxyl radicals, rate constants of $k = 8.5\text{-}12 \times 10^9 M^{-1}s^{-1}$ have been reported.[44,78] Aromatic amino acids on peptides react with hydroxyl radicals with rate constants of $k = 10^9$ to $10^{10} M^{-1}s^{-1}$ depending on this overall structure and the steric hindrance.[32,44,79] Reaction rates with the Fenton substrates Fe^{2+} ($k = 3 \times 10^8 M^{-1}s^{-1}$) [80] and H_2O_2 ($k = 2 \times 10^7 M^{-1}s^{-1}$) [77] are about 100 fold lower than the reaction rates with the amino acid residues, making them the less likely targets for the hydroxyl radical attack.

3.1.6 Reaction of hydroxyl radicals and sulfur containing amino acids

Cys, Met and disulfide bridges are known to be facile targets for a hydroxyl radical attack.[44] The Met oxidation on the sulfur group yields Met sulfoxide.[81] The enzyme family of Met sulfoxide reductases can reduce either free or protein bounds sulfoxide.[82,83] Therefore, Met can act as protecting agent for proteins from irreversible damage occurring on other amino acids.[84] The rate of Met oxidation in proteins depends on the accessibility for a radical attack, Met residues buried within the hydrophobic area of a protein are less likely to be attacked than well-exposed Met residues.[85,86]

A disulfide bond has similar reactivity towards hydroxyl radicals compared to Phe.[44] The disulfide groups of peptides show a slower reaction rate when the amino groups

are protonated.[87] The oxidation of sulfur containing amino acids yields sulfoxides of Met or H-abstraction and further disulfide or C-S bond formation of Cys. The disulfide bond of two Cys can be oxidized to yield thiosulfinate, sulfinic or sulfonic acid or new formation of C-S bonds via one-electron oxidation[86] Disulfide scrambling, which promotes protein aggregation, can occur in acidic solutions. First the disulfide bridge is reduced by the proton and a thiol and sulfenium cation is formed, **Reaction 8**, followed by the disulfide bond interchange and formation of a new sulfenium cation as shown in **Reaction 9**.[86] Steric hindrance and the accessibility of the solvent are other factors determining the formation of products through a radical attack.[44]

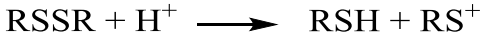

Reaction 8

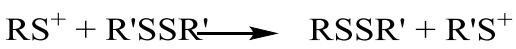

Reaction 9

The one-electron oxidation of sulfur through hydroxyl radicals results in the formation of a radical cation, a sulfuranyl radical (**Scheme 5**).[88] The newly formed sulfuranyl radical cations can react with each other to form $RSSR^{2+}$ and RSSR or a carbon centered radical, see **Scheme 6** and **Scheme 7**, and in both cases form thiosulfinate.[44,79]

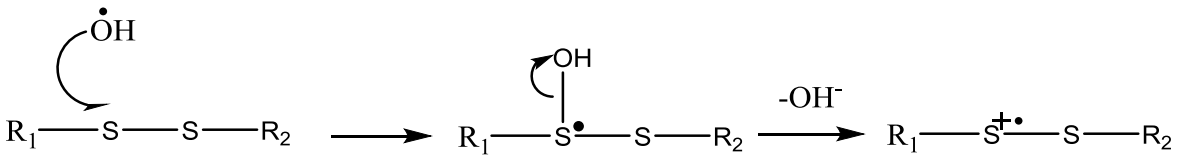

Scheme 5: Mechanism of the formation of a sulfuranyl radical cation

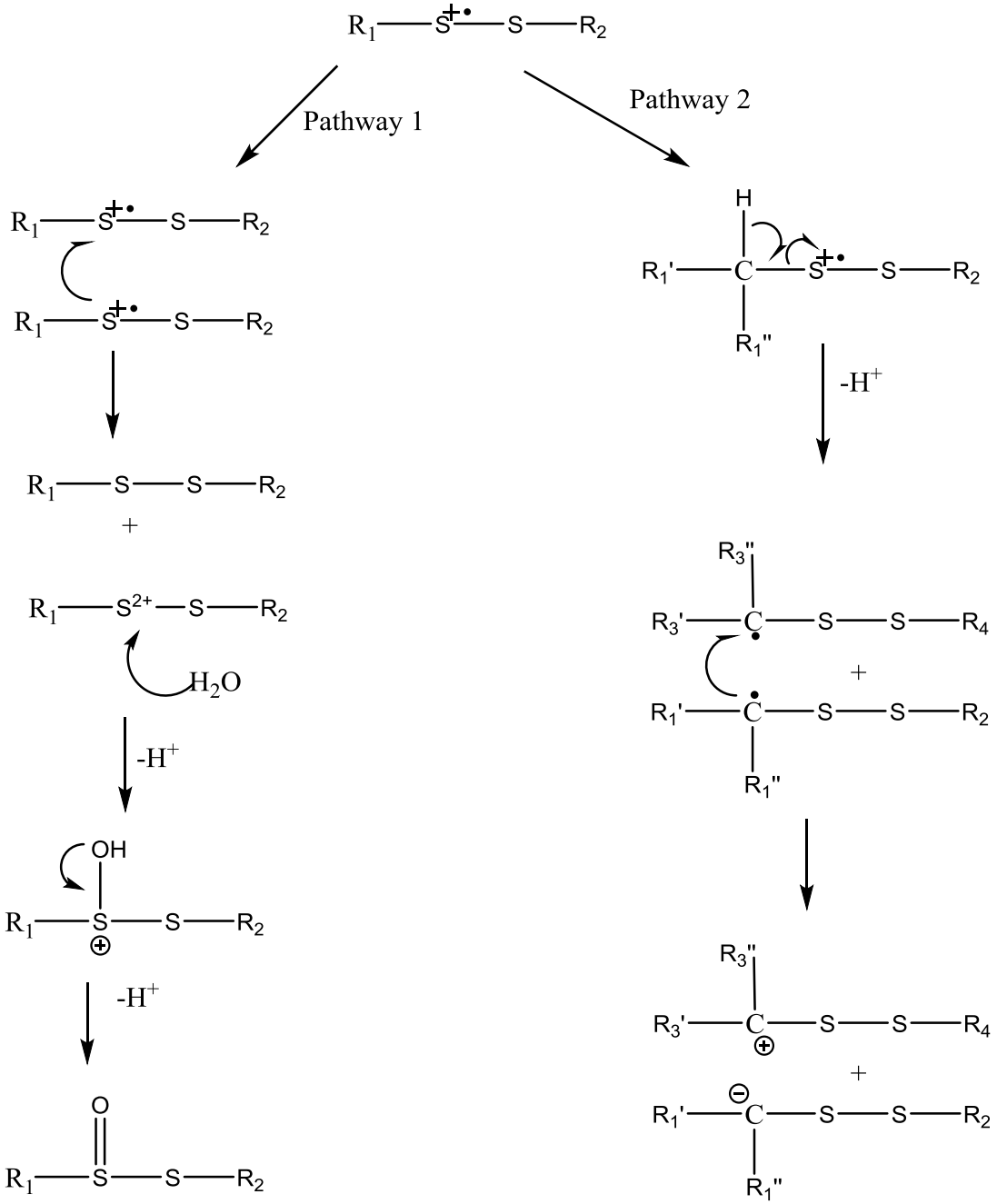

Scheme 6: Mechanism of thiosulfinate formation

Pathway 2 cont.

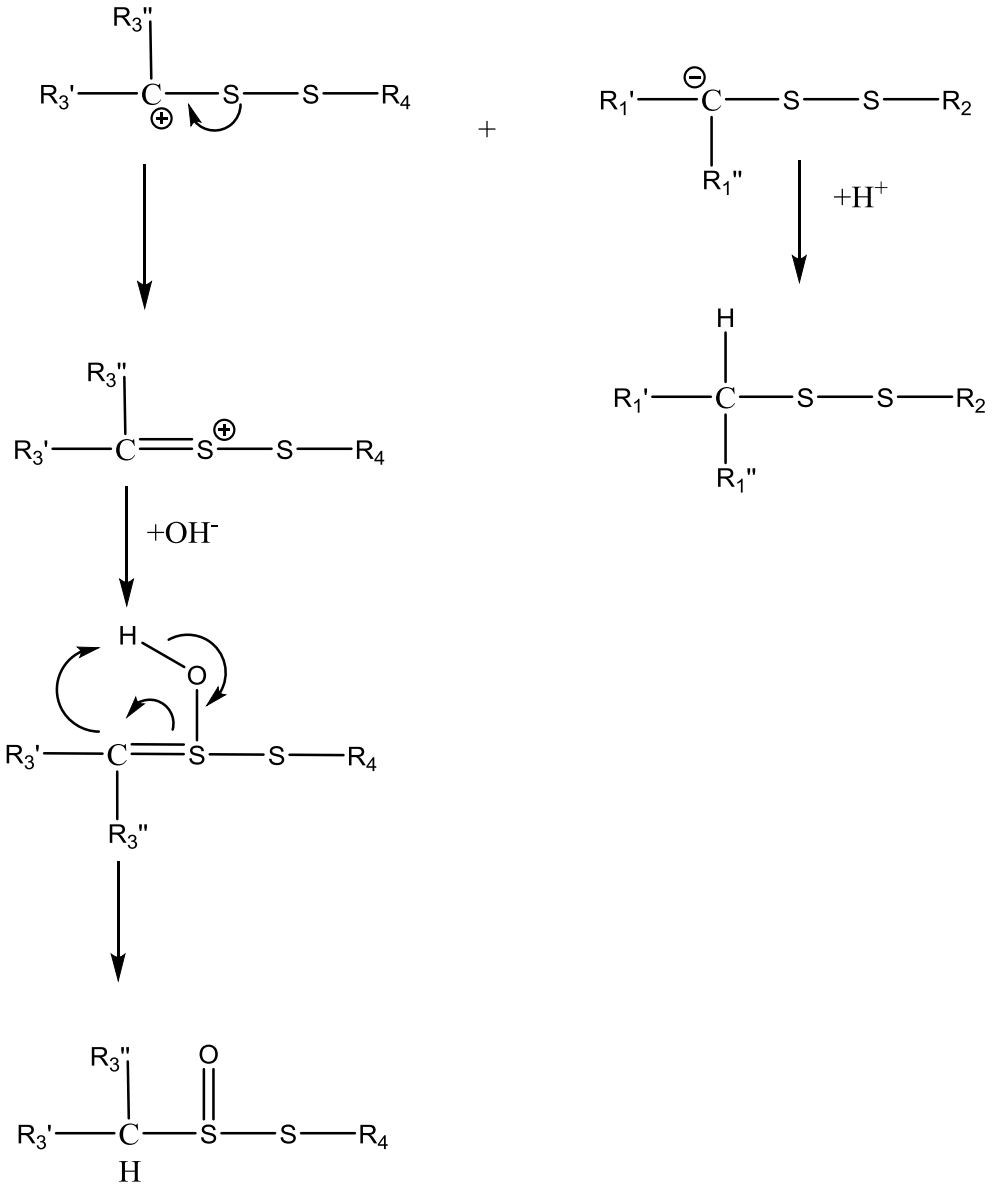

Scheme 7: Mechanism of thiosulfinate formation continued

The sulfuranyl radical cation formed by the reaction with a hydroxyl radical can further oxidize Fe^{2+} to reform the original disulfide bridge. It can also react with another organic

disulfide with a rate constant in the range of $k = 5.4 \times 10^5$ $M^{-1}s^{-1}$ to 5.2×10^6 $M^{-1}s^{-1}$ depending on the steric hindrance of the reactants.[79]

3.1.7 Reaction of hydroxyl radicals with aromatic amino acids

Hydroxyl radicals add to an aromatic system as shown in **Scheme 8** which shows the radical attack on a Phe residue. The hydroxyl radical attacks the aromatic ring and yields a hydroxycyclohexadienyl radical by abstracting an electron from the ring and forming a hydroxide anion. The hydroxycyclohexadienyl radical can be further oxidized, for example by a ferric iron ion (Fe^{3+}) that is formed during the Fenton reaction (**Reaction 2**)[89] and then releases a positive charge in form of a proton to form 4-hydroxylphenylalanine in this example, also 2- or 3-hydroxyphenylalanine can be formed by this reaction with equal yields.[32,37,58,90]

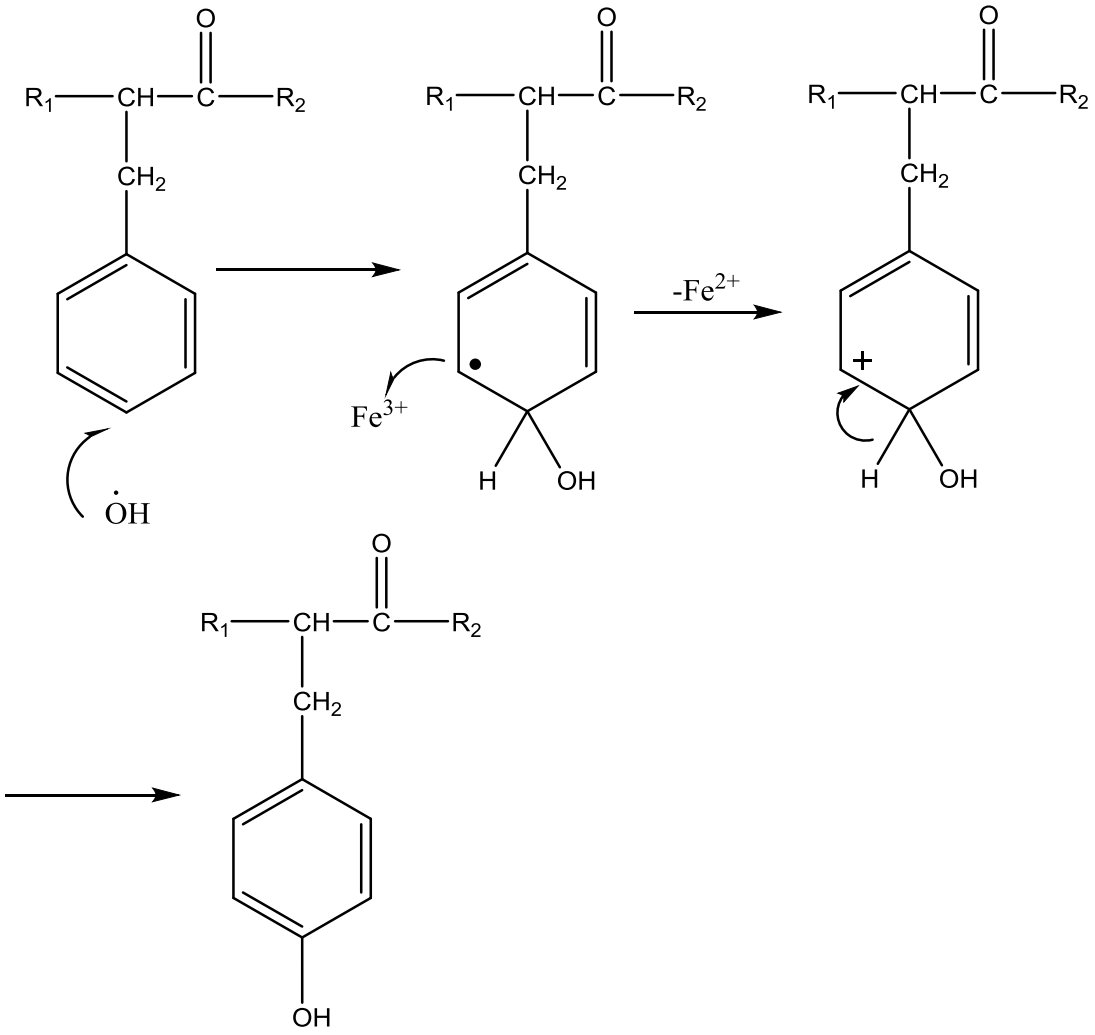

Scheme 8: Mechanism of the hydroxylation of Phe by a hydroxyl radical

Aromatic groups can stabilize radicals through their resonance.[91] In the absence of oxygen also dimerization of Tyr can occur.[92]

A ferryl ion can add to the aromatic ring shown in **Scheme 9**.[37]

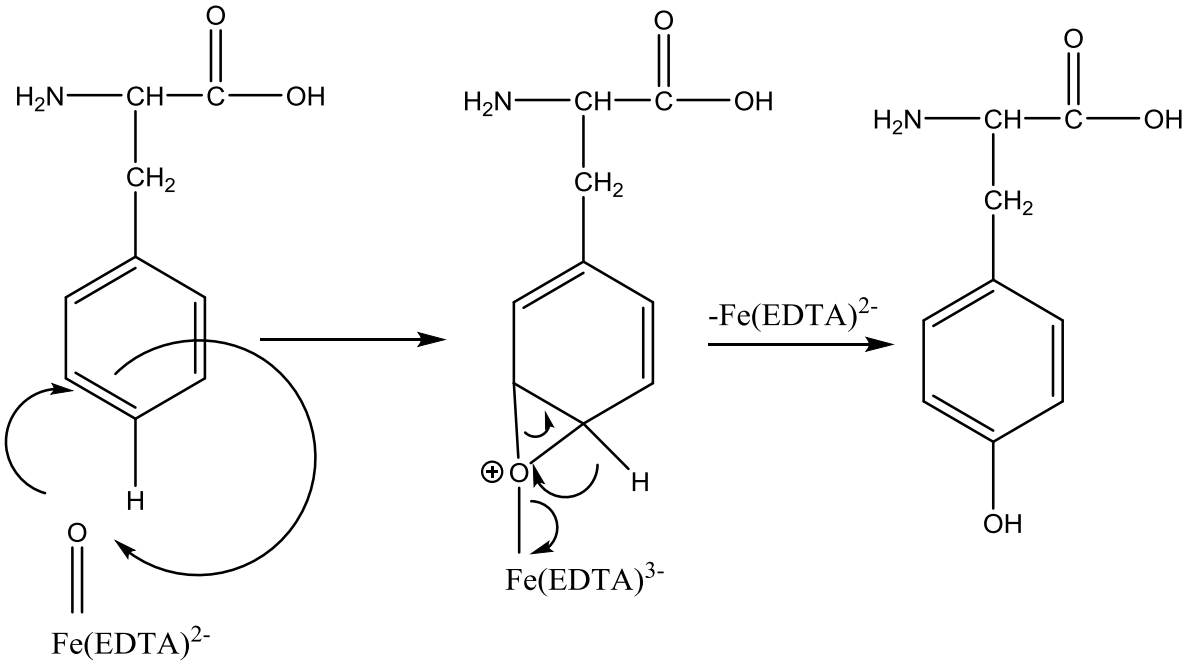

Scheme 9 – Ferryl ion attack on an aromatic residue

Phe is the most abundant aromatic amino acid found in proteins.[93] In the absence of oxygen, hydroxyl radicals add to Phe at all positions to form 2-, 3- or 4-hydroxyphenylalanine. Tyr can be hydroxylated to yield DOPA and can also form 3,3′-dityrosine cross links.[44,90,94-96] Dityrosine can be detected by its intrinsic fluorescence which can be detected at excitation wavelength of 320 nm and emission wavelength of 405 nm.[97]

3.1.8 Intermolecular radical transfer

The damage on peptides and proteins from radicals can be transferred to aromatic and sulfur containing residues, i.e. Trp, Tyr and Cys residues. Thiyl radicals formed from cleavage of disulfide radical anions can oxidize Tyr residues.[98] Electron transfer can

occur over long distances within a protein with the rates depending on the protein structure resulting in different products than expected. For example glutamine synthetase is mainly oxidized on its His residues even though they are adjacent to Met or Cys which are usually very easily oxidized.[99]

3.2 Materials and methods

3.2.1 Chemicals

Tert-butyloxycarbonyl-Pressinoic acid (PA) was purchased from Bachem (Torrance, CA, USA). Hydrogen peroxide (30% H_2O_2); ethylendiamine tetraacetatic acid (EDTA); ferrous ammonium sulfate, hexahydrate; sodium phosphate, mono and dibasic; sodium pyruvate; acetonitrile (ACN), HPLC grade; tetrahydrofuran (THF); trifluoracetic acid (TFA); formic acid (FA); hydrochloric acid (HCl); phenol (liquefied, 90% in H_2O); 4-hydroxyphenylalanine; 2-hydroxyphenylalanine; 3,4-dihydroxyl-phenylalanine (DOPA); (tris(2-carboxyethyl)phosphine (TCEP); n-ethylmaleimide (NEM); 2,2'-azino-bis(3-ethylbenzothiazoline-6-sulfonic acid) diammonium salt (ABTS); potassium ferricyanide were all purchased from Sigma-Aldrich (St. Louis, MO, USA); compressed gases were purchased from Matheson Tri-Gas, Inc. (Montgomeryville, PA, USA), oxygen traces from Argon (Ar) were removed with an Oxyclear DGP-250R2 gas purifier (Labclear, Oakland, CA, USA) ; D_2O:H_2O, 99.8%:0.2%, was obtained from Cambridge Isotopes; 2-hydroxyphenylalanine, 95% was purchased from Alfa Aesar (Ward Hill, MA, USA).

3.2.2 Instrumentation

HPLC analysis was performed on a Shimadzu SIL20 system equipped with a 20X autosampler, an SPD-M20 photodiode array detector and an RF-20A fluorescence detector. For analysis and separation of the samples a Vydac 218TP C18 ODS2 (250x4.6 mm, 5 micron) analytical column and for amino acid analysis a Thermo C18 ODS Hypersil (250x4.6 mm; 5 micron) column was used.

Solid phase extraction (SPE) was performed using 50mg/1ml C18 Hypersep columns purchased from Thermo Scientific, (Bellefonte, PA, USA). SPE was performed on a Supelco (Bellefonte, PA, USA) vacuum manifold.

MS and MS/MS data were acquired on a Synapt G2 mass spectrometer (Micromass Ltd. Manchester, UK) coupled to an Acquity UPLC system (Waters Corp., Milford, MA, USA). The ESI was operated at +2.5k V, tube lens offset at 75 V and the capillary temperature was set to +250 °C. For the product separation a Vydac MS C18 300A column with the dimensions of 250 mm length, 0.5 mm diameter and 5 micron particle size (Fisher Scientific, Pittsburg, PA, USA) was used.

NMR experiments were performed on a Bruker Avance III 600 MHz instrument equipped with an X-channel observe quadruple nuclei probe.

3.2.3 Methods

3.2.3.1 Preparation of the reactants

The Fenton reaction was performed with Fe(II). To avoid any oxidation of the iron before the Fenton reaction started, all solutions were kept oxygen-free by purging with Argon (Ar). Phosphate buffer was prepared by mixing 10 mM $Na_2H_3PO_4$ with 40 mM NaH_2PO_4 in water and degassed with Ar for at least 30 min. The pH (6.1) was measured before purging. $Fe(EDTA)^{2-}$ solution was prepared by first dissolving EDTA in phosphate buffer to yield a 10 mM concentration and purging the solution with Ar for 30 min. Then 10 mM ferrous ammonium sulfate was added to the solution. The H_2O_2 solution was prepared by diluting 7 M (30% v/v) H_2O_2 in phosphate buffer to yield 105 mM concentration and purged with Ar. Sodium pyruvate (150 mM) solution was prepared in H_2O.

3.2.3.2 Experimental setup for the Fenton reaction with PA

The experimental setup for the Fenton reaction with PA is shown in **Figure 26**.

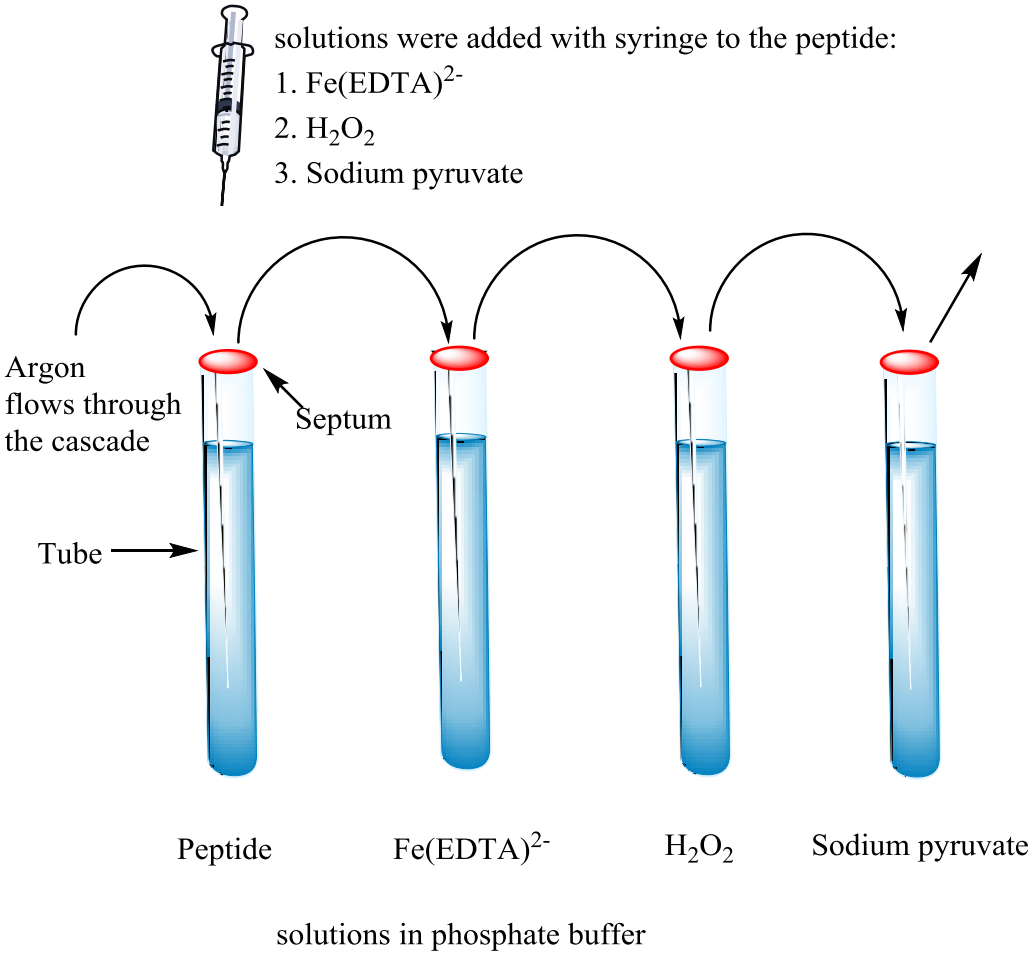

Figure 26: Experimental setup for the Fenton reaction

The solutions were kept in individually rubber septum-sealed glass vials. The vials were connected with tubes attached to syringe needles that were punched through the septa. This cascade setup allowed to purge all solutions simultaneously with Ar and minimize the oxygen uptake when a sample was withdrawn or injected.

The PA in H_2O (1 mM) solution was continuously purged with Ar for at least 10 min. Then $Fe(EDTA)^{2-}$ was transferred into the PA solution and the reaction was started by

injecting the H_2O_2 solution. This resulted in final concentrations of 0.45 mM PA, 4.5 mM $Fe(EDTA)^{2-}$ and 10.5 mM H_2O_2. After 2 min, the reaction was stopped by addition of 15 mM sodium pyruvate. Sodium pyruvate has been used to break down residual H_2O_2 as described in Chapter 2. During the analytical workflow, which included several purification steps, significant losses during the individual steps resulting in product concentrations below the detection limit of the analytical instruments occured. Therefore excess amounts of $Fe(EDTA)^{2-}$ and H_2O_2 were used in order to gain sufficient product concentrations.

3.2.3.3 Solid phase extraction (SPE)

SPE is a simple and efficient method to separate a peptide from its reactants that may interfere with the quality of the analytical data. The SPE protocol was applied after the Fenton reaction and after the reduction and alkylation process in order to obtain clean peptide samples and prevent further reaction with the reactants used.

The flow rate through the C18 SPE cartridges was manually set to approximately 1 ml/min. The cartridge was activated with 2 ml methanol and the solvent flow was stopped for 1 min after half of the solvent had eluted to allow the solvent to soak fully into the resin bed. Then the cartridge was equilibrated with 1 ml 99.9%:0.1% H_2O:TFA and the sample solution with peptide and reactant was added. An additional 1 ml 99.9%:0.1% H_2O:TFA was used to clean the sample. The eluents were discarded. For the elution of the peptide, 2 ml ACN were added to the column and the solvent flow was

stopped for 1 min after half of the solvent had been eluted to allow full elution of the peptide from the resin bed. The collected eluted sample was then freeze-dried in order to remove ACN and reconstituted to the original sample volume with H_2O.

This protocol was tested with a PA standard sample. In order to verify that the sample had been eluted during the desired separation step, all eluted fractions were separately freeze dried and reconstituted in H_2O. The samples were then analyzed with HPLC by means of UV and fluorescence detection. PA was only detected in the ACN fractions, confirming the functionality of the SPE protocol.

3.2.3.4 Product separation with HPLC

HPLC by means of UV and fluorescence detection was used to separate the major products of PA formed during the Fenton reaction. The fluorescence of the Tyr residues in PA allowed the detection of PA and its oxidation products with the fluorescence detector using an excitation wavelength of 275 nm and an emission wavelength of 305 nm. The sample/solvent mixture eluting from the detector was collected for further analysis.

For the elution a linear gradient was used with solvent A: H_2O:ACN:TFA (v:v:v) 95:5:0.1 and solvent B: H_2O:ACN:TFA (v:v:v) 5:95:0.1 increasing from 30% B to 40% B over 10 min.

3.2.3.5 Reduction and alkylation of the disulfide bridge

In order to obtain reproducible MS/MS data the disulfide bond of the PA samples had to be reduced with TCEP to open the ring structure. TCEP also removes oxygen from potentially formed thiosulfinate.[100] The reduction mechanism that removes oxygen from the disulfide bridge is shown in **Scheme 10**. Oxygen removal can be easily identified by comparing the masses before and after reduction.

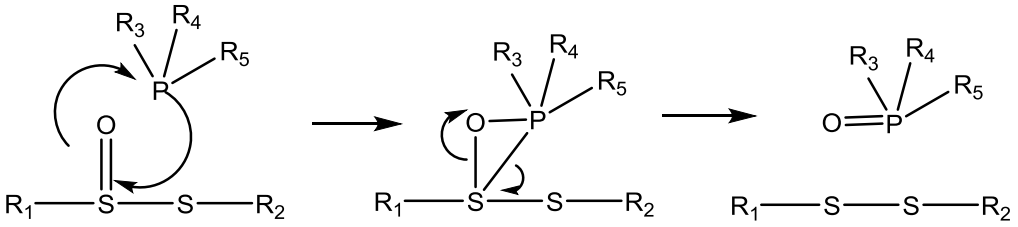

Scheme 10: Reduction mechanism of thiosulfinate with TCEP

The PA samples were reduced by adding 2 mM TCEP in H_2O solution to the 1 mM PA sample and incubated for 1 h at 37 °C. Then 4 mM NEM solution in H_2O was added and incubated for 2 h at 37 °C to block the newly formed thiol groups and prevent the reformation of a disulfide bridge.

The samples were cleaned using SPE as described above in order to remove excess substances and then freeze-dried and reconstituted to the original volume with H_2O.

3.2.3.6 Mass spectrometry analysis

For MS analysis the flow rate of the HPLC was set to 15 µl x min^{-1}. The mobile phase was composed of solvent A, that is, 100:0:0 (v:v:v) H_2O:ACN:FA, and solvent B, that is, 0:99.9:0.1 (v:v:v) H_2O:ACN:FA. The injection volume was 5 µl. For the first 5 min, the pump flow was set to 25% solvent B, while a linear gradient from 25% to 41% B was applied over the next 10 min. Mass spectrometry data was analyzed with Mass Lynx 4.0 software.

For the MS/MS analysis the flow rate of the HPLC was set to 15 µl x min^{-1}. The mobile phase was composed of A: 99.9:0:0.1 (v:v:v) H_2O:ACN:FA and B: 0:99.9:0.1 (v:v:v) H_2O:ACN:FA. The injection volume was 5 µl. The linear gradient was set from 20% to 44% B over 15 min. Mass spectrometry data was analyzed with Mass Lynx 4.0 software. The MS/MS spectra were obtained from extracted ion chromatograms of the mass spectrometer based on the predicted m/z values of the precursor ions. The intensities of the fragment ions were compared by defining the ion with the highest count in the spectrum as 100%. The other ions occurring were converted into relative % compared to the 100% ion.

The m/z values of the MS/MS fragments were predicted by the MS-product function of the Protein Prospector v 5.14.0 by the University of Southern California.

3.2.3.7 Peptide hydrolysis

Amino acid analysis allows identifying specific hydroxyphenylalanine isomers (**Scheme 11**). Most amino acids need modification with fluorescent groups to carry out amino acid analysis. Considering the inherent fluorescence and hydrophobicity of Tyr and its isomers they are separable by RP-HPLC without further modification.

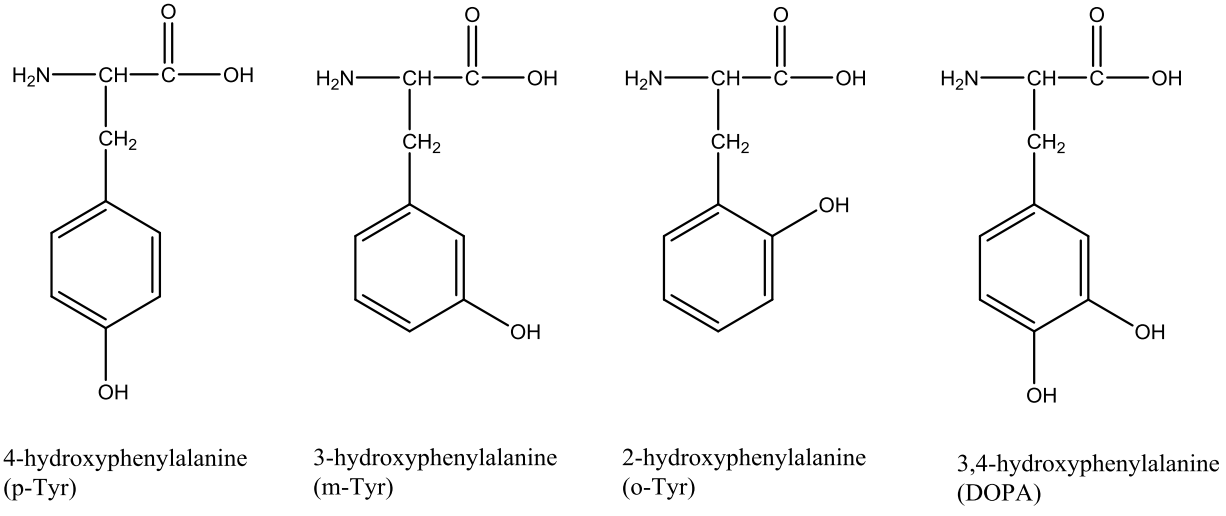

Scheme 11: Tyr isomers detected in the hydrolzyed PA samples drawn with ChemDraw.

The samples collected after the Fenton chemistry was applied, see section 3.2.3.4, were reduced and alkylated, section 3.2.3.5, and used for Tyr isomer analysis. For the hydrolysis the PA samples were dissolved in 6 M HCl containing 1% v:v phenol (liquefied), which served as antioxidant.[101] The hydrolysis solutions were first degassed with He for 2 min and then O_2 was removed from the solution by alternating evacuation and N_2 addition. Degassing with He prevented the formation of air bubbles during the

evacuation that caused sample loss due to splashing. The PA samples were then incubated for 3 h at 120 °C. After the hydrolysis process the PA samples were freeze-dried to remove HCl and were reconstituted to their original volume with H_2O.

3.2.3.8 Amino acid analysis of the hydroxyphenylalanine isomers

For identification of the hydroxyphenylalanine isomers shown in **Scheme 11** a solution of 1% NaCl (w:v) and 1% acetic acid (v:v) was used for isocratic elution by HPLC.[84,94,102] The Tyr isomers were identified by comparison of their elution time with 1 mM standard solutions in H_2O of 2-, 3-, 4-, and 3,4-hydroxyphenylalanine. Tyr isomer standards were treated according to the protocol for acid hydrolysis before chromatographic analysis. Treatment of the amino acid standards under the same conditions as applied to the hydrolysis of the amino acids in the peptides allowed identifying newly formed products, which may be detected in the chromatograms.

3.2.3.9 Synthesis of 3-hydroxyphenylalanine

3-hydroxyphenylalanine was not readily available and had to be synthesized. 1mM Phe standard solution was hydroxylated using the Fenton protocol described above. This method yields 2-, 3- and 4-hydroxyphenylalanine isomers.[94,102] Based on the elution times of the known standards the elution time of 3-hydroxyphenylalanine was predicted to be between the elution times of 4- and 2-hydroxyphenylalanine. The sample that was believed to be 3-hydroxyphenylalanine was collected from the fluorescence detector

outlet. After repeated collection, in order to allow accumulation of enough sample concentration for ^{1}H NMR spectroscopy, the sample was freeze dried and reconstituted with 2 ml of H_2O, enough to keep all solid residues in solution.

The collected 3-hydroxyphenylalanine sample contained a high concentration of NaCl. The sample was desalted by HPLC to enable successful characterization by means of 1H-NMR spectroscopy. High salt concentrations absorb the radio-frequency field applied during NMR spectroscopy which leads to less excitation of the sample. This makes longer pulse sequences necessary which can heat the sample and broaden the observed peaks.[103]

A linear gradient with solvent A = 99.9:0.1 (v:v) H_2O:TFA and solvent B = 5:95:0.1 (v:v:v) THF:ACN:TFA was applied for the desalting process. The flow rate was set to 1 ml x min^{-1}. For the first 3 min after injection 100% solvent A was used in order to remove the salt from the sample, then a linear gradient over 3 min from 0% to 30% was applied.

The desalted product eluted with the organic phase and the fluorescence signal of 3-hydroxyphenylalanine was observed. After the desalting process the sample was freeze-dried and reconstituted to its original volume with D_2O. The structure of the Tyr isomers was analyzed by means of ^{1}H NMR spectroscopy.

3.2.3.10 Fenton reaction with ABTS

2,2′-azinobis(3-ethylbenzthiazoline-6-sulfonate) (ABTS) can undergo one–electron oxidation and form a ABTS radical cation as shown in **Reaction 10**.[104]

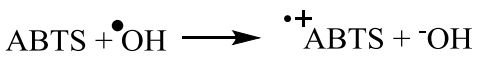

Reaction 10

Due to its low reduction potential of E^0 = 0.62 V [105] ABTS can be easily oxidized by the hydroxyl radical. The ABTS cation radical ($ABTS^{\bullet+}$) is rather stable and has an absorption maximum at 414 nm which can be measured spectroscopically. The time required for the Fenton reaction to produce hydroxyl radicals or ferryl ions can be measured by observation of the absorption spectrum of the ABTS solution at 414 nm during Fenton reaction. The Fenton reaction, which yields hydroxyl radicals (**Reaction 1**), is faster than the formation of superoxide radicals (**Reaction 6**). Therefore, formation of the ABTS radical cation absorption is expected to slow down after the Fenton reaction process comes to an end and only superoxide formation is expected to take place.[106]

A 10 mM ABTS solution containing 10 mM $Fe(EDTA)^{2-}$ in an phosphate buffer (pH 6.1) was prepared, filled into a quartz cuvette, and placed into a UV-VIS absorption spectrophotometer. Next, the absorption at 414 nm was recorded as a function of time. Hereby, the reaction was started by means of injecting 10 mM H_2O_2 with a syringe.

3.2.3.11 NMR analysis

In the context of available standards of 2- and 4-hydroxyphenylalanine (1 mM in D_2O:H_2O 99.8 %:0.2 %), their ^1H chemical shifts were recorded. The lock signal was set to D_2O. Recording the spectra required 128 FID (scans).

The spectra were analyzed with the MestReNova Software v 10.0 package (Mestrelab Research, Santiago de Compostela, Spain). The hydrogen on the aromatic residues were numbered according to the IUPAC recommendations.[107]

3.3 Results

3.3.1 Fenton reaction observed with ABTS

The absorption of an ABTS solution in the presence of the Fenton reagent was monitored to determine the time needed for the Fenton reaction to come to an end. The corresponding relationship is shown in **Figure 27**. After injection of H_2O_2 the absorption increased rapidly until it nearly plateaued after ca. 1 min followed by a slow increase. From the latter a time window of 2 min has been set for the Fenton reaction experiments with PA in order to allow the Fenton reaction to be completed.

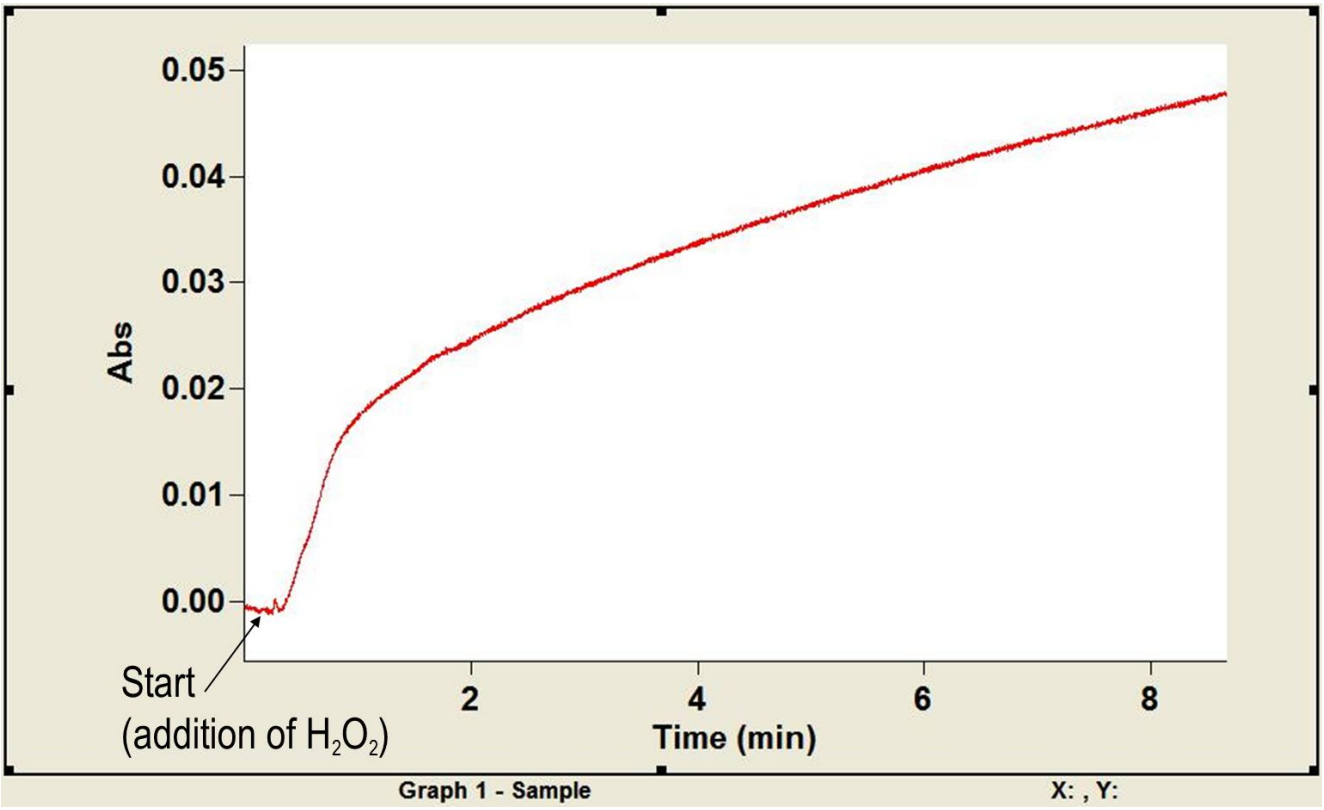

Figure 27: Time evolution of ABTS absorption at 414 nm upon H_2O_2 addition.

After the recording was started the H_2O_2 solution was injected (Start) and the absorption at 414 nm was detected over a time interval of 9 min.

3.3.2 Product detection of PA after Fenton reaction and separation with HPLC

The chromatograms obtained after Fenton reaction was applied to PA showed that four new substances had formed (**Figure 28**). The main products eluted after 8.9 min (product #1), 10.6 min (product #2), 12.5 min (product #3) and 13.7 min (product #4) in addition a peak occurred after 15.3 min, which was identical with the PA standard. Product #3 featured a lower peak intensity relative to the other products. Additionally,

substances eluting after 2.3 min and 19 min were collected and analyzed by means of MS. The MS spectra of these two products could not be assigned to a specific substance.

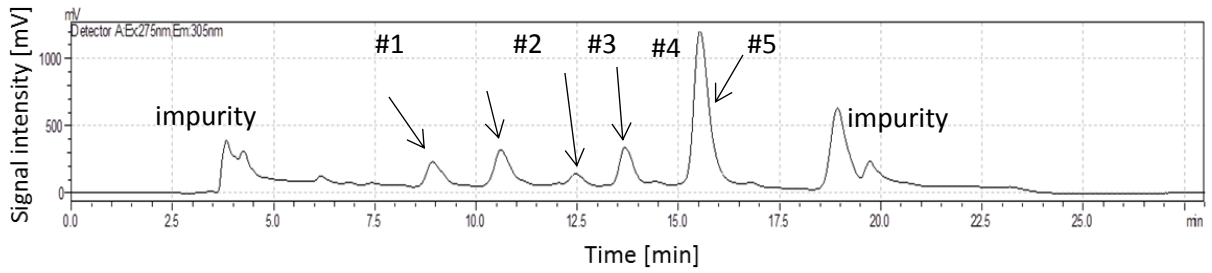

Figure 28 – Chromatogram of PA after Fenton reaction

The chromatogram of 1mM PA after Fenton reaction is showing the four major oxidation products #1-4 and the unmodified PA #5. Fluorescence detector Ex: 275 nm; Em: 305 nm. Recorded over 30 min.

3.3.3 Fenton product separation and identification by HPLC with MS detection

The PA standard has a predicted precursor m/z = 875 (874 Da + 1, because the ion is singly charged). The extracted MS chromatograms, showed m/z = 875 and m/z = 775 for the PA standard sample. The mass loss of 100 Da is due to the t-boc group, which degrades under the conditions as they occur in the positive mode of the mass spectrometer (**Scheme 12**).

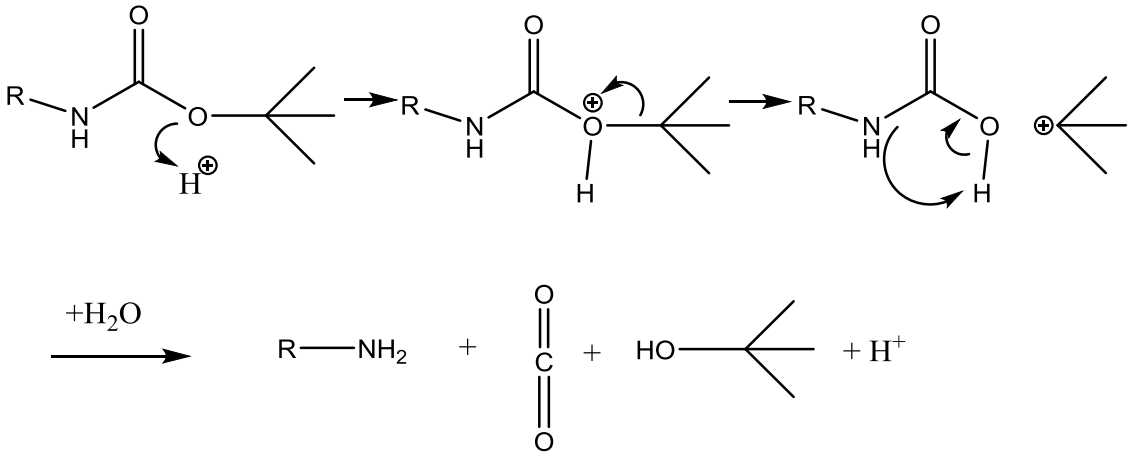

Scheme 12: Acidic t-boc removal mechanism

The m/z ratios of the separated products #1 to #4 all showed an increase of 16 Da from m/z = 875 to m/z = 891. The addition of 16 Da indicates the addition of one oxygen to the peptide for each product formed during the reaction. No products with +32 Da (i.e., the addition of two oxygen) were detected.

For further elucidation of the oxidation sites the individual samples were reduced and alkylated in order to obtain MS/MS data.

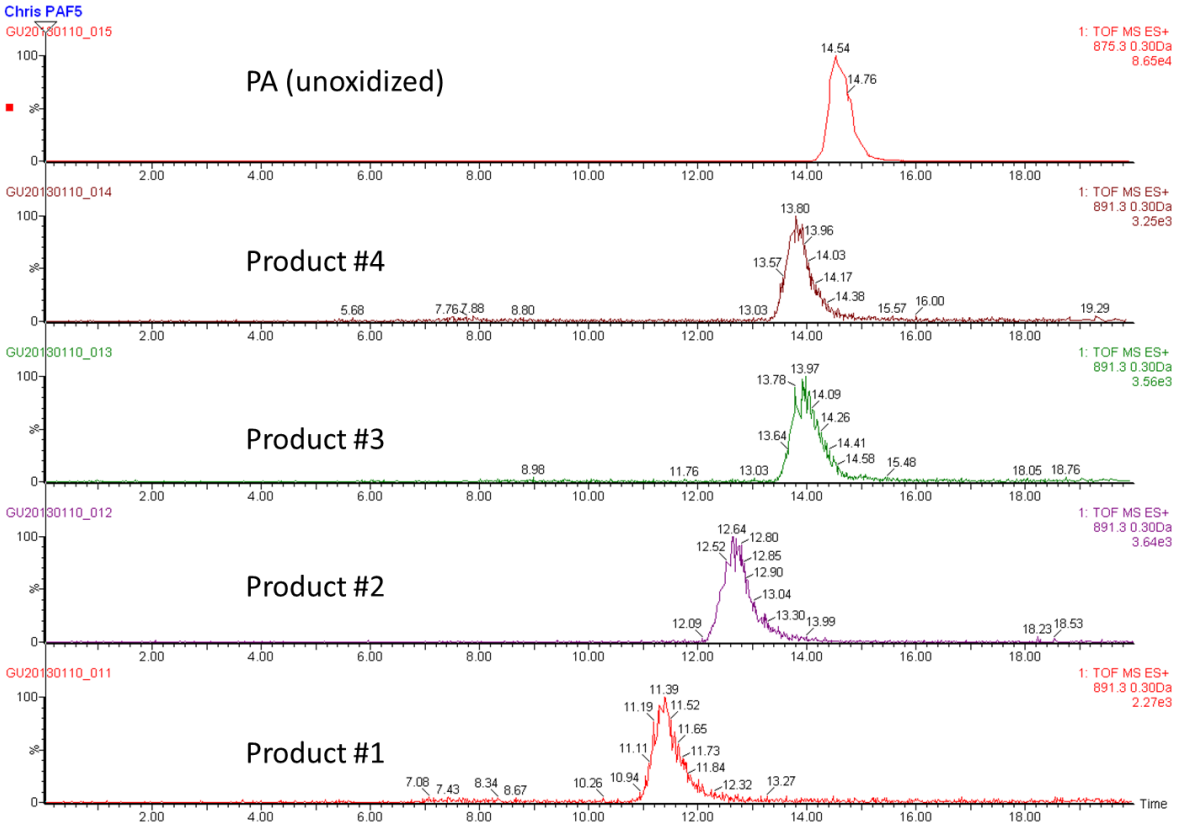

Figure 29: MS chromatograms of PA and the separated PA products stemming from a reaction with the Fenton reagent. The graphs show the extracted ion chromatograms of the four products formed from PA after the Fenton reaction and that of unreacted PA.

The PA samples were collected as described in section 3.3.2. and individually analyzed by mass spectrometry, see **Figure 29**. Products #1-4 were eluted after 11.39, 12.64 min, 13.97, and 13.80 min. respectively. Unoxidized PA was eluted after 15.54 min. After the subsequent reduction and alkylation the MS chromatograms shown in **Figure 30** indicated elution of products #1-4 after 14.94, 15.52, 16.30, and 16.66 min, respectively, while the PA standard eluted after 17.06 min. Based on only the elution times none of

these substances are identical. If a thiosulfinate had been formed during the Fenton reaction it would have been reduced by TCEP to yield the original PA peptide.[100] Considering that the elution times of all products differ, it is inferred that no thiosulfinate has been formed during the Fenton reaction.

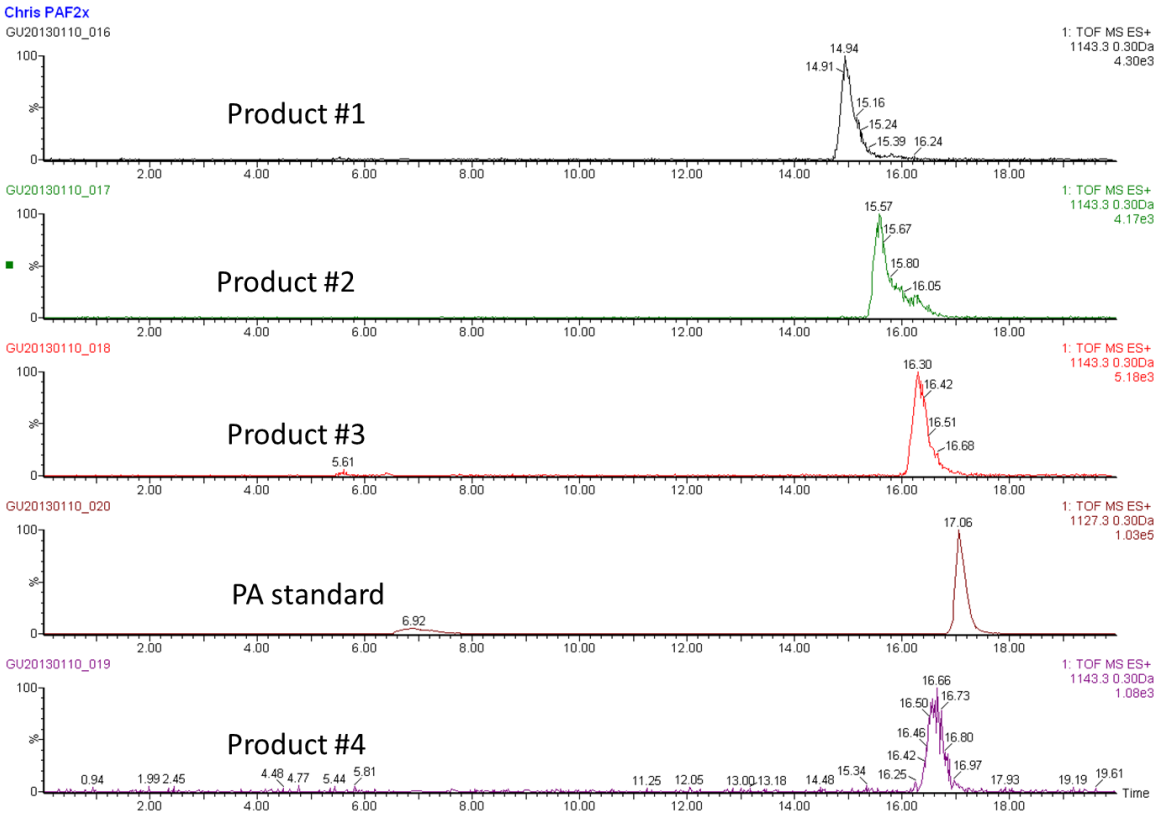

Figure 30: MS chromatograms of PA and the separated PA products stemming from a reaction with the Fenton reagent and following subsequent reduction and alkylation.

The graphs in **Figure 30** show the chromatograms of the four products formed from PA after the Fenton reaction and the unoxidized PA sample after reduction with TCEP and alkylation with NEM.

3.3.3.1 Experiments performed with equimolar and double concentration of the Fenton reagents

Experiments were performed with equimolar amounts of the Fenton reactants. In particular, PA (0.1 mM) was subjected to the Fenton reaction with Fe(II) (0.1mM) and H_2O_2 (0.1 mM) to as described in the methods section.

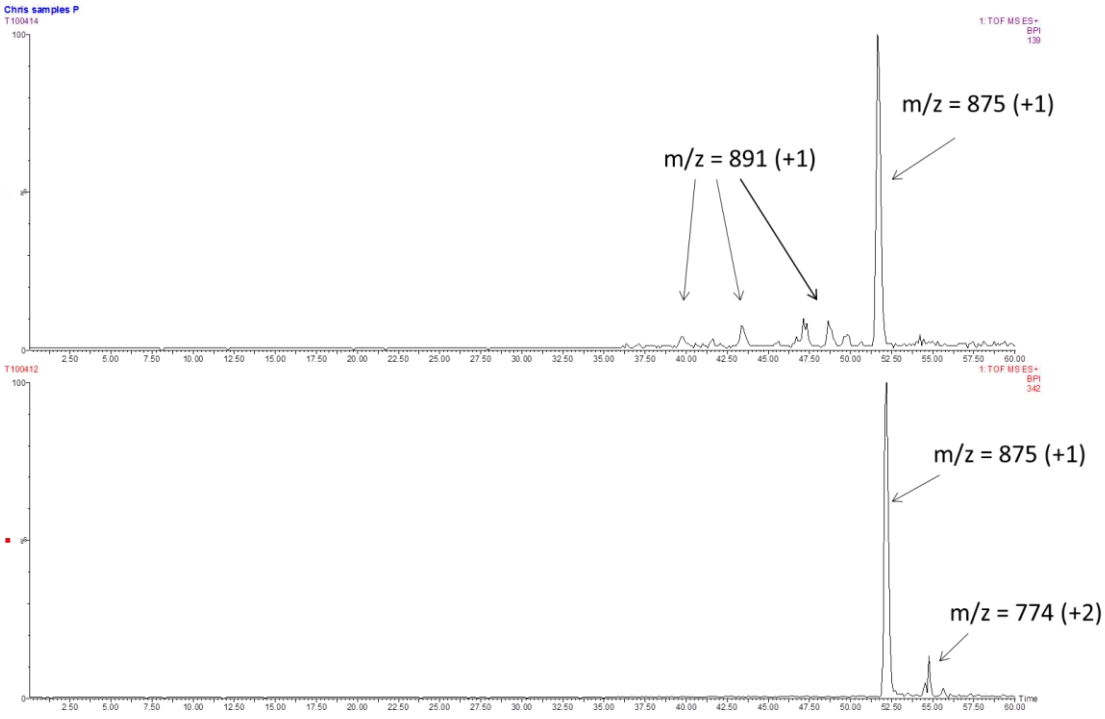

Figure 31: MS chromatogram of PA standard – upper part – and of PA after the Fenton reaction was performed with equimolar concentrations of the Fenton reagents – lower part. A linear gradient was applied with solvent A: 100% H_2O and solvent B 99.9:0.1 (v/v) ACN:TFA from 10% solvent B to 33% solvent B over 50 min.

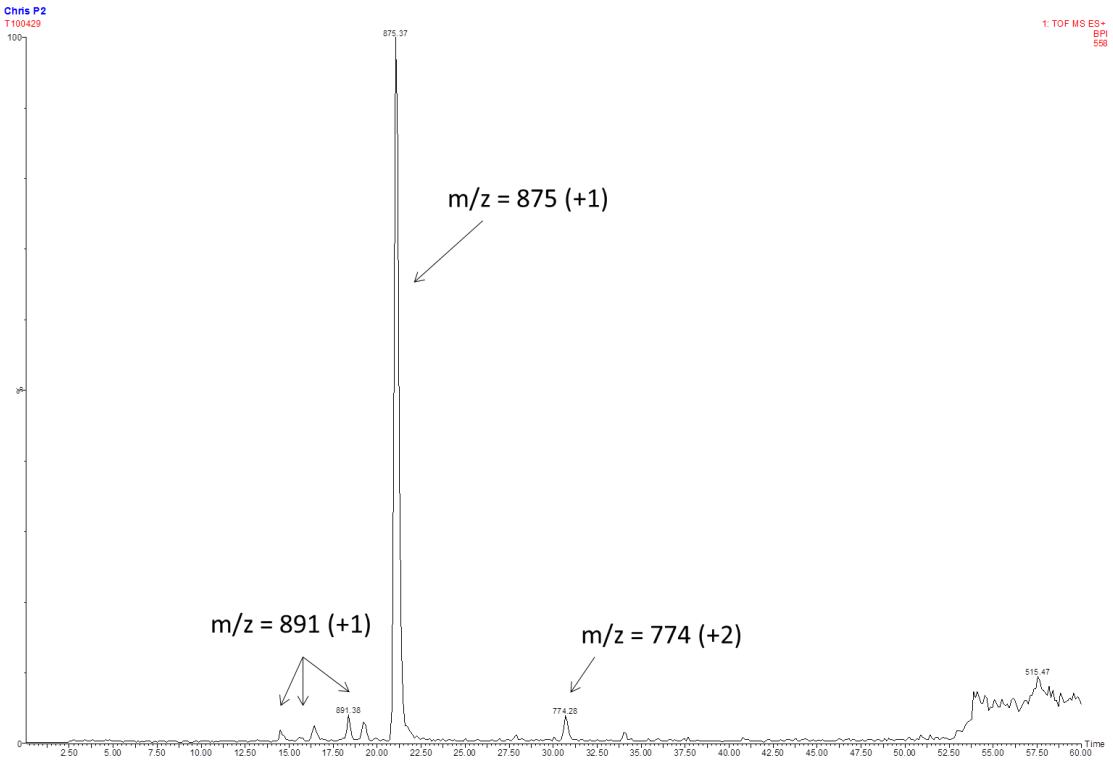

Figure 32: MS chromatogram of PA after the Fenton reaction was performed with double concentrations of the Fenton reagents. A linear gradient was applied with solvent A: 100% H_2O and solvent B: 99.9:0.1 (v/v) ACN:TFA from 20% solvent B to 65% solvent B over 50 min.

3.3.4 MS/MS data of individually reduced and alkylated oxidation products

The assignment of b^+ and y^+ ions was based on the predicted fragment ion masses minus 100 Da. Because the t-boc group of the peptide is unstable under the conditions under which the mass spectrometry is performed, the product ions did not contain the additional mass of the t-boc group.

The most abundant m/z signals recorded in all samples matched the a2 ion and the b2 ion. No b1 ions were found in the spectra as b1 ions can be considered as unstable, they are transformed to immonium ions by elimination of CO and H_2O, see **Scheme 13**.[108] The carboxyl group is protonated which leads to the loss of H_2O and the formation of an instable acylium ion which further cleaves off CO and results in the formation of a more stable immonium ion.

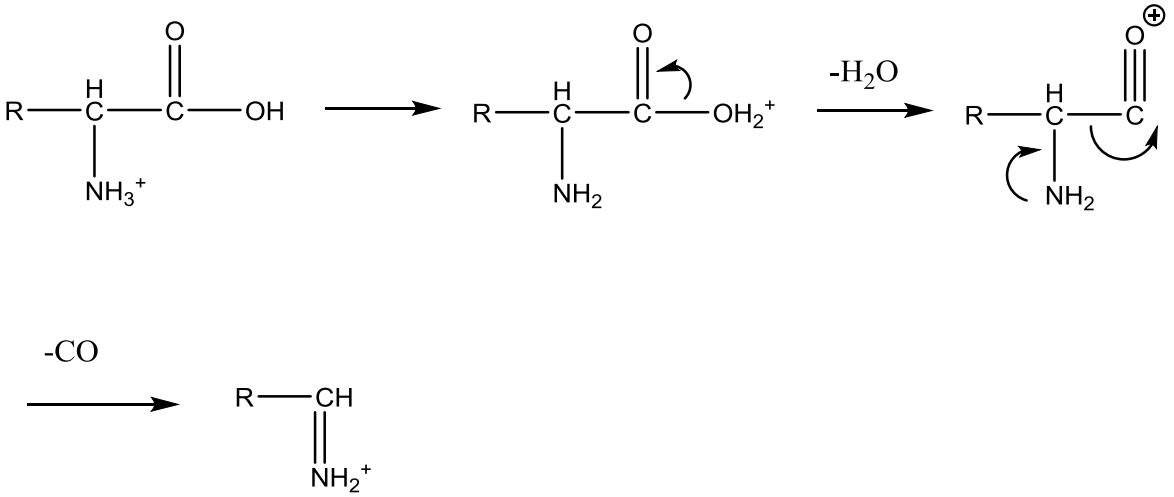

Scheme 13: Mechanism of the degradation of b1 ions

Ion fragments of the b class with two or more residues are stable enough to be observed in the mass spectra. The b2 ion formed from the precursor ion (MH+) is a positively charged, five membered, oxazolone ring, see **Scheme 14**.[109] The amide of the C-terminal amino acid (R_2) is positively charged by a proton. In a concerted reaction, the bond between this amide and the adjacent carbonyl group is likely to be broken. Then, a new bond involving the carbonyl group adjacent to the amino acid at the N-terminal

direction is formed followed by the formation of a C=N double bond. This results in a positive charge on the nitrogen in the newly formed oxazolone ring.

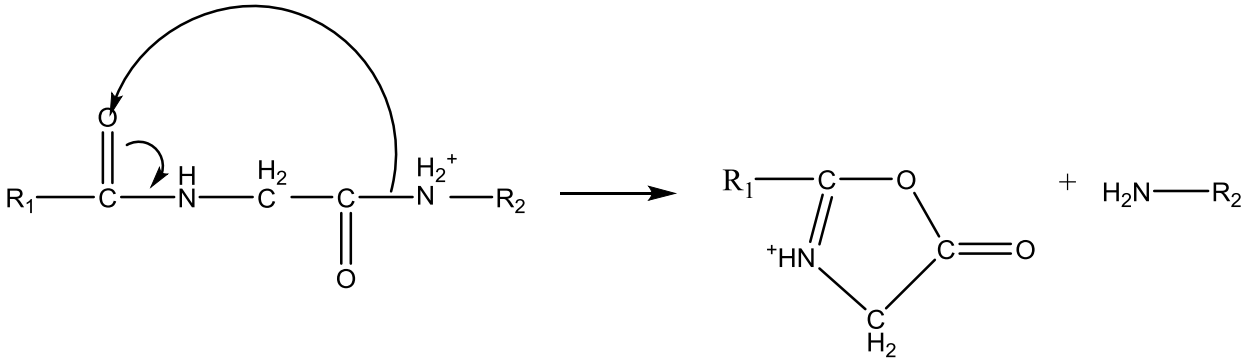

Scheme 14: Mechanism of the formation of a b2 ion

The b2 fragmentation ions can cleave CO (mass loss of 28 Da) to form a2 ions.[110] This loss is increased at higher collision energy.[110,111] The formation of a2 ions can occur during the $b_x \rightarrow b_{x-1}$ pathway. During this mechanism an a_x ion is formed, see **Scheme 15**.[112] In a concerted pathway the two bonds connected to the carbonyl group in the oxazolone ring are breaking off and release a neutral CO residue. This mechanism has been found to be energetically favored over a stepwise breakdown.[113] As shown in **Scheme 15** the two bonds connected to the carbonyl group are cleaved off and release CO.

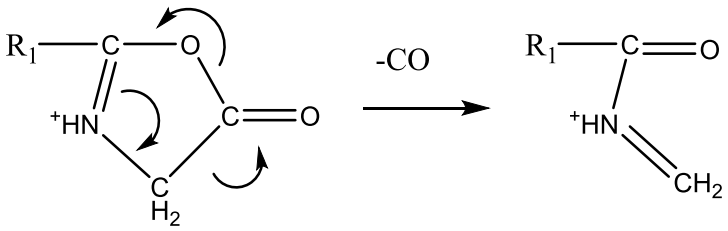

Scheme 15: Mechanism of the formation of an a2 ion

3.3.4.1 MS/MS data of the PA standard

From the MS/MS data of the PA standard sample, shown in **Figure 33**, a very good coverage of b+ and y+ product ions is derived. The precursor ion with m/z = 1127 (singly charged) was the predicted value for PA after reduction and alkylation with two NEM (one at each Cys residue). The m/z value was calculated as follows. 874 (PA) + 1 (+1 proton for the charge) + 2x125 (two NEM) + 2 (two hydrogen added during reduction) = 1127.

Due to the loss of the t-boc group under the MS/MS conditions the precursor ion had an m/z value of 1027.

The most abundant product ions are the a2 ion and b2 ion. No b1 ion has been detected. The b3, b4 ions show about 40% intensity relative to the a2 ion and b5 ion shows 20% intensity. The y2, y3 and y4 ions have a relative intensity of ca. 30% and the y1 has 20% relative intensity. The relative signal intensities of the MH+ and MH+ -NH_3 are 30% and 15%.

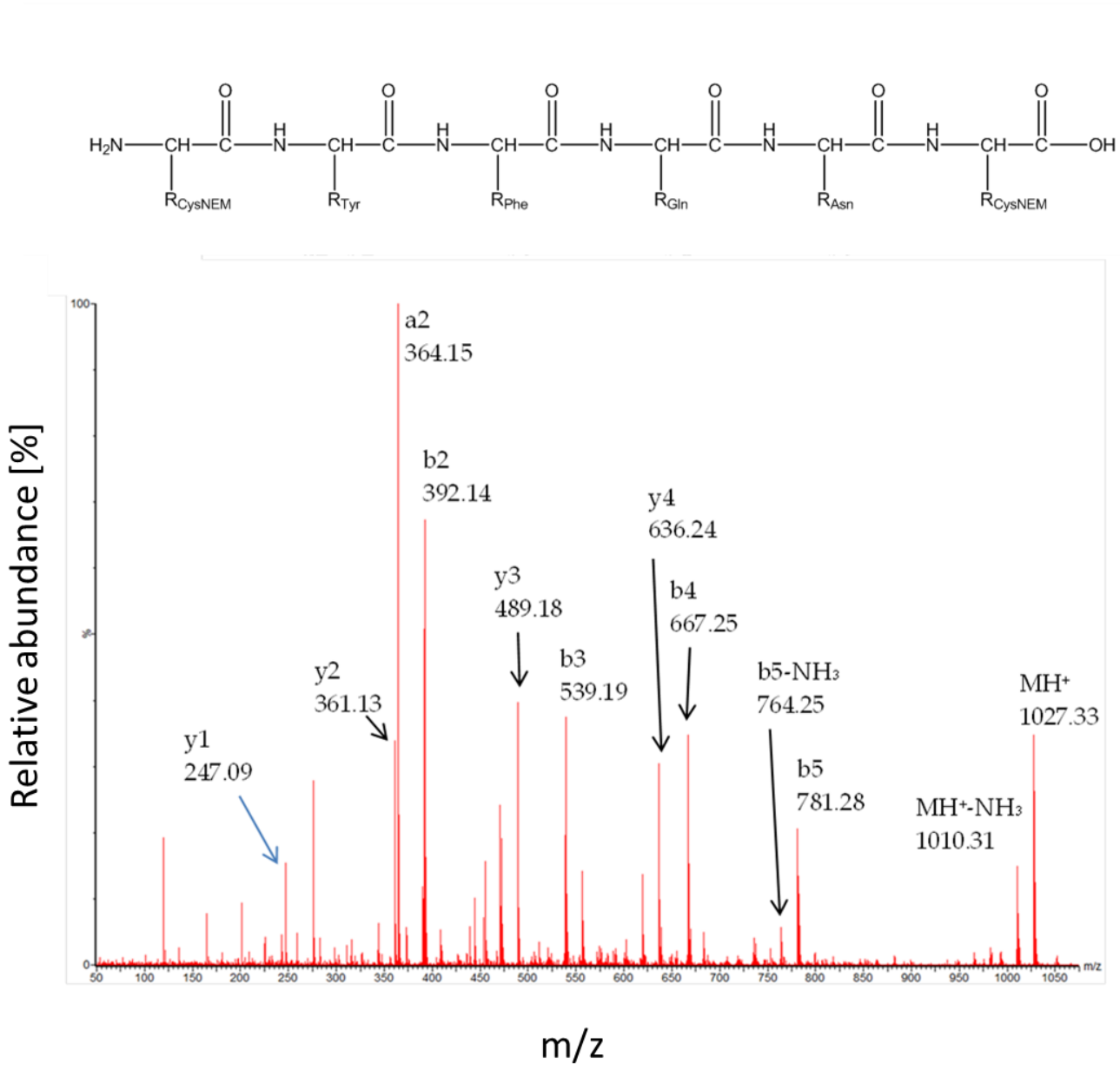

Figure 33: MS/MS spectrum of 1mM PA after reduction with TCEP and alkylation of the Cys-residues with NEM. The precursor ion has an m/z=1127.3. The ions have a mass of 100 Da less due to loss of the t-boc group during the fragmentation process.

3.3.4.2 MS/MS data of the separated PA products after the Fenton reaction

The MS/MS data of products #1 to #4 (**Figure 34** to **Figure 38**) are all based on the precursor ion m/z = 1143. This is the predicted value for PA after reduction and alkylation with two NEM attached to the Cys residues plus one additional oxygen present in the peptide. This also shows the presence of a non-reducible oxygen, i.e. it excludes the formation of a thiosulfinate which can be reduced by TCEP, see section 3.2.3.5 and **Scheme 10**.[100] Products # 1, 2 and 4 had identical ion coverage and match the product ion distribution for a predicted oxidized Phe residue. The ion coverage for product #3 fits the product ions distribution for the prediction of oxidized Tyr in the peptide.

According to the MS and MS/MS data the Gln, Asn and Cys residues were not oxidized during Fenton reaction. Since the four oxidation products were well separated it was possible to further identify the exact position of the additional oxygen on the respective aromatic residue.

3.3.4.3 MS/MS data of PA product #1

The predicted ion coverage for an oxidized phenylalanine residue matched the MS/MS data shown in **Figure 34** that has been recorded for product #1. The most intense ions are the a2 (100% signal intensity relative to a2) and b2 (65%) ions. Both m/z values consistent with a Cys(NEM)-Tyr residue. The b3 ion has 26%, b4 and b5 ions have 5% of the signal intensity of the a2 ion. The b3, b4 and b5 ions match the predicted m/z values

for a hydroxylated Phe residue (+16 Da). The y2 ion has a signal intensity of 33% and the other y-ions 6-10%. The y4 ion matches the predicted m/z value for an hydroxylated Phe residue (+16 Da) and the y3, y2 and y1 ions match the m/z values of the PA standard indicating no oxidation of the Asn, Gln or Cys(NEM) residues. The precursor ion (MH+) was not detected but the fragmentation pattern is based on the precursor m/z = 1143.3 which is the predicted value for product #1.

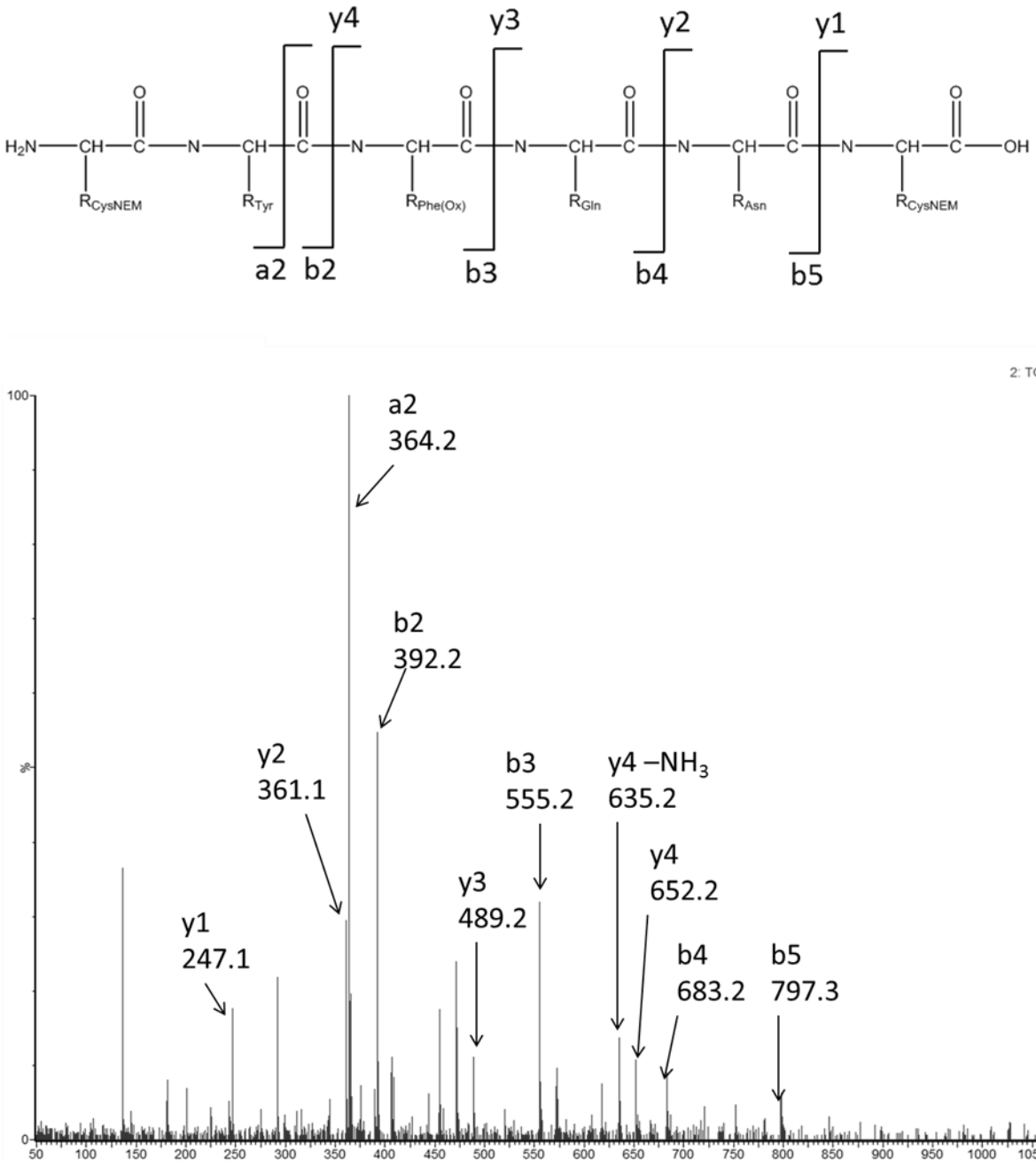

Figure 34: MS/MS spectrum of product #1 after reduction with TCEP and alkylation of the Cys-residues with NEM.

The ions have a mass of 100 Da less due to loss of the t-boc group during the fragmentation process. MS/MS spectrum of Product #1 after reduction and alkylation with NEM

3.3.4.4 MS/MS data of PA product #2

The MS/MS data of product #2, shown in **Figure 35**, matched the ions predicted for a hydroxylated Phe residue. The a2 ion (100%) and the b2 ion (79%) contained no additional oxygen on the Tyr residue. The b3 ion (43%) and the b4, b5 ions (9-12%) had an additional mass of 16 Da indicating one additional oxygen had been attached to the Phe residue. The y4 ion (6%) had an additional 16 Da and the y3 (16%), y2 (40%) and y1 (9%) ions had the same mass as the standard sample ions. This verified the hydroxylation of the Phe residue. The relative signal intensities were similar to the results for product #1, spectrum shown in **Figure 34**. As in the MS/MS spectrum of product #1 the precursor ion (MH+) has not been detected, probably due to high fragmentation energy.

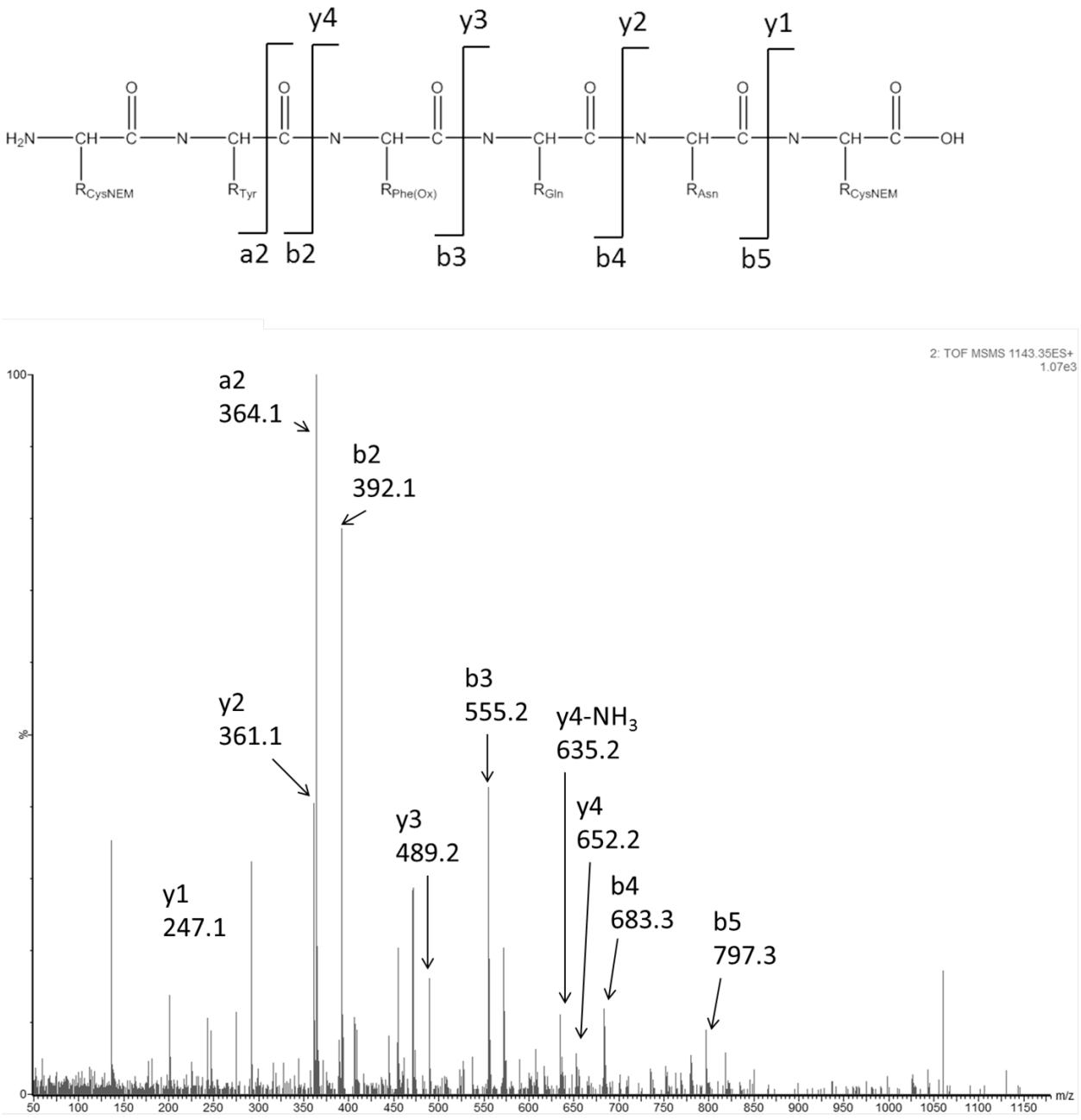

Figure 35: MS/MS spectrum of product #2 after reduction with TCEP and alkylation of the Cys-residues with NEM. The ions have a mass of 100 Da less due to loss of the t-boc group during the fragmentation process.

3.3.4.5 MS/MS data of PA product #3

For product #3 the MS/MS data (**Figure 36**) matched the predicted fragmentation pattern of PA with the Tyr residue hydroxylated to 2,4-dihydroxyphenylalanine or 3,4-dihydroxyphenylalanine. The most abundant fragment ion is the b2 ion, the a2 ion accounts for only 55% relative intensity. Both the b2 and a2 ion as well as the b3 (58%), b4 (50%) and b5 (31%) ion match the predicted m/z value of DOPA in this PA sample. The y5-NH_3 ion (51%) but not the y5 ion was found matching the predicted value of DOPA in the PA sample. The y5-NH_3 ion may have formed from the MH+ -NH_3 ion. The y4 (36%), y3 (66%), y2 (55%) and y1 (22%) ions are consistent with the predicted values for non-oxidized residues as they occur in the standard sample. The MH+ (59%) and MH+ -NH_3 (16%) match the predicted value for an oxidized PA species.

The ion count of the fragments differs from the products #1 and #2 because Tyr but not Phe has been hydroxylated during the Fenton reaction. Also, the a2 ion intensity was less than that of the b2 ion. It appears that the a2 ion formation is less favored for DOPA compared to Tyr.

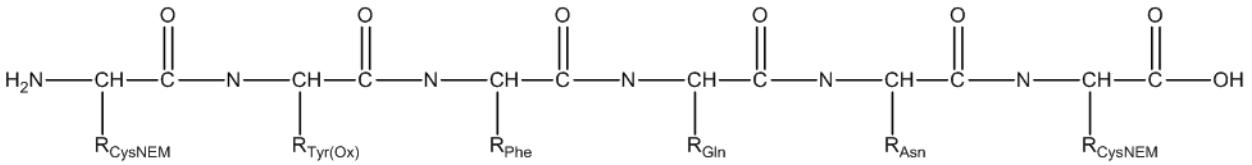

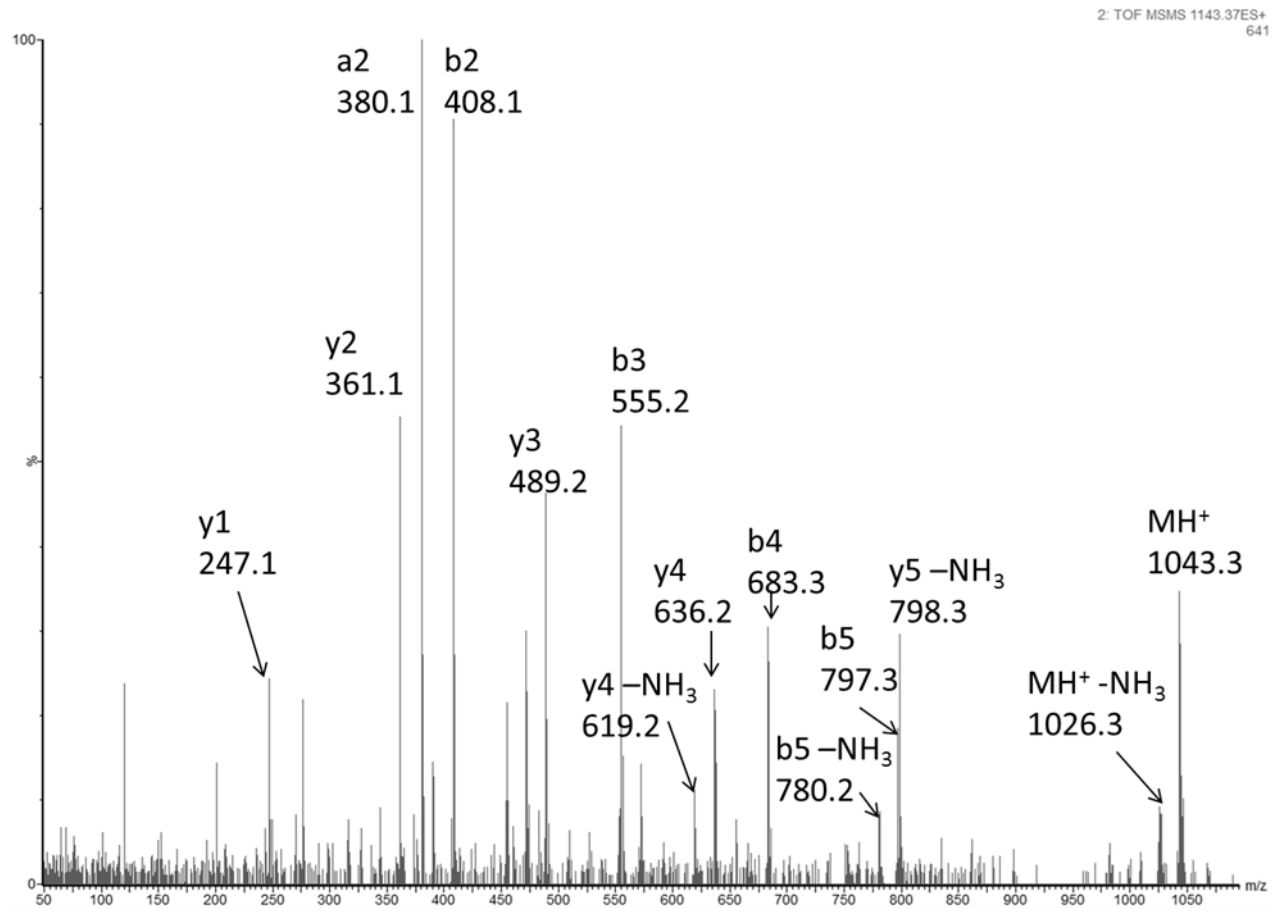

Figure 36: MS/MS spectrum of product #3 after reduction with TCEP and alkylation of the Cys-residues with NEM. The ions have a mass of 100 Da less due to loss of the t-boc group during the fragmentation process.

3.3.4.6 MS/MS data of PA product #4

The MS/MS spectrum of product #4 (**Figure 37**) matched the predicted ion coverage for a hydroxylated Phe residue. The a2 (100%) and b2 (51%) ions indicate that the Tyr residue remained unoxidized. The b3 (59%), b4 (71%) and b5 (18%) ions all match the predicted values for hydroxylated Phe residues in PA. The y4 (35%) and y4-NH_3 (16%) ions included the hydroxylated Phe residue, while the y3 (54%), y2 (29%) and y1 (18%) ions contained no oxidized residues matching the data of the standard sample. The MH+ (52%) and MH+ -NH_3 (13%) ions showed an additional 16 Da compared to the PA standard sample.

In comparison with the spectra of products #1 and #2 (**Figure 34** and **Figure 35**) which also contained hydroxylated phenylalanine, the intensities of the ion count of the b4 and y3 ions was significantly higher in the spectrum #4. The precursor ion MH+ was detected only in the spectrum of product #4 indicating less intensive fragmentation which resulted in a different overall distribution of the fragment ion.

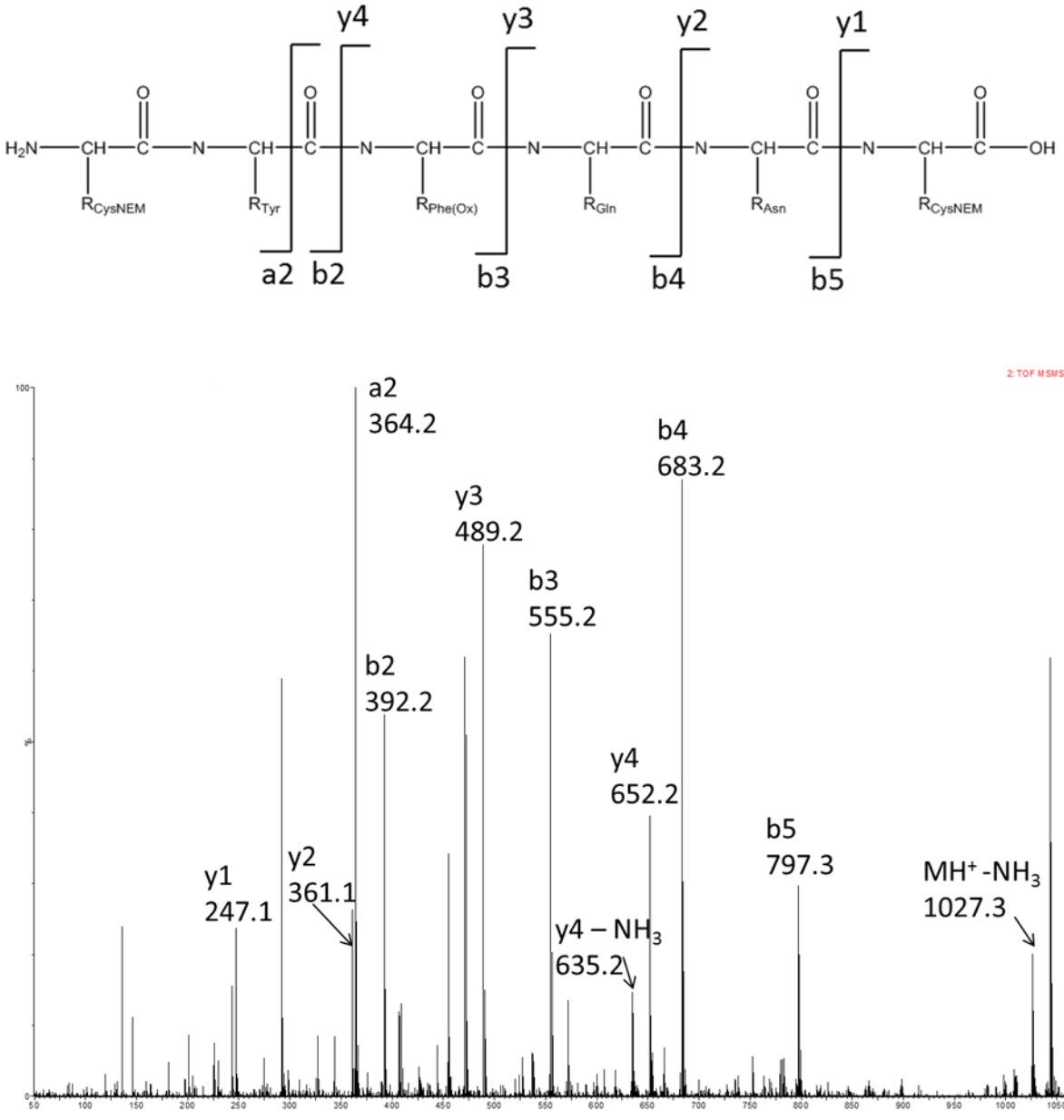

Figure 37: MS/MS spectrum of product #4 after reduction with TCEP and alkylation of the Cys-residues with NEM. The ions have a mass of 100 Da less due to loss of the t-boc group during the fragmentation process.

3.3.4.7 MS/MS data of PA product #5

The MS/MS data of product #5 (**Figure 38**) matched the predicted ions for PA standard. The a2 (100%), b2 (67%), b3 (37%) and b2 (67%) ions were all matching the predicted values for unmodified PA residues. The y1 (15%), y2 (34%), y3 (40%), y4-NH_3 (14%) ions and y4 (30%) ion as well as the MH^+ -NH_3 (15%) and MH^+ (35%) ion values are in agreement with this finding. Product #5 was the most abundant of the five products isolated after Fenton reaction was applied to PA. No oxidation or dimerization has been detected in product #5.

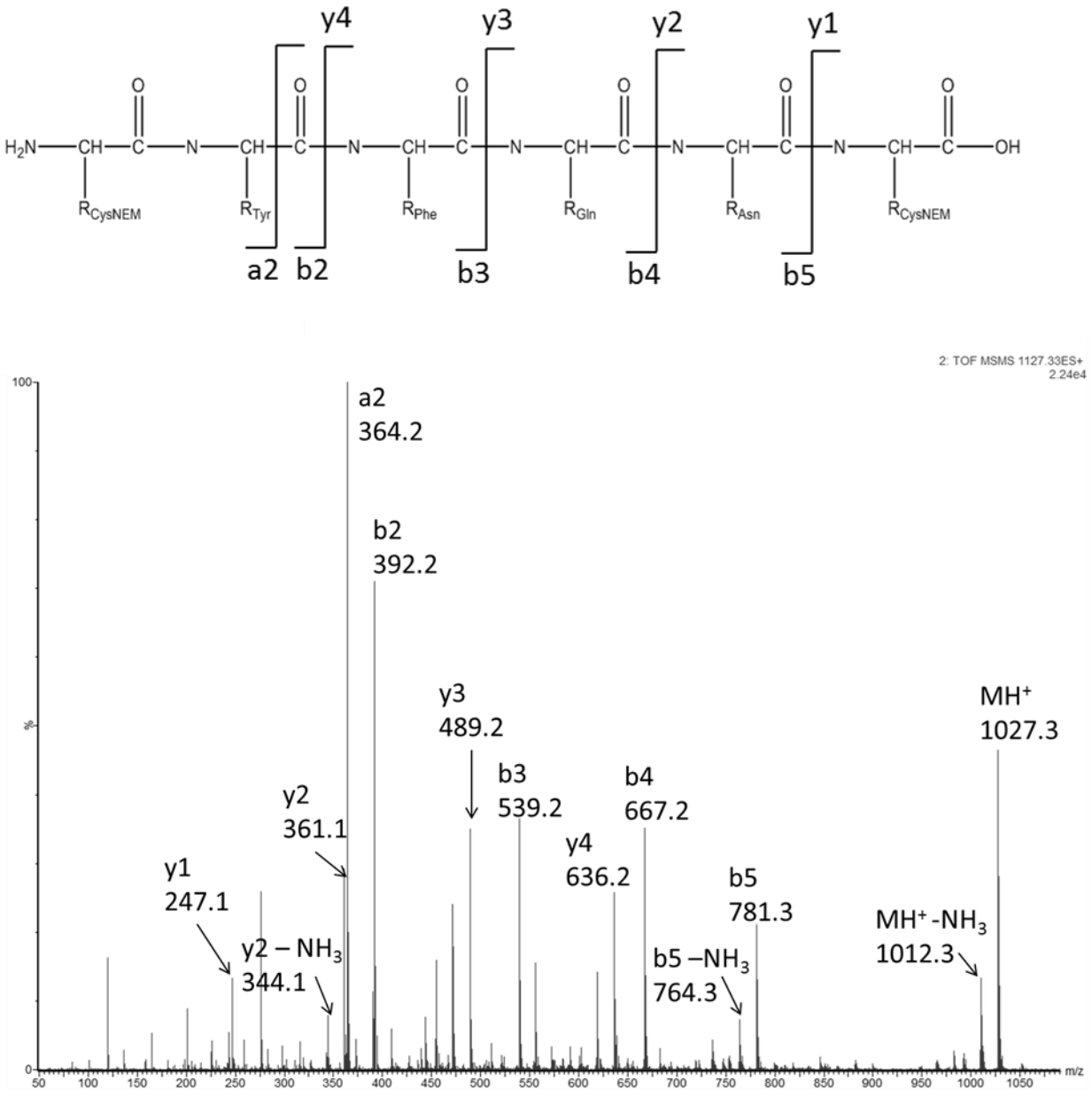

Figure 38: MS/MS spectrum of product #5 after reduction with TCEP and alkylation of the Cys-residues with NEM. The ions have a mass of 100 Da less due to loss of the t-boc group during the fragmentation process.

3.3.5 Identification of hydroxyphenylalanine isomers by amino acid analysis

Amino acid analysis allowed to identify hydroxyphenylalanine isomers formed during Fenton reaction. The amino acids 2-, 3- and 4-hydroxyphenylalanine were well separated (**Figure 44**) and their elution times had been assigned as follows: 4-hydroxyphenylalanine eluted after 7.8 min and 2-hydroxyphenylalanine after 11.2 min. The substance eluting after 8.9 min was proposed to be 3-hydroxyphenylalanine.[114] No additional products were detected of these standards. After hydrolysis was performed with these standards no additional products have been detected. The DOPA standard sample eluted after 5.8 min and after hydrolysis of the DOPA standard an additional product was detected after 4.5 min. This additional product did not form in sufficient yields for performing a meaningful ^{1}H-NMR spectrum interpretation. Nevertheless, the additional DOPA product has been formed only after its hydrolysis.

3.3.5.1 Amino acid analysis of PA standard

The samples used for amino acid analysis were individually collected after the Fenton reaction and were further processed. The preparation steps required for the amino acid analysis lead to significant sample loss as some sample may have spilled during the hydrolyzation process. Therefore the amino acid analysis data are of interest only qualitatively. Individual peak heights can therefore not represent the total amount of product formed. **Figure 39** shows the chromatogram of the hydrolyzed PA standard sample. It contained 4-hydroxyphenylalanine, eluting after 7.9 min and maximum peak

height of 4000 mV, and traces of the other hydroxyphenylalanine isomers. The trace levels of those isomers may have originated from the hydrolysis process. Although the samples were evacuated several times before hydrolysis some oxygen may have remained in the sample solution. Those oxygen residues may be responsible for the formation of hydroxyphenylalanine isomers. Due to its low fluorescence intensity Phe could not be detected but it was confirmed by MS-analysis that Phe was not modified in this sample.

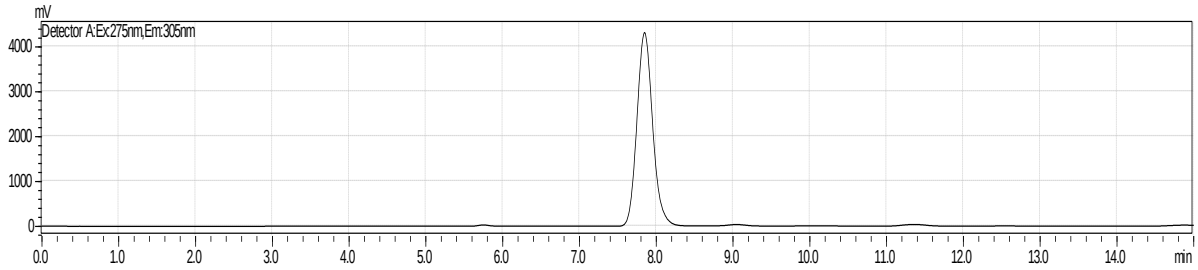

Figure 39: HPLC chromatogram of hydrolyzed PA standard

HPLC chromatogram with a fluorescence detector of hydrolyzed PA standard. 1% NaCl + 1% acetic acid in H_2O, isocratic elution. Ex: 275 nm; Em: 305 nm. Recorded over 15 min.

3.3.5.2 Amino acid analysis of PA Fenton product #1

The chromatogram of hydrolyzed product #1 contained 4-hydroxyphenylalanine, eluting after 7.8 min and a max. peak height of 800 mV, and traces of other hydroxyphenylalanine isomers, see **Figure 40**. Hereby, the signals of the trace levels

appear more intense than in the standard sample. For example, the peak height of 4-hydroxyphenylalanine with 800 mV is less than that of the standard sample with 4000 mV. Considering that the additional peaks occur at the same levels they appear more intense compared to the main peak.

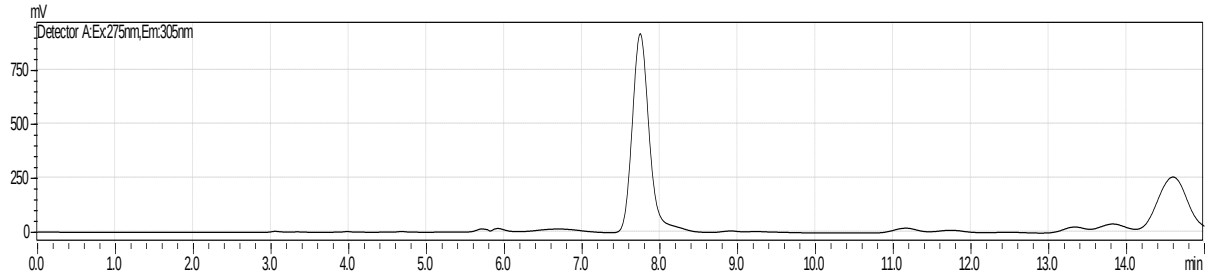

Figure 40: HPLC chromatogram of hydrolyzed product #1

HPLC chromatogram from a fluorescence detector of hydrolyzed product #1 following the Fenton reaction. 1% NaCl + 1% acetic acid in H_2O, isocratic elution. Ex: 275 nm; Em: 305 nm. Recorded over 15 min.

This suggests that Phe was oxidized to 4-hydroxyphenylalanine during the Fenton reaction. The new PA product therefore contained two 4-hydroxyphenylalanine residues. One was originally present in PA and one was newly formed. The MS/MS data supported this notion since they prompt to the fact that no hydroxylated Tyr, but a hydroxyphenylalanine has been formed.

3.3.4.3 Amino acid analysis of PA Fenton product #2

The chromatogram of hydrolyzed product #2, **Figure 41**, contained 4- and 3-hydroxyphenylalanine eluting after 7.2 and 8.4 min with max. peak heights of 750 and 460 mV.

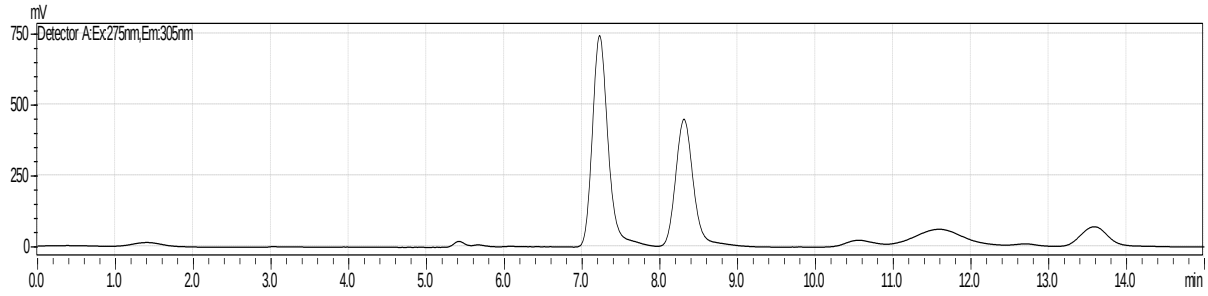

Figure 41: HPLC chromatogram of hydrolyzed product #2

HPLC chromatogram from a fluorescence detector of hydrolyzed product #2 following the Fenton reaction. 1% NaCl + 1% acetic acid in H_2O, isocratic elution. Ex: 275 nm; Em: 305 nm. Recorded over 15 min.

It is likely that 3-hydroxyphenylalanine was formed through Fenton reaction induced oxidation of the Phe residue in PA. Please note that 4-hydroxyphenylalanine was already present in the sample according to the MS/MS data.

3.3.5.4 Amino acid analysis of PA Fenton product #3

Product #3 contained DOPA, eluting after 4.5 and 6.0 min with peak heights of 40 mV and 80 mV. Due to the very low peak intensities of the main product trace amounts of the other hydroxyphenylalanines occurred in the spectrum, **Figure 42**.

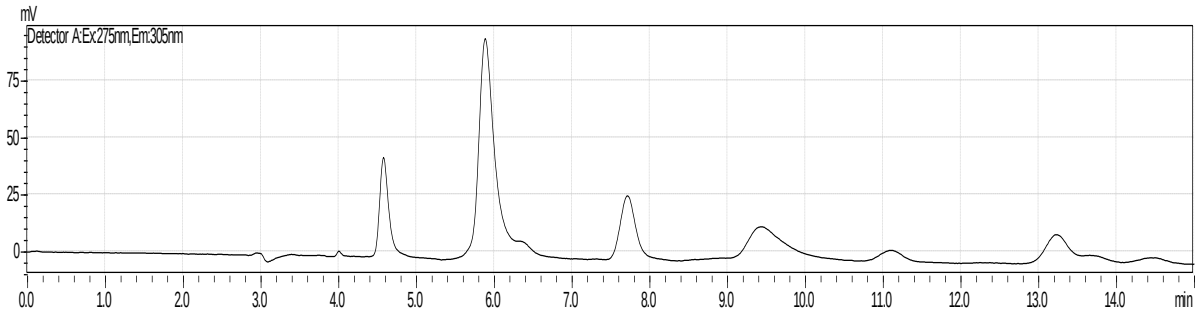

Figure 42: HPLC chromatogram from a fluorescence detector of hydrolyzed product #3 following the Fenton reaction. 1% NaCl + 1% acetic acid in H_2O, isocratic elution. Ex: 275 nm; Em: 305 nm. Recorded over 15 min.

No Phe residue could be detected due to its low fluorescence yield. However, the presence of unmodified Phe and hydroxylated Tyr in this sample was proven by the MS/MS data.

3.3.5.5 Amino acid analysis of PA Fenton product #4

Product #4 contained 4- and 2-hydroxyphenylalanine eluting after 7.8 min and 11.4 min, respectively, with peak heights of 1000 mV and 500 mV indicating that Phe was oxidized to 2-hydroxyphenylalanine, see **Figure 43**. No oxidation occurred on the Tyr residue according to the MS/MS data.

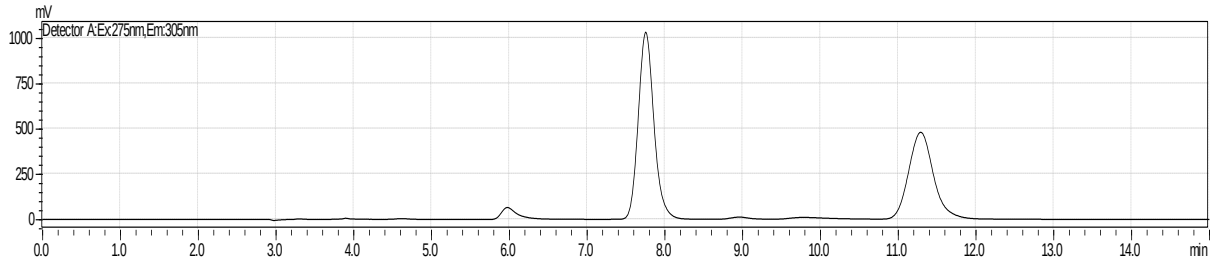

Figure 43: HPLC chromatogram of hydrolyzed product #4

HPLC chromatogram from a fluorescence detector of hydrolyzed product #4 following the Fenton reaction. 1% NaCl + 1% acetic acid in H_2O, isocratic elution. Ex: 275 nm; Em: 305 nm. Recorded over 15 min.

3.3.6 Preparation of Tyr isomers

The chromatogram that has been recorded during the separation of three hydroxyphenylalanine isomers formed from Phe by the Fenton reaction is shown in **Figure 44**.

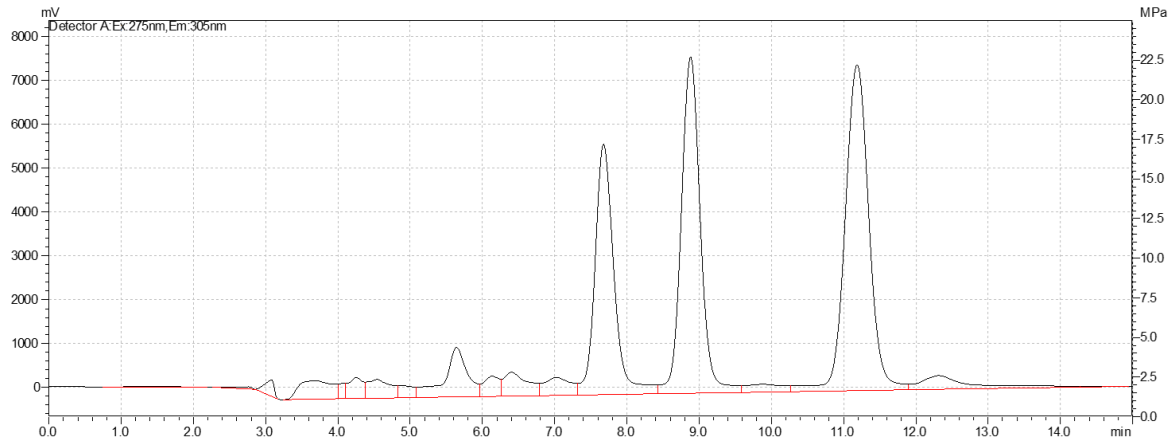

Figure 44: HPLC chromatogram of Phe after Fenton reaction

HPLC chromatogram from a fluorescence detector of 1mM Phe following the Fenton reaction. 1% NaCl + 1% acetic acid in H_2O, isocratic elution. Ex: 275 nm; Em: 305 nm. Recorded over 15 min.

The elution times of 2- and 4-hydroxyphenylalanine were verified by comparison with elution times of the known standards. 3-hydroxyphenylalanine eluted after 8.9 min. The structures were verified with collection of the fractions by NMR analysis.

3.3.7 Structural verification of the Tyr isomers by ^{1}H NMR analysis

The structure of Tyr isomers was verified by ^{1}H NMR analysis. Of particular interest was the aromatic region of chemical shifts in the range of 6-8 ppm. The NMR spectra were assigned according to the predicted chemical shifts and the expected peak splitting. 3-hydroxyphenylalanine was synthesized as it was unavailable as a standard and its structure needed to be verified by NMR. Structures of 2- and 4-hydroxyphenylalanine, which were commercially available, were verified by ^{1}H-NMR to strengthen the assignments of their elution times in the amino acid analysis section.

3.3.7.1 3-Hydroxyphenylalanine

The ^{1}H NMR spectrum of 3-hydroxyphenylalanine is shown in **Figure 45**. The chemical shifts are as follows: ^{1}H NMR (600 MHz, D_2O) δ 7.27 (t, J = 8 Hz, 1H), 6.85 (d, J = 7 Hz, 1H), 6.82 (d,d J = 8Hz J= 3Hz, 1H), 6.79 (s, 1H).

Based on the chemical shifts and the J-coupling values the substance was identified as 3-hydroxyphenylalanine. The signal at 7.27 ppm shows a triplet with 8 Hz J-coupling which indicates two hydrogens in ortho position on the ring. This peak was assigned to the hydrogen #5. The signal at 6.79 ppm showed a single peak indicating no adjacent hydrogen. This signal was assigned to hydrogen #2. The signals at 6.85 and 6.82 ppm both showed doublets with 8 Hz J-coupling indicating one neighboring hydrogen in ortho position. At 6.82 ppm a doublet of a doublet was identified with 2 Hz J-coupling which indicates one hydrogen in meta position. The signals were assigned to hydrogens #4 and #6. Both have adjacent hydrogens at the same relative positions and the assignment was based on prediction of the chemical shift.

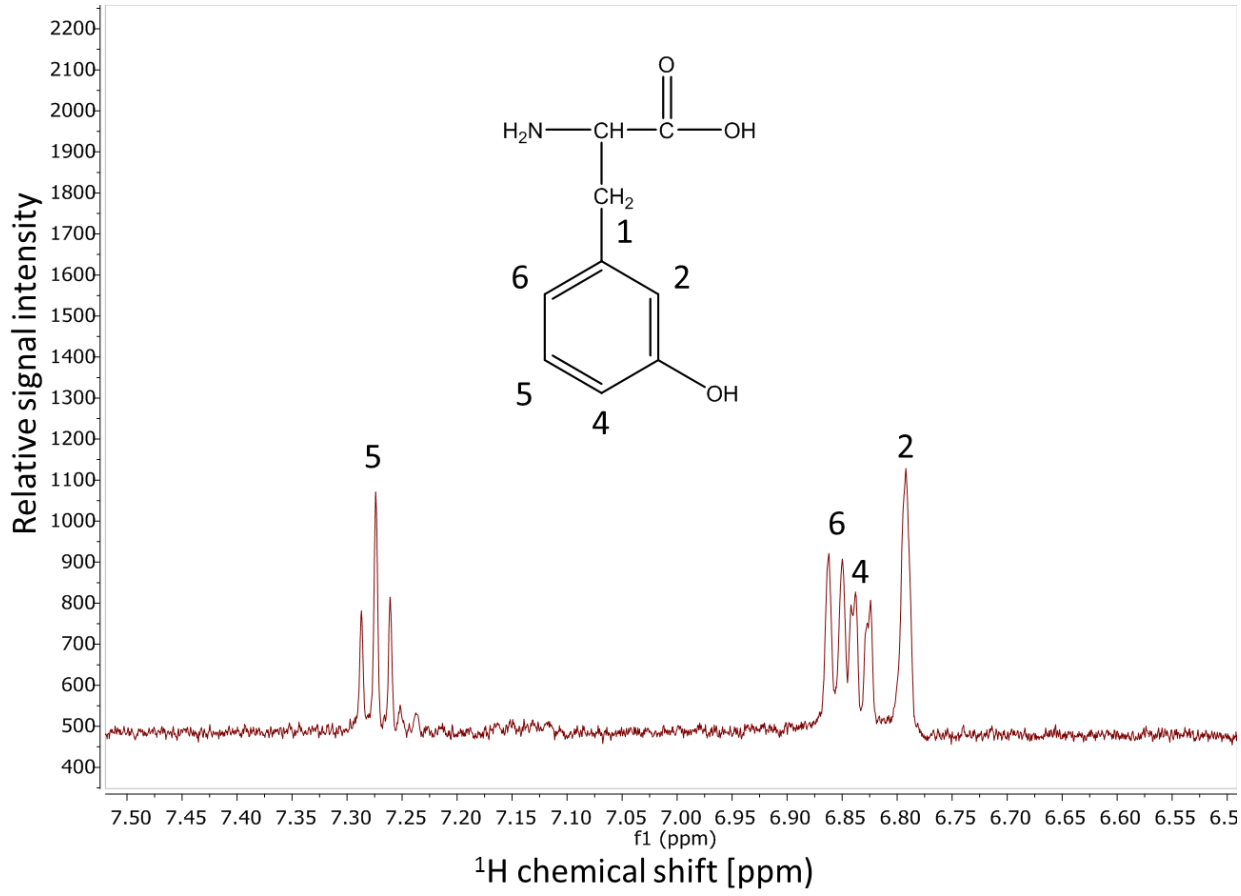

Figure 45: ^{1}H-NMR spectrum of 3-hydroxyphenylalanine, extracted from Phe oxidized by the Fenton reaction. The ^{1}H-NMR spectrum was recorded with 3-hydroxyphenylalanine dissolved in D_2O and a 600 MHz NMR instrument. The spectrum shows aromatic residues between 6.7 and 7.4 ppm.

3.3.7.2 2-hydroxyphenylalanine

Chemical shifts of 2-hydroxyphenylalanine (**Figure 46**): ^{1}H NMR (600 MHz, D_2O) δ 7.17 (t, J = 8 Hz, 1H), 7.14 (d, J = 7 Hz, 1H), 6.86 (t, J = 8 Hz, 1H), 6.87 (d, J = 7 Hz).

The signal at 7.17 ppm shows a triplet with 8 and 2 Hz J-coupling. This means it has two hydrogens in ortho position and one hydrogen in meta position. Based on the predicted chemical shift the signal was assigned to hydrogen #4. The signal at 7.14 ppm shows a doublet with 7 Hz J-coupling indicating one hydrogen in ortho position. It was assigned to hydrogen #6.

The signal at 6.86/6.87 ppm is a triplet. The chemical shifts of both hydrogen #3 and #5 were predicted in this range. The triplet showed a 2nd order coupling effect rising in the upfield direction, however, in this case a downfield direction was expected. Integration of the three peaks of the triplet showed a ratio of 1:3:2. The same ratio can be expected if a triplet signal of hydrogen #5 and a doublet of hydrogen #3 are overlaid. Therefore hydrogen #5 was assigned to 6.86 ppm and hydrogen #3 was assigned to 6.87 ppm.

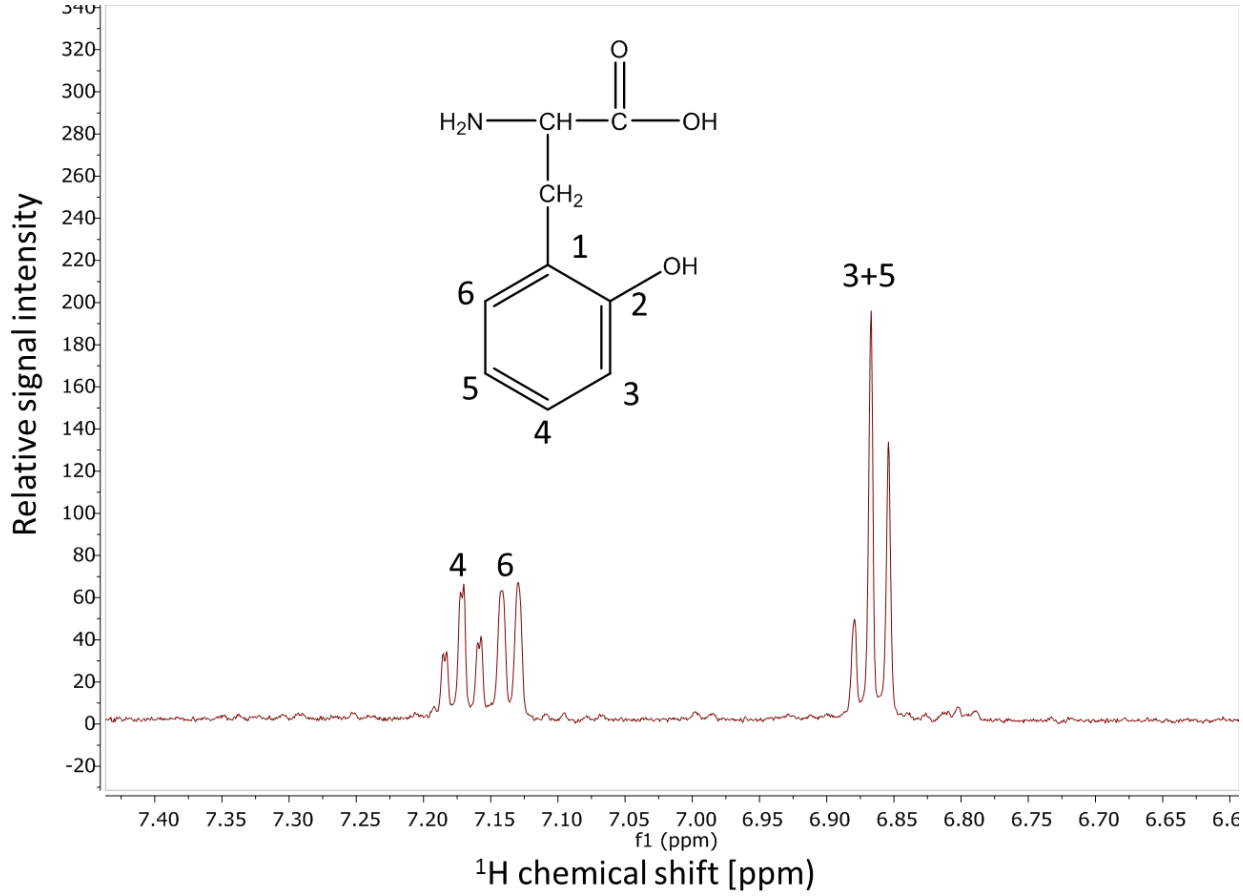

Figure 46: ^{1}H-NMR spectrum of 2-hydroxyphenylalanine.

The ^{1}H-NMR spectrum was recorded with 2-hydroxyphenylalanine dissolved in D_2O and a 600 MHz instrument. The spectrum shows the aromatic residues between 6.8 and 7.3 ppm. The numbers indicate the hydrogen signals occurring in the spectrum and their assigned position on the aromatic ring

3.3.7.3 4-hydroxyphenylalanine

The chemical shifts of 4-hydroxyphenylalanine (**Figure 47**) are: ^{1}H NMR (600 MHz, D_2O) δ 7.11 (d, J = 9 Hz), 6.82 (d, J = 9 Hz).

Due to the symmetric structure of 4-hydroxyphenylalanine hydrogen #1and #5 as well as #2 and #4 have identical chemical shifts. The signal at 7.11 ppm showed a doublet and was assigned to hydrogen #1 and #5 and the signal at 6.82 ppm with a doublet was assigned to hydrogen #2 and #4. The additional peak splitting can be attributed to virtual coupling which is a common effect in aromatic systems.

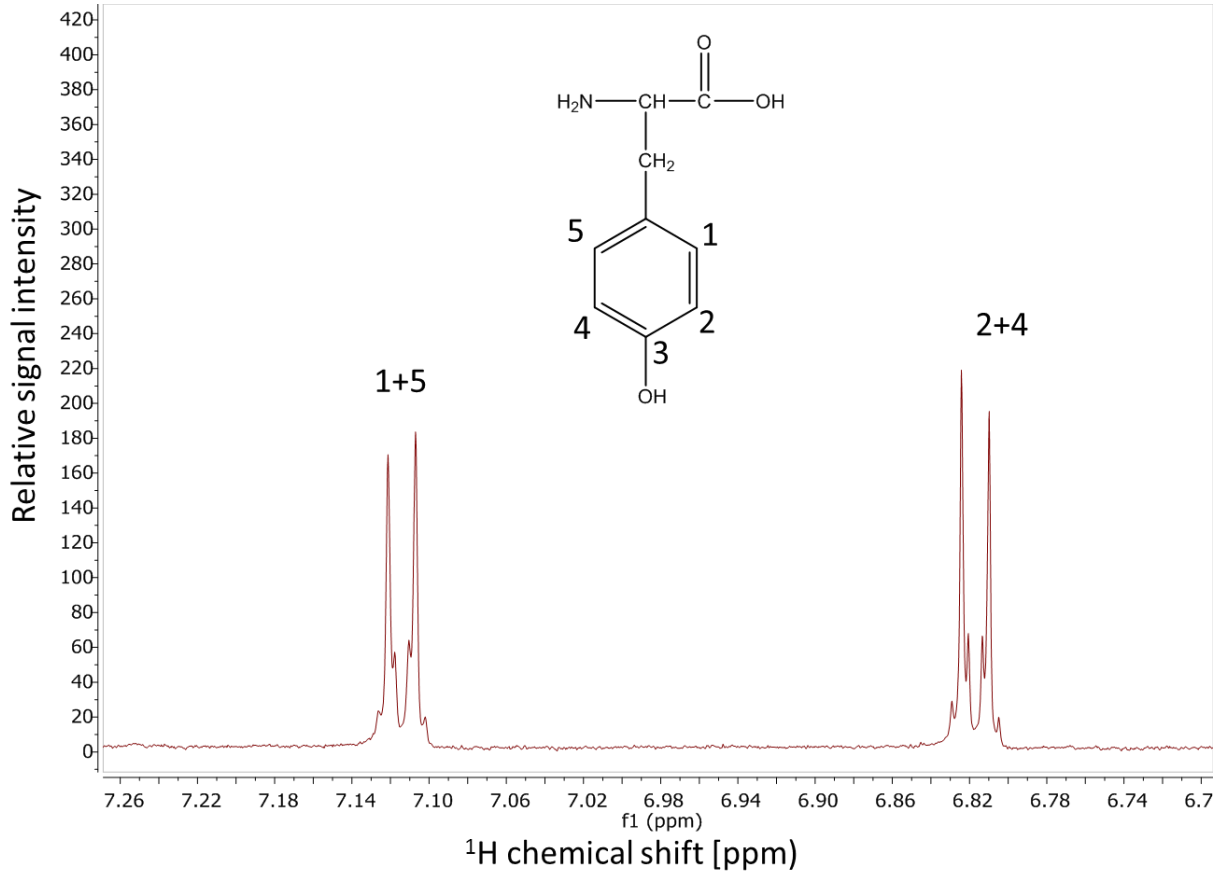

Figure 47: ^{1}H-NMR spectrum of 4-hydroxyphenylalanine.

The ^{1}H-NMR spectrum was recorded with 4-hydroxyphenylalanine dissolved in D_2O and a 600 MHz instrument. The spectrum shows the aromatic residues between 6.7

and 7.2 ppm. The numbers indicate the hydrogen signals occurring in the spectrum and their assigned position on the aromatic ring

3.3.8 Radical scavenger MeOH

The solubility of PA in H_2O is limited to a concentration of 1 mM. To increase the product yield without increasing the total volume methanol and acetonitrile were considered as additives to increase the solubility. Both of these additives are radical scavengers.[45] The reduction potential of deprotonation of the hydroxyl group of an alcohol is about $E^0 = 1.6$ V.[72]

When the experiments, as they are described in the methods section, but here with equimolar concentrations of PA, Fe(II) and H_2O_2, were performed with 10% of MeOH or ACN as additive, no oxidation products were detected (**Figure 48**). For example, only one product was seen for the PA standard sample to elute after 9.1 min with m/z = 875. The sample of PA after Fenton reaction had a major peak eluting after 9.0 min with m/z = 875 and two additional products, which eluted after 8.4 min with m/z = 891. The latter are the oxidation products stemming from the Fenton reaction. The samples where 10% ACN or MeOH were added to the Fenton reaction mix showed that almost no products formed. This prompts to the fact that hydroxyl radicals, which have been formed during the Fenton reaction have been scavenged.

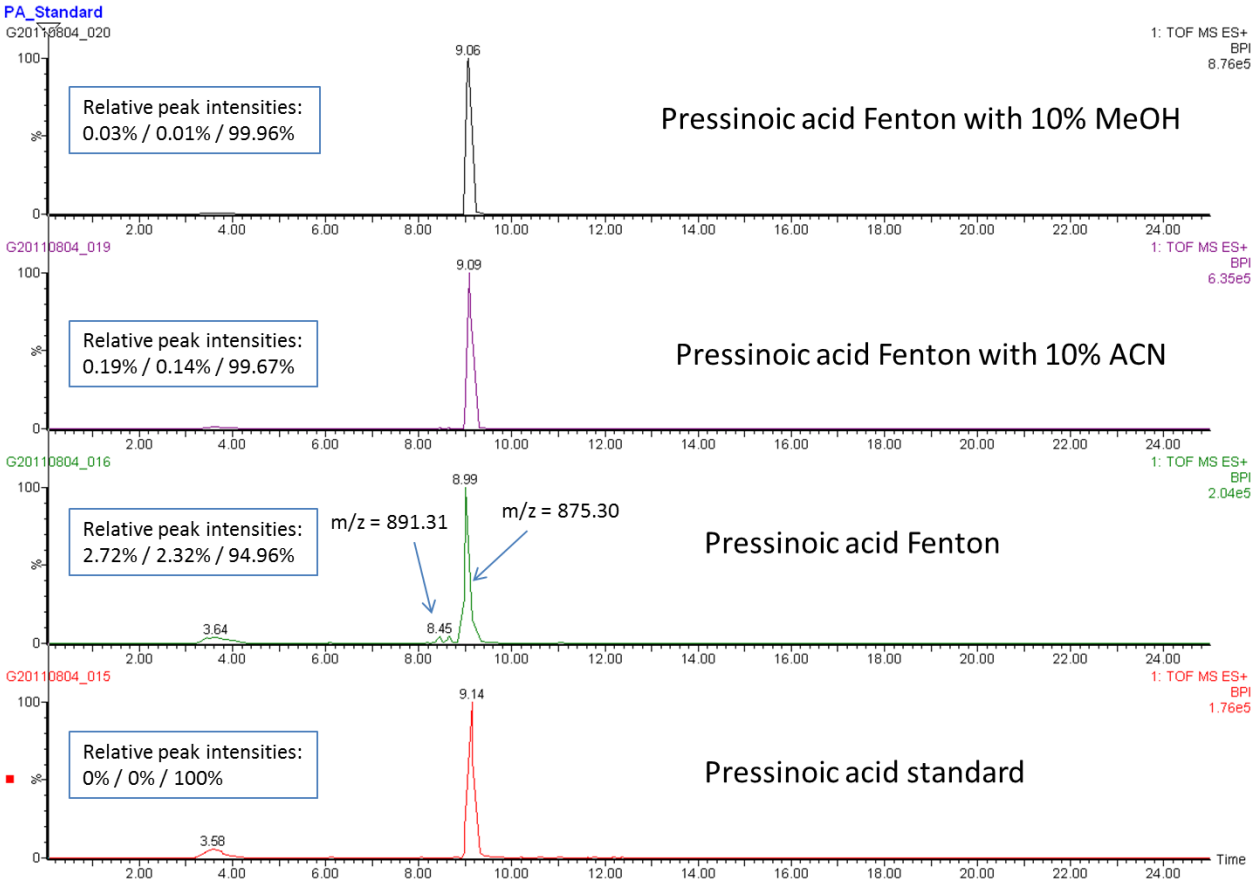

Figure 48: MS chromatograms of PA after the Fenton reaction was performed with radical scavengers

MS chromatograms of PA, which are shown as base peak integrated chromatograms. The gradient of solvent A (100% H_2O) and solvent B (99.9:0.1% v/v ACN:TFA) was set to 20-35% B over 20 min.

Pressinoic acid Fenton with 10% MeOH: The experiment of PA with the Fenton reagents was performed in 10:90 (v:v) MeOH:H_2O solution.

Pressinoic acid Fenton with 10% ACN: The experiment of PA with the Fenton reagents was performed in 10:90 (v:v) ACN:H_2O solution.

Pressinoic acid Fenton with 10 %MeOH: The experiment of PA with the Fenton reagents was performed in 10:90 (v:v) MeOH:H_2O solution.

Pressinoic acid Fenton: The experiment of PA with the Fenton reagents was performed in H_2O solution.

Pressinoic acid standard: The original PA in H_2O solution was injected

3.3.9 Tboc group removal from PA samples before MS/MS analysis

From the MS/MS data of the reduced and alkylated PA samples it was concluded that tboc groups have been cleaved off during fragmentation. To verify that the mass loss of 100 Da, which was observed during MS/MS analyses, is, in fact, accountable by the removal of tboc groups, the tboc group was removed from the PA sample. In particular, 1 mM PA solution was incubated with an equal volume of TFA for 2 h and then neutralized with NH_4OH. After freeze-drying, the sample was cleaned by SPE to remove nonvolatile ammonium-triflouracetate. The MS chromatograms of PA prior and after tboc removal are shown in Figure 49. For the PA standard sample one major peak eluting after 9.02 min with m/z = 875 was noted. This corresponds to PA with a tboc group. An additional small fraction eluted after 6.1 min with m/z = 775. This relates to PA minus a tboc group. In contrast, the chromatogram of PA after tboc removal showed only one major peak eluting after 6.5 min with m/z = 775. Again, this matches the value

for PA without a tboc group. The spectrum of the substance eluting before the PA sample without the tboc group could not be assigned to any particular product.

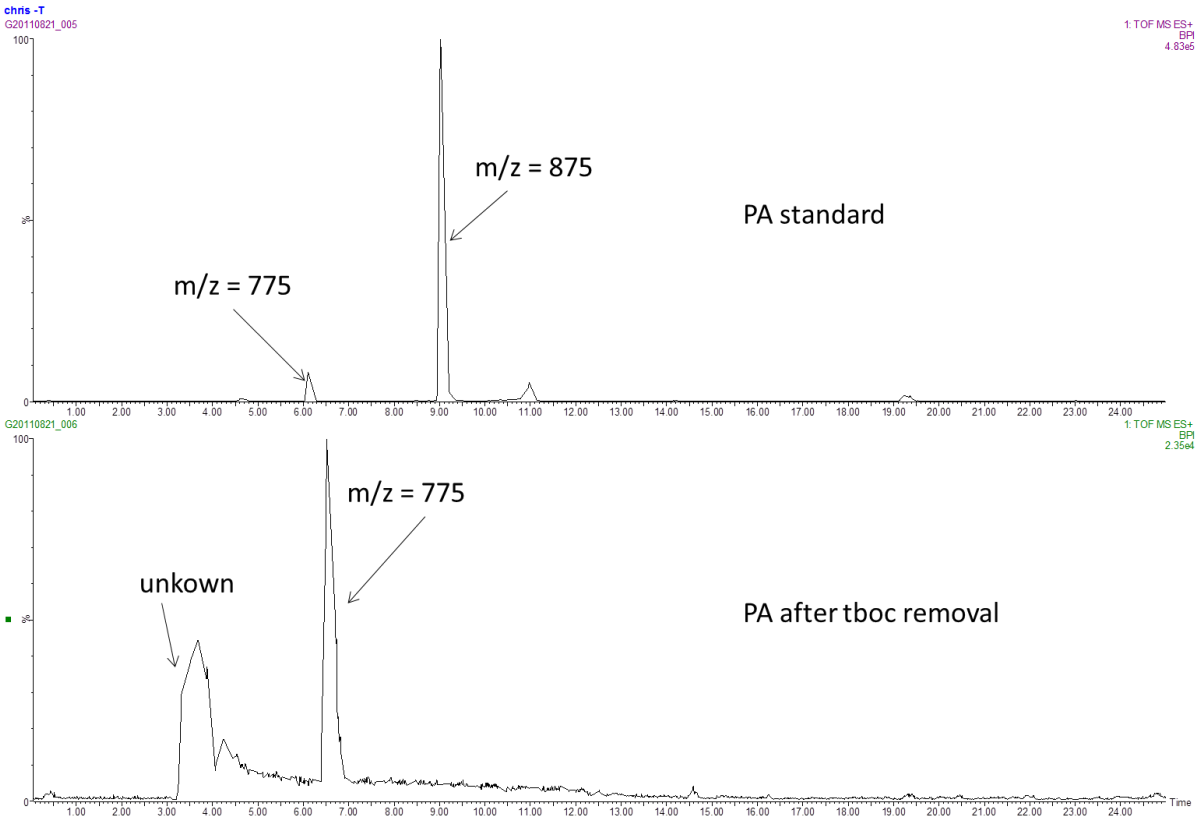

Figure 49 – MS chromatogram of PA before and after tboc removal

MS chromatogram of PA before and after tboc removal, which are shown as base peak integrated chromatograms. The gradient of solvent A (100% H2O) and solvent B (99.9:0.1% v/v ACN:TFA) was set to 20-35% B over 20 min.

3.4 Discussion

Four major oxidation products have been identified after PA was exposed to Fenton reaction. Oxidation occurred only on the aromatic residues of the peptide even though the disulfide bond was also well exposed.[4] The possible oxidation of the disulfide bond

did not occur. As such, the oxidation products contained 2-, 3- and 4-hydroxyphenylalanine, which resulted from hydroxylation of the Phe residue, and 3,4-dihydroxyphenylalanine, which is derived from the hydroxylation of the Tyr residue of PA.

Notably, none of the oxidation products have seemingly lost oxygen during the reduction. The retention times shown in **Figure 30** confirm this notion. Following the reduction and alkylation process, none of the retention times seen for the products of the Fenton reaction matched those of the reduced and alkylated PA standard. In addition, the masses of the products prior and after reduction and alkylation indicated that one oxygen of PA was not reduced by TCEP. TCEP is known to reduce disulfide bonds[100] and to remove oxygen from sulfoxides and thiosulfinate. TCEP, however, cannot reduce the C-OH bond of an aromatic residues such as hydroxyphenylalanine.[100]

Free hydroxyl radicals have a very high reduction potential (E^0 = 2.72 V)[72] and are therefore very strong oxidants capable of reacting with all amino acids of PA since they have a lower reduction potential.[115]

Previous experiments showed that Met is a good target for oxidation by the Fenton reaction.[74] In small model peptides which contained both Tyr and Met adjacent to each other only the Met residue was oxidized meaning Tyr had no protecting effect.[99] The reduction potential of Met (E^0 = +1.46 V[3]) and Tyr (at neutral pH E^0 = +0.93 V[75]) suggest that the Tyr residue is the primary target for oxidation if hydroxyl radicals are formed. It

was in fact shown that no free hydroxyl radical has been formed and the Met oxidation occurred via a two electron oxidation mechanism, see reactions 11-13. Under slightly acidic conditions $[Fe(OH)]^{3+}$ can be formed which may transfer a hydroxyl cation to the sulfur of Met and yield a sulfoxide after deprotonation.[99]

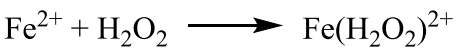

Reaction 11

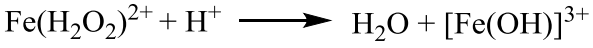

Reaction 12

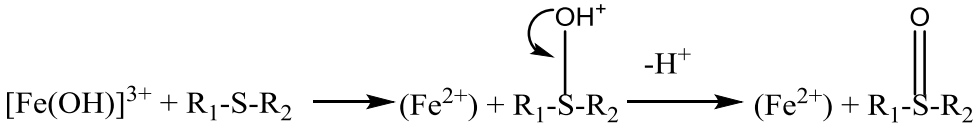

Reaction 13

Since the reduction potential of a disulfide bridge (dimethyldisulfide E^0 = +1.39 V)[1] is lower than the reduction potential of Met (E^0 = +1.46 V)[3], the disulfide bridge in PA is believed to be a facile target for hydroxyl radical attack. In fact, it has been shown before that hydroxyl radicals formed by irradiation oxidized the disulfide bridge and the Tyr and Phe residues of PA.[116,117] If the experimental conditions applied here would have formed free hydroxyl radicals, a significant amount of oxidation products on the Cys residues, i.e. the disulfide bridge, should have been observed.

Although the current experiments were performed under slightly acidic conditions a mechanism as it is summarized in reactions 11-13 yielding sulfoxide or thiosulfinate via hydroxyl cation transfer is ruled out.[99]

In the presence of 10% methanol or ACN in the reaction solution no products have been formed during the Fenton reaction with PA.

Fenton reaction performed with EDTA as chelating agent can form both hydroxyl radicals and ferryl ions[45] and both can react with amino acid residues to yield identical products.[53] With the formation of free hydroxyl radicals excluded, either complexed hydroxyl radicals or ferryl ions are formed. Both are more selective oxidizing species than free hydroxyl radicals.

The experiments for understanding the potential oxidation of the disulfide bridge were performed with large excess of $Fe(EDTA)^{2-}$ and H_2O_2. This allowed the creation of larger quantities of oxidation products in order to perform all analytical tests required. During the preparation steps a significant amount of sample was lost and, therefore, more sample had to be prepared. Higher concentrations of reactants for the Fenton reaction are believed to yield more hydroxyl radicals than ferryl ions.[45]

This indicates that the experimental conditions created complexed hydroxyl radicals that selectively oxidized the aromatic residues of PA. However, a radical attack on the disulfide bridge cannot be excluded. No oxidation of the disulfide bridge has been detected but the possibility of a radical transfer remains. It is possible that a sulfuranyl

radical cation was formed which was repaired too fast for an oxidation product to form. In fact, it appears as if the aromatic residues are protecting the disulfide bond from radical attack.

The 3-D structure of PA[118] indicates that the disulfide bond and the aromatic residues are well exposed and therefore easily accessible for hydroxyl radicals. Although the aromatic residues as well as the disulfide bond are located on the hydrophobic side of the peptide,[118] the hydrophilic site, containing Gln and Asn was not subject to radical attack. Therefore steric hindrance as well as solvent accessibility did not have a significant influence on the oxidation site.

Phe yielded three hydroxyphenylalanine isomers after the Fenton reaction. The hydroxylation of Phe is likely to follow the pathway shown in **Scheme 8**.

Hydroxyl radicals add to an aromatic system to form a hydroxycyclohexadienyl radical, which may be oxidized by Fe^{3+} and will later detach a proton.[32,37,58,90] Alternatively if the Fenton reaction yields a ferryl ion the reaction can follow the pathway shown in **Scheme 9**.

A similar pathway can occur for the hydroxylation of Tyr to form 3,4-dihydroxyphenylalanine and the other Tyr isomers.

As it is still discussed whether the Fenton reaction yields free hydroxyl radicals[33] at least these results indicate that no free radicals were formed. From these experiments it is,

however, impossible to conclude if the hydroxylated Phe or Tyr had changed the three-dimensional structure of PA and its biological activity. Hydroxylation by means of the Fenton reaction is increasing the hydrophilicity of the peptide and allows exposure of the aromatic residues to the aqueous environment. This was also verified by the reduced retention times of the products shown in the MS chromatograms. In fact, the PA peptides with newly formed Tyr isomers from Phe eluted in the same order as single amino acid Tyr isomers.

3.4.1 Isomers formed

The oxidation of Phe residues of PA via Fenton reaction yielded 2-, 3- and 4-hydroxyphenylalanine. The oxidation of free Phe through the Fenton reaction is also known to yield these three isomers.[44] Since the Phe residue of PA is well accessible the hydroxyl radicals formed during Fenton reaction could attack the aromatic ring at all three positions. Tyr was oxidized to 3,4-dihydroxyphenylalanine. The elution order of the newly formed Tyr isomers in the peptide agreed with the expected order based on the elution order of the single amino acids. The fact that the hydrophilicity of the peptide is significantly influenced by the oxidized Phe indicates that the exposed Phe residues remained exposed even after oxidation. The 3-D structure showed that the two aromatic AA are perpendicular to each other. Addition of oxygen to Phe will still allow the two AA to remain in this position. Also the formation of DOPA, which appears to be

limited to one site, as the other site is blocked by the Phe residue, is possible without reformation of the peptide structure.

MS/MS data showed very good ion coverage for all four products and the PA standard. The high yield of a2 ions in all samples can be attributed to the Tyr residue. The b2 ion formed further fragments to an a2 ion by release of the CO residue.[111]

3.5 Summary

The effect of oxidizing species created via Fenton chemistry on PA has been investigated. Each oxidation product contained one additional oxygen.

Scheme 16 shows the structures of PA and all of the products identified after Fenton reaction. The data show that only the aromatic residues of PA were subject to oxidation from hydroxyl radicals formed through Fenton reaction. No evidence for the oxidation of the disulfide group was found.

The Phe residue of PA was oxidized to either 2-, 3- or 4- hydroxyphenylalanine and Tyr was oxidized to DOPA. None of the products contained two additional oxygen atoms and no dimerization or polymerization of PA was identified.

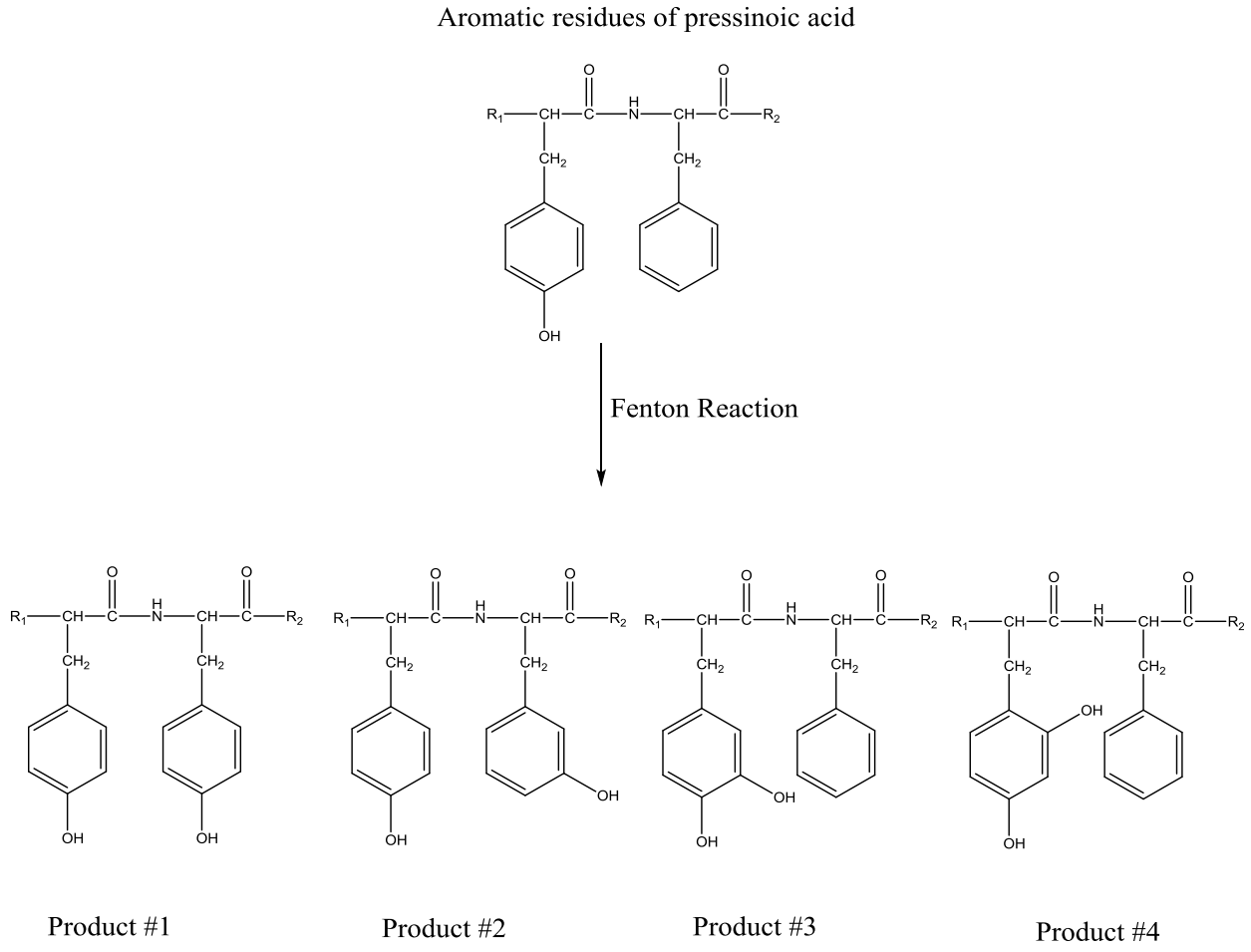

Scheme 16: The hydroxylation products of the aromatic residues of PA after Fenton reaction

The two aromatic residues of PA, Tyr and Phe, have been hydroxylated during Fenton reaction. The four products, separated with HPLC, were numbered according to their elution order.

3.6 Additional experiments performed

3.6.1 Test of the isocratic elution of hydroxyphenylalanine isomers with several salt and solvent mixtures

Several different isocratic solutions were tested for the separation of Tyr isomers. To this end, solutions of 5% methanol in H_2O with 2.5, 25, or even 250 mM potassium phosphate were tested. The pH was adjusted to 3.1 by addition of 85% phosphoric acid. As a matter of fact, the solution with 25 mM potassium phosphate gave the best results in terms of separation. Nevertheless, solutions of 1% NaCl and 1% acetic acid in H_2O were preferred for the isocratic elution, because it gave similar separation results and required less preparation effort.

Notable is the fact that solutions with 5% ACN or THF and 25 mM potassium phosphate failed to improve the separation of the hydroxyphenylalanine isomers.

At this point it is important to define how the buffer is produced. Buffers are often described as a salt in solution, whose pH is adjusted to a required value. It may, however, not be evident if a 25 mM potassium phosphate buffer (pH 3.1) is made by mixing 25 mM KH_2PO_4 in H_2O, followed by a titration with H_3PO_4 to obtain the desired pH, or if a solution of 25 mM H_3PO_4 in H_2O should be titrated to the desired pH by addition of NaOH.

3.6.2 IR-spectroscopy

Infrared spectroscopy was employed to identify potentially formed thiosulfinate in PA by the Fenton reaction. For IR spectroscopy, 1 mM samples of PA and the samples collected after Fenton reaction including reduction and alkylation have been tested on a Bruker (Billerica, MA, USA) Vertex 70 FTIR instrument with 256 scans per sample. Sulfoxide groups are IR active in the region of 1050 cm^{-1}.[22] Other bonds in PA are IR inactive in this range of the spectrum. The IR spectra are shown in **Figure 50.** On one hand, the spectrum of PA reveals no significant resonance in the 1050 cm^{-1} region. On the other hand, PA samples treated with the Fenton reagent showed a strong signal at ca. 1070 cm^{-1}. However, the latter was absent upon reduction and alkylation. This lead to the false conclusion that thiosulfinate has been created by the Fenton reaction. The observed transition originates from phosphate, which was introduced to the observed sample by phosphate buffer used for the SPE. Phosphate bonds absorb in the same IR wavelength region as sulfoxide.[23] In addition, after reduction with TCEP these transitions disappeared from the spectra as it was expected for the sulfoxide bands. This may be due to removal or dilution of the phosphate during the reduction and alkylation step. As a consequence, phosphate buffer was no longer used for the SPE protocol.

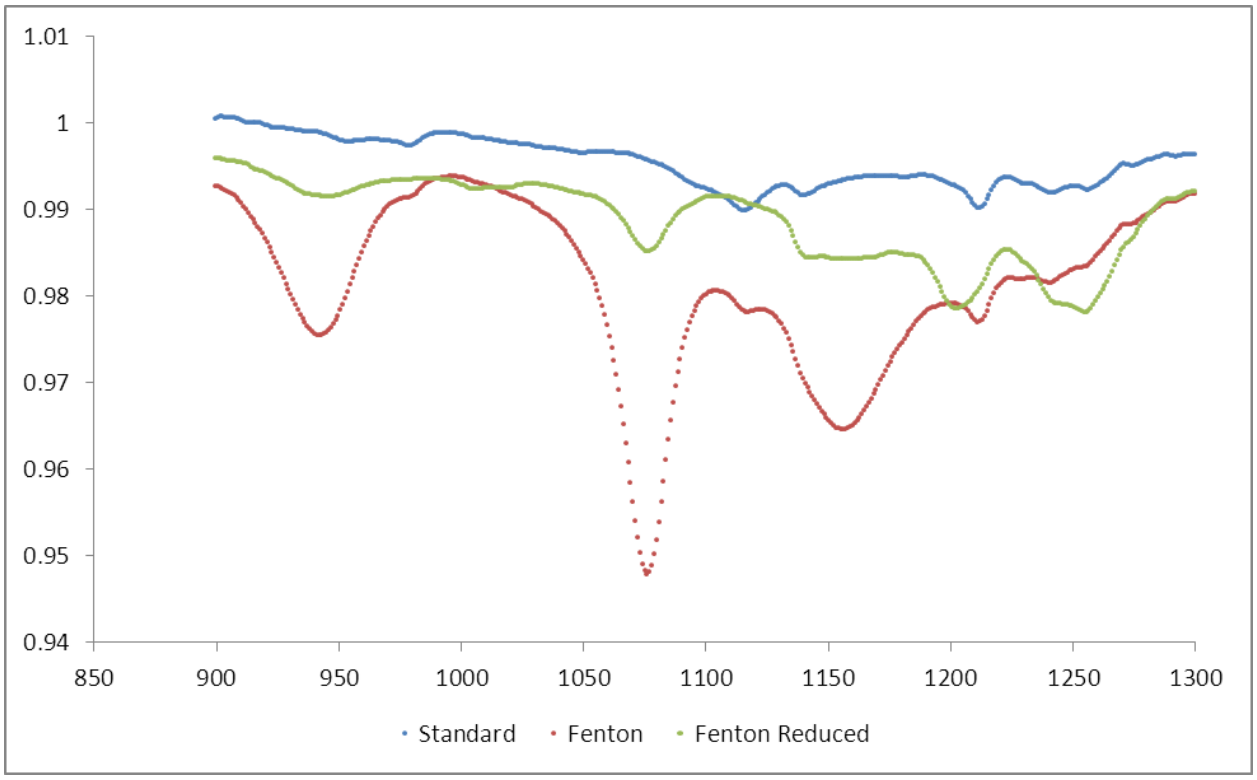

Figure 50: IR spectra of pressinoic acid recorded over 850 to 1300 cm^{-1} of PA samples before and after Fenton reaction and after reduction and alkylation.

3.6.3 COSY NMR for PA

Correlation spectroscopy (COSY) NMR is a two-dimensional NMR method that shows the interaction of adjacent protons on a molecule. A COSY NMR spectrum was recorded of PA standard and one of the separated products of PA modified with Fenton reaction. The COSY spectrum was recorded on a 600 MHz NMR spectrometer. For the standard the spectrum of 1 mM PA in D_2O was recorded, see **Figure 51**. While it was possible to distinguish between the signals occurring from Phe (7.2-7.5 ppm) and Tyr (6.7-7.1 ppm)

the assignment of the individual hydrogen on the Phe residue and their correlation to adjacent hydrogen was difficult due to the very close signals.

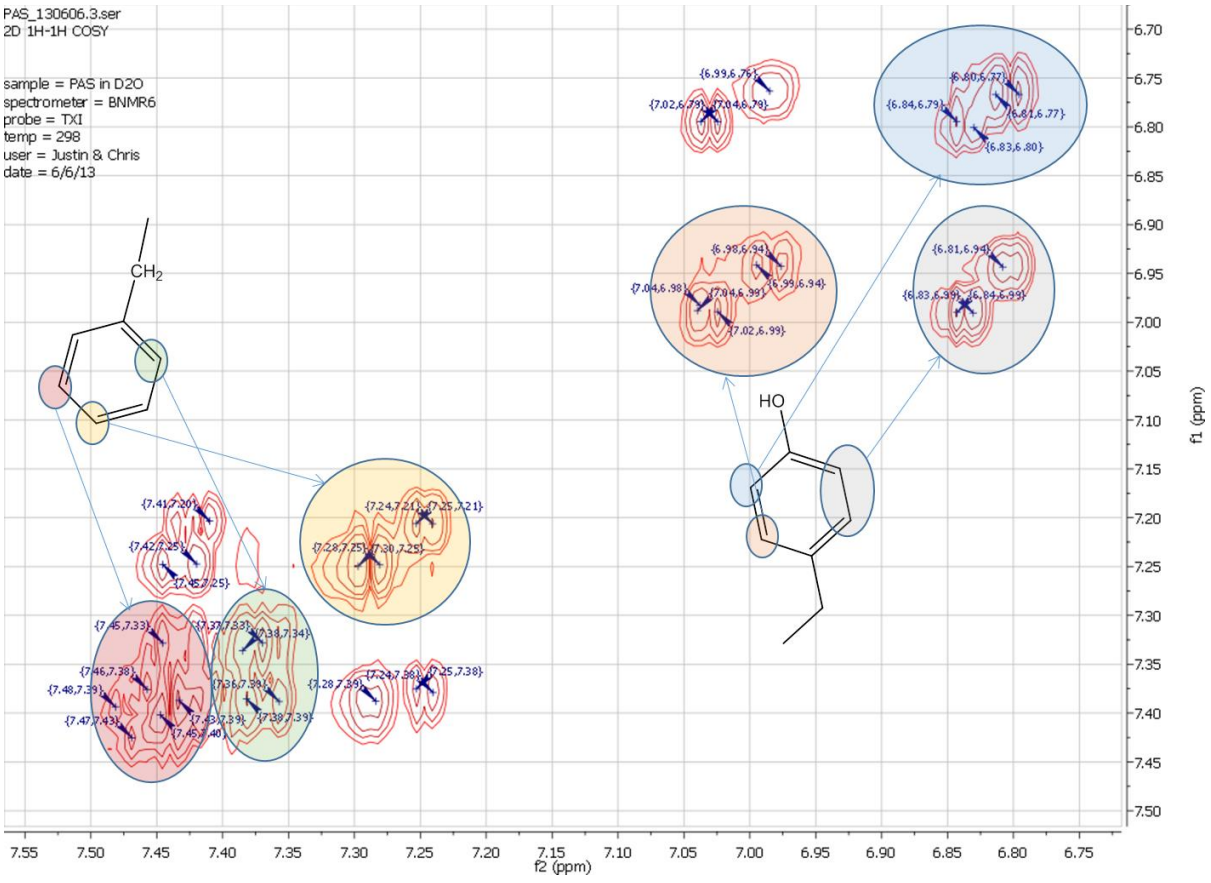

Figure 51: COSY NMR spectrum of PA standard

The spectrum shows the chemical shifts at 6.5-7.5 ppm, which represents the chemical shifts of the aromatic region of Phe and Tyr. Spectra were recorded at room temperature and neutral pD. Frequency 1 (f1) first hydrogen chemical shift in ppm; Frequency 2 (f2) second hydrogen chemical shift in ppm.

In order to record the spectrum of PA following the Fenton reaction, the separated samples had to be synthesized several times in order to yield enough concentration for the NMR observation. Figure 5 shows the spectrum of sample #4. It was still possible to assign the chemical shifts of the Tyr residue, but the additional signals that occurred could not be assigned to a specific hydroxyphenylalanine isomer and the prediction software of ChemDraw is not accurate enough for clear assignments of the chemical shifts.

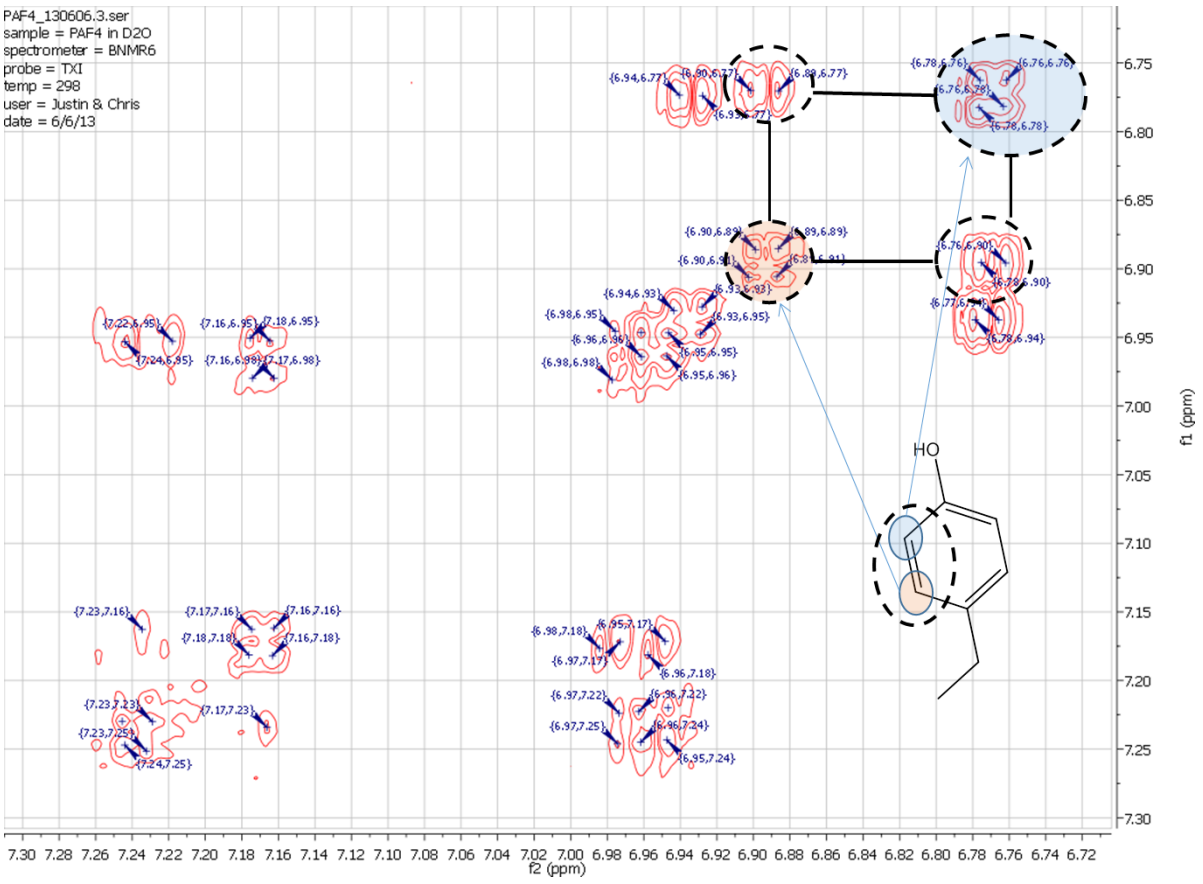

Figure 52: COSY NMR spectrum of PA product #4

The spectrum shows the chemical shifts at 6.6-7.3 ppm, which represents the chemical shifts of the aromatic region of Phe and Tyr. Spectra were recorded at room temperature and neutral pD. Frequency 1 (f1) first hydrogen chemical shift in ppm; Frequency 2 (f2) second hydrogen chemical shift in ppm.

3.6.4 Rose Bengal dye irradiation for singlet oxygen formation

Rose Bengal dye can be irradiated with UV-light to produce singlet oxygen which readily reacts with sulfur and aromatic amino acids.[98,119] This may be used to form samples with oxidized disulfide bridges and verify that thiosulfinates can be detected as described in the methods section. A 1 mM Rose Bengal solution was made and 50 µl of PA standard (1mM) were mixed with 450 µl Rose Bengal solution and irradiated with UV lamps at 365 nm for 30 min. The samples were analyzed as described in section 3.2.3.4 but no additional products have been detected. Only the unmodified PA sample has been observed.

3.6.5 Synthesis of pressinoic acid out of known amino acid standards

The option of synthesizing product standards that contain the predicted hydroxyphenylalanine isomers would allow to compare elution times and fragmentation pattern of known standards with the separated products of PA after Fenton reaction. Those product standards could be made with Fmoc peptide synthesis[120] and subsequent disulfide ring closure by dimethylsulfoxide (DMSO).[121]

A 1 mM PA standard solution was reduced with 2 mM TCEP solution as described in section 3.2.3.5. The reaction mixture was cleaned with SPE, see section 3.2.3.3 and the freeze dried samples were then reconstituted in DMSO and purged with O_2. The chromatographic data in **Figure 53** shows that it rendered impossible to oxidize the reduced PA sample by DMSO. The reduced PA sample eluted later than the PA standard sample, probably due to its increased space use of its open chain form. The DMSO sample had the same elution time as the reduced sample indicating no reclosing of the ring structure.

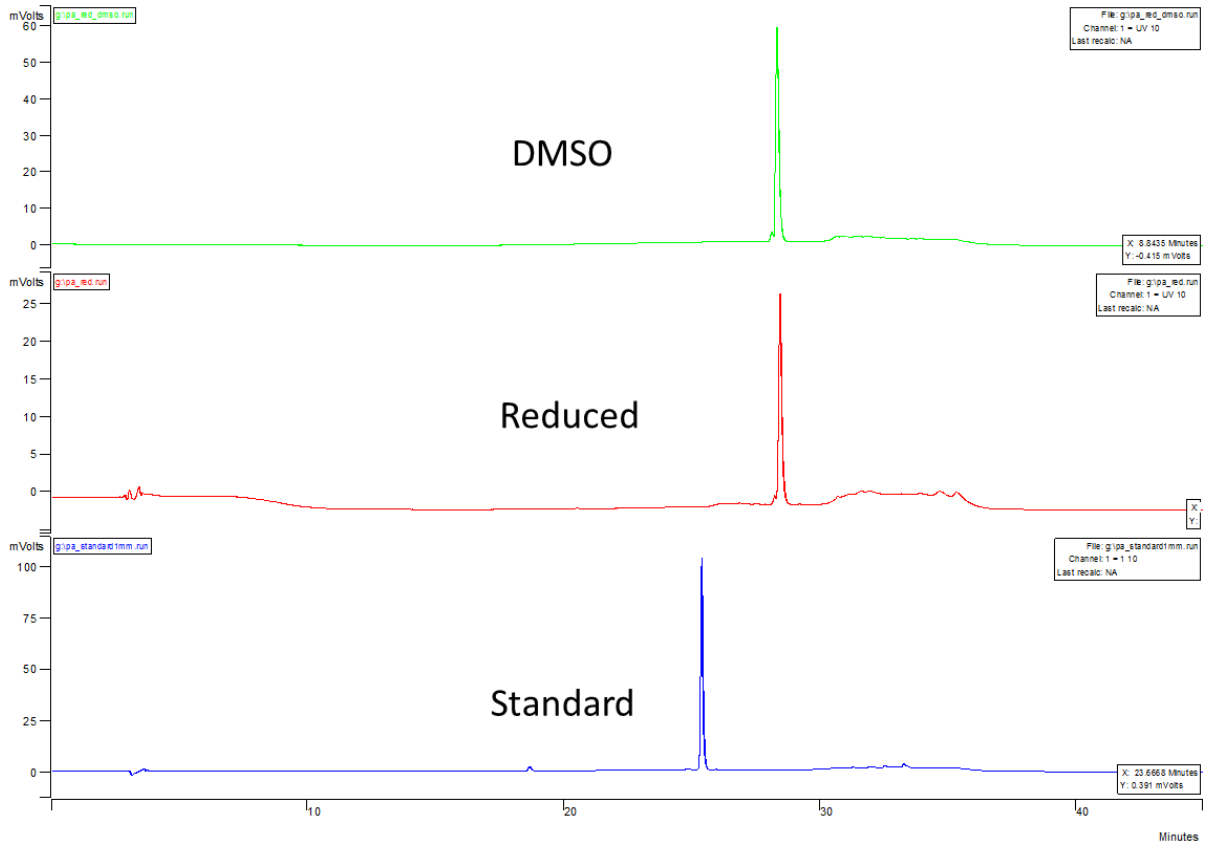

Figure 53: Chromatographic spectra of PA standard, after reduction and after reconstitution in DMSO. Elution with solvent A: 95% H_2O, 5% ACN, 0.1 %TFA and solvent B: 5% H_2O, 95 %ACN and 0.1% TFA. Gradient 10-40% B over 30 min.

3.7 References

(1) Bonifacic, M.; Asmus, K.-D. *J Chem Soc, Perkin Trans 2* **1986**, 1805.
(2) Koppenol, W. H.; Butler, J. *Adv. Free Radical Biol. Med.* **1985**, *1*, 91.
(3) Brunelle, P.; Schoeneich, C.; Rauk, A. *Can. J. Chem.* **2006**, *84*, 893.
(4) Langs, D. A.; Smith, G. D.; Stezowski, J. J.; Hughes, R. E. *Science* **1986**, *232*, 1240.
(5) Ervin, M. G.; Leake, R. D.; Ross, M. G.; Calvario, G. C.; Fisher, D. A. *J of Clinical Investigation* **1985**, *75*, 1696.
(6) Sharman, A.; Low, J. *Continuing Education in Anaesthesia, Critical Care & Pain* **2008**, *8*, 134.
(7) Baumann, G.; Dingman, J. F. *J of Clinical Investigation* **1976**, *57*, 1109.
(8) Czaczkes, J. W.; Kleeman, C. R.; Koenig, M.; Boston, R. *J of Clinical Investigation* **1964**, *43*, 1625.
(9) Nielsen, S.; Chou, C. L.; Marples, D.; Christensen, E. I.; Kishore, B. K.; Knepper, M. A. *Proc of the Nat Acad of Sci* **1995**, *92*, 1013.
(10) Sands, J. M.; Blount, M. A.; Klein, J. D. *Trans of the Am Clinical and Climatological Ass* **2011**, *122*, 82.
(11) ANG, V. T. Y.; JENKIS, J. S. *J of Clinical Endocrinology & Metabolism* **1984**, *58*, 688.
(12) MARKWICK, A. J.; LOLAIT, S. J.; FUNDER, J. W. *Endocrinology* **1986**, *119*, 1690.
(13) Russell, J. T.; Brownstein, M. J.; Gainer, H. *Endocrinology (Baltimore)* **1980**, *107*, 1880.
(14) Amico, J. A.; Finn, F. M.; Haldar, J. *Am J Med Sci* **1988**, *296*, 303.
(15) Whitton, P. D.; Rodrigues, L. M.; Hems, D. A. *Biochem J* **1978**, *176*, 893.
(16) Keppens, S.; De Wulf, H. *Biochimica et Biophysica Acta (BBA) - General Subjects* **1979**, *588*, 63.
(17) Dunning, B. E.; Moltz, J. H.; Fawcett, C. P. *Peptides (Fayetteville, N. Y.)* **1984**, *5*, 871.
(18) Yibchok-Anun, S.; Cheng, H.; Heine, P. A.; Hsu, W. H. *Am. J. Physiol.* **1999**, *277*, E56.
(19) Kirk, C. J.; Rodrigues, L. M.; Hems, D. A. *Biochem. J.* **1979**, *178*, 493.
(20) Grazzini, E.; Lodboerer, A. M.; Perez-Martin, A.; Joubert, D.; Guillon, G. *Endocrinology* **1996**, *137*, 3906.
(21) Xiao, X.; Zhu, Y.; Zhen, D.; Chen, X. M.; Yue, W.; Liu, L.; Li, T. *J. Surg. Res.* **2015**, Ahead of Print.
(22) Malay, M. B.; Ashton, R. C., Jr.; Landry, D. W.; Townsend, R. N. *J. Trauma: Inj., Infect., Crit. Care* **1999**, *47*, 699.
(23) Landry, D. W.; Levin, H. R.; Gallant, E. M.; Ashton, R. C., Jr.; Seo, S.; D'Alessandro, D.; Oz, M. C.; Oliver, J. A. *Circulation* **1997**, *95*, 1122.
(24) Holmes, C. L.; Patel, B. M.; Russell, J. A.; Walley, K. R. *CHEST* **2001**, *120*, 989.
(25) Ferger, M. F.; Jones, W. C.; Dyckes, D. F.; Du Vigneaud, V. *J Am Chem Soc* **1972**, *94*, 982.
(26) Saffran, M.; Pearlmutter, A. F.; Rapino, E.; Upton, G. V. *Biochem and Biophys Res Com* **1972**, *49*, 748.
(27) Salata, R. A.; Jarrett, D. B.; Verbalis, J. G.; Robinson, A. G. *J of Clinical Investigation* **1988**, *81*, 766.
(28) Tilders, F. J. H.; Berkenbosch, F.; Vermes, I.; Linton, E. A.; Smelik, P. G. *Fed. Proc., Fed. Am. Soc. Exp. Biol.* **1985**, *44*, 155.
(29) Hagler, A. T.; Osguthorpe, D. J.; Dauber-Osguthorpe, P.; Hempel, J. C. *Science (Washington, D. C., 1883-)* **1985**, *227*, 1309.

(30) Burley, S.; Petsko, G. *Science* **1985**, *229*, 23.
(31) Fenton, H. J. H. *J Chem Soc, Trans* **1894**, *65*, 899.
(32) Walling, C. *Acc. Chem. Res.* **1975**, *8*, 125.
(33) Goldstein, S.; Meyerstein, D.; Czapski, G. *Free Radical Biol. Med.* **1993**, *15*, 435.
(34) Wardman, P.; Candeias, L. P. *Radiat Res* **1996**, *145*, 523.
(35) Harmon, P. A.; Kosuda, K.; Nelson, E.; Mowery, M.; Reed, R. A. *J. Pharm. Sci.* **2006**, *95*, 2014.
(36) Koppenol, W. H. *Free Rad Biol and Med* **1993**, *15*, 645.
(37) Brook, M. A.; Castle, L.; Lindsay Smith, J. R.; Higgins, R.; Morris, K. P. *J. Chem. Soc., Perkin Trans. 2* **1982**, 687.
(38) Ponganis, K. V.; De Araujo, M. A.; Hodges, H. L. *Inorg. Chem.* **1980**, *19*, 2704.
(39) Pecht, I.; Anbar, M. *J. Chem. Soc., A* **1968**, 1902.
(40) Kaur, H.; Halliwell, B. In *Met in Enzym*; Lester, P., Ed.; Academic Press: 1994; Vol. Volume 233, p 67.
(41) Czapski, G.; Samuni, A.; Meisel, D. *J. Phys. Chem.* **1971**, *75*, 3271.
(42) Davies, G.; Sutin, N.; Watkins, K. O. *J. Amer. Chem. Soc.* **1970**, *92*, 1892.
(43) Moorhouse, C. P.; Halliwell, B.; Grootveld, M.; Gutteridge, J. M. C. *Biochim. Biophys. Acta, Gen. Subj.* **1985**, *843*, 261.
(44) Xu, G.; Chance, M. R. *Chem. Rev. (Washington, DC, U. S.)* **2007**, *107*, 3514.
(45) Yamazaki, I.; Piette, L. H. *J. Am. Chem. Soc.* **1991**, *113*, 7588.
(46) Winterbourn, C. C. *Free Radical Biol. Med.* **1987**, *3*, 33.
(47) Nakken, K. F.; Pihl, A. *Radiat. Res.* **1965**, *26*, 519.
(48) Allen, A. O. *The Radiation Chemistry of Water and Aqueous Solutions*; D. Van Nostrand, 1961.
(49) Janata, E.; Schuler, R. H. *Journal of Phys Chem* **1982**, *86*, 2078.
(50) Schwarz, H. A. *J. Phys. Chem.* **1969**, *73*, 1928.
(51) Bors, W.; Michel, C.; Saran, M. *Eu J of Biochem* **1979**, *95*, 621.
(52) Bray, W. C.; Gorin, M. H. *J. Am. Chem. Soc.* **1932**, *54*, 2124.
(53) Rush, J. D.; Maskos, Z.; Koppenol, W. H. *Methods Enzymol.* **1990**, *186*, 148.
(54) Yamamoto, N.; Koga, N.; Nagaoka, M. *J. Phys. Chem. B* **2012**, *116*, 14178.
(55) Rahhal, S.; Richter, H. W. *J. Am. Chem. Soc.* **1988**, *110*, 3126.
(56) Yamazaki, I.; Piette, L. H. *J. Biol. Chem.* **1990**, *265*, 13589.
(57) Bull, C.; McClune, G. J.; Fee, J. A. *J. Am. Chem. Soc.* **1983**, *105*, 5290.
(58) Jefcoate, C. R. E.; Smith, J. R. L.; Norman, R. O. C. *J. Chem. Soc. B* **1969**, 1013.
(59) Farber, J. M.; Levine, R. L. *J. Biol. Chem.* **1986**, *261*, 4574.
(60) Creeth, J. M.; Cooper, B.; Donald, A. S. R.; Clamp, J. R. *Biochem. J.* **1983**, *211*, 323.
(61) Kaur, H.; Fagerheim, I.; Grootveld, M.; Puppo, A.; Halliwell, B. *Anal. Biochem.* **1988**, *172*, 360.
(62) Manzanares, D.; Rodriguez-Capote, K.; Liu, S.; Haines, T.; Ramos, Y.; Zhao, L.; Doherty-Kirby, A.; Lajoie, G.; Possmayer, F. *Biochemistry* **2007**, *46*, 5604.
(63) Turell, L.; Botti, H.; Carballal, S.; Ferrer-Sueta, G.; Souza, J. M.; Duran, R.; Freeman, B. A.; Radi, R.; Alvarez, B. *Biochemistry* **2008**, *47*, 358.
(64) Kroon, D. J.; Baldwin-Ferro, A.; Lalan, P. *Pharm. Res.* **1992**, *9*, 1386.
(65) Meyer, T. E.; Przysiecki, C. T.; Watkins, J. A.; Bhattacharyya, A.; Simondsen, R. P.; Cusanovich, M. A.; Tollin, G. *Proc Nat Academy of Sciences* **1983**, *80*, 6740.
(66) Griffiths, P. R. *Anal. Bioanal. Chem.* **2009**, *393*, 409.
(67) Hildebrand, J. H. *J. Am. Chem. Soc.* **1913**, *35*, 847.
(68) Biegler, T.; Woods, R. *J. Chem. Educ.* **1973**, *50*, 604.
(69) Ramette, R. W. *J. Chem. Educ.* **1987**, *64*, 885.

(70) Buettner, G. R. *Arch. Biochem. Biophys.* **1993**, *300*, 535.
(71) Wardman, P. *J. Phys. Chem. Ref. Data* **1989**, *18*, 1637.
(72) Wood, P. M. *Biochem. J.* **1988**, *253*, 287.
(73) Chu, J.-W.; Yin, J.; Brooks, B. R.; Wang, D. I. C.; Speed Ricci, M.; Brems, D. N.; Trout, B. L. *J. Pharm. Sci.* **2004**, *93*, 3096.
(74) Hong, J.; Schoneich, C. *Free Radic Biol Med* **2001**, *31*, 1432.
(75) Harriman, A. *J. Phys. Chem.* **1987**, *91*, 6102.
(76) Bergès, J.; de Oliveira, P.; Fourré, I.; Houée-Levin, C. *J Phys Chem B* **2012**, *116*, 9352.
(77) Buxton, G. V.; Greenstock, C. L.; Helman, W. P.; Ross, A. B. *J Phys and Chem Ref Data* **1988**, *17*, 513.
(78) Bobrowski, K.; Holcman, J. *J Phys Chem* **1989**, *93*, 6381.
(79) Bonifacic, M.; Schaefer, K.; Moeckel, H.; Asmus, K. D. *J. Phys. Chem.* **1975**, *79*, 1496.
(80) Walling, C.; Johnson, R. A. *J. Am. Chem. Soc.* **1975**, *97*, 363.
(81) Berlett, B. S.; Stadtman, E. R. *J Biol Chem* **1997**, *272*, 20313.
(82) Davies, M. J. *Biochim. Biophys. Acta, Proteins Proteomics* **2005**, *1703*, 93.
(83) Cabreiro, F.; Picot, C. R.; Friguet, B.; Petropoulos, I. *Ann N Y Acad Sci* **2006**, *1067*, 37.
(84) Dalle-Donne, I.; Scaloni, A.; Giustarini, D.; Cavarra, E.; Tell, G.; Lungarella, G.; Colombo, R.; Rossi, R.; Milzani, A. *Mass Spectrom Rev* **2005**, *24*, 55.
(85) Teh, L. C.; Murphy, L. J.; Huq, N. L.; Surus, A. S.; Friesen, H. G.; Lazarus, L.; Chapman, G. E. *J. Biol. Chem.* **1987**, *262*, 6472.
(86) Cornell Manning, M.; Chou, D. K.; Murphy, B. M.; Payne, R. W.; Katayama, D. S. *Pharm. Res.* **2010**, *27*, 544.
(87) Elliot, A. J.; McEachern, R. J.; Armstrong, D. A. *J Phys Chem* **1981**, *85*, 68.
(88) Asmus, K. D. *Accounts of chemical research* **1979**, *12*, 436.
(89) Bhatia, K.; Schuler, R. H. *J. Phys. Chem.* **1974**, *78*, 2335.
(90) Maskos, Z.; Rush, J. D.; Koppenol, W. H. *Arch. Biochem. Biophys.* **1992**, *296*, 521.
(91) Hovorka, S. W.; Schoneich, C. *J. Pharm. Sci.* **2001**, *90*, 253.
(92) Karam, L. R.; Dizdaroglu, M.; Simic, M. G. *Intern J of Rad Biol* **1984**, *46*, 715.
(93) Galano, A.; Cruz-Torres, A. *Organic & Biomolecular Chem* **2008**, *6*, 732.
(94) Molnar, G. A.; Nemes, V.; Biro, Z.; Ludany, A.; Wagner, Z.; Wittmann, I. *Free Radical Res.* **2005**, *39*, 1359.
(95) Themann, C.; Teismann, P.; Kuschinsky, K.; Ferger, B. *J Neurosc Meth* **2001**, *108*, 57.
(96) Musso, H. *Angew. Chem.* **1963**, *75*, 965.
(97) Kungl, A. J.; Visser, A. J.; Kauffmann, H. F.; Breitenbach, M. *Biophys J* **1994**, *67*, 309.
(98) Pattison, D. I.; Rahmanto, A. S.; Davies, M. J. *Photochem. Photobiol. Sci.* **2012**, *11*, 38.
(99) Dufield, D. R.; Wilson, G. S.; Glass, R. S.; Schoeneich, C. *J. Pharm. Sci.* **2004**, *93*, 1122.
(100) Faucher, A.-M.; Grand-Maitre, C. *Synth. Commun.* **2003**, *33*, 3503.
(101) Amorati, R.; Valgimigli, L. *Organic & Biomolecular Chemistry* **2012**, *10*, 4147.
(102) Ishimitsu, S.; Fujimoto, S.; Ohara, A. *J chromato* **1986**, *378*, 222.
(103) Rule, G. S.; Hitchens, T. K., SpringerLink, Eds.; Dordrecht : Springer: Dordrecht, 2006.
(104) Wolfenden, B. S.; Willson, R. L. *J. Chem. Soc., Perkin Trans. 2* **1982**, 805.
(105) Fabbrini, M.; Galli, C.; Gentili, P. *J. Mol. Catal. B: Enzym.* **2002**, *16*, 231.
(106) Hovorka, S. W.; Hong, J.; Cleland, J. L.; Schoneich, C. *J Pharm Sci* **2001**, *90*, 58.
(107) *Biochemical Journal* **1984**, *219*, 345.
(108) Bouchoux, G.; Bourcier, S.; Hoppilliard, Y.; Mauriac, C. *Org. Mass Spectrom.* **1993**, *28*, 1064.
(109) Paizs, B.; Lendvay, G.; Vwkey, K.; Suhai, S. *Rapid Commun. Mass Spectrom.* **1999**, *13*, 525.
(110) Yalcin, T.; Khouw, C.; Csizmadia, I. G.; Peterson, M. R.; Harrison, A. G. *J Am Soc Mass Spectrom* **1995**, *6*, 1165.

(111) Ambihapathy, K.; Yalcin, T.; Leung, H.-W.; Harrison, A. G. *J Mass Spectrom* **1997**, *32*, 209.
(112) Paizs, B.; Suhai, S. *Mass Spectrom Rev* **2005**, *24*, 508.
(113) Paizs, B.; Szlávik, Z.; Lendvay, G.; Vékey, K.; Suhai, S. *Rapid Com in Mass Spectrom* **2000**, *14*, 746.
(114) Biondi, R.; Xia, Y.; Rossi, R.; Paolocci, N.; Ambrosio, G.; Zweier, J. L. *Anal. Biochem.* **2001**, *290*, 138.
(115) Stadtman, E. R. *Science (Washington, D. C., 1883-)* **1992**, *257*, 1220.
(116) Klassen, N. V.; Purdie, J. W.; Lynn, K. R.; D'Iorio, M. *Int. J. Radiat. Biol. Relat. Stud. Phys., Chem. Med.* **1974**, *26*, 127.
(117) Purdie, J. W.; Lynn, K. R. *Int J Radiat Biol Relat Stud Phys Chem Med* **1973**, *23*, 583.
(118) Langs, D. A.; Smith, G. D.; Stezowski, J. J.; Hughes, R. E. *Science* **1986**, *232*, 1240.
(119) Kautsky, H.; de Bruijn, H. *Naturwissenschaften* **1931**, *19*, 1043.
(120) Gawande, M. B.; Branco, P. S. *Green Chemistry* **2011**, *13*, 3355.
(121) Tam, J. P.; Wu, C. R.; Liu, W.; Zhang, J. W. *J Am Chem Soc* **1991**, *113*, 6657.

4 Metal-catalyzed degradation pathway of hydrogen peroxide and its effect on oxytocin and a peptide that contains no aromatic residues via Fenton Reaction

4.1 Introduction

The effect of oxytocin (Oxt) causing contraction of the uterus in mammalians has led to its name derived from the greek words for "quick birth".[1,2] The key functions from oxytocin created in the posterior pituitary gland are uterine contraction[1] and milk ejection after birth.[3,4]

Before oxytocin had been discovered as a hormonal peptide, evidence was found that a component extracted from the pituitary gland and intravenously injected lead to elevated blood pressure and increased heart rate.[5] Oxt is a neurohypophysial nonapeptide hormone, primarily synthesized in the posterior lobe of the pituitary gland of the hypothalamus, and has similar effects as vasopressin.[2] Almost all vertebrate species possess Oxt and vasopressin hormone peptides with similar structures. All those peptides have a disulfide bridge which connects the two Cys residues at positions 1 and 6 as well as at the 5-Asn, 7-Pro and 9-Gly(amidated) residues. The genetic information for Oxt and vasopressin genes are located on the same gene but they are transcribed in the opposite direction.[6] The gene that encodes the Oxt sequence also encodes the carrier protein neurophysin, which is responsible for delivery and storage of the Oxt hormone in the granula before release into the blood stream.[7] Oxt occurs in several other organs,

e.g. heart, placenta, testis, and it has also influence on social behavior and sexual activity.[8,9]

Oxt is used to prevent postpartum hemorrhage, the largest contributor to maternal mortality, occurring in between 1 and 5% of deliveries.[10-13] Therefore Oxt is listed in the WHO Model List of Essential Medicines.[14] Its stability and bioavailability during storage is therefore essential.

The structure of Oxt was originally elucidated by the Edman degradation method.[15] Followed by its structural analysis the first synthetic version of Oxt has been presented.[16] The structure of Oxt is shown in **Scheme 17**.

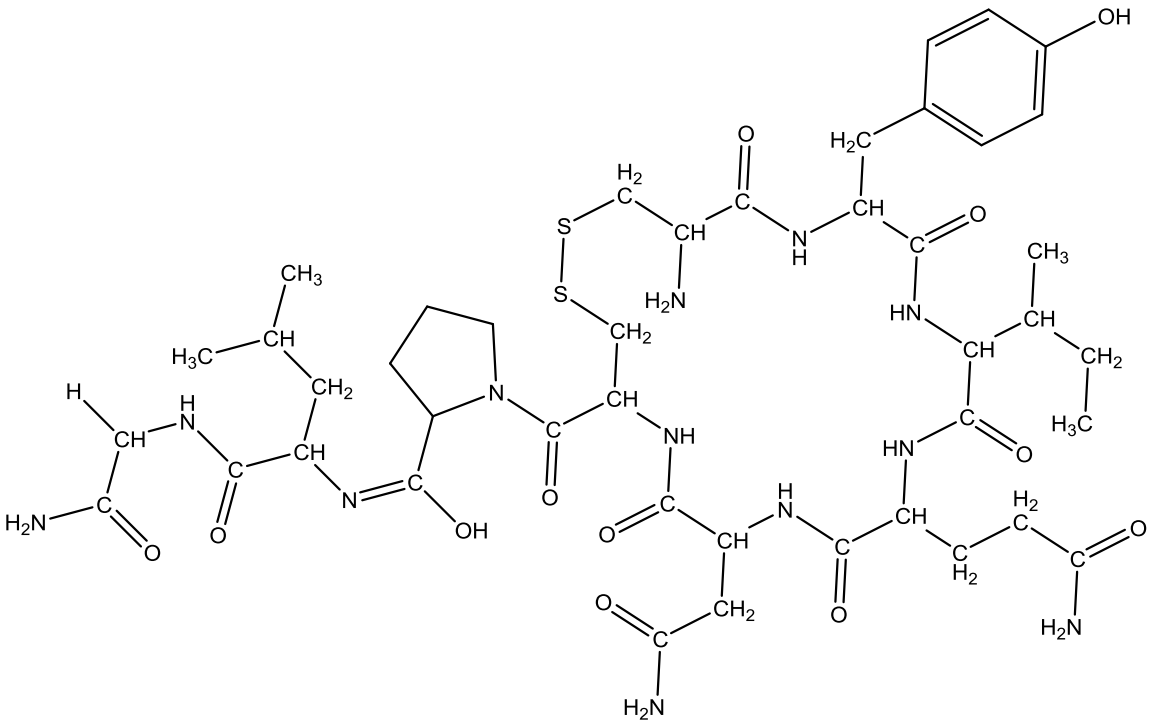

Scheme 17: Structure of Oxt drawn with ChemDraw

The active part of Oxt consists of the Ile, Gln, Pro and Leu residues. These amino acids are responsible for the biological activity and the other amino acids stabilize the three-dimensional structure of the peptide. Even slight changes to the dihedral angle of the disulfide bridge impact the biological activity of Oxt. Importantly, conformational changes have been detected by circular dichroism upon substitution of sulfur with selenium in Cys residues.[17] The biological activity of Oxt samples with selenium substitutes was significantly reduced despite the fact that the disulfide bridge is not part of the biological active part of Oxt.[18] Both the disulfide bridge and the Tyr residue are well exposed and are therefore facile targets for oxidative damage. Alkylation of the Tyr residue with bulky groups such as methyl or ethyl groups lead to decrease of the activity.[17]

Oxt is most stable at pH 4.5. Storage at high temperatures and increasing pH triggers the Tyr dimerization and the deamidation of Gln and Asn. Aggregation, which is due to the formation of dimers and trimers via disulfide bridge exchanges, is the main pathway of Oxt degradation. Under acidic conditions, the disulfide interchange occurs via the formation of a sulfenium cation as a consequence of disulfide protonation. Notably, the sulfenium cation may further react with another disulfide bridge.[19] Under neutral or basic conditions a free thiolate anion reacts with another disulfide bridge.[19,20]

In comparison to PA, Oxt is made of three additional amino acids: Pro-Leu-Gly and the Phe is substituted by an Ile residue. Ile is an aliphatic amino acid and much less reactive towards hydroxyl radicals than Phe.[18]

The experiments and the results in Chapter 3 dealt with the effect of the Fenton reaction on PA. One of the main targets for hydroxylation by the Fenton reagents was the Phe residue. Considering that the Phe residue is replaced in Oxt by Ile this facile target is eliminated. With the substitution of the Phe residue by a more stable Ile residue, insights into the role of Phe in terms of hydroxyl radical scavenging are enabled. According to the redox potential and the reaction kinetics, Phe, unlike Ile, is likely to react very efficiently with hydroxyl radicals.[22,23]

It has been shown that free hydroxyl radicals that were formed by g-irradiation in N_2O saturated solution of Oxt are capable of oxidizing the cystine disulfide bridge as well as the Tyr and Leu residues.[24]

4.2 Methods

The methods described in Chapter 3 for PA were applied to Oxt. Modifications to those experiments are described here.

4.2.1 Chemicals used

Oxytocin (Oxt) was purchased from Bachem (Torrance, CA, USA). Hydrogen peroxide, (30% H_2O_2); ethylendiamine tetraacetatic acid (EDTA); ferrous ammonium sulfate,

hexahydrate (Fe^{2+}); sodium phosphate, mono and dibasic; sodium pyruvate; acetonitrile, HPLC grade (ACN); tetrahydrofuran (THF); trifluoracetic acid (TFA); hydrochloric acid (HCl); phenol (liquefied, 90%); n-ethylmaleimide (NEM) were purchased from Sigma-Aldrich (St. Louis, MO, USA); compressed gases were purchased from Matheson Tri-Gas, Inc. (Montgomeryville, PA)

4.2.2 Instruments used

HPLC analysis was performed on a Shimadzu SIL20 system equipped with a 20X autosampler and an SPD-M20 PDA and a RF-20A fluorescence detector. For the analysis and separation a Vydac 218TP C18 ODS2 (250x4.6 mm, 5 micron) analytical column and for the amino acid analysis a Thermo C18 ODS Hypersil (250x4.6 mm; 5 micron) column were used. A linear gradient of solvent A (95:5:0.1 H_2O:ACN:TFA) and solvent B (5:95:0.1 H_2O:ACN:TFA) was applied from 15% to 22% solvent B over 10 min.

Solid phase extraction (SPE) was performed using 50mg/1ml C18 Hypersep columns purchased from Thermo Scientific (Bellefonte, PA, USA).

MS and MS/MS data were acquired on a Waters Xevo G2-S QTof mass spectrometer with HPLC solvent delivery systems from Waters (Manchester, UK). ESI was operated at 2.8 kV cone voltage, tube lens offset at 70 V, and the capillary temperature was 350 °C. For the separation a Vydac MS C18 300A column (250x0.5 mm; 5 micron) was used. The injection volume was 3 µl. A linear gradient of solvent A (100% H_2O) and solvent B (99.9% ACN: 0.1% TFA) was applied from 15% to 30% solvent B over 50 min.

4.2.3 Experimental protocol

A standard solution of phosphate buffer (pH = 6.1) was prepared by mixing 10 mM Na_2HPO_4 with 40 mM NaH_2PO_4 in water followed by at least 30 min of degassing with Ar. To a solution of EDTA in phosphate buffer the Fe^{2+} has been added. 7 M (30% v/v) H_2O_2 was diluted in phosphate buffer to yield a 105 mM solution. 150 mM sodium pyruvate solution was prepared in H_2O. All subsequent steps were performed while purging the solutions with argon to avoid oxygen uptake. The analytical workflow is summarized in **Table 8**. For details see the methods section of chapter 3. The final concentrations were 0.45 mM Oxt, 4.5 mM $Fe(EDTA)^-$ and 10.5 mM H_2O_2.

Table 8: Workflow for the Oxt experiment

Step	**Purpose**
Fenton reaction with Oxt	Formation of oxidation products
Solid phase extraction (offline)	Separation of the peptide from the buffered Fenton reaction solution
Freeze-dry and reconstitute in H_2O	Removal of solvents used for SPE
Product separation with UV/Fluorescence HPLC	Individual collection of the products formed during the Fenton reaction
Freeze-dry and reconstitute in H_2O	Removal of solvents used for HPLC
MS analysis	Characterization of the products
Reduction/alkylation	Preparation for subsequent analytical methods
Solid phase extraction (offline)	Separation of the peptide from reduction/alkylation substances

Freeze-dry and reconstitute in H_2O	Removal of solvents used for SPE
MS/MS analysis	Identification of the oxidation site of the peptide, exclusion of disulfide bridge oxidation
Hydrolysis	Preparation for amino acid analysis
Freeze-dry and reconstitute in H_2O	Removal of solvents from the hydrolysis
Aromatic amino acid analysis	Identification of the isomers formed by the Fenton reaction

4.3 Results

4.3.1 Chromatograms of the Fluorescence HPLC experiment for product separation

After the Oxt sample was exposed to Fenton reaction one additional substance occurred in the chromatogram shown in **Figure 54**.

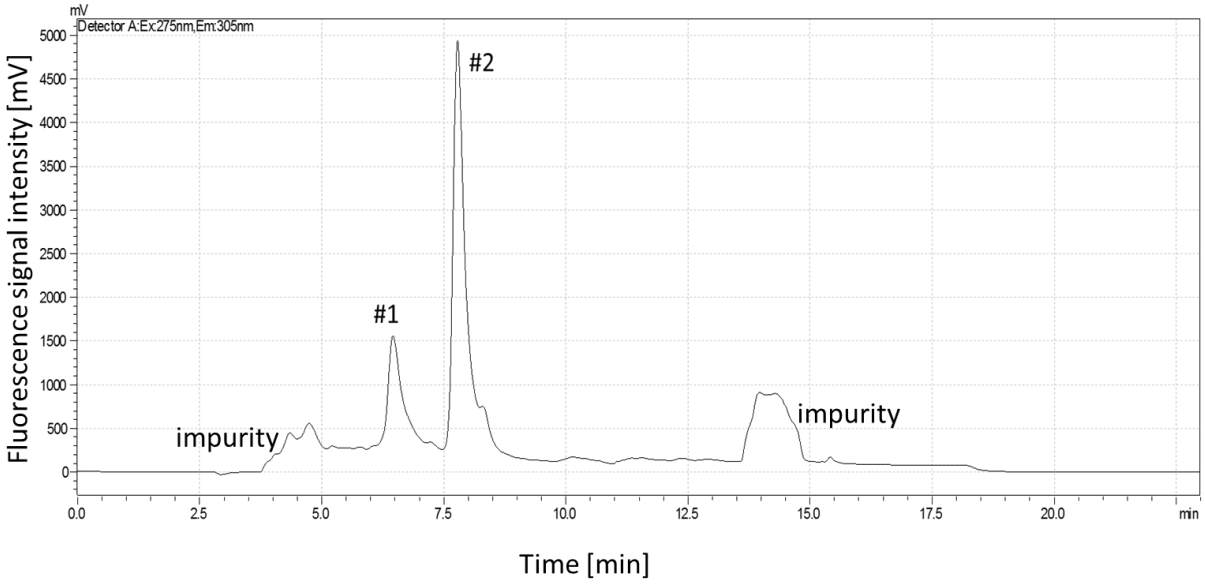

Figure 54: HPLC chromatogram recorded with a fluorescence detector of Oxt after Fenton reaction. A linear gradient of solvent A (100% H_2O) and solvent B (99.9% ACN: 0.1% TFA) was applied from 15% to 22% solvent B over 10 min.

Peak #1 shows the new product formed from Oxt by the Fenton reaction. Peak #2 represents unmodified Oxt. The structure of unmodified Oxt was verified by comparing the elution times with Oxt standard and by mass spectrometry. The two impurities eluting after 4 and 13 min were collected and analyzed by mass spectrometry. No specific substances could be identified. Interestingly, none of the impurities were observed in the mass spectrum when the sample mixture was injected into the mass spectrometer after the Fenton reaction. This indicates that the impurities were no products formed during the Fenton reaction with Oxt. Although the analytical column

was flushed over night with a high concentration of organic solvent these impurities still eluted at the same time during the analysis.

4.3.2 MS data

The MS data of Oxt exposed to Fenton reaction, shown in **Figure 55**, indicate that the main product formed contained an additional oxygen. The MS chromatogram showed that besides the unreacted Oxt with m/z = 1007.4 eluting after 35.2 min, three products with m/z = 1023.4 were formed. The mass difference of 16 Da indicates the addition of one oxygen. The small product peak that eluted after 30.3 min had m/z = 1023.4. The other two product peaks with m/z = 1023.4 eluted after 33.2 and 34.1 min, respectively. It was not possible to separate these substances by means of chromatography coupled to fluorescence detection. Therefore, it was impossible to separately collect those individual oxidation products and analyze them following reduction and alkylation.

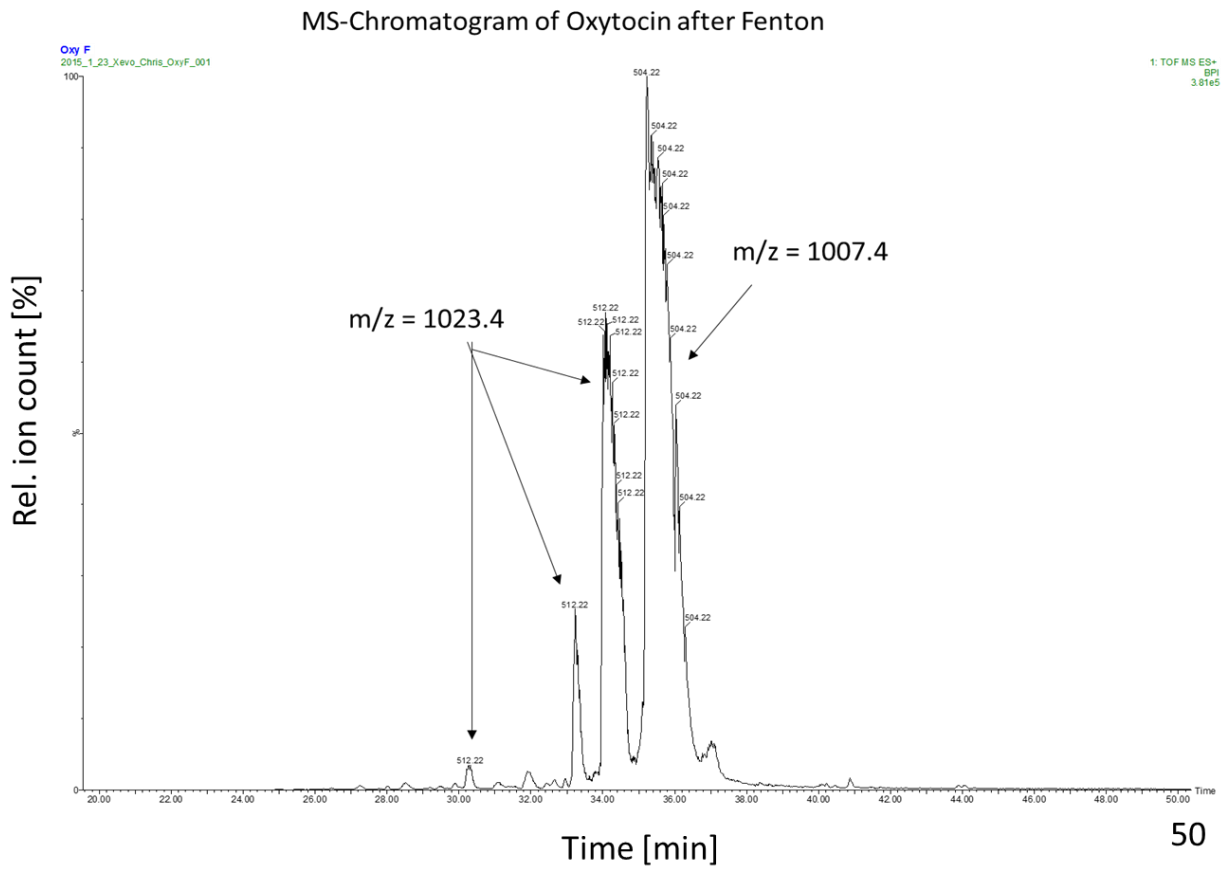

Figure 55: MS chromatogram of oxytocin after Fenton reaction was applied, MS chromatogram recorded over 50 min and the base peak integration method has been applied

4.3.3 MS data after reduction and alkylation

After reduction and alkylation of unmodified Oxt standard four isobaric peaks, matching the mass of the reduced and alkylated Oxt were observed in the MS spectrum. The occurrence of four isobaric peaks can be explained by the formation of four possible

combinations of how the two Cys residues are attached to the N-ethylsuccinimide residues.

The carbon of N-ethylsuccinimide attached to the sulfur is chiral and can have either R or S configuration, see **Scheme 18**. With two Cys residues in the peptide this results in four possible configurations: RR, RS, SR, SS. The column used for MS analysis is actually capable of separating those products.

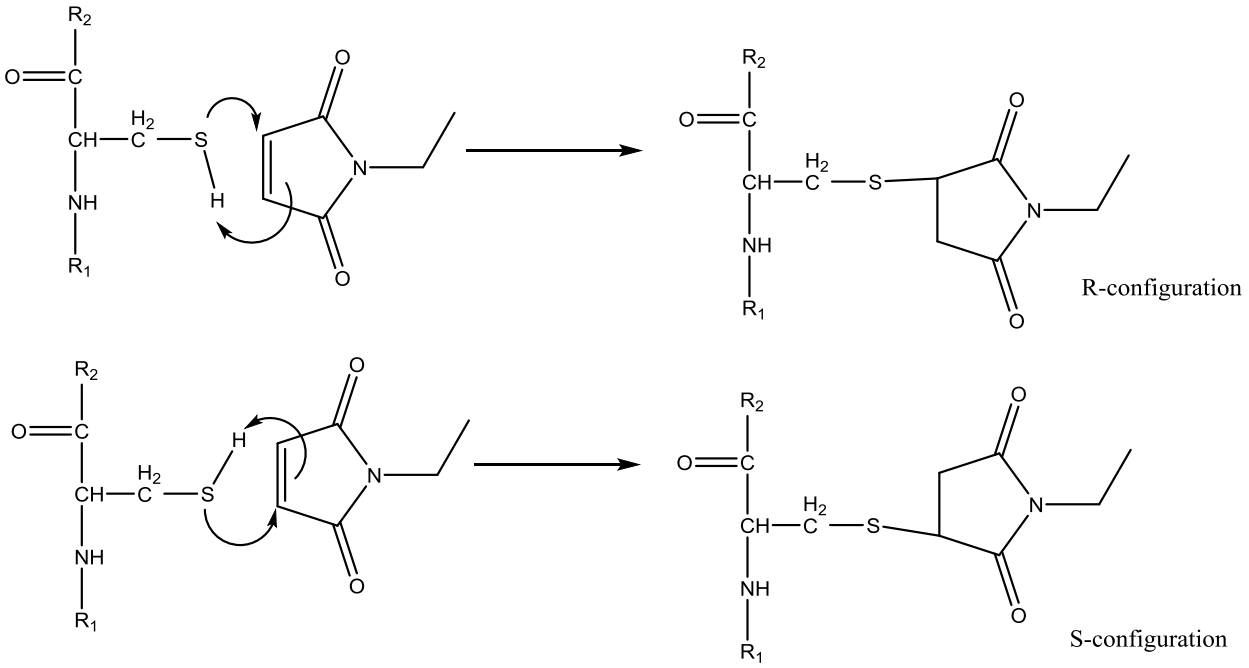

Scheme 18: Formation of Cys-N-ethylsuccinimide isomers

Figure 56 shows the MS data of reduced and alkylated oxytocin after the Fenton reaction. The peaks are not well separated since four products were formed during alkylation for each species making it difficult to analyze them. Therefore the

individually separated products #1 and #2 (**Figure 54**) were reduced and alkylated for further analysis.

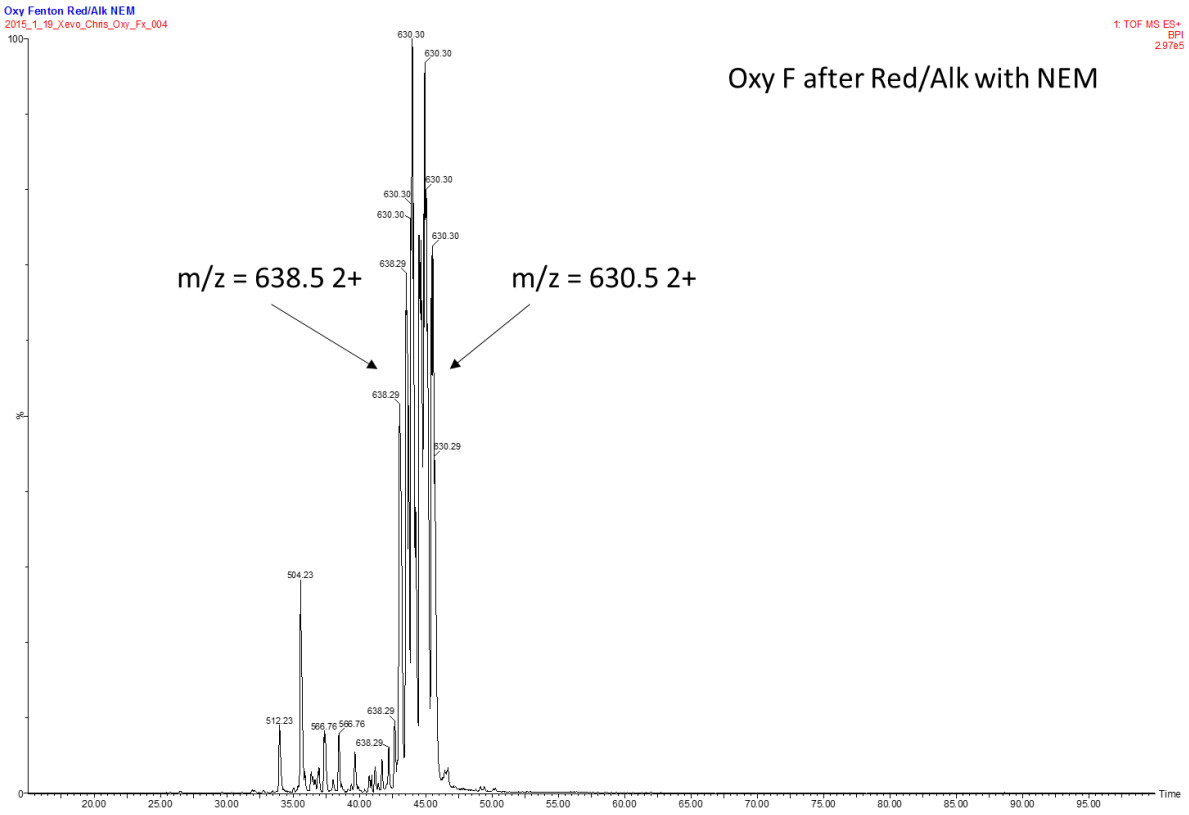

Figure 56: MS chromatogram of reduced and alkylated oxytocin after the Fenton reaction was applied, chromatogram recorded over 95 min and the base peak integration method was applied.

4.3.4 MS/MS data after reduction and alkylation

The MS/MS data obtained of the reduced and alkylated Oxt standard as well as the Fenton oxidized samples #1 and #2 showed very good b and y ion coverage. The product formed by Fenton reaction matched the predictions for Tyr that is hydroxylated

to yield 3,4-dihydroxyphenylalanine. Similar to the PA samples a strong signal occurred from the a2 ion which can also be accounted for by CO loss from the b2 ion. **Figure 57** shows the ion coverage for the unmodified Oxt and for product #2 after reduction and alkylation. **Figure 58** shows the MS/MS spectrum of reduced and alkylated product #1 of Oxt after Fenton reaction. In addition to the assigned b and y ions a large peak with m/z = 636.26 2+ occurred, which represents the doubly charged precursor ion of Oxt.

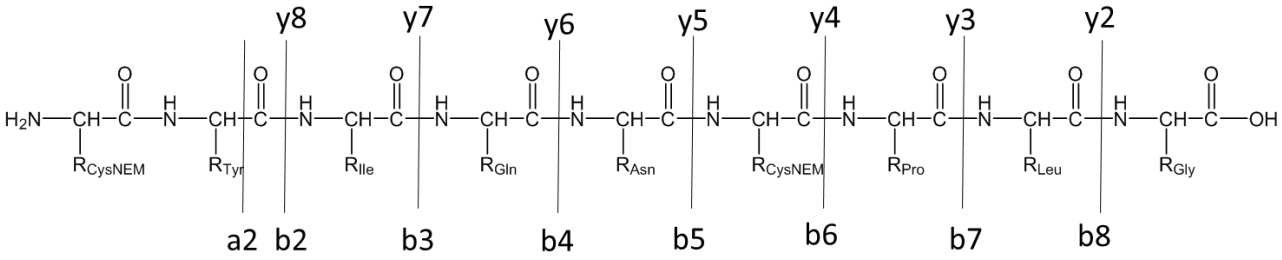

Figure 57: Ion coverage for product #2 and Oxt standard after reduction and NEM alkylation

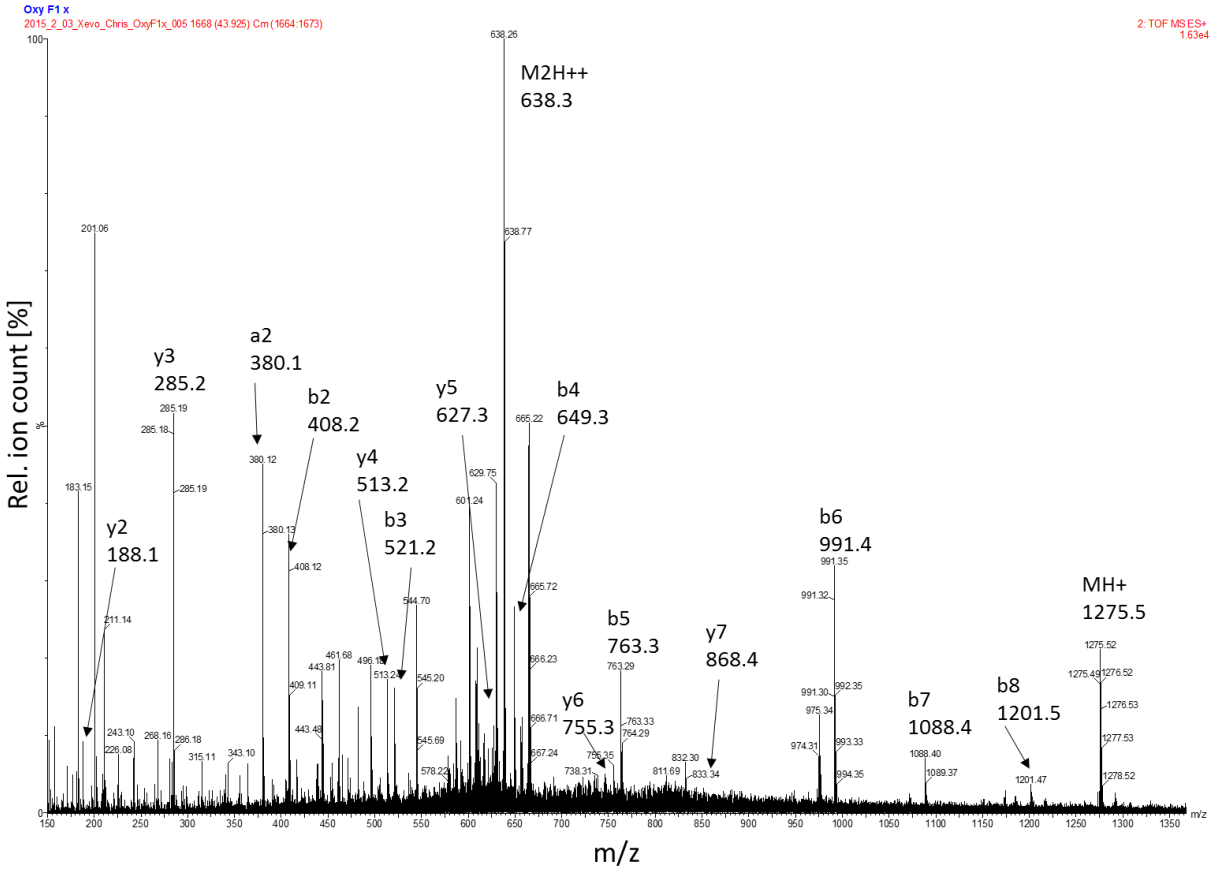

Figure 58: MS/MS spectrum of reduced and alkylated product #1 of Oxt. The spectrum shows the ions detected and asssigned for the predicted fragments in the range of m/z = 150 to 1350

Figure 59 and **Figure 60** show the ion coverage and the spectrum of product #1 after reduction and alkylation. Again, this very good coverage proves the formation of 3,4-dihydroxyphenylalanine from Tyr.

In both cases oxygen remained on the peptide after reduction, indicating that no thiosulfinate had been formed.

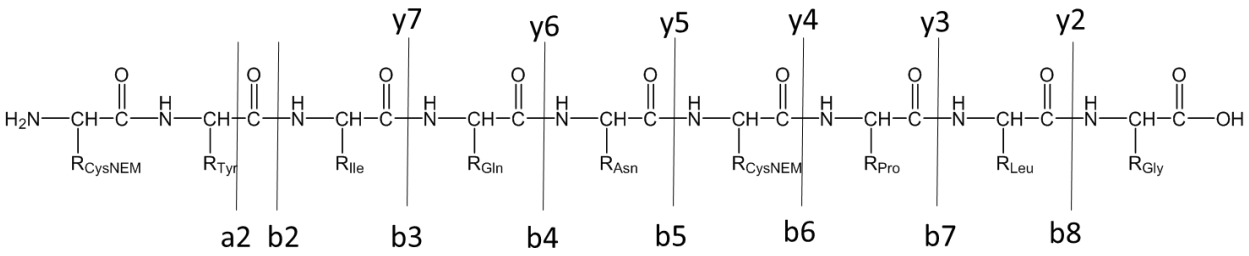

Figure 59 – ion coverage for product #2 after reduction and alkylation with NEM

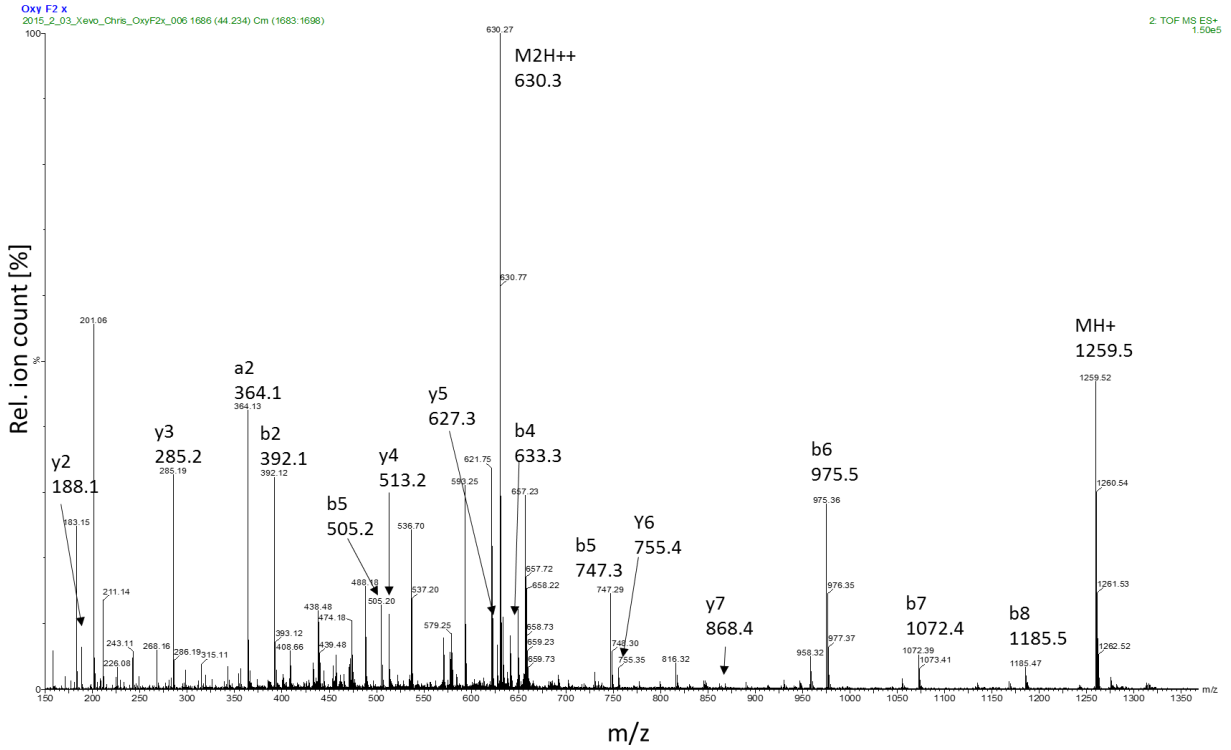

Figure 60 – MS/MS-spectrum of reduced and alkylated sample #2. The spectrum shows the ions detected and assigned for the predicted fragments in the range of m/z = 150 to 1350

4.3.5 Amino acid analysis

Oxt standard and the separated products #1 and #2 were hydrolyzed after reduction and alkylation to perform amino acid analysis. The Oxt standard and product #2 both contained Tyr, shown in **Figure 61** is the data of Oxt standard after hydrolysis.

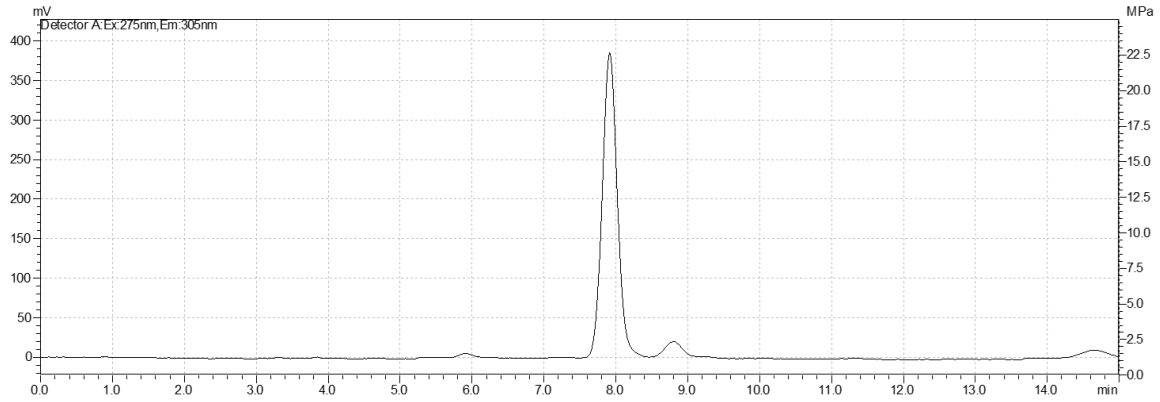

Figure 61: Fluorescence signal of hydrolyzed Oxt standard

HPLC chromatogram recorded with a fluorescence detector of hydrolyzed Oxt standard. 1% NaCl + 1% acetic acid in H_2O, isocratic elution. Ex: 275 nm; Em: 305 nm. Recorded over 15 min.

In product #1 the elution time of the hydrolysis products matched the elution time of 3,4-hydroxyphenylalanine (DOPA) standard as shown in **Figure 62**. This supported the findings from the mass spectra that the oxidation product of Oxt is containing DOPA. Similar to the results of product #3 of PA the DOPA residue showed three products

during the amino acid analysis. During the hydrolysis process the rather instable DOPA starts to degrade leading to the formation of three substances, DOPA, Tyr, and an unidentified product. This result is reproducible as it was also found when DOPA standard solutions were hydrolyzed.

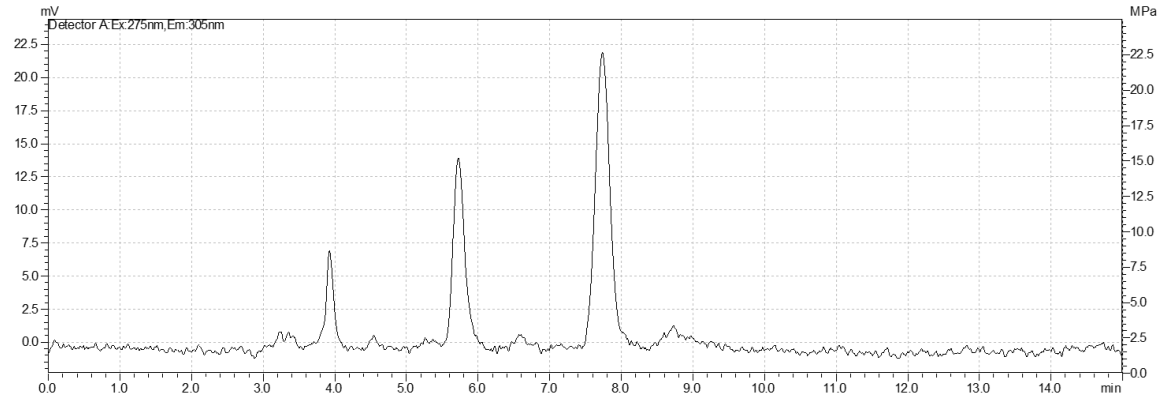

Figure 62: HPLC chromatogram of hydrolyzed Oxt product #1

HPLC chromatogram of hydrolyzed Oxt product #1 following the Fenton reaction. 1% NaCl + 1% acetic acid in H_2O, isocratic elution. Ex: 275 nm; Em: 305 nm. Recorded over 15 min.

4.4 Additional experiment with a peptide that contains no aromatic residue

The Fenton reaction described before was applied to a custom made peptide, subsequently referred to as Arg-peptide, that contained no aromatic residues in order to eliminate possible radical scavenging from an aromatic residue. The Arg-peptide had the following structure:

Gly-Gly-Cys-Arg-Gly-Gly-Leu-Leu-Gly-Gly-Arg-Cys-Gly-Gly (the two Cys residues are connected with a disulfide bridge), see **Figure 63**.

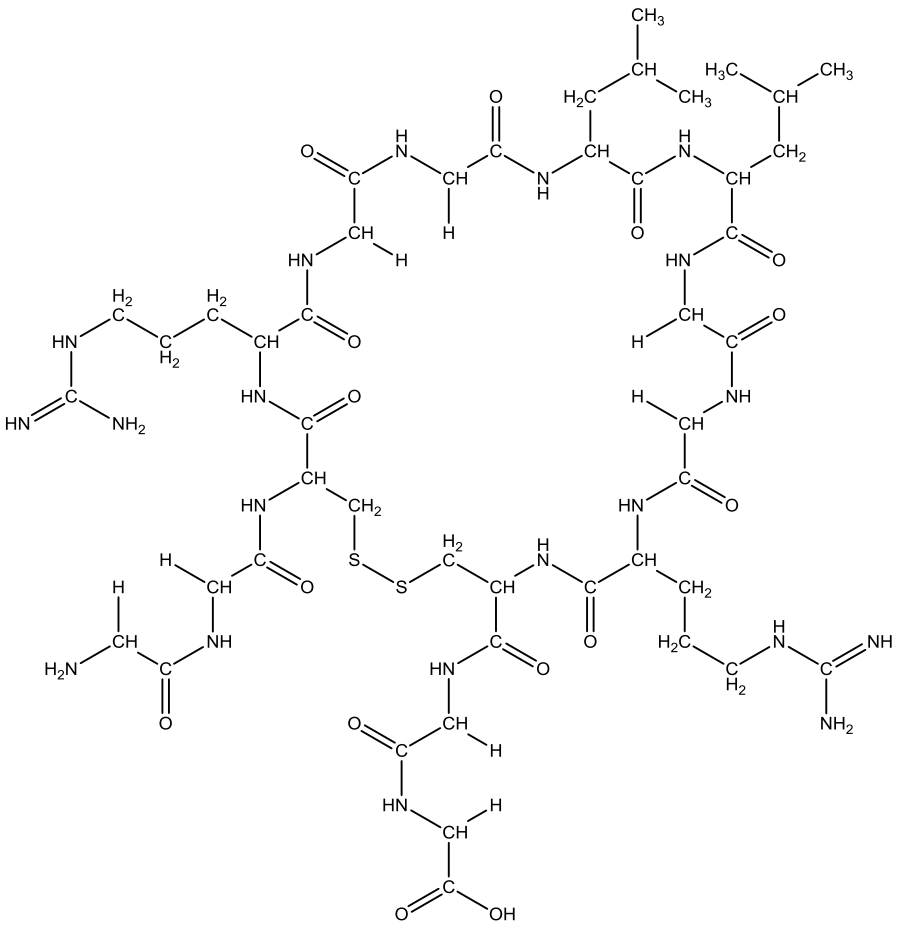

Figure 63: Structure of the Arg-peptide drawn with ChemDraw

The MS data of the original peptide (**Figure 64**) showed m/z = 406.5 (3+) which is the expected value for the peptide mass (406.5 x 3 – 3 = 1216.5 Da).

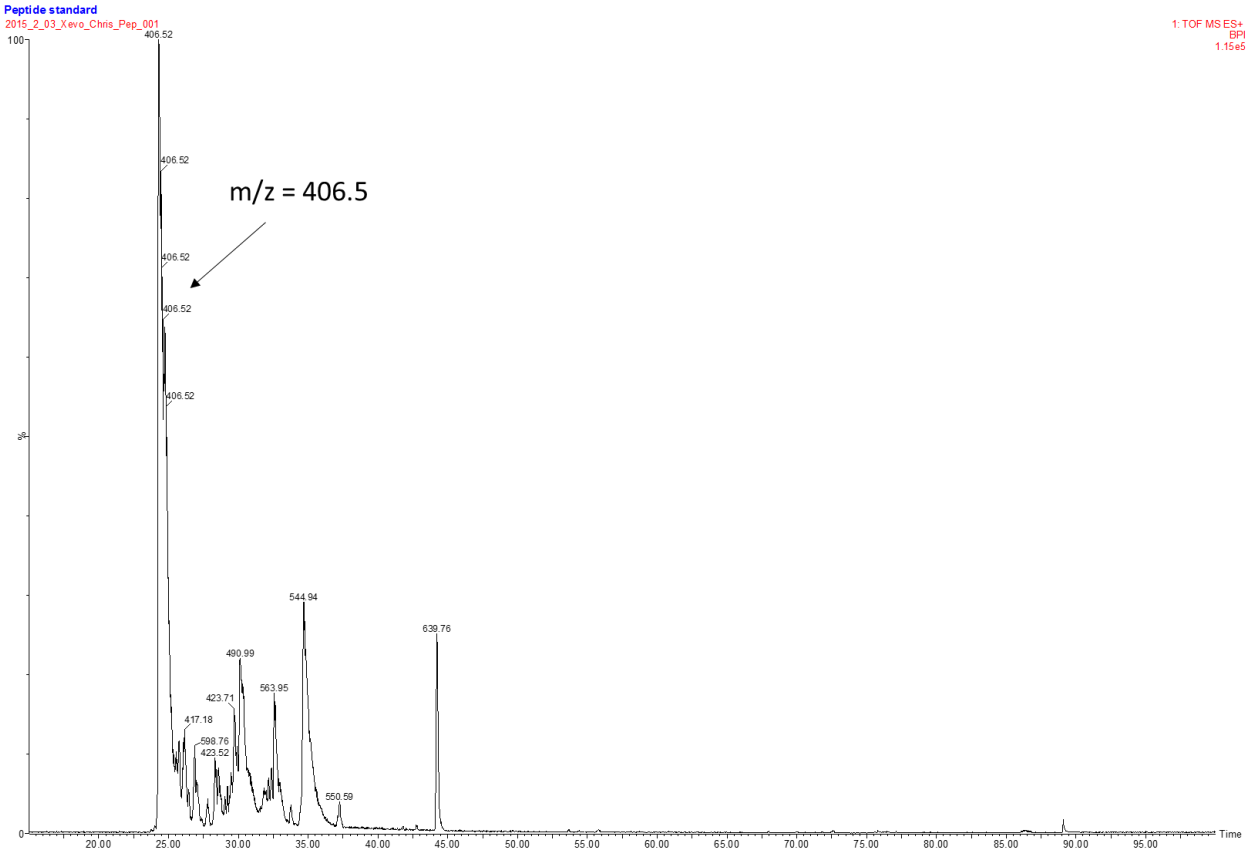

Figure 64: MS chromatogram of the Arg-peptide

MS chromatogram of the Arg peptide, MS chromatogram recorded over 95 min and the base peak integration method has been applied.

Due to its unexpected intense hydrophilicity the HPLC gradient for the observation of the mass spectrometry data was not optimized for the Arg-peptide and therefore the samples eluted too early and the products could not be well separated.

The MS chromatogram recorded from the Arg-peptide after Fenton reaction is shown in **Figure 65**. Besides the unmodified Arg-peptide (m/z = 406.5 3+), two other major

products were found. One product had an m/z = 587.8 2+ which gives a mass of 587.8 x 2 -2 = 1173.6 Da.

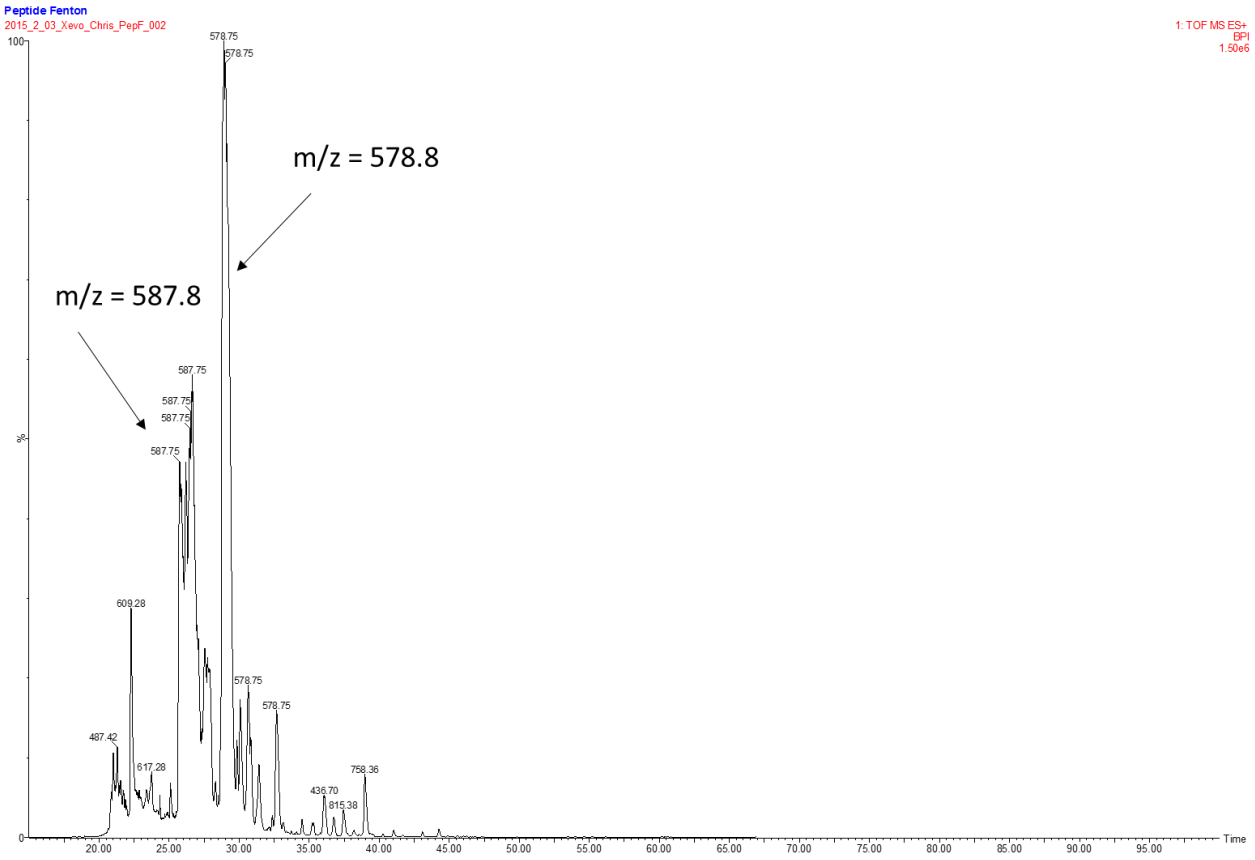

Figure 65: MS chromatogram of the Arg-peptide after Fenton reaction

MS chromatogram of the Arg-peptide Fenton reaction was applied, MS chromatogram recorded over 50 min and the base peak integration method has been applied.

This is a mass difference of 43 Da compared to the unmodified peptide. This can be referred to the reaction of the hydroxyl radical with the Arg residue that results in deguanidination indicated by the mass loss of 43 Da.[19] The other major product had m/z

= 578.8 2+ which gives a total mass of 578.8 x 2 -2 = 1155.6 Da or a difference of 60 Da compared to the original mass. This mass was not assigned to a specific product.

4.5 Discussion

Hydroxyl radicals formed by Fenton reaction formed one major product with oxytocin. This product was identified as tyrosine that had been hydroxylated to 3,4-dihydroxyphenylalanine. Since Oxt contains no Phe residue the major oxidation site was Tyr. Close proximity of the disulfide bridge to Tyr may have prevented its oxidation. It can be assumed that Tyr is protecting the disulfide bridge of Oxt and PA from radicals formed by the Fenton reaction. **Scheme 19** shows the electron pair distribution in 4-hydroxyphenylalanine. A free electron pair of oxygen can form a double bond to the carbon in the ring system and the adjacent double bond electron pair can be distributed to the carbon in ortho position to the hydroxyl group. A negative charge is less likely to occur on the meta position and therefore the electrophilic hydroxyl radical is more likely to form 3,4-dihydroxyphenylalanine than 2,4-dihydroxyphenylalanine. **Scheme 20** shows the hydroxylation pathway of Tyr with a free hydroxyl radical,[20] the same products will be formed if the Tyr residue is attacked by a bound hydroxyl radical or a ferryl ion.[20]

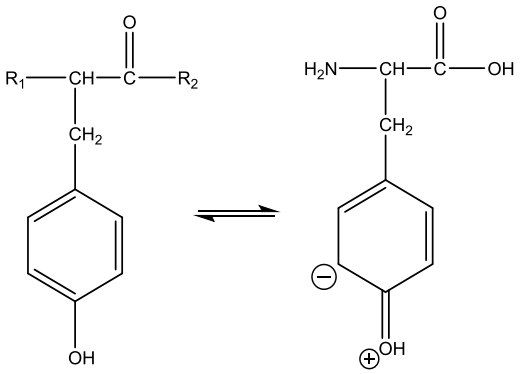

Scheme 19: Electron pair distribution of 4-hydroxyphenylalanine

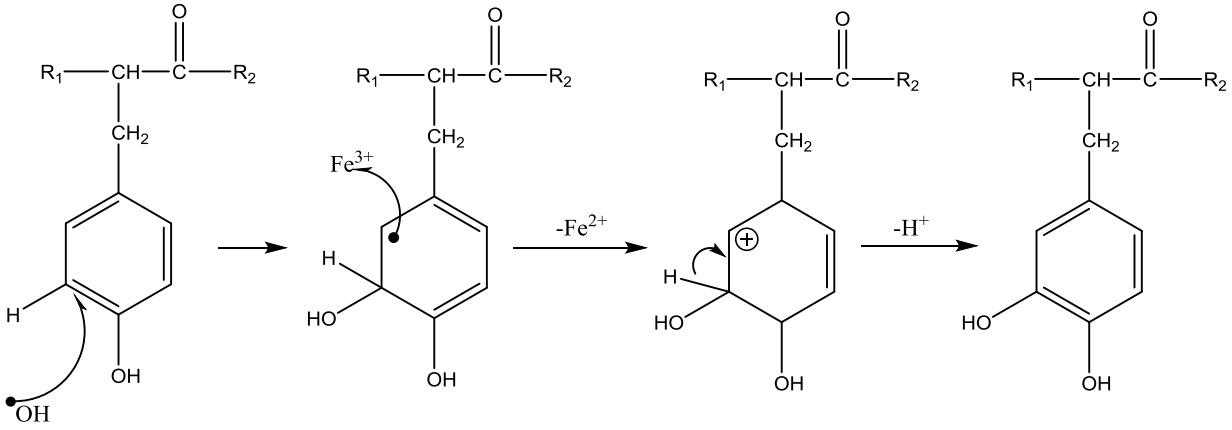

Scheme 20: Formation mechanism of 3,4-dihydroxyphenylalanine by a hydroxyl radical

Like in PA, the disulfide bridge of Oxt lacks susceptibility for any attack by the reactive species formed in the Fenton reaction. From the aforementioned the question arises whether the Tyr residue acts as a radical scavenger and, in turn, protects the disulfide bridge.

The additional experiment with the Arg-peptide that contained no aromatic residues shows that the disulfide bridge is not necessarily protected by aromatic residues. Arg

and cystine disulfide bridges have a similar reaction rate constant for the reaction with hydroxyl radicals.[19] The mass loss of 43 Da observed after Fenton reaction can be attributed to the deguanidation of the Arg residue.[19] The reaction mechanism is presented in **Scheme 21**.

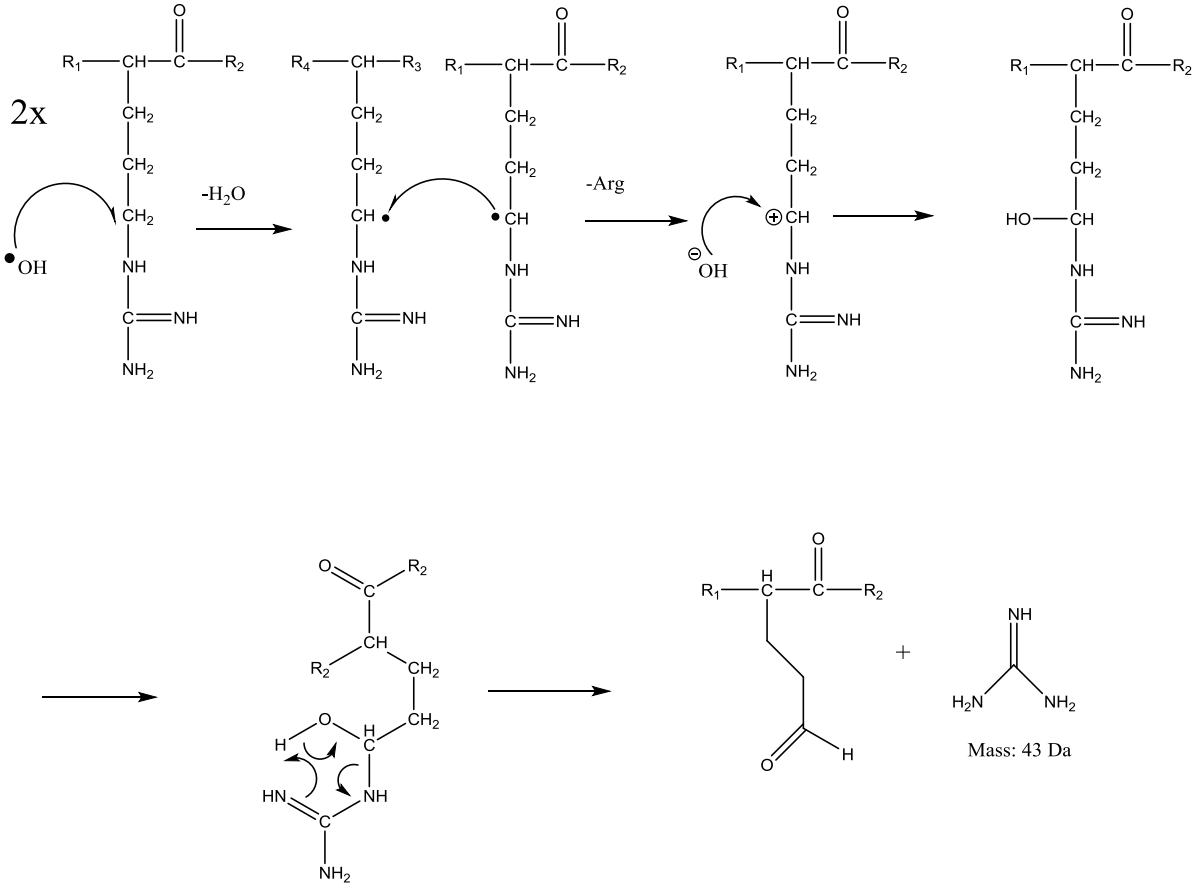

Scheme 21: Deguanidation mechanism of Arg after hydroxylation

The hydroxyl radical abstracts a hydrogen from the Arg residue and leaves an Arg radical which can abstract an electron from another Arg radical. The newly formed Arg cation can attract a hydroxide ion followed by a concerted cleavage of a guanidine group.

However, no formation of a thiosulfinate has been detected according to the MS data. This leads to the question whether the disulfide bridge is too inert to react with a hydroxyl radical that has been created by the Fenton reaction or if the sulfuranyl radical is able to repair itself by reacting with the adjacent amino acid residue.

Previous studies showed that the cystine disulfide bridge of Oxt can be degraded by free hydroxyl radicals.[21,22] As it is widely discussed whether the Fenton reaction yields free or bound hydroxyl radicals or Ferryl ions the disulfide bridge was either not attacked by the reactive species of the Fenton reaction or the radical damage was repaired before the oxidation could occur. The Fenton system contains Fe^{2+} which reacts with H_2O_2 yielding Fe^{3+}.[20,23,24] During the hydroxylation of aromatic residues or the deguanidation of Arg an electron can be transferred to Fe^{3+} in order to form a cation. This will yield Fe^{2+} again which can either react with H_2O_2 again or transfer an electron to a potentially formed sulfuranyl radical. That means the radical on the disulfide bridge can be repaired.

4.6 Additional experiments performed

4.6.1 MS^3 Fragmentation of the ring structure

MS/MS analysis requires that the ring structure of PA and Oxy is opened in order to form fragment ions. Reduction and alkylation of TCEP may induce oxygen removal attached to sulfur as described in section 3.2.3.5. The combination of source fragmentation followed by MS/MS analysis during the MS analysis allows opening a peptide ring and forming fragment ions with predictable m/z values without the

reduction and alkylation process being necessary.[30] The corresponding spectra did not allow to assign specific fragments to the m/z values. Therefore, this method was not further applied.

4.6.2 Enzymatic digest of peptides

Next, the enzymatic cleavage of Oxt and PA was tested with chymotrypsin. The latter is known to cleave on the C-terminal site of aromatic amino acid residues.[31] Digests were performed with PA and Oxt as well as Insulin Chain B for comparison. Insulin Chain B was used to corroborate the digestive ability of the enzyme.For the digest, chymotrypsin with a concentration of 1 µg/µl was added to 1 mM Oxt, PA and Insuin Chain B solution with a ratio of 1:200 (Enzyme:Peptide). The solution was incubated for 18 hours at 25 °C. Chymotrypysin MS data showed that only insulin chain B was digested, indicating that the enzymes were active but unable to cleave the rigid ring structure of the Oxt and PA. **Figure 66** shows the MS data of the chymotrypsin digest experiments.

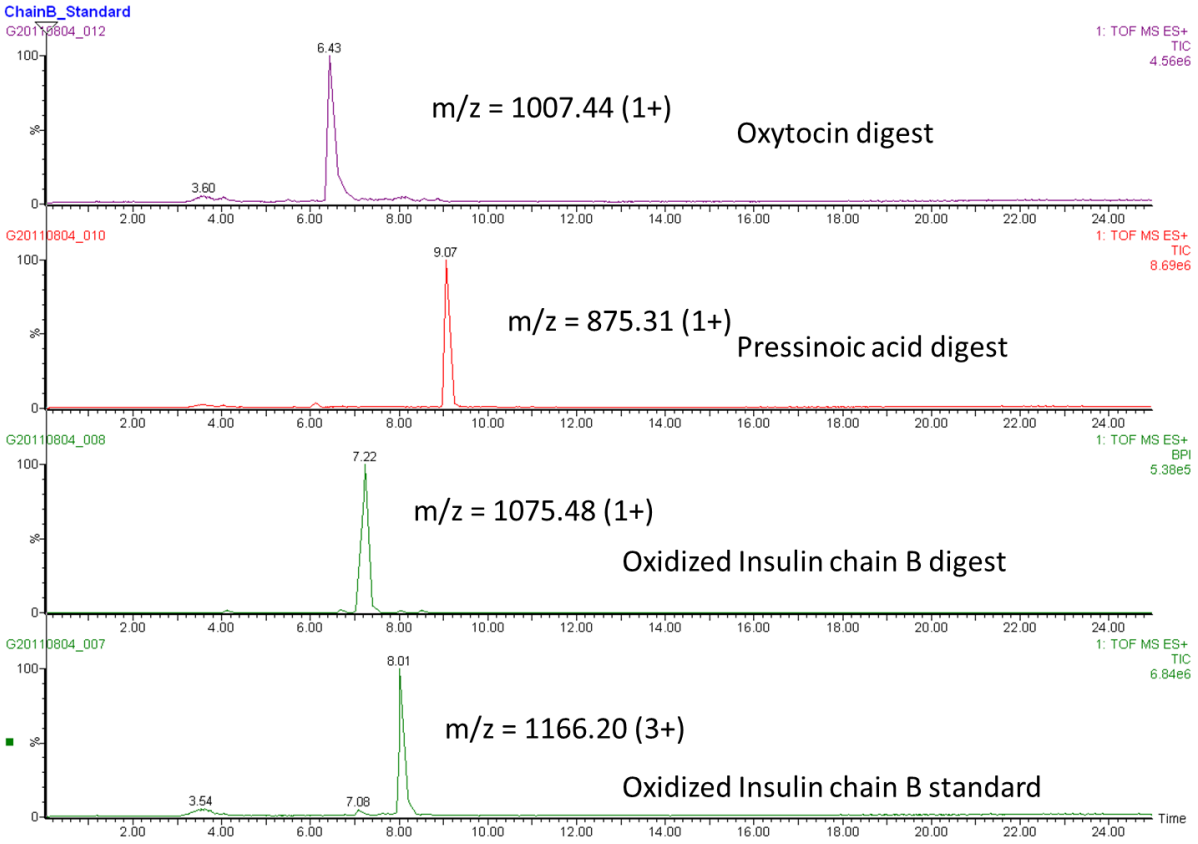

Figure 66: MS data of the chymotrypsin digest experiment, linear gradient with solvent A (100% H_2O) and solvent B (99.9% ACN, 0.1% TFA) of solvent B 10%-80% over 20 min, chromatograms displayed as base peak integrated.

4.7 References

(1) Dale, H. H. *J Physiology* **1906**, *34*, 163.
(2) Lee, H.-J.; Macbeth, A. H.; Pagani, J.; Young, W. S. *Prog neurobiol* **2009**, *88*, 127.
(3) Ott, I.; Scott, J. C. *Proc. Soc. Exp. Biol. Med.* **1910**, *7*, 48.
(4) Schafer, E. A.; Mackenzie, K. The Action of Animal Extracts on Milk Secretio*n*, 1911; Vol. 84.
(5) Oliver, G.; Schafer, E. A. *J Physiol* **1895**, *18*, 277.
(6) Gainer, H. In *Vasopressin and Oxytocin*; Zingg, H., Bourque, C., Bichet, D., Eds.; Springer US: 1998; Vol. 449, p 15.
(7) Renaud, L. P.; Bourque, C. W. *Prog. Neurobiol. (Oxford)* **1991**, *36*, 131.
(8) Amico, J. A.; Finn, F. M.; Haldar, J. *Am J Med Sci* **1988**, *296*, 303.
(9) Gimpl, G.; Fahrenholz, F. The Oxytocin Receptor System: Structure, Function, and Regulation, 2001; Vol. 81.
(10) Gizzo, S.; Patrelli, T. S.; Di Gangi, S.; Carrozzini, M.; Saccardi, C.; Zambon, A.; Bertocco, A.; Fagherazzi, S.; D'Antona, D.; Nardelli, G. B. *Reprod. Sci.* **2013**, *20*, 1011.
(11) Ayadi, A. M. E.; Robinson, N.; Geller, S.; Miller, S. *Expert Rev. Obstet. Gynecol.* **2013**, *8*, 525.
(12) Rath, W.; Bohlmann, M. K. *Gynaekologe* **2011**, *44*, 538.
(13) Van, D. P. W.; Van, R. J.; De, B. C. N.; Van, R. J. *Pharm Weekbl Sci* **1991**, *13*, 238.
(14) Anonymous *WHO Technical Report Series* **2014**, I.
(15) du Vigneaud, V.; Ressler, C.; Trippett, S. *J Biol Chem* **1953**, *205*, 949.
(16) du Vigneaud, V.; Ressler, C.; Swan, J. M.; Roberts, C. W.; Katsoyannis, P. G. *J Am Chem Soc* **1954**, *76*, 3115.
(17) Walter, R.; Schwartz, I. L.; Darnell, J. H.; Urry, D. W. *Proc. Nat. Acad. Sci. U. S.* **1971**, *68*, 1355.
(18) Langs, D. A.; Smith, G. D.; Stezowski, J. J.; Hughes, R. E. *Science* **1986**, *232*, 1240.
(19) Xu, G.; Chance, M. R. *Chem. Rev. (Washington, DC, U. S.)* **2007**, *107*, 3514.
(20) Walling, C. *Acc. Chem. Res.* **1975**, *8*, 125.
(21) Klassen, N. V.; Purdie, J. W.; Lynn, K. R.; D'Iorio, M. *Int. J. Radiat. Biol. Relat. Stud. Phys., Chem. Med.* **1974**, *26*, 127.
(22) Purdie, J. W.; Lynn, K. R. *Int J Radiat Biol Relat Stud Phys Chem Med* **1973**, *23*, 583.
(23) Goldstein, S.; Meyerstein, D.; Czapski, G. *Free Radical Biol. Med.* **1993**, *15*, 435.
(24) Wardman, P.; Candeias, L. P. *Radiat Res* **1996**, *145*, 523.

5 Outlook

In the following section, the current findings are placed in a context of future experiments.

5.1 The degradation pathway of sodium pyruvate

In this thesis, evidence by means of ^{13}C-NMR corroborates that the reaction of sodium pyruvate and H_2O_2 yields an intermediate, which has been identified as 2-hydroperoxy-2-hydroxypropanoate, for the experiments performed with deuterated solvents referred to as 2-deuteroperoxy-2-deuteroxypropanoate. Kinetic analyses of experiments with ^{13}C-enriched sodium pyruvate assisted in calculating the activation parameters for the formation and breakdown of the intermediate. Notably, the kinetic experiments were performed at neutral pD*. Further experiments should focus on performing the experiments at different pDs*. At, for example, low pD*, an increased amount of the hydrate form (2,2 dihyroxypropanoate) may crossover the rate limiting step from just a decarboxylation to the formation of the intermediate. At a higher pD*, an increased amount of ionized H_2O_2 is likely to facilitate a reaction with pyruvate.

Sodium pyruvate is meant to break down H_2O_2 into non-reactive products. It should be tested in future assays if intermediates, which are formed during this process, are more or less reactive than molecular H_2O_2. The impact of these assays is significant since the presence of pyruvate is supposed to protect drug formulations from oxidation.

Met as single amino acid is oxidized rather easily.[1] Experiments, which focus on investigating the potential of 2-hydroperoxy-2-hydroxypropanoate as an intermediate, need to be performed both at room temperature and low temperature. The presence of Met is vital in this context, especially to simulate different storage conditions. The oxidation of the sulfur group in Met in the presence and absence of sodium pyruvate and H_2O_2 should be analyzed.

A different interest lies in the Fenton reaction. In particular, a reaction with either PA or Oxt, as described in Chapters 3 and 4, respectively, should be initiated and followed regarding the extend of oxidation products if the peptide solutions contain sodium pyruvate prior to the addition of H_2O_2. A potential outcome of these investigations would be the verification of the H_2O_2 degradation to occur fast and efficient and to prevent potentially the formation of reactive species through the Fenton reaction.

Little is known about the scavenging of organic peroxides by pyruvate. For example, peroxides, which are formed on polysorbate 80 (PS80), are likely to interact with transition-metal residues and, as such, to form highly reactive species through the Fenton reaction.[2,3] Future work should clarify if sodium pyruvate might be active in terms of break downing the peroxides on PS80. If so, the reaction mechanisms should be elucidated by applying a similar protocol as developed in this thesis.

In order to ensure pseudo first-order kinetics, the experiments described in Chapter 2 required a tenfold excess of H_2O_2 over sodium pyruvate. Under these conditions the

hemiacetal formed in the presence of d4-methanol appeared, however, to be rather inert against the degradation induced by H_2O_2. Similarly, the experiments in section 2.6.5 were performed with a 30-fold excess of H_2O_2. Again, no visible change of the hemiacetal concentration was observed during the course of the reaction. Considering that experiments, as they were described in Chapter 2, suggested that the equilibrium is shifted to the intermediate rather than the hemiacetal form, however there was no indication of a hemiacetal degradation even after all of the sodium pyruvate has been consumed. It seems of interest to see the effect of a 100-fold or even 200-fold excess of H_2O_2 – reaching molar concentrations – on the degradation of the hemiacetal even at low temperatures.

The methyl group of sodium pyruvate contains an acidic proton, which facilitates the formation of pyruvate dimers and polymers under neutral or basic conditions.[4] It was established in this thesis that the dimer form of sodium pyruvate is inert against degradation through H_2O_2 and loses its scavenging function. Substitution of the methyl group with an electron-withdrawing functionality further decreases the electron density on the C2 position of an alpha-keto acid like pyruvic acid. It is expected that this modification results in a facilitation of the nucleophilic attack of H_2O_2. In addition, dimerization might be prevented from occurring. For the substitution of the methyl group a functional group, similar to the Met residue, can allow to synthesize an effective

scavenger against both molecular oxygen and H_2O_2. Provided that the substrates and all products are not subject to further unwanted reactions and are non-toxic.

5.2 The Fenton reaction and the effect of the reactive species formed on PA and Oxt

Based on the results presented in Chapters 3 and 4 the hypothesis was made that the cystine disulfide bridge is not a facile target for the different radical species created by the Fenton reaction. The experiments were, however, performed with peptides that contained aromatic amino acids, that is, Phe or Tyr. These are known to initiate the facile hydroxylation at positions adjacent to the disulfide bridge. A model peptide with the disulfide bridge adjacent to Arg also failed in terms of attacks on the disulfide bridge. Please note that Met is known to be a facile target for hydroxyl radicals.[5] Taken the aforementioned into concert, further experiments should shed light on the oxidation of Met, which is placed adjacent to a disulfide bridge, and the inertness of the disulfide bridge.

The effect of the Fenton reaction on model peptides made out of aliphatic amino acids such as glycine or leucine adjacent to a cystine disulfide bridge is another unanswered question. Both intermolecular, namely two peptide chains that are connected, and intramolecular, namely a ring shaped peptide, disulfide bridges should be tested towards their reactivity with Fenton reaction based radical species.

A common feature of the experiments is that the aromatic amino acid residues are located in close proximity to the disulfide bridge of PA and Oxt. The Fenton reaction should be applied in complementary work to model peptides, in which the aromatic amino acids or even Met are placed further away from the disulfide bridge. The objective of such work would be to demonstrate if an intermolecular radical transfer occurs as the key step to protect the disulfide bridge from radical attack.

No modification of the cystine disulfide bond was detectable in the products formed when the Fenton reaction was applied to the model peptides. However, it is impossible to conclude from the products if any reaction at all occurred on the disulfide bridge or if any damage or radical formation on the disulfide bridge was repaired through, for example, an intermolecular electron transfer.[6] It seems reasonable to postulate that sulfuranyl radicals were formed, which were repaired faster than the formation of any oxidation products. Electron spin resonance is the method of choice to detect potentially formed sulfuranyl radical cations.[7]

Free hydroxyl radicals, formed by γ-irradiation of N_2O saturated water were reported to degrade the Cys residues in Oxt.[8] Such experiments should be applied to the current samples in order to verify that the cystine disulfide bridge is indeed a target, which is susceptible for free hydroxyl radicals. Another incentive for such experiments is the proof of principle for the analytical methods, which were developed in the current

work, for the identification of modifications on the Cys residues including the oxidation of the disulfide bridge, etc.

Larger proteins such as enzymes or even antibodies should be subjected to the Fenton reaction experiments as well. Likewise, proteins featuring a large number of disulfide bridges with different neighboring amino acids and accessibility to oxidizing species should be probed. Some disulfide bridges may be more susceptible for radical attack or may promote damage to adjacent amino acids.

Even if a disulfide bridge is considered resistant against radical attack it is important to know if the overall stability is based on its intrinsic inertness or its repair mechanism, the latter being a potential problem for all adjacent amino acid residues.

5.3 References

(1) Brunelle, P.; Schoeneich, C.; Rauk, A. *Can. J. Chem.* **2006**, *84*, 893.
(2) Wardman, P.; Candeias, L. P. *Radiat. Res.* **1996**, *145*, 523.
(3) Cohen, G.; Sinet, P. M. *Dev. Biochem.* **1980**, *11A*, 27.
(4) Margolis, S. A.; Coxon, B. *Anal Chem* **1986**, *58*, 2504.
(5) Chu, J.-W.; Yin, J.; Brooks, B. R.; Wang, D. I. C.; Speed Ricci, M.; Brems, D. N.; Trout, B. L. *J. Pharm. Sci.* **2004**, *93*, 3096.
(6) Pattison, D. I.; Rahmanto, A. S.; Davies, M. J. *Photochem. Photobiol. Sci.* **2012**, *11*, 38.
(7) Bunce, N. J. *J Chem Educ* **1987**, *64*, 907.
(8) Klassen, N. V.; Purdie, J. W.; Lynn, K. R.; D'Iorio, M. *Int. J. Radiat. Biol. Relat. Stud. Phys., Chem. Med.* **1974**, *26*, 127.